• Institute of Fundamental Technological Research
• Polish Academy of Sciences
• Warsaw • Poland

LECTURE NOTES 14

Gerhard Nägele

The Physics of Colloidal Soft Matter

Centre of Excellence for
Advanced Materials and Structures

WARSAW 2004

AMAS LECTURE NOTES

Production of this volume has been partially supported by the European Commission

Published and distributed by
Institute of Fundamental Technological Research
Świętokrzyska 21, 00-049 Warszawa, Poland

ISSN 1642-0578

Papier offset. kl. III, 70 g, B1
Ark. wyd.: 13,6; ark. druk.: 11,5
Skład w systemie LaTeX: T.G. Zieliński
Oddano do druku i druk ukończono: V 2004
Druk i oprawa: Drukarnia Braci Grodzickich, Piaseczno, ul. Geodetów 47a

Contents

Preface

These Lecture Notes include material from 12 lectures and two seminars which I have given in March-April 2003 as a Visiting Professor at the Centre of Excellence for Advanced Materials and Structures (AMAS) in the Institute of Fundamental Technological Research, Polish Academy of Sciences, in Warsaw. It is my pleasure to thank Prof. Zenon Mróz for inviting me to visit AMAS and to present a series of lectures on Colloid Physics. I am grateful to Ms. Izabela Śleczkowska for her help with travel and accommodation, and for an endless supply of transparencies. Moreover, I am grateful to Mr. Tomasz Zieliński for assistance in preparing these lecture notes for publication. Many thanks to Prof. Tomasz Kowalewski for explaining me the interesting activities in his lab, for helping me to connect my notebook to the internet, and for having shared with me the wonderful experience of Mozart's *Don Giovanni* at the Warsaw opera. I thank Prof. Andrzej Majhofer for having explained to me part of the history of Warsaw. I am obliged to Prof. Jan Dhont, Research Centre Jülich, who wrote Chapter 7 on dynamic light scattering. Most notably, I want to express my deepest gratitude to Dr. Maria Ekiel-Jeżewska and to Prof. Bogdan Cichocki for their overwhelming hospitality, for fruitful scientific collaboration, and for sharing with me their deep insights into (hydro)dynamic problems. I really enjoyed the numerous discussions with Maria and Bogdan, and I have benefitted a lot from it.

Chapter 1

Static properties: introduction

Liquids and dense atomic or colloidal fluids are distinguished from dilute gases by the importance of short-range correlations and particle collision processes, and from crystalline solids by the lack of long-range order. The distinction between a liquid and a gas is only a quantitative one, since there is no change in symmetry in going from the gas phase to the liquid phase.

The most simple liquid systems are monoatomic liquids consisting of spherically shaped atoms (e.g., argon or neon), or else of quasi-spherical molecules such as methane. The interactions between the atoms can be characterized by simple pair potentials which depend only on the interatomic distances. Colloidal fluids consist of mesoscopically large colloidal particles, typically a few hundred nanometers in size, dispersed in a low-molecular solvent such as water. There are strong local correlations in the positions of these particles ("super atoms") so that they form a colloidal liquid in the liquid (solvent). The omnipresence of colloidal dispersions in chemistry and biology, and the unsurpassed variety and tunability of their particle interactions explains their importance both in industrial applications and fundamental research. Well-studied examples of simple colloidal fluids are suspensions of silica and polymethyl-methacrylate spheres in organic solvents, and aqueous dispersions of globular proteins or polystyrene latex spheres.

While the friction-dominated, diffusive dynamics of colloidal particles is quite different from the ballistic one of atomic liquids, atomic and colloidal liquids are very similar in terms of their equilibrium microstructure, i.e. in terms of the average particle ordering. There are just orders of magnitude

differences in the relevant length and time scales. Diffusion of colloidal particle suspensions will be explored in great detail in the second part of these lecture notes (Chapters 6-9).

In the first part of the present lecture notes (Chapters 1-5), I will discuss a versatile class of liquid state theory methods which allows to determine theoretically the microstructural and thermodynamic properties, both for colloidal and atomic liquids, from the knowledge of the particle interactions. These so-called integral equation schemes are based on the Ornstein–Zernike (OZ) equation. Some of the most relevant OZ schemes will be introduced, and we will explore their predictive power in comparison with computer simulations and experiment. The quantities of central importance calculated using these integral equation schemes are the radial distribution function, $g(r)$, of an isotropic liquid, and the associated static structure factor $S(q)$. The latter quantity is essentially the Fourier transform of $g(r)$, and it is directly measurable by appropriate static scattering techniques. A Fourier analysis of $S(q)$ provides then information about $g(r)$. In case of suspensions of large micron-sized colloidal particles, $g(r)$ is more directly accessible by means of video microscopy or confocal scanning microscopy.

Typical atomic and colloidal liquids of spherically shaped particles will be briefly characterized in Chapter 2 in terms of their interaction potentials. Chapter 3 provides an overview on general properties of $g(r)$ and $S(q)$, and on their relation to scattering experiments and thermodynamic properties. Chapter 4 introduces the fundamental Ornstein–Zernike equation with the associated concept of direct orrelations. As a first application of the OZ equation, I will address the phenomenon of critical opalescence in near-critical liquids. Various approximate closure relations are discussed which lead to closed integral equations for $g(r)$. Particular focus is given to hard-sphere fluids, since they can serve as a reference system of uncharged liquids, similar to the harmonic solid in solid-state physics. Chapter 5, finally, deals with the generalization of the Ornstein–Zernike integral equation schemes to liquid mixtures. These generalizations will be applied to the important case of a suspension of charge-stabilized colloidal particles. We will calculate the screened electrostatic interaction between the colloidal particles by contracting the neutralizing counter- and salt ions out of the description. For this purpose and for analytic simplicity, we use the so-called mean-spherical approximation (MSA), which is a direct generalization of the celebrated Debye–Hückel (DH) theory for dilute electrolytes to dense systems.

Chapter 2

Model systems and pair potentials

In the following we exemplify pair potentials suitable for describing the pair forces acting in simple and colloidal fluids of spherical particles. Simple fluids of non-polar atoms or molecules will be considered first, followed by a discussion of pair interactions in suspensions of spherical colloidal particles.

The Lennard–Jones 12-6 potential [1, 2]

$$u(r) = 4\epsilon \left[\left(\frac{\sigma}{r}\right)^{12} - \left(\frac{\sigma}{r}\right)^{6} \right] \quad \text{for} \quad r > 0 \tag{2.1}$$

provides a fair description of the interaction between pairs of rare-gas atoms like in argon, krypton and xenon, and also of quasi-spherical molecules such as CH_4. A sketch of the potential curve is provided in Fig. 2.1. Two parameters characterize the potential: the collision diameter σ where $u(r) = 0$, and the depth, ϵ, of the potential minimum at $r = 2^{1/6}\sigma$. The values of σ

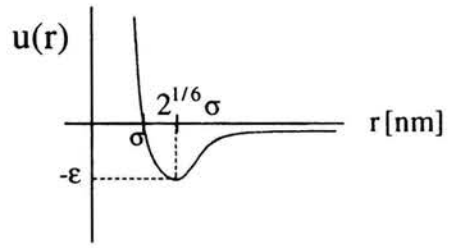

FIGURE 2.1. Lennard–Jones pair potential for atomic liquids.

and ϵ have been determined for a large number of atoms using, e.g., atomic scattering techniques. For argon, $\sigma_{Ar} = 0.34\,\text{nm}$ and $\epsilon_{Ar}/k_B = 119.8\,\text{K}$. The short-range repulsive part of the pair potential proportional to r^{-12} represents approximately the electronic repulsion of two atoms. The longer-range van der Waals attraction between two atoms at a distance r is described by the r^{-6} part.

The most simple pair potential one can think of is the potential between hard spheres of diameter σ, i.e.

$$u(r) = \begin{cases} \infty & \text{for } r < \sigma, \\ 0 & \text{for } r > \sigma. \end{cases} \tag{2.2}$$

While there exists no atomic fluid of hard atoms, colloidal suspensions of hard spheres are realized within good approximation, by coated polymethylmethacrylate (PMMA) spheres dispersed in a refractive index-matched non-polar solvent like cyclohexane. The coating consists of a thin layer, as compared to σ, of adsorbed polymer chains (cf. Fig. 2.2). The polymer brush gives rise to a short-range repulsion between the colloidal spheres which counterbalances the remnants of the van der Waals attraction. The sizes of the colloidal hard spheres are in the range of several hundred to a few thousand nanometers.

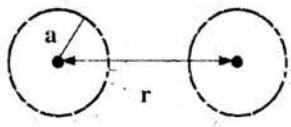

FIGURE 2.2. Model of colloidal hard spheres: PMMA spheres in non-polar solvent with surface-grafted polymer hairs.

PMMA particles in a non-organic solvent are a paradigm for sterically stabilized dispersions.

A well-studied example of charge-stabilized colloidal dispersions are polystyrene latex spheres dispersed in a polar solvent like water [3]. The latex particles acquire a high surface charge through the dissociation of ionizable surface groups. Each colloidal particle is surrounded by a diffuse layer of oppositely charged counterions, which are monovalent in the simplest case. Overlap of the electric layers of two colloidal macroions leads to an electrostatic repulsion which counteracts the van der Waals attraction and prevents

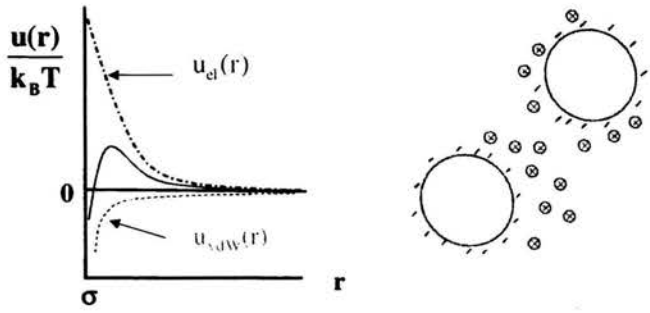

FIGURE 2.3. Left: electrostatic and van der Waals potential contributions to the total effective pair potential $u(r)$ (inner curve). Right: colloidal macroions and dissociated counterions.

the particles from irreversible aggregation (cf. Fig. 2.3). As will be shown in Sec. 5.2 the screened electrostatic repulsion between the charged colloidal spheres in a solvent of dielectric constant ϵ is approximately described by the effective pair potential

$$\beta u_{el}(r) = L_B Z^2 \left(\frac{e^{\kappa a}}{1+\kappa a} \right)^2 \frac{e^{-\kappa r}}{r}, \quad r > \sigma, \tag{2.3}$$

which is the repulsive electrostatic part of the celebrated Derjaguin–Landau–Verwey–Overbeek (DLVO) potential. Here, Z is an *effective* or dressed surface charge number of a colloidal particle of radius $a = \sigma/2$, $\beta = 1/(k_B T)$, and $L_B = e^2/(\epsilon k_B T)$ is the so-called Bjerrum length. This length is the characteristic distance, for a pair of elementary charges e, where their Coulomb interaction energy is comparable to the thermal energy $k_B T$. For water at room temperature, $L_B = 0.71$ nm. In case of dispersions of highly charged colloidal particles, the effective charge number in Eq. (2.3) can be substantially smaller than the *bare* macroion charge as defined in a more refined many-component Primitive Model picture of spherical macroions and microions (cf. Sec. 5.2)

The Debye–Hückel screening length, κ^{-1}, is defined through

$$\kappa^2 = 4\pi L_B \sum_\alpha \rho_\alpha Z_\alpha^2 \tag{2.4}$$

where the sum is taken over all types of microions (i.e. counter- and salt ions) of number densities ρ_α and charge numbers Z_α. For a concentrated suspension, the densities ρ_α refer actually to the fluid volume accessible to

the microions. The right-hand-side of Eq. (2.4) includes then an extra factor of $1/(1-\Phi)$, where Φ is the volume fraction of colloidal spheres.

Notice that the range of the potential can be controlled by adding or removing small ions. The total effective pair potential, $u(r)$, of charge-stabilized colloidal particles is the sum $u(r) = u_{el}(r) + u_{vdW}$ of $u_{el}(r)$, and of the attractive van der Waals pair potential, $u_{vdW}(r)$. The van der Waals part for two identical colloidal spheres can be described as

$$u_{vdW}(r) = -\frac{A_{eff}}{6}\left[\frac{2a^2}{r^2-4a^2} + \frac{2a^2}{r^2} + \ln\left(1-\frac{4a^2}{r^2}\right)\right], \qquad r > \sigma, \qquad (2.5)$$

with $u_{vdW}(r) \sim -r^{-6}$ for large r, and $u_{vdW}(r) \sim -(r-\sigma)^{-1}$ near contact distance $r = \sigma$ (cf. Fig. 2.3). The effective Hamaker constant, A_{eff}, incorporates to some extent electrodynamic retardation and non-additivity effects on the dispersion forces. For non-metallic colloidal spheres, A_{eff} is typically of the order of a few k_BT. For more details on dispersion forces, we refer to the textbooks of Russel, Saville and Schowalter [4], and of Mahanty and Ninham [5]. Recall that the van der Waals forces between two identical particles are always attractive. However, repulsive dispersion forces can occur for non-identical particles when the dielectric susceptibility of the dispersing medium is of a value in between the ones of the two particles.

For dispersions of highly charged colloidal particles, $u_{vdW}(r)$ becomes completely masked by the electrostatic part $u_{el}(r)$. In this case one frequently refers to the colloidal particles (with associated microion layer) as Yukawa spheres, since their microstructural properties are determined only by the Yukawa-like, exponentially screened Coulomb potential $u_{el}(r)$.

It is commonly assumed that the potential energy, $U(\mathbf{r}^N)$, of a N-particle liquid system can be approximated by a sum of pair interactions

$$U(\mathbf{r}^N) \approx \sum_{i<j}^{N} u(|\mathbf{r}_i - \mathbf{r}_j|) = \sum_{i<j}^{N} u(r_{ij}) \qquad (2.6)$$

for any configuration $\mathbf{r}^N = \{\mathbf{r}_1, \ldots, \mathbf{r}_N\}$ of position vectors $\{\mathbf{r}_i\}$ pointing to the particles centres. The quality of this pairwise additivity assumption depends on the choice of $u(r)$, and on how certain many-body aspects (non-additive dispersion forces, influence of solvent molecules, electrostatic screening et cetera) are approximately included in the pair potential. Typically, $u(r)$ is temperature and density dependent. Notice that $U(\mathbf{r}^N)$ is exactly pairwise additive only for systems of ideal hard spheres.

Under the premise of Eq. (2.6), the thermodynamic and microstructural properties of the fluid are solely expressible in terms of $u(r)$, and of its associated radial distribution function $g(r)$. The latter constitutes the most simple and most relevant reduced distribution function.

Chapter 3

Pair distribution functions

In this Chapter we discuss salient properties of $g(r)$, and of its associated Fourier transform pair $S(q)$, denoted as static structure factor. From a knowledge of $g(r)$, one can calculate macroscopic thermodynamic properties and analyze the local microstructure. Furthermore, knowledge of static pair correlations is an essential ingredient of most theoretical approaches to the transport and rheology of simple and complex fluids. The aim of the liquid state theory is therefore to calculate $g(r)$ from the particle interactions and to determine from it scattering properties and the thermodynamics.

3.1. Basic properties

The concept of reduced distribution functions has proven to be most useful in liquid state theory. Consider a system of N identical spherical particles in a volume V at temperature T (canonical NVT ensemble). The function

$$P_N(\mathbf{r}^N) = \frac{e^{-\beta U(\mathbf{r}^N)}}{Z_N(V,T)}, \tag{3.1}$$

with configurational integral

$$Z_N(V,T) = \int d\mathbf{r}_1 \cdots d\mathbf{r}_N \, e^{-\beta U(\mathbf{r}^N)} = \int d\mathbf{r}^N \, e^{-\beta U(\mathbf{r}^N)}, \tag{3.2}$$

is the probability density that the N particles are at the positions $\mathbf{r}_1, \ldots, \mathbf{r}_N$. It provides far more information than is necessary for the calculation of

scattering properties and thermodynamic functions. What is really needed for are the reduced distribution functions for a small subset of $n \ll N$ particles irrespective of the positions of the remaining $N - n$ particles.

Hence we introduce the n-particle distribution function [1, 6]

$$\rho_N^{(n)}(\mathbf{r}^n) = N(N-1)\cdots(N-n+1)\int d\mathbf{r}_{n+1}\cdots d\mathbf{r}_N\, P_N(\mathbf{r}^N) \tag{3.3}$$

of finding any set of n particles at a specified configuration $\mathbf{r}^n = \{\mathbf{r}_1, \ldots, \mathbf{r}_n\}$, regardless of how these n identical particles have been labelled. Of major importance are the reduced distribution functions of order $n = 1, 2$. For a homogeneous system

$$\rho_N^{(n)}(\mathbf{r}_1, \ldots, \mathbf{r}_n) = \rho_N^{(n)}(\mathbf{r}_1 + \mathbf{t}, \ldots, \mathbf{r}_n + \mathbf{t}) \tag{3.4}$$

for an arbitrary displacement vector $\mathbf{t}$. Then $\rho_N^{(1)} = \rho = N/V$ is equal to the average particle number density, ρ, and $\rho_N^{(2)}(\mathbf{r}_1, \mathbf{r}_2) = \rho_N^{(2)}(\mathbf{r}_1 - \mathbf{r}_2)$ depends only on the vector distance $\mathbf{r}_{12} = \mathbf{r}_1 - \mathbf{r}_2$ (to see this choose $\mathbf{t} = -\mathbf{r}_2$).

The correlation length $\xi(T)$ is a characteristic distance over which two particles are correlated. For fluids, ξ is typically of the range of $u(r)$ or larger to some extent, but under certain conditions (i.e., at a critical point) it can become extremely large. For a n-particle cluster of large mutual distances $r_{ij} = |\mathbf{r}_i - \mathbf{r}_j| \gg \xi$ and $N \gg 1$

$$\rho_N^{(n)}(\mathbf{r}_1, \ldots, \mathbf{r}_n) \approx \prod_{i=1}^{n} \rho_N^{(1)}(\mathbf{r}_i) = \rho^n \tag{3.5}$$

since these particles are then uncorrelated. To describe pair correlations in a fluid relative to a classical ideal gas of uncorrelated particles at the same density and temperature, we introduce the pair distribution function, $g_N(\mathbf{r}_1, \mathbf{r}_2)$, in the NVT-ensemble as

$$g_N(\mathbf{r}_1, \mathbf{r}_2) := \frac{\rho_N^{(2)}(\mathbf{r}_1, \mathbf{r}_2)}{\rho_N^{(1)}(\mathbf{r}_1)\,\rho_N^{(1)}(\mathbf{r}_2)}, \tag{3.6}$$

such that $g_N(\mathbf{r}_1, \mathbf{r}_2) \to 1$ for $r_{12} \to \infty$. If the system is isotropic as well as homogeneous (no spatially varying external force field, no crystals), $\rho_N^{(2)}$ and g_N are functions only of the separation $r = r_{12}$. Then, $g_N(r)$, with

$$g_N(r) = \frac{\rho_n^{(2)}(r)}{\rho^2} = \frac{N(N-1)}{\rho^2}\int d\mathbf{r}_3 \cdots d\mathbf{r}_N\, P_N(\mathbf{r}^N) \tag{3.7}$$

is usually called the radial distribution function. It plays a central role in one-component fluids, since it is indirectly measurable by radiation scattering experiments. Moreover, thermodynamic quantities can be written as integrals over $g_N(r)$ and $u(r)$, provided that the particles interact by pairwise additive forces (cf. Secs. 3.3-4).

As an important observation, we note that $\rho g_N(r)$ is the average density of particles a distance r apart from a given one. In fact, integration of $\rho g(r)$ over the system volume leads to

$$\rho \int d\mathbf{r}\, g_N(r) = \frac{N(N-1)}{\rho} \int d\mathbf{r}_{12} \int d\mathbf{r}_3 \cdots d\mathbf{r}_N\, P_N(\mathbf{r}^N) = N-1 \qquad (3.8)$$

since $\int d\mathbf{r}_{12} = V^{-1} \int d\mathbf{r}_1 d\mathbf{r}_2$. Likewise, Eq. (3.8) can be rewritten as

$$1 + \rho \int_V d\mathbf{r}\, [g_N(r) - 1] = 0\,. \qquad (3.9)$$

Notice in this context for the canonical $g_N(r)$ that $g_N(r \to \infty) = 1 - N^{-1}$ since there are $N-1$ particles left besides the one at $r = 0$. Equations (3.8) and (3.9) are only valid for a system of finite and fixed N, where particle number fluctuations are absent. In order to be independent of the specific statistical ensemble used in calculating static properties, it is understood that the thermodynamic limit of very large systems, i.e. $N, V \to \infty$ with $\rho = N/V$ kept fixed, is taken at the end of each calculation. Then

$$g(r) := \lim_{N,V\to\infty} g_N(r) \qquad (3.10)$$

defines the ensemble-independent radial distribution function, $g(r)$, of a macroscopic system.

Let us summarize general properties of $g(r)$ which follow readily from the definition of $g_N(r)$ in Eq. (3.7):

$$g(r) \geq 0\,, \quad g(r \to \infty) = 1, \qquad (3.11)$$

$$g(r) \approx 0\,, \quad \text{for } \beta u(r) \gg 1, \qquad (3.12)$$

$$g(r) = e^{-\beta u(r)} + \mathcal{O}(\rho), \qquad (3.13)$$

$$g(r) \quad \text{continuous for } u(r) \text{ continuous.} \qquad (3.14)$$

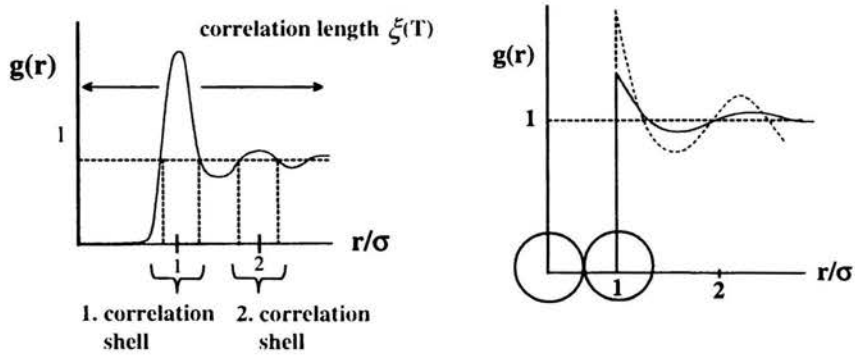

FIGURE 3.1. The $g(r)$ of a Lennard–Jones liquid (left), and of hard spheres (right).

The typical behavior of $g(r)$ for an atomic liquid with a soft pair potential of Lennard–Jones type, and for a hard-sphere fluid is sketched in Fig. 3.1. Regions of r with $g(r) > 1$ ($g(r) < 1$) have a larger (lower) probability of finding a second particle from a given one at $r = 0$, than for an ideal gas at the same T and ρ. The main features are a small-r region where $g(r) = 0$ owing to strong repulsive forces exerted by the particle at the origin, and several peaks representing increasingly diffuse shells, for increasing r, of next neighbors, second next neighbors and so on. This shell layering manifests the granularity (non-continuum nature) of the fluid. The oscillations in $g(r)$ decrease in amplitude with increasing r. Eventually, $g(r)$ approaches its asymptotic value one for $r > \xi(T, \rho)$. The oscillations in $g(r)$ become more pronounced with increasing ρ. Whereas the Lennard–Jones $g(r)$ is continuous at any r, the hard-sphere $g(r)$ jumps from zero to values ≥ 1 at $r = \sigma$, due to the singular nature of the hard-sphere $u(r)$. For hard spheres, $g(r) = \theta(r - \sigma) + \mathcal{O}(\rho)$ according to Eq. (3.13). Hard-sphere systems are athermal (i.e., T-independent) since the probability for a given particle configuration is either zero or one, independent of β, depending only on whether two or more spheres overlap or not.

3.2. Potential of mean force

There is a remarkable relation between $g(r)$ and the so-called potential of mean force, $w(r)$. For $N \gg 1$, $w(r)$ is defined in terms of $g(r)$ by

$$g(r) =: e^{-\beta w(r)} \tag{3.15}$$

or

$$\begin{aligned} w(r_{12}) &= -k_B T \ln g(r_{12}) \\ &= -k_B T \left[\ln \int d\mathbf{r}_3 \cdots d\mathbf{r}_N \, e^{-\beta U(\mathbf{r}^N)} + \ln \left(\frac{V^2}{Z_N} \right) \right] . \end{aligned} \tag{3.16}$$

To reveal the physical meaning of $w(r)$, we take the derivative of $-w$ with respect to the position vector $\mathbf{r}_1$:

$$-\nabla_1 w(\mathbf{r}_{12}) = \frac{\int d\mathbf{r}_3 \cdots d\mathbf{r}_N \left(-\frac{\partial U}{\partial \mathbf{r}_1} \right) e^{-\beta U}}{\int d\mathbf{r}_3 \cdots d\mathbf{r}_N \, e^{-\beta U}} = \left\langle -\nabla_1 U(\mathbf{r}^N) \right\rangle_{1,2} . \tag{3.17}$$

The quantity on the right can be interpreted as the force on particle 1 if we hold particle 2 fixed, and average over the positions of all the other particles (as denoted by $\langle \cdots \rangle_{1,2}$). $w(r)$ is the potential for that force and is therefore called the potential of mean force. Likewise, $w(r)$ can be interpreted as the reversible work for a process in which two particles are moved through the system, at constant N, V and T, from infinite separation to a relative separation r. To see this explicitly, recall from statistical mechanics that

$$F(r_{12}) = -k_B T \ln \int d\mathbf{r}_3 \cdots \mathbf{r}_N e^{-\beta U(\mathbf{r}^N)} + F_0(N-2, V, T) \tag{3.18}$$

is the Helmholtz free energy of a $N-2$-particle system in the presence of two fixed spheres at a distance r_{12}. The spheres 1 and 2 influence the system through their excluded volume and longer-ranged interactions. Moreover, F_0 is the (non-interesting) configuration-independent part of the free energy. Consequently

$$-\frac{\partial w(r_{12})}{\partial \mathbf{r}_{12}} = -\frac{\partial F(r_{12})}{\partial \mathbf{r}_{12}} \tag{3.19}$$

and

$$w(r_{12}) = F(r_{12}) - F(\infty) , \tag{3.20}$$

with $w(r)$ defined such that $w(r \to \infty) = 0$. The first and second laws of thermodynamics tell us for a reversible displacement that

$$dF = -SdT - pdV + \mu dN + \delta W_{rev} . \tag{3.21}$$

This means that $dF = \delta W_{rev} = -\nabla_{12} w(r_{12}) \cdot d\mathbf{r}_{12}$ is the reversible (maximal) work done by the $N-2$ particle system to achieve an infinitesimal displacement $d\mathbf{r}_{12}$ of the two boundary particles at fixed temperature, system volume and particle number.

The function $w(r)$ is generally a considerably more complicated object than the mere pair potential $u(r)$, since it involves the effects of particles 1 and 2 on the configurations of the other particles. Only in the limit $\rho \to 0$ follows that

$$w(r) \to u(r) \quad \text{i.e.} \quad g(r) \to e^{-\beta u(r)}, \tag{3.22}$$

as will be shown shortly. A sketch of $w(r)$ for hard spheres at finite density is shown in Fig. 3.2. As seen, two hard spheres effectively attract each other at distances $r \leq 1.5\sigma$. This many-body effect arises from an unbalance of forces on the two spheres when the gap between the two particles is depleted from the other ones. Depletion interactions of this kind may occur in any system with excluded volume interaction contributions. This explains why depletion effects have attracted considerable interest in the past few years.

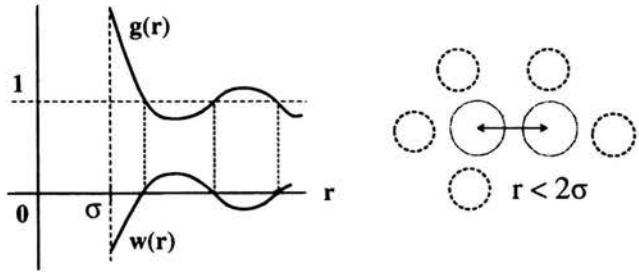

FIGURE 3.2. Potential of mean force of hard spheres (left) and depletion attraction (right).

Assuming pairwise additive interactions where

$$-\nabla_1 U(\mathbf{r}^N) = -\sum_{i>1} \nabla_1 u(r_{1i}), \tag{3.23}$$

the force law for w in Eq. (3.17) can be rewritten as

$$-\nabla_1 w(r_{12}) = -\nabla_1 u(r_{12}) - \rho \int d\mathbf{r}_3 \frac{g^{(3)}(\mathbf{r}_1, \mathbf{r}_2, \mathbf{r}_3)}{g(r_{12})} \nabla_1 u(r_{13}), \tag{3.24}$$

or likewise,

$$-\nabla_1 w(r_{12}) = -\nabla_1 u(r_{12}) - \rho \int d\mathbf{r}_3 \left[\frac{g^{(3)}(\mathbf{r}_1, \mathbf{r}_2, \mathbf{r}_3)}{g(r_{12})} - 1 \right] \nabla_1 u(r_{13}), \tag{3.25}$$

since the surface integral vanishes for a sufficiently short-ranged pair potential. Here,

$$g^{(3)}(\mathbf{r}_1, \mathbf{r}_2, \mathbf{r}_3) := \frac{\rho_N^{(3)}(\mathbf{r}_1, \mathbf{r}_2, \mathbf{r}_3)}{\rho^3} \tag{3.26}$$

is the triplet distribution function of an isotropic and homogeneous liquid. Actually $g^{(3)}$ depends only on the separations r_{12}, r_{13}, and on the angle between $\mathbf{r}_{13}$ and $\mathbf{r}_{12}$. The mean force on particle 1 in the presence of particle 2 at distance r_{12} is thus the sum of a direct interaction between 1 and 2, and the interaction of 1 with a third particle at $\mathbf{r}_3$, weighted by the factor $g^{(3)}(\mathbf{r}_1, \mathbf{r}_2, \mathbf{r}_3)/g(r_{12})$. The latter gives the probability of finding a particle at $\mathbf{r}_3$, given that there are certainly particles at $\mathbf{r}_1$ and $\mathbf{r}_2$. The above equation is the lowest order one of the Yvon-Born-Green hierarchy of equations for the reduced equilibrium probability density functions. Finally, Eqs. (3.13) and (3.22) are limiting cases, for $\rho \to 0$, of Eq. (3.24).

3.3. Static scattering experiments

In the following, we briefly explain how pair correlations can be measured indirectly by radiation scattering. A scattering experiment will have to probe distances of the order of the particle sizes and next neighbor distances, which are Ångstroms in case of atomic liquids, and fractions of microns in case of colloidal dispersions. Therefore, X-rays and neutrons are used for atomic liquids whereas colloids are probed by light scattering and small angle neutron scattering.

A schematic view of a scattering experiment is shown in Fig. 3.3. Monochromatic radiation of wavelength λ impinges on a fluid sample and is scattered at an angle ϑ into a detector which measures the average intensity, $I(q)$, of scattered neutrons or photons.

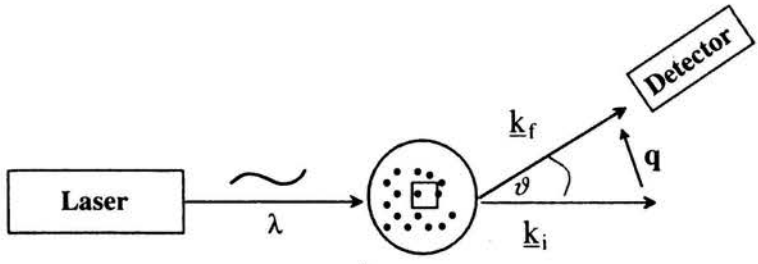

FIGURE 3.3. Typical scattering experiment setup.

For single and quasi-elastic scattering from spherical particles

$$I(q) \propto \langle N \rangle \, P(q) \, S_c(q) \tag{3.27}$$

where $q = (4\pi/\lambda)\sin(\vartheta/2)$ is the modulus of the scattering wave vector $\mathbf{q} = \mathbf{k}_f - \mathbf{k}_i$, and $\langle N \rangle$ is the average number of particles in the illuminated volume part of the sample. The so-called (normalized) form factor $P(q)$ contains information on the scattering material distribution inside a particle, i.e. information on the particle size (and form). The most relevant quantity in Eq. (3.27) including information on inter-particle correlations is called the (collective) static structure factor $S_c(q)$. Its statistical mechanical definition reads

$$S_c(q) = \left\langle \frac{1}{N} \sum_{l,p=1}^{N} e^{i\mathbf{q}\cdot[\mathbf{r}_l - \mathbf{r}_p]} \right\rangle = \left\langle \left| \frac{1}{\sqrt{N}} \sum_{l=1}^{N} e^{i\mathbf{q}\cdot\mathbf{r}_l} \right|^2 \right\rangle \geq 0 \tag{3.28}$$

where $\langle \cdots \rangle$ denotes an equilibrium ensemble average. By expanding the double sum into self, $l = p$, and distinct, $l \neq p$, parts, it can be shown that

$$S_c(q) = 1 + \rho \int d\mathbf{r}\, e^{i\mathbf{q}\cdot\mathbf{r}}\, h(r) = 1 + 4\pi\rho \int_0^\infty dr\; r^2 h(r)\, \frac{\sin(qr)}{qr}\,, \tag{3.29}$$

where, $h(r)$, with

$$h(r) = g(r) - 1 \tag{3.30}$$

is called the total correlation function. Notice that $h(r \to \infty) = 0$, and $S_c(q \to \infty) = 1$. As a result, the static structure factor determines the Fourier transform, $h(q)$, of $h(r)$. Since Fourier transforms are one-to-one mappings, $S_c(q)$ can be inverted to determine $h(r)$ and thus $g(r)$:

$$g(r) = \mathcal{F}^{-1}\left[\frac{S_c(q) - 1}{\rho}\right] = 1 + \frac{1}{2\pi^2 \rho\, r} \int_0^\infty dq\, q\, \sin(qr)[S_c(q) - 1]\,. \tag{3.31}$$

In principle, this would require to measure $S_c(q)$ at all wave numbers q where $S_c(q)$ exhibits significant oscillations. This is often not possible to do since the largest accessible q is limited by $q_{max} = 4\pi/\lambda$, which corresponds to backward scattering.

We have used here the following basic result on Fourier transforms: suppose $h(r)$ is an arbitrary isotropic function, with $h(r) \to 0$ sufficiently fast for $r \to \infty$. The three-dimensional Fourier transform, $h(q)$, of $h(r)$ is defined as

$$h(q) := \mathcal{F}\{h(r)\} = \int d\mathbf{r}\, e^{i\mathbf{q}\cdot\mathbf{r}}\, h(r) = 4\pi \int_0^\infty dr\; r^2 h(r)\, \frac{\sin(qr)}{qr} \tag{3.32}$$

where the third equality follows from performing two angular integrals in spherical coordinates. The Fourier inversion theorem states then that

$$h(r) = \mathcal{F}^{-1}\{h(q)\} = \frac{1}{(2\pi)^3}\int d\mathbf{q}\, e^{-i\mathbf{q}\cdot\mathbf{r}}\, h(q) = \frac{1}{2\pi^2}\int_0^\infty dq\; q^2\, h(q)\,\frac{\sin(qr)}{qr}\,. \tag{3.33}$$

For notational simplicity, Fourier transformed functions are distinguished from their real-space counterparts only by their argument q. As an important example we quote the following Fourier transform pair:

$$f(r) = \frac{e^{-\kappa r}}{r}\,, \tag{3.34}$$

with Fourier transform

$$f(q) = \frac{4\pi}{q^2+\kappa^2} \tag{3.35}$$

for $\kappa \geq 0$. This result will be used subsequently.

3.4. Thermodynamic properties

There exist several routes through which thermodynamic properties of liquids can be related to integrals involving $g(r)$ and $u(r)$. In the following, we review the three most important ones.

The energy equation

$$E = \langle T_{kin}\rangle + \langle U(\mathbf{r}^N)\rangle = \frac{3}{2}\,NK_BT + \frac{1}{2}\,\rho N\int_0^\infty dr\, 4\pi r^2 g(r)\,u(r) \tag{3.36}$$

expresses the internal energy, E, of a one-component N-particle system in terms of $u(r)$ and $g(r)$. The internal energy is the sum of a kinetic part, $(3/2)Nk_BT$, and an interaction part, $\langle U(\mathbf{r}^N)\rangle$. The latter can be understood on physical grounds as follows: for each particle out of N, there are $4\pi r^2\,\rho\, g(r)\, dr$ neighbors in a spherical shell of radius r and thickness dr, and the interaction energy between the central particles and these neighbors is $u(r)$. Integration from 0 to ∞ gives the interaction energy part of E, with the factor $1/2$ correcting for the double counting of particle pairs.

The pressure equation

$$p = p_{kin} + p_{int} = \rho k_B T - \frac{2\pi}{3}\rho^2 \int_0^\infty dr\, r^3 g(r)\, u'(r) \tag{3.37}$$

relates the thermodynamic pressure, p, to an integral over $g(r)$ and the derivative, $u'(r)$, of the pair potential. Here, $p_{kin} = \rho k_B T$ is the kinetic pressure of an ideal gas. The pressure contribution, p_{int}, due to particle interactions can be derived along the same lines as the energy equation. For a repulsive pair potential with $u'(r) < 0$, p_{int} is a positive pressure contribution originating from the stronger thermal bombardment of container walls by the mutually repelling particles. A colloidal dispersion consists of colloidal particles *and* of the solvent. For colloids, Eq. (3.37) gives the osmotic pressure exerted by the particles on a membrane permeable to the solvent.

The compressibility equation,

$$\frac{\chi_T}{\chi_T^{id}} = \lim_{q\to 0} S_c(q) = 1 + \rho \int d\mathbf{r}\, [g(r) - 1]\,, \tag{3.38}$$

links the (osmotic, in case of colloids) isothermal compressibility, χ_T, defined as

$$\chi_T := -\frac{1}{V}\left(\frac{\partial V}{\partial p}\right)_T = \frac{1}{\rho}\left(\frac{\partial \rho}{\partial p}\right)_T \tag{3.39}$$

to an integral involving only $g(r)$. Here, $\chi_T^{id} = (\rho k_B T)^{-1}$ is the compressibility of an ideal gas. The compressibility equation holds more generally than the energy and pressure equations, since it is valid even when the interparticle forces are not pairwise additive. According to Eqs. (3.29) and (3.38), χ_T can be determined experimentally from measuring $S_c(q)$ in the long-wavelength limit $q \to 0$ (i.e., for $q\xi \ll 1$).

The compressibility equation can be derived only in the grand canonical ensemble representing an open system, at constant V and T, which allows for fluctuations in the particle number. This is perfectly appropriate since $S_c(q)$ is related to the intensity of quasi-elastically scattered radiation. The radiation beam samples only a fraction of the system volume, and in this subvolume the number of particles, while macroscopically large, fluctuates.

To derive the compressibility equation, we need thus the definition of $g(r)$ in the grand canonical ensemble. For N finite and fixed, we know

from Eq. (3.7) that

$$\begin{aligned}\rho^2 g_N(r) &= N(N-1)\int d\mathbf{r}_3\cdots\mathbf{r}_N P_N(\mathbf{r}^N)\\ &= N(N-1)\int d\mathbf{r}_3\cdots\mathbf{r}_N P_N(\mathbf{r}^N)\frac{1}{V}\int d\mathbf{r}_1 d\mathbf{r}_2\,\delta(\mathbf{r}-\mathbf{r}_{12})\\ &= \frac{N(N-1)}{V}\langle\delta(\mathbf{r}-\mathbf{r}_{12})\rangle_N = \frac{1}{V}\left\langle\sum_{i\neq j}^{N}\delta(\mathbf{r}-\mathbf{r}_{ij})\right\rangle_N \end{aligned} \tag{3.40}$$

where $\langle\cdots\rangle_N$ denotes the canonical (i.e., fixed N) ensemble average. The canonical $g_N(r)$ has been formulated by the most right equality in terms of an ensemble average invoking Dirac δ functions. Next, to obtain the grand-canonical $g(r)$, we merely need to replace the canonical average by the grand canonical one, denoted as $\langle\cdots\rangle_{gc}$:

$$\langle(\cdots)\rangle_N = \int d\mathbf{r}_N P_N(\mathbf{r}^N)(\cdots) \;\rightarrow\; \langle(\cdots)\rangle_{gc} := \sum_N P(N)\langle(\cdots)\rangle_N\,. \tag{3.41}$$

We have introduced here the grand canonical probability, $P(N)$, of finding a system with exactly N particles. The grand-canonical pair distribution function is thus defined as

$$\rho^2 g(r) := \frac{1}{V}\left\langle\sum_{i\neq j}^{N}\delta(\mathbf{r}-\mathbf{r}_{ij})\right\rangle_{gc}\,. \tag{3.42}$$

For finite and fixed N, it follows from Eq. (3.8) that

$$\rho^2\int d\mathbf{r}\, g_N(r) = \frac{N(N-1)}{V}\,. \tag{3.43}$$

For an open system this leads to

$$\begin{aligned}\rho^2\int d\mathbf{r}\,[g(r)-1] &= \frac{\langle N(N-1)\rangle_{gc}}{V} - \frac{\langle N\rangle_{gc}^2}{V}\\ &= \rho\left[\frac{\langle N^2\rangle_{gc}-\langle N\rangle_{gc}^2}{\langle N\rangle_{gc}} - 1\right]\end{aligned} \tag{3.44}$$

with $\rho = \langle N\rangle_{gc}/V$. The variance of the number fluctuations in an open system is related to the isothermal compressibility through the thermodynamic relation

$$\rho k_B T\chi_T = \frac{\left\langle(N-\langle N\rangle_{gc})^2\right\rangle_{gc}}{\langle N\rangle_{gc}}\,. \tag{3.45}$$

This completes our derivation of the compressibility equation. There is no contradiction between the compressibility equation and the canonical ensemble result in Eq. (3.9). On first sight the latter might suggest that $\lim_{q\to 0} S_c(q) = 0$ is exactly valid. However, Eq. (3.9) applies only to a closed system with zero particle number fluctuations. Notice further, for N and V finite and fixed (at given density ρ), that physically allowed wave numbers are restricted to $q > V^{-1/3}$: it makes no sense to consider particle density fluctuations of wave lengths ($\sim q^{-1}$) larger than the system size. The thermodynamic limit of a macroscopic system should be performed first, then the limit $q \to 0$.

The particles of a liquid near the triple point of the gas-liquid-solid coexistence are densely packed such that χ_T is very small. Furthermore, the compressibility is nearly zero for a classical crystal near $T = 0$, since there are hardly any vibrations of the atoms around their equilibrium positions. In contrast, χ_T diverges at the critical point which is the terminal point of the gas-liquid coexistence line. The divergence is due to a long distance tail in $h(r)$ which causes the phenomenon of critical opalescence observed in light scattering studies near critical points. We will study critical opalescence in Sec. 4.2. As a summary, we note

$$\frac{\chi_T}{\chi_T^{id}} \approx \begin{cases} 0, & \text{fluid near triple point,} \\ 0, & \text{ideal crystal,} \\ \infty, & \text{fluid at critical point.} \end{cases} \tag{3.46}$$

Special care is needed for the case of state-dependent effective pair potentials $u(r) = u(r;\rho,T)$. Potentials of this type occur for liquid mixtures in the process of tracing out the particle degrees of freedom associated with all but a single component. The liquid mixture is hereby mapped onto an equivalent system of pseudo-particles governed by an effective state-dependent pair potential. An example of such a one-component reduction is given in Sec. 5.2, for the case of charged colloidal particles, with a resulting effective pair potential as quoted already in Eq. (2.3). In case of a state-dependent $u(r)$, the energy and pressure equations must be generalized, in particular, to

$$E = \frac{3}{2}Nk_BT + Nu_0(\rho) + \frac{1}{2}\rho N \int_0^\infty dr\, 4\pi r^2 g(r) \frac{\partial}{\partial\beta}(\beta u(r)) , \tag{3.47}$$

and

$$p = \rho k_B T + \rho^2 \frac{du_0(\rho)}{d\rho} - \frac{2\pi}{3}\rho^2 \int_0^\infty dr\, r^2\, g(r) \left(r\frac{\partial}{\partial r} - 3\,\rho \frac{\partial}{\partial \rho} \right) u(r)\,. \quad (3.48)$$

Here, $u_0(\rho)$ is a structure-independent free energy contribution, called volume energy, which depends on the average density of pseudo-particles. The volume energy is a consequence of the one-component reduction. It may significantly influence, e.g., the thermodynamic properties of charge-stabilized dispersions in the limit of low added salt concentrations. For an interesting derivation of the effective pair potential and volume energy of charged colloids based on the analogy between charge-stabilized colloidal dispersions and liquid metals the reader is advised to consult [7] and [8].

Chapter 4

Ornstein–Zernike integral equation methods

We proceed to discuss theoretical methods which allow to calculate the $g(r)$ and $S_c(q)$ of dense liquids from a given pair potential. All these methods are based on the so-called Ornstein–Zernike (OZ) equation, initially introduced by Ornstein and Zernike (1914) in their investigations of critical opalescence in near-critical liquids. The OZ equation introduces the direct correlation function, $c(r)$, as a very useful concept. Closed integral equations determining $g(r)$ can be derived from the OZ equation, when $c(r)$ is additionally involved in some physically appealing approximation to $g(r)$ and $u(r)$. These additional relations are known as closure relations. We will introduce various closure relations, and discuss their merits and shortcomings.

4.1. Ornstein–Zernike equation and direct correlations

The Ornstein–Zernike equation of a homogeneous and isotropic system is given by

$$h(r_{12}) = c(r_{12}) + \rho \int d\mathbf{r}_3 \, c(r_{13}) \, h(r_{23}) \, . \tag{4.1}$$

It introduces the direct correlation function, $c(r)$, as a new function and can be viewed as the definition of $c(r)$ in terms of the total correlation function, $h(r) = g(r) - 1$, of two particles a distance $r = r_{12}$ apart. Equation (4.1) can

be recursively solved for $h(r_{12})$ to give

$$h(r_{12}) = c(r_{12}) + \rho \int d\mathbf{r}_3\, c(r_{13})c(r_{23}) + \rho^2 \int d\mathbf{r}_3\, d\mathbf{r}_4\, c(r_{13})\, c(r_{24})\, c(r_{34}) + \mathcal{O}(c^4)\,. \quad (4.2)$$

This leads to the following physical interpretation of the OZ equation: the total correlations between particles 1 and 2, described by $h(r_{12})$, are due in part to the direct correlations, $c(r_{12})$, of these particles but also to an indirect correlation propagated by direct correlations via increasingly large numbers of intermediate particles.

Once information is available about $c(r)$ in form of a closure relation involving $u(r)$, the OZ equation can be viewed also as a closed integral equation for $h(r)$. Some information on $c(r)$ derives from Eq. (4.1) in the low-density limit $\rho \to 0$ where $c(r) \to h(r)$. With Eq. (3.13) follows then

$$c(r) \to f(r) \text{ for } \rho \to 0\,, \quad (4.3)$$

where

$$f(r) := e^{-\beta u(r)} - 1 \quad (4.4)$$

is called a Mayer-f function. It follows then that

$$c(r) = -\beta u(r) \quad (4.5)$$

for $r \to \infty$. Without proof we note that the long-distance asymptotic result (4.5) holds true for a wide class of pair potentials even at finite densities. The range of $c(r)$ is thus comparable with that of $u(r)$, and the fact that $h(r)$ is generally longer ranged than $u(r)$ can be ascribed to indirect correlation effects. One word of warning: we refer here and in what follows to one-component liquids of electrically neutral particles. Ionic fluids must be distinguished from neutral fluids in that the effect of screening (cf. Sec. 5.2) in such systems is to cause $h(r)$ to decay exponentially at large r, whereas $c(r)$ still has the range of the infinite Coulomb potential and therefore decays as r^{-1}. In principle, ionic liquids consist of at least two charged components of opposite sign to enforce overall charge neutrality.

To relate $c(r)$ to $S_c(q)$, we slightly rewrite the OZ equation as

$$h(r) = c(r) + \rho \int d\mathbf{r}'\, c(|\mathbf{r} - \mathbf{r}'|)\, h(r') \quad (4.6)$$

using $\mathbf{r} = \mathbf{r}_{12}$, $\mathbf{r}' = \mathbf{r}_{23}$ and $|\mathbf{r} - \mathbf{r}'| = \mathbf{r}_{13}$. Fourier transformation of both sides of the OZ equation leads to

$$h(q) = c(q) + \rho\, c(q)\, h(q) \tag{4.7}$$

or

$$\rho\, h(q) = \frac{\rho\, c(q)}{1 - \rho\, c(q)}\,, \tag{4.8}$$

where $c(q)$ is the three-dimensional Fourier transform of $c(r)$. Noting that $S_c(q) = 1 + \rho\, h(q)$, we obtain $S_c(q)$ in terms of $c(q)$:

$$S_c(q) = \frac{1}{1 - \rho\, c(q)} \geq 0\,, \tag{4.9}$$

from which we learn that $\rho\, c(q) \leq 1$.

In the derivation of Eq. (4.7), we have employed the convolution theorem of Fourier transformation theory. The convolution (german: "Faltung"), $f_1 * f_2$, of two integrable functions $f_1(\mathbf{r})$ and $f_2(\mathbf{r})$ is defined as

$$(f_1 * f_2)(\mathbf{r}) := \int d\mathbf{r}'\, f_1(\mathbf{r}') f_2(\mathbf{r} - \mathbf{r}') = \int d\mathbf{r}'\, f_2(\mathbf{r}') f_1(\mathbf{r} - \mathbf{r}')\,. \tag{4.10}$$

The convolution theorem states that

$$\int d\mathbf{r}\, e^{i\mathbf{q}\cdot\mathbf{r}}\, (f_1 * f_2)(\mathbf{r}) = f_1(\mathbf{q}) f_2(\mathbf{q}) \tag{4.11}$$

i.e. the Fourier transform of the convolution of two functions is equal to the product of their Fourier transforms.

Using Eq. (4.9), we finally obtain the compressibility equation in terms of $c(q)$:

$$\frac{1}{\rho\, k_B T \chi_T} = 1 - \rho\, c(q \to 0) = 1 - 4\pi\rho \int_0^\infty dr\, r^2\, c(r)\,. \tag{4.12}$$

4.2. Theory of critical opalescence

In the following, we explore the behavior of $g(r)$ near a critical point. Consider a one-component system with an attractive part in the pair potential, like a Lennard–Jones-type system (say, argon) or a suspension of sticky colloidal spheres. For a purely repulsive $u(r)$ like the hard-sphere potential,

there is only one fluid phase and thus there is no liquid-gas critical point in the one-component case. However, a critical point of a liquid-gas-type demixing transition may occur in two-component, size-asymmetric dispersions of colloidal hard spheres due to the depletion attraction effect discussed earlier (cf. Fig. 3.2).

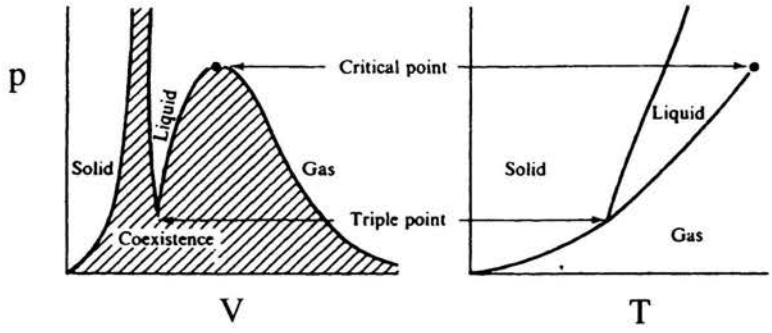

FIGURE 4.1. Schematic $p - V$ and $p - T$ phase diagrams of a Lennard–Jones system (argon).

Schematic $p - V$ and $p - T$ phase diagrams of a Lennard-Jones system are displayed in Fig. 4.1. The gas-liquid coexistence line in the $p-T$ diagram terminates in a critical point at the critical temperature T_c and pressure p_c. It is the location of a continuous (i.e., 2nd order) phase transition. On approaching the critical point along the coexistence line, the (density-) difference between liquid and gas phases ceases to exist. At the critical point, strong and long-living density fluctuations occur (cf. Eq. (3.45)) such that χ_T becomes arbitrarily large in the thermodynamic limit (cf. Fig. 4.1):

$$\left(\frac{\partial p}{\partial V}\right)_T = 0 \quad \text{i.e.} \quad \chi_T = \infty\,. \tag{4.13}$$

According to Eqs. (3.38) and (4.9),

$$\lim_{q\to 0} S_c(q) = 1 + \rho \int d\mathbf{r}\, h(r) = \frac{1}{1 - \rho c(q \to 0)} \to \infty \quad \text{for} \quad T \to T_c\,, \tag{4.14}$$

which means that $S_c(q)$ becomes very large for small q as the critical point is approached. Then, regions of larger and smaller densities develop. As the size of these regions approaches the wavelength of visible light, there is in fact so much scattering that the fluid appears cloudy or opalescent. This phenomenon is therefore called critical opalescence. It is due to the occurrence

of long-range spatial correlations between particles in the vicinity of a critical point such that the volume integral over $h(r)$ diverges in the limit of an infinite volume. As $T \to T_c$,

$$c(q \to 0) = 4\pi \int_0^\infty dr\, r^2\, c(r) \to \frac{1}{\rho} \tag{4.15}$$

which means that, contrary to $h(r)$ and $g(r)$, $c(r)$ remains short-ranged with finite second moment.

Since $c(q)$ is well behaved at T_c, we assume that it can be expanded in a truncated Taylor series around $q = 0$ up to $\mathcal{O}(q^2)$. Using $\sin(x)/x \approx 1 - x^2/6 + \mathcal{O}(x^4)$, $c(q)$ is thus approximated, for small q, by

$$\rho c(q) = 4\pi\rho \int_0^\infty dr\, r^2\, \frac{\sin(qr)}{qr}\, c(r) = c_0 - c_2 q^2 + \mathcal{O}(q^4) \tag{4.16}$$

with expansion coefficients

$$c_0 = 4\pi\rho \int_0^\infty dr\, r^2\, c(r) \to 1 \quad \text{for} \quad T \to T_c\,, \tag{4.17}$$

$$c_2 = \frac{2\pi}{3}\rho \int_0^\infty dr\, r^4\, c(r)\,. \tag{4.18}$$

We restrict here our attention to small q and thereby to large distances r. Note that $c_0 = \rho\, c(q = 0) \leq 1$. Substitution of this truncated expansion into Eq. (4.9) then gives

$$S_c(q) \approx \frac{1}{1 - c_0 + c_2\, q^2} = \frac{1}{c_2}\, \frac{1}{\xi^{-2} + q^2} \tag{4.19}$$

as an approximation of $S_c(q)$ for small q, more precisely for $qR_U \ll 1$. This is the small-q approximation for the near-critical structure factor originally proposed by Ornstein and Zernike around 1917. The range of the interaction potential is denoted as R_U, and we have further introduced the correlation length

$$\xi(T) := \left(\frac{c_2}{1 - c_0}\right)^{1/2} = [c_2\, S(0)]^{1/2} = \left(c_2\, \frac{\chi_T}{\chi_T^{id}}\right)^{1/2}, \tag{4.20}$$

by assuming the fourth moment, c_2, of $c(r)$ to exist and to be positive. With the compressibility diverging for $T \to T_c$ in a power-law fashion

as $\chi_T \propto (T - T_c)^{-\gamma}$, it follows that the correlation length diverges like $\xi \propto (T - T_c)^{-\gamma/2}$. The numerical value of the critical exponent γ is predicted as $\gamma = 1$ in a simple Landau-type mean-field approximation. However, the accepted value of γ for the liquid-gas transition is 1.24, as derived from renormalization group calculations of critical phenomena and verified by high-precision experiments on critical fluids [9, 10].

Fourier inversion of the OZ approximation for $S_c(q)$, using Eqs. (3.34)-(3.35), gives the asymptotic form of $h(r)$ for large pair separation $r \gg R_U$

$$h(r) = \frac{1}{(2\pi)^3 \rho} \int d\mathbf{q}\, e^{-i\mathbf{q}\cdot\mathbf{r}} \, [S_c(q) - 1] \approx \frac{1}{4\pi\rho\, c_2} \frac{e^{-r/\xi}}{r} . \tag{4.21}$$

At the critical temperature, ξ becomes infinite with

$$h(r)|_{T=T_c} \sim \frac{1}{r} \quad \text{for } r \gg R_U \tag{4.22}$$

which corresponds to

$$S_c(q)|_{T=T_c} \sim \frac{1}{q^2} \quad \text{for } q \ll {R_U}^{-1} . \tag{4.23}$$

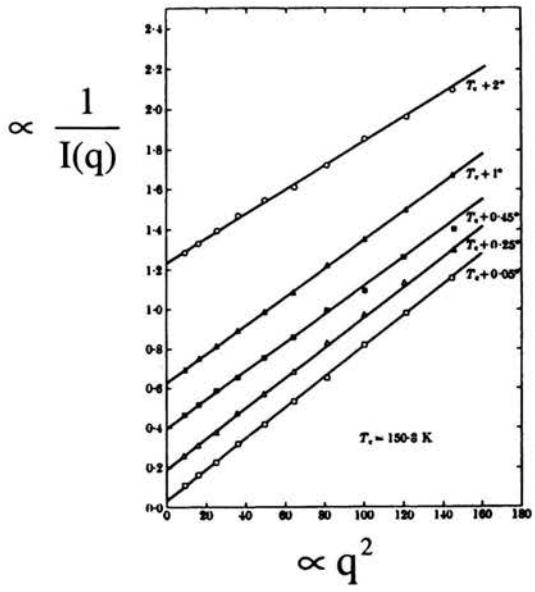

FIGURE 4.2. Experimental Ornstein–Zernike plot of argon. After [11].

The total correlation function decays thus algebraically, and not exponentially, at the critical point.

If the OZ approximation (Eqs. (4.19)-(4.23)) is valid, then

$$\frac{1}{I(q)} \propto \frac{1}{S_c(q)} = c_2 \left[\xi^{-2} + q^2\right] \tag{4.24}$$

i.e. a plot of the reduced inverse scattered intensity against q^2 should yield a straight line of practically constant slope, c_2, and an intercept c_2/ξ^2 that approaches zero for $T \to T_c$. Figure 4.2 shows such an experimental Ornstein–Zernike plot for argon. It suggests that the mean-field-type OZ approximation is valid to good approximation at least as long as q and $|T - T_c|$ are not very close to zero.

Experiments performed very close to T_c reveal in fact deviations at small q from the OZ approximation prediction for $S_c(q)$. Improved modern renormalization group theory calculations of critical phenomena lead to a corrected asymptotic scaling behavior of $h(r)$ at T_c, given in three dimensions by [9, 10]

$$h(r)|_{T=T_c} \sim \frac{1}{r^{1+\eta}} \tag{4.25}$$

or, equivalently,

$$S_c(q)|_{T=T_c} \sim \frac{1}{q^{2-\eta}}\,, \tag{4.26}$$

with a small but nonzero critical exponent η. The accepted theoretical value for η is 0.04. The reason for the failure of the OZ approximation very close to T_c is that, by assuming a truncated small-q expansion of $c(q)$ to hold, one does not account for the full spectrum of correlation fluctuations existing at *all* length scales. We finally remark that the liquid-gas transition at T_c belongs to the same universality class of second-order phase transitions as the ferromagnetic-paramagnetic transition in uniaxial ferromagnets (cf. the three-dimensional Ising model). All members of the same universality class show the same critical exponents.

4.3. Various closure relations

After having explored the long-distance behavior of $g(r)$ in a near-critical liquid, we discuss now various closure relations which express $c(r)$ approximately in terms of $h(r)$ and a given pair potential $u(r)$. These relations, and

a deeper understanding of the meaning of $c(r)$, can be obtained by diagrammatic and density functional derivative methods. We take here a pragmatic point of view and establish the closure relations most simply using plausibility arguments. In combination with the OZ equation, the closures lead to closed integral equations for $g(r)$. These integral equations have been found, in comparison with computer simulation results and scattering data, to be most useful in calculating the full r-dependence of $g(r)$ and thermodynamic properties of dense liquids.

For a system with a hard-core excluded volume part in $u(r)$, any closure relation should be consistent with the exact condition

$$h(r < \sigma) = -1\,, \quad \text{i.e.} \quad g(r < \sigma) = 0\,, \tag{4.27}$$

which states that two spheres of hard-sphere diameter σ can not interpenetrate, and the asymptotic result

$$c(r) = -\beta u(r)\,, \text{ for } r \to \infty \tag{4.28}$$

valid for a wide class of pair potentials.

Mean-spherical approximation (MSA)

The exact asymptotic form of $c(r)$ forms the basis of the so-called mean-spherical approximation, first introduced into liquid state theory by Lebowitz and Percus (1966). In MSA, $c(r)$ is assumed to be given approximately by the closure relation

$$c(r) \approx -\beta u(r) \tag{4.29}$$

for all non-overlap distances $r > \sigma$. Together with Eqs. (4.27) and (4.29), the OZ equation (4.6) becomes a *linear* integral equation determining $g(r)$ for $r > \sigma$, and $c(r)$ for $r < \sigma$. The most attractive feature of the MSA closure, as compared to other ones, is that analytic solutions exist, even in the many-component case, for various pair potential models, namely for the hard and sticky hard-sphere potentials, the square well potential, the Coulomb potential, attractive and repulsive Yukawa-type potentials, and for the dipolar hard-sphere potential. These potentials are of particular interest for molten salts, electrolyte solutions and in colloid science. No analytic MSA solution exists for the Lennard–Jones potential.

While the MSA is well suited for short-range attractive and repulsive potentials, it can predict non-physical negative values for $g(r)$ close to contact

distance in case of dilute systems of strongly repelling particles. At very low density (more precisely, small volume fractions Φ), the MSA predicts that

$$g(r) = 1 + c(r) + \mathcal{O}(\Phi) \approx 1 - \beta u(r) + \mathcal{O}(\Phi), \quad r > \sigma, \tag{4.30}$$

with a negative $g(r)$ for $\beta u(r) > 1$. This wrong prediction should be contrasted with the exact zero-density form of $g(r)$ given in Eq. (3.13). The volume fraction $\Phi = (\pi/6)\rho\sigma^3$ is defined as the fraction of the system volume filled by the spherical particles.

Rescaled MSA

For fluids of (colloidal) particles, where the physical hard core is masked by strong and long-range repulsive forces, there exists an improved variant of the MSA which preserves the positive semi-definiteness of $g(r)$. This variant is called the rescaled MSA (Hansen and Hayter, 1982). It is based on the fact that the $g(r)$ of such systems is continuous at all distances r. Moreover and most importantly, two particles in these systems are virtually never closer to each other than a certain distance $\sigma' > \sigma$, so that $g(r) \approx 0$ for $r < \sigma'$.

In RMSA, the actual system is replaced by a fictitious system consisting of particles of enlarged diameter $\sigma' > \sigma$, at the same number density ρ and, for $r > \sigma'$, with the same pair potential $u(r)$ than the original one. The

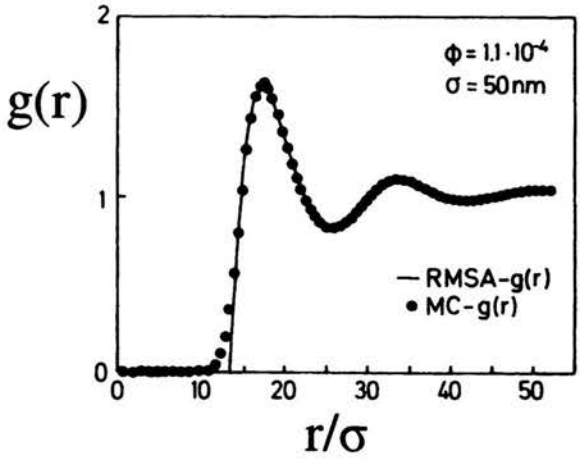

FIGURE 4.3. Radial distribution function of a charge-stabilized Yukawa-type dispersion. Comparison between RMSA-$g(r)$ and Monte Carlo computer simulation results. After [3].

(density-dependent) effective diameter, σ', is determined from the continuity of $g(r)$ at $r = \sigma'$, by demanding that

$$g(r = \sigma'; \rho, \Phi') = 0\,, \tag{4.31}$$

with $g(r)$ calculated in MSA for a larger rescaled volume fraction $\Phi' = \Phi(\sigma'/\sigma)^3 > \Phi$. The RMSA-$g(r)$ is positive semi-definite since the volume fraction, Φ', of the fictitious system is so much larger than Φ that Eq. (4.30) does not apply any more.

Figure 4.3 includes the RMSA-$g(r)$ for a dilute aqueous suspension of highly charged polystyrene spheres interacting by the Yukawa-type DLVO potential of Eq. (2.3). The charge number, $Z_{RMSA} = 257$, employed in the RMSA calculation has been selected such that the height of the principal peak of the RMSA $g(r)$ is coincident with that of the "exact" $g(r)$, generated by Monte Carlo (MC) computer simulations using a smaller charge number $Z_{MC} = 205$. Since $Z_{RMSA} > Z_{MC}$, the RMSA underestimates the structural ordering in systems of strongly correlated particles. However, once Z has been adjusted to fit the actual peak height, the overall shape of $g(r)$ is remarkably well predicted by the semi-analytical RMSA solution. The RMSA has been extended to multi-component systems of mutually repelling Yukawa particles (cf. Ref. [3]). The predictions of the RMSA for the effective charge number Z can be further improved by correcting for the penetrating background of (uniform) microion charge density which maintains electroneutrality [12].

Percus–Yevick (PY) closure relation

Aside from the linear MSA, there exist a variety of non-linear integral equation schemes. The Percus–Yevick approximation (Percus and Yevick, 1958) is among the most popular ones. To introduce the PY closure relation, we reformulate the OZ equation as

$$c(r) = g(r) - \left[1 + \rho \int d\mathbf{r}'\, c(r') \left\{g(|\mathbf{r} - \mathbf{r}'|) - 1\right\}\right] =: g(r) - g_{ind}(r)\,. \tag{4.32}$$

The term in brackets, $g_{ind}(r)$, describes the indirect part of the pair correlations. Since $g(r) = \exp[-\beta w(r)]$, one can approximate $g_{ind}(r)$ by

$$g_{ind}(r) \approx e^{-\beta[w(r)-u(r)]}\,, \tag{4.33}$$

or, equivalently, $c(r)$ by

$$c(r) \approx g(r)\left[1 - e^{\beta u(r)}\right] = g(r) - y(r) = f(r)y(r)\,. \tag{4.34}$$

This is the PY closure relation for $c(r)$. It is an exact relation up to first order in the density, as one can show from a density expansion of $h(r)$ and $c(r)$ based on the iterated OZ Eq. (4.2). We have introduced here the so-called cavity function, $y(r)$, defined as

$$y(r) := e^{\beta u(r)}\, g(r)\,. \tag{4.35}$$

Contrary to $g(r)$, which for hard spheres has a jump discontinuity at $r = \sigma$ wholly contained in the factor $\exp[-\beta u(r)]$, $y(r)$ has the useful property of being continuous at all r. It agrees with $g(r)$ for all r where $u(r) = 0$. In PY approximation, $c(r)$ is thus assumed to be zero whenever the pair potential vanishes. The continuity of $y(r)$ is easy to see, using Eq. (3.7), and noting that

$$y(r_{12}) = \frac{V^2}{Z_N} \int d\mathbf{r}_3 \cdots d\mathbf{r}_N \exp\left[-\beta {\sum_{i<j}}' u(r_{ij})\right] \tag{4.36}$$

for pairwise additive forces, with the pair $\{i,j\} = \{1,2\}$ omitted from the sum. Hence $y(r)$ is a smooth and non-zero continuation of $g(r)$ into the overlap region ("cavity") $r < \sigma$.

Substitution of Eq. (4.34) into the OZ equation gives the non-linear PY integral equation

$$y(r) = 1 + \rho \int d\mathbf{r}' \left[e^{-\beta u(|\mathbf{r}-\mathbf{r}'|)}\, y(|\mathbf{r}-\mathbf{r}'|) - 1\right] \left[e^{-\beta u(r')} - 1\right] y(r') \tag{4.37}$$

for $y(r)$ or, likewise, $g(r)$. This equation can be solved analytically in three dimensions for the important case of hard spheres (cf. Sec. 4.4), and by numerical methods for arbitrary pair potentials.

Hypernetted-chain (HNC) approximation

Another frequently used approximate integral equation scheme is the hypernetted-chain approximation (van Leeuwen et al., 1959). The name stems from its diagrammatic derivation. The HNC closure relation in terms of $c(r)$ is

$$c(r) \approx -\beta u(r) + h(r) - \ln\left[1 + h(r)\right] = h(r) - \ln y(r)\,. \tag{4.38}$$

Exponentiation gives

$$g(r) \approx e^{-\beta u(r) + h(r) - c(r)}\,, \tag{4.39}$$

showing that in HNC approximation the positive definiteness of the exact $g(r)$ is preserved at any density. Since from Eq. (4.38)

$$c(r) \approx -\beta u(r)\,, \quad r \to \infty \tag{4.40}$$

the HNC approximation leads further to the correct asymptotic behavior of $c(r)$ for arbitrary ρ. On the other hand the PY-$c(r)$ gives the correct long-distance behavior in general only for small densities.

The HNC closure combined with the OZ equation leads to

$$\ln\left[e^{\beta u(r)}\, g(r)\right] \approx h(r) - c(r) = \rho \int d\mathbf{r}'\, c(|\mathbf{r} - \mathbf{r}'|)\, h(r')\,. \tag{4.41}$$

Introducing the cavity function, Eq. (4.41) can be re-expressed as

$$\ln\left[y(r)\right] = \rho \int d\mathbf{r}'\, h(r')\, \left[-\beta u(|\mathbf{r} - \mathbf{r}'|) + h(|\mathbf{r} - \mathbf{r}'|) - \ln g(|\mathbf{r} - \mathbf{r}'|)\right]\,. \tag{4.42}$$

This is the non-linear HNC integral equation for $g(r)$. It can be solved only numerically even for hard spheres. Like in the PY approximation, the HNC approximation predicts $g(r)$ correctly to first order in the density.

The PY is quite successful for hard spheres but, contrary to the MSA, does not work so well for systems with attractive tails. The HNC is complementary to the PY in the sense that it is unsatisfactory for hard spheres but appears to account satisfactorily for the effects of soft cores and, in particular, for long-range repulsive potential tails as given in ionic fluids and dispersions of Yukawa particles. All three integral equation schemes have severe deficiencies near a critical point.

HNC results for a Yukawa system (cf. Eq. (2.3)) of moderately charged colloidal particles (Z = 107) of diameter $\sigma = 160\,\mathrm{nm}$ and fixed screening parameter $\kappa\sigma$ in an organic solvent ($\epsilon = 10$) are shown in Fig. 4.4. The charge Z was determined from a fit of the HNC peak height of $S_c(q)$ to the experimentally given one. There is then rather good agreement between the theoretical and experimental $S_c(q)$. The deviations at small q and around the minimum can be attributed to polydispersity effects, that is to a spread in the experimental particle sizes. With increasing volume fraction Φ, there is increasing ordering visible through more pronounced undulations in $g(r)$, and the system becomes less compressible (decreasing $S(0)$). The particles avoid each other as much as possible because of the strong and longer-ranged electrostatic repulsion so that $g(r < 1.5\sigma) = 0$. In monodisperse systems with

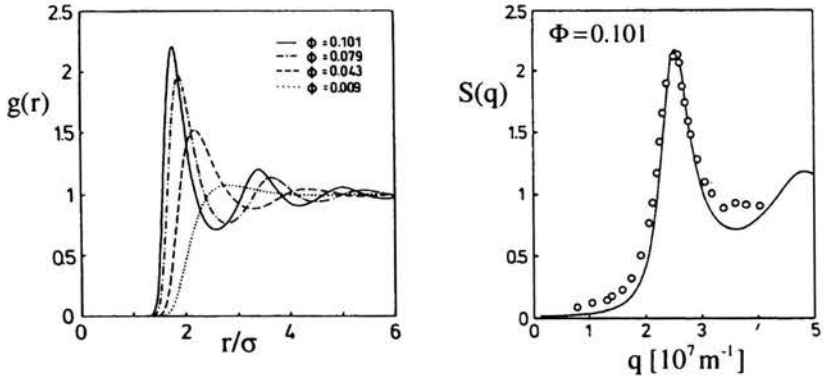

FIGURE 4.4. HNC radial distribution function $g(r)$ at various volume fractions (left), and static structure factor $S(q) = S_c(q)$ (right) of charge-stabilized dispersions of silica spheres. Open circles: light scattering results of $S_c(q)$. After [13].

long-range repulsion, the position, q_m, of the principal peak of $S_c(q)$ increases with volume fraction approximately as $q_m \sim \Phi^{1/3}$. Away from a critical point, the location, r_m, of the main peak of $g(r)$ is approximately related to q_m by

$$r_m \sim \frac{2\pi}{q_m} . \tag{4.43}$$

Random phase approximation (RPA)

Suppose we can separate the pair potential of a liquid system into a short-range reference part, $u_0(r)$, and a long-range perturbational part, $u_l(r)$ (cf. Fig. 4.5), with

$$u(r) = u_0(r) + u_l(r) . \tag{4.44}$$

Let us further assume that the direct correlation function, $c_0(r)$, of the reference system (where $u = u_0$) is known exactly or to a good approximation. For a reference system of hard spheres, e.g., we could use the analytic PY solution for $c_0(r)$ derived in Sec. 4.4. The true direct correlation function, $c(r)$, of the system can then be approximated by

$$c(r) \approx c_0(r) - \beta u_l(r) \ , \ r > 0 \tag{4.45}$$

which is asymptotically correct at long pair separations. For historical reasons, this closure relation is referred to as the random phase approximation.

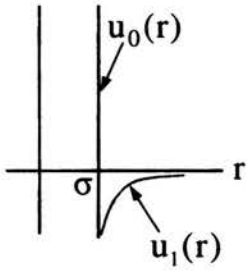

FIGURE 4.5. Pair potential consisting of hard-sphere reference part, $u_0(r)$, and a longer-ranged, attractive perturbational part $u_l(r)$.

In this approximation one obtains

$$S_c(q) = \frac{1}{1-\rho c(q)} \approx \frac{1}{1-\rho c_0(q)+\beta\rho\, u_l(q)}\,. \tag{4.46}$$

The static structure factor is thus expressed in terms of the structure factor, $S_c^0(q)$, of the reference system and the Fourier transform,

$$u_l(q) = \int_0^\infty d\mathbf{r}\, e^{i\mathbf{q}\cdot\mathbf{r}}\, u_l(r)\,, \tag{4.47}$$

of the perturbational part of $u(r)$. Eq. (4.46) can be rewritten in the mnemonic form

$$\frac{1}{S_c(q)} \approx \frac{1}{S_c^0(q)} + \beta\rho u_l(q)\,. \tag{4.48}$$

The RPA is the most simple perturbation theory for fluid microstructures, usually suited only for small wave numbers. Its multi-component extension has been successfully used for the calculation of monomer-monomer structure factors of polymer blends [14]. For an ideal gas as reference system, one has $c_0(r) = 0$ and $S_c^0(q) = 1$. The RPA reduces then to the MSA for point-like particles, referred to in the literature as a version of the Debye–Hückel approximation. One should notice that the perturbation must be sufficiently weak, or the density sufficiently low, to ensure that $\beta\rho u_l(q) S_c^0(q) > -1$ with $S_c(q) > 0$. Furthermore, the RPA does not ensure that $g(r<\sigma) = 0$ in case of a hard-sphere reference system. This non-physical feature of the RPA is related to an ambiguity in the choice of the perturbation potential $u_l(r)$ for $r < \sigma$ in Eq. (4.47). The true $g(r)$ should not depend on this choice.

In the optimized random phase approximation (ORPA), $u_l(r)$ is extended into the hard-core regime $r < \sigma$ such that $g(r<\sigma) = 0$. While the ORPA is

a considerable improvement of the RPA, there is a price to pay in form of a much larger numerical effort to calculate $S_c(q)$.

4.4. Percus–Yevick solution for hard spheres

Hard spheres serve as a reference system in the theory of uncharged liquids, as an ideal gas does in the theory of dilute gases, and a harmonic solid in solid-state physics. The PY approximation leads to an integral equation for the hard-sphere cavity function $y(r)$ which can be solved analytically.

The solution proceeds as follows. For hard spheres,

$$c(r) = g(r)\left[1 - e^{\beta u(r)}\right] = 0, \quad r > \sigma \tag{4.49}$$

in PY approximation, i.e. the hard-sphere direct correlation is approximately set equal to zero for non-overlap distances. As a matter of fact, the true $c(r)$ has a small but non-vanishing tail for $r > \sigma$. As can be noticed here, the PY closure becomes identical to the MSA closure (cf. Eq. (4.29)) in case of a hard-sphere fluid.

The hard-sphere cavity function reads

$$y(r) = e^{\beta u(r)} g(r) = \begin{cases} g(r), & r > \sigma, \quad \text{exact}, \\ -c(r), & r < \sigma, \quad \text{PY aproximation}, \end{cases} \tag{4.50}$$

where the lower equality follows from the PY closure in Eq. (4.34). It follows that $c(r)$ and $g(r)$ have a jump discontinuity at $r = \sigma$, with $g(r = \sigma^+) = -c(r = \sigma^-)$, since $y(r)$ is continuous everywhere.

Upon inserting the hard-sphere potential into Eq. (4.37), one obtains a quadratic integral equation for $y(r)$ of the form

$$y(r) = 1 + \rho \int\limits_{r'<\sigma} d\mathbf{r}'\, y(r') - \rho \int\limits_{r'<\sigma,\, |\mathbf{r}-\mathbf{r}'|>\sigma} d\mathbf{r}'\, y(r')\, y(|\mathbf{r} - \mathbf{r}'|)\,. \tag{4.51}$$

It is required to solve this integral equation within $r < \sigma$ for $c(r) = -y(r)$, since $c(r > \sigma) = 0$ is known already. Following Wertheim [15], we use a third-order polynomial

$$c(r) = a_0 + a_1 r + a_2 r^2 + a_3 r^3 \tag{4.52}$$

as a trial solution of $c(r < \sigma)$, with yet unknown density-dependent expansion coefficients $\{a_i\}$. This ansatz is suggested from the low density form of $c(r)$,

which is a third order polynomial in case of hard spheres. For a proof of this statement use Eq. (4.2) to show that to first order in density (volume fraction Φ), $y(r)$ is given by

$$y(r) = 1 + \rho \int d\mathbf{r}' f(r') f(|\mathbf{r} - \mathbf{r}'|) + \mathcal{O}(\rho^2) . \tag{4.53}$$

For hard spheres, the Mayer-f function is $f(r) = -1$ for $r < \sigma$ and zero otherwise. The convolution integral in Eq. (4.53) is then equal to the volume of overlap of two spheres of equal radii σ with centres separated by r. As a consequence

$$y(r) = 1 + 8\Phi \left[1 - \frac{3}{4} x + \frac{1}{16} x^3\right] \theta(2 - x) + \mathcal{O}(\Phi^2) , \tag{4.54}$$

with $x = r/\sigma$. The overlap volume is zero for $x > 2$ as expressed by the unit step function $\theta(2 - x)$. Recall that the PY approximation is correct for $g(r)$ to first order in ρ. In using the polynomial ansatz in Eq. (4.52), it is assumed that the functional form of $c(r)$ is the same for all volume fractions.

The four expansion coefficients, $\{a_i\}$, are determined by employing the continuity of $y(r)$ and its first two derivatives at $r = \sigma$. Their continuity follows from Eq. (4.51) and its first two derivatives. A fourth condition follows from the PY integral equation (4.51) evaluated at $r = 0$:

$$y(0) = 1 + \rho \int_{r' < \sigma} d\mathbf{r}' \, y(r') . \tag{4.55}$$

After inserting Eq. (4.52) in Eq. (4.51) and making use of the four boundary conditions to determine the $\{a_i\}$, a lengthy calculation gives the following PY result for the hard-sphere $c(r)$:

$$c(r < \sigma) = -\left[\lambda_1 \left(1 + \frac{1}{2} \Phi x^3\right) + \lambda_2 x\right] \tag{4.56}$$

with

$$\lambda_1 = \frac{(1 + 2\Phi)^2}{(1 - \Phi)^4} , \qquad \lambda_2 = -\frac{6\Phi (1 + 0.5\Phi)^2}{(1 - \Phi)^4} . \tag{4.57}$$

The PY result for $-c(r)$ reduces, for small Φ, to the correct first order density form of $y(r)$ given in Eq. (4.54).

Fourier transformation of $c(r)$ leads with Eq. (4.9) to an analytic expression for $S_c(q)$. This expression reads explicitly [3]

$$S(y) = \frac{1}{X^2(y) + Y^2(y)} \tag{4.58}$$

with

$$X(y) = 1 - 12\,\Phi\,[\,A\,f_1(y) + B\,f_2(y)\,]\,, \tag{4.59}$$

$$Y(y) = -12\,\Phi\,[\,A\,f_3(y) + B\,f_4(y)\,]\,, \tag{4.60}$$

where

$$A = \frac{1+2\Phi}{(1-\Phi)^2}\,, \qquad B = \frac{1+0.5\Phi}{(1-\Phi)^2}\,, \tag{4.61}$$

and

$$f_1(y) = \frac{y-\sin(y)}{y^3}\,, \qquad f_2(y) = \frac{\cos(y)-1}{y^2}\,, \tag{4.62}$$

$$f_3(y) = \frac{f_2(y)}{y} + \frac{1}{2y}\,, \qquad f_4(y) = -y f_1(y)\,. \tag{4.63}$$

We have introduced here the reduced wave number $y = q\sigma$.

The reduced isothermal compressibility follows in PY approximation as

$$\lim_{q\to 0} S_c(q) = \frac{(1-\Phi)^4}{(1+2\Phi)^2}\,, \tag{4.64}$$

which is a monotonically decreasing function in Φ. For given analytical $S_c(q)$, the hard-sphere $g(r)$ can be determined in principle by numerical Fourier-inversion. However, to avoid problems caused by the jump discontinuity in $g(r)$, it is safer to calculate first the function $\gamma(r) := h(r) - c(r)$ by Fourier-inverting $\gamma(q) = \rho c(q)h(q) = [S_c(q)-1]^2/(\rho S_c(q))$. The hard-sphere $g(r)$ follows then in PY approximation from $g(r) = y(r) = 1 + \gamma(r)$ for $r > \sigma$. Contrary to $g(r)$, $\gamma(r)$ is continuous also at $r = \sigma$ as one can deduce directly from the OZ equation. Notice here that the identity $y(r) = 1 + \gamma(r)$ holds true only within PY approximation.

While the full PY-$g(r)$ of hard spheres can not be represented analytically, one can derive closed expressions for the contact values of $g(r)$ and its first derivative from the continuity of $y(r)$ and its derivative at $r = \sigma$:

$$g(r = \sigma^+) = \frac{1+0.5\,\Phi}{(1-\Phi)^2}\,, \tag{4.65}$$

and

$$\sigma\,\frac{dg}{dr}(r = \sigma^+) = -\frac{4.5\Phi\,(1+\Phi)}{(1-\Phi)^3}\,. \tag{4.66}$$

An analytic expression for the Laplace transform of $rg(r)$ has been derived by Wertheim [15], viz.

$$\widetilde{G}(s) = \int_0^\infty dx \exp\{-sx\}\, xg(x) = \frac{\exp\{-s\}\,[A + Bs]}{s^2\,[1 - 12\Phi(A\,\phi_2(s) + B\,\phi_1(s))]} \tag{4.67}$$

with $\phi_1(s) = (1 - s - \exp\{-s\})/s^2$ and $\phi_2(s) = (1 - s + s^2/2 - \exp\{-s\})/s^3$. As seen, $\widetilde{G}(s)$ decays exponentially for large s, and it diverges at $s = 0$ like s^{-2}. The pole at the origin originates from $g(r \to \infty) = 1$. The static structure factor follows directly from Eq. (4.67) by noting that

$$S_c(y) = -\frac{24\,\Phi}{y}\,\Im\{\widetilde{G}(s = iy)\}\,. \tag{4.68}$$

The analytic form for $\widetilde{G}(s)$ is useful in evaluating the specific integrals,

$$\int_1^\infty dx\,\frac{g(x)}{x^n}\,\exp\{-sx\} = \int_s^\infty du\,\widetilde{G}(u)\,\frac{(u-s)^n}{n!}\,, \tag{4.69}$$

and

$$\int_1^\infty dx\, g(x)\, x^{n+1}\,\exp\{-sx\} = (-1)^n\,\frac{d^n}{ds^n}\,\widetilde{G}(s)\,, \tag{4.70}$$

for $n = 0, 1, \ldots$ and $s \geq 0$. These integrals are needed when thermodynamic properties like the isothermal compressibility (cf. Eq. (3.38)), and diffusion coefficients (cf. Chapter 9) are calculated.

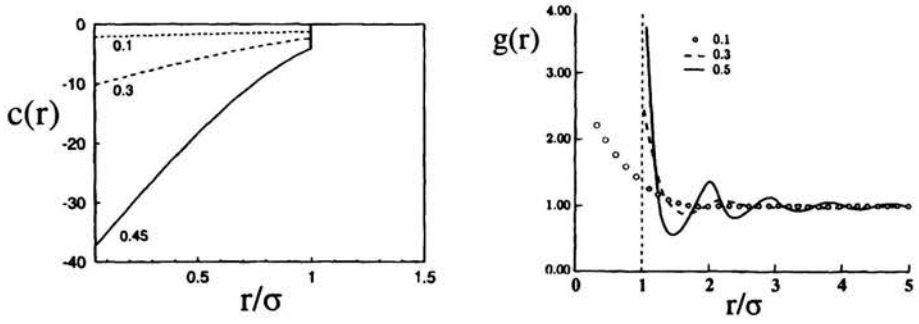

FIGURE 4.6. Percus–Yevick direct correlation function (left) and radial distribution function (right) of hard spheres.

PY results for the hard-sphere $c(r)$ and $g(r)$, and for the static structure factor, are shown in Figs. 4.6 and 4.7, respectively, for various volume fractions. For $\Phi = 0.1$, we further show the cavity function with $y(r) = -c(r)$ for $r < \sigma$. The PY approximation provides a quite good representation of the true hard-sphere $S_c(q)$ and $g(r)$ for volume fractions $\Phi \leq 0.35$. At larger values of Φ it underestimates the contact value of $g(r)$, as can be seen

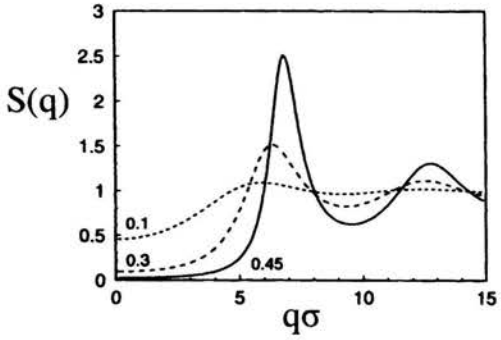

FIGURE 4.7. Percus–Yevick static structure factor $S(q) = S_c(q)$ of hard spheres.

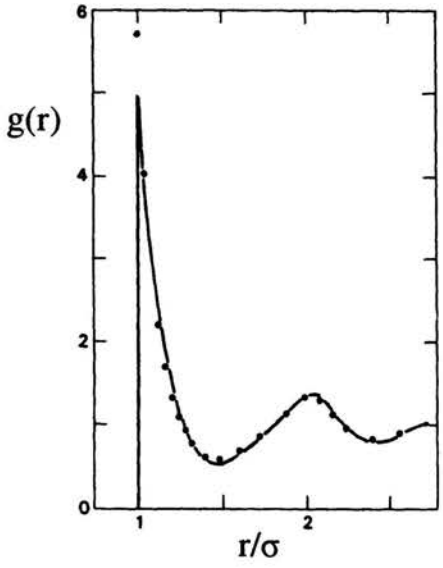

FIGURE 4.8. Hard-sphere $g(r)$ for a volume fraction $\Phi = 0.49$ close to the freezing transition. Comparison between PY (solid line) and MC computer simulations (filled circles).

from Fig. 4.8 in comparison with Monte Carlo (MC) computer simulation results. The PY approximation further fails to predict the liquid-solid freezing transition which occurs for hard spheres at $\Phi_f = 0.49$. This failure is not restricted to the PY approximation: none of the Ornstein–Zernike integral equations discussed in this lecture can, per se, predict a first-order liquid-crystal phase transition.

Verlet–Weis (VW) correction for hard spheres

Based on the analytic PY solution for hard spheres, Verlet and Weis [16] have provided a simple prescription to obtain results for the hard-sphere $g(r)$ and $S(q)$, which are in very good agreement with computer simulation results up to the freezing volume fraction.

For given physical diameter σ and volume fraction Φ, the Verlet–Weis-corrected $g(r)$ is determined, for $x = r/\sigma > 1$, by

$$g_{VW}(x;\Phi) = g_{PY}(x\frac{\sigma}{\sigma'};\Phi') + A\,\frac{e^{-(\mu-1)x}}{x}\,\cos\left[\mu(x-1)\right], \tag{4.71}$$

with a rescaled volume fraction

$$\Phi' = \Phi(1 - \frac{1}{16}\Phi), \tag{4.72}$$

and a rescaled diameter $\sigma' = (\Phi'/\Phi)^{1/3}\sigma < \sigma$. Moreover,

$$A(\Phi') = \frac{3\Phi'^2\,(1 - 0.7117\,\Phi' - 0.114\,\Phi'^2)}{4(1-\Phi')^4} \tag{4.73}$$

and

$$\mu(\Phi') = \frac{24\,A(\Phi')}{\Phi'\,g_{PY}(1^+;\Phi')}\,. \tag{4.74}$$

The PY hard-sphere contact value as quoted in Eq. (4.65) is evaluated at the rescaled volume fraction.

Equation (4.72) for the rescaled volume fraction has been obtained from minimizing the integral over $|g(r/\sigma;\Phi) - g_{PY}(r/\sigma';\Phi')|$ for an interval ranging from $r = 1.6\,\sigma$ to $r = 3\,\sigma$. Thus, the region close to contact is ignored. Here, $g(r)$ is the 'exact', i.e., computer-simulated radial distribution function. In Eq. (4.71), the amplitude A of the exponentially decaying and thus short-range correction term added to $g_{PY}(r/\sigma';\Phi')$, has been determined from demanding that

$$g_{VW}(\sigma^+;\Phi) \equiv g_{PY}(\sigma/\sigma';\Phi') + A = g_{CS}(\sigma^+;\Phi)\,, \tag{4.75}$$

where

$$g_{CS}(\sigma^+;\Phi) = \frac{1}{4\Phi}\left(\frac{p_{CS}}{p_{id}} - 1\right) = \frac{1-0.5\Phi}{(1-\Phi)^3} \tag{4.76}$$

is the contact value of $g(r)$ derived from the accurate Carnahan–Starling equation of state in Eq. (4.81). The exponent μ was determined from enforcing the isothermal compressibility in the Verlet–Weis prescription to be equal to the Carnahan–Starling expression,

$$S_c^{VW}(q=0;\Phi) = S_c^{CS}(q=0;\Phi)\,, \tag{4.77}$$

with

$$S_c^{CS}(q=0;\Phi) = k_B T\left(\frac{\partial n}{\partial p_{CS}}\right)_T = \frac{(1-\Phi)^4}{(1+2\Phi)^2 + \Phi^3(\Phi-4)}\,. \tag{4.78}$$

The static structure factor in the Verlet–Weis prescription follows from a Fourier-sine integration of Eq. (4.71). It is nearly sufficient to integrate over the PY-part of $g_{VW}(r)$ only, i.e. $S_c^{VW}(q\sigma;\Phi) \approx S_c^{PY}(q\sigma';\Phi')$, since the near-contact region contributes only little to the Fourier integral.

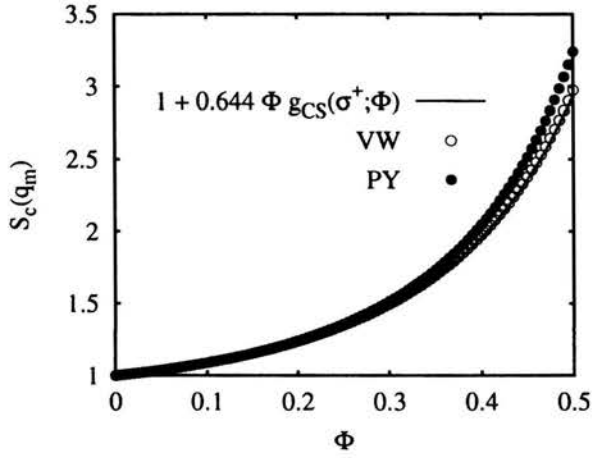

FIGURE 4.9. Hard-sphere principal peak of $S_c(q)$ versus Φ, as predicted in PY and in the Verlet–Weis scheme. Solid line is drawn according to Eq. (9.75).

In Fig. 4.9, the principal peak height, $S_c(q_m)$, of the structure factor is plotted versus Φ. The PY approximation overestimates the peak height near the freezing concentration, but the agreement with the Verlet–Weis corrected scheme is good for $\Phi < 0.42$. The solid line is the result of an accurate parametrization for the peak height given in Eq. (9.75). See the text following this equation for a discussion of the Hansen–Verlet freezing criterion [17].

4.5. Thermodynamic consistency and Rogers–Young scheme

One important reason for the failure of the PY approximation at higher densities is its thermodynamic inconsistency: due to the approximate nature of the PY-$g(r)$, the thermodynamic routes in Eqs. (3.36-3.38) give pressure curves, $p(\rho)$, which become increasingly different from each other with increasing density. The results for the thermodynamic properties obtained via the three routes are in general different for all OZ integral equations discussed so far. This lack of thermodynamic consistency is a common feature of approximate theories.

To illustrate the thermodynamic inconsistency of the PY approximation for the case of hard spheres we integrate the compressibility in (4.64) with respect to Φ. This yields the compressibility equation of state

$$\frac{\beta p^c}{\rho} = \frac{1+\Phi+\Phi^2}{(1-\Phi)^3} . \tag{4.79}$$

Using instead the pressure (or virial) equation of state, Eq. (3.37), one obtains

$$\frac{\beta p^v}{\rho} = 1 + 4\,\Phi g(r=\sigma^+) = \frac{1+2\Phi+3\Phi^2}{(1-\Phi)^2} , \tag{4.80}$$

which agrees with the pressure, p^c, derived from the compressibility equation only up to third order in the volume fraction. The pressure Eq. (3.37) is referred to also as virial equation of state, since it can be derived from the virial theorem of classical mechanics. The first equality in Eq. (4.80) between pressure and contact value of $g(r)$ is an exact statement for hard spheres.

The energy equation, Eq. (3.36), can not be used to derive the excess pressure, since the internal energy of hard spheres is of purely kinetic origin.

The PY and HNC compressibility and pressure (virial) equation of states for hard spheres are plotted in Fig. 4.10, in comparison with the "exact" pressure curve obtained from computer simulations. The exact hard-sphere equation of state is very well described in the fluid regime ($\Phi \leq 0.49$) by the Carnahan–Starling formula

$$\frac{p_{CS}}{p_{id}} = \frac{1}{p_{id}}\left[\frac{1}{3}p^v + \frac{2}{3}p^c\right] = \frac{1+\Phi+\Phi^2-\Phi^3}{(1-\Phi)^3} . \tag{4.81}$$

The exact pressure is bracketed by p^c and p^v, with increasing differences between p^c and p^v for increasing Φ. The PY is obviously a better approximation for hard spheres than the HNC.

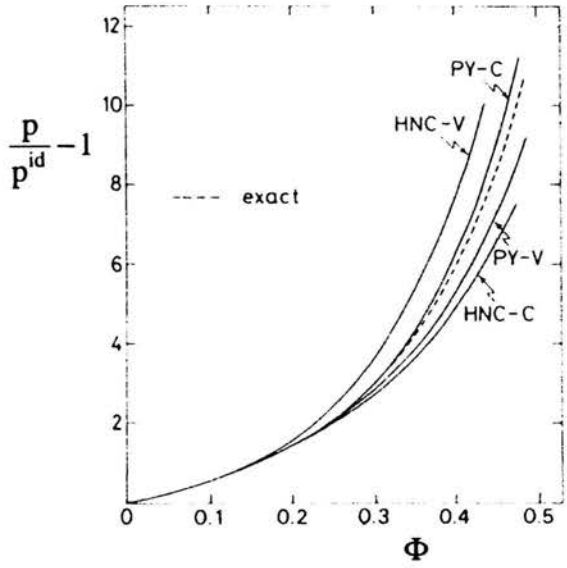

FIGURE 4.10. Hard-sphere compressibility and pressure (virial) equations of states in PY and HNC approximations. Dashed line: exact pressure curve. After [1].

Rogers–Young (RY) approximation

Rogers and Young [18] have combined the PY and HNC approximations in an integral equation scheme which removes part of their thermodynamic inconsistencies. This hybrid scheme was suggested from the observation (cf. Fig. 4.11) that computer simulation data for the structure factor of systems with purely repulsive pair potentials are bracketed, around q_m, by the PY and HNC structure factors. The RY closure relation is given by

$$g(r) \approx e^{-\beta u(r)} \left\{ 1 + \frac{1}{f(r)} \left[e^{f(r)[h(r)-c(r)]} - 1 \right] \right\} \tag{4.82}$$

with a mixing function

$$f(r) = 1 - e^{-\alpha r} \tag{4.83}$$

including a mixing parameter $\alpha \in \{0, \infty\}$. The closure relation is constructed in such a way that for

$$\begin{aligned} r \text{ or } \alpha \to 0: \quad & f(r) \to 0 \quad \text{RY} \to \text{PY}, \\ r \text{ or } \alpha \to \infty: \quad & f(r) \to 1 \quad \text{RY} \to \text{HNC}. \end{aligned} \tag{4.84}$$

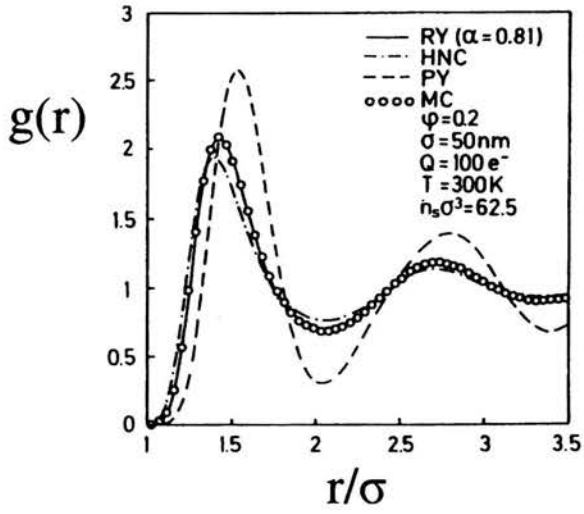

FIGURE 4.11. Radial distribution functions of an aqueous charge-stabilized Yukawa-like suspension with monovalent counterions at volume fraction $\Phi = 0.2$, diameter $\sigma = 50\,\mathrm{nm}$, $L_B = 0.71\,\mathrm{nm}$, $Z = 100$, and number density $\rho_s = n_s/2 = 415\,\mu\mathrm{M}$. Reduced screening parameter: $\kappa\sigma = 4.25$ with $(\kappa\sigma)^2 = (L_B/\sigma)\left[24\Phi|Z| + 8\pi\rho_s\sigma^3\right]$. Comparison of the RY, HNC, and PY approximations with MC results. After [19].

Hence the RY $y(r)$ reduces to its PY value for $r \to 0$ and to its HNC value for $r \to \infty$. This is consistent with the observation that whereas the HNC closure is correct at large separations, the PY approximation is expected to be more reliable at small r, at least for strongly repulsive potentials. The parameter α determines the proportion in which HNC and PY are mixed at intermediate r. Its numerical value follows from requiring partial thermodynamic consistency by demanding the equality, $\chi_T^p = \chi_T^c$, of the compressibilities obtained from the pressure and compressibility equations od state. Since χ_T is directly related to the long-wavelength limit of the static structure factor, one may expect that the RY approximation will provide reliable results for $S_c(q)$ at finite q.

The RY mixing scheme has been found to perform very well for three-dimensional liquids with purely repulsive pair potentials. Its predictions of the pair structure are less precise for two-dimensional systems. Monolayers of charged or magnetic colloidal particles at a liquid-gas interface or between two narrowly spaced plates are well-studied examples of such (quasi-) two-dimensional systems. Figure 4.11 includes a comparison of RY, HNC and PY

results for $g(r)$ with Monte Carlo simulations of a three-dimensional colloidal dispersion of Yukawa spheres, with a pair potential as given in Eq. (2.3).

The true (i.e., Monte Carlo) $g(r)$ is strongly overestimated by the PY approximation, whereas the fluid microstructure is somewhat underestimated by the HNC approximation, and even more so when the RMSA is used (the $g(r)$ of the latter is not included in Fig. 4.11). The RY approximation, on the other hand, reproduces the MC data rather perfectly. The suspension in Fig. 4.11 includes 415 μM of added 1-1 electrolyte. Figures 4.12 and 4.13, respectively, show the $g(r)$ and $S(q)$ of a dei-ionized (i.e., salt-free) suspension of charge-stabilized spheres close to the freezing transition. In this numerically more demanding case of strongly interacting spheres, even the RY scheme underestimates somewhat the oscillations in the pair distribution function. In comparison, $g(r)$ is tremendously overestimated by the PY scheme (not included in the Figure).

We observe here the ordering relations $g^{max}_{RMSA} < g^{max}_{HNC} < g^{max}_{RY} \leq g^{max}_{MC} < g^{max}_{PY}$, typical for a system of Yukawa-like particles. Addition of a modest

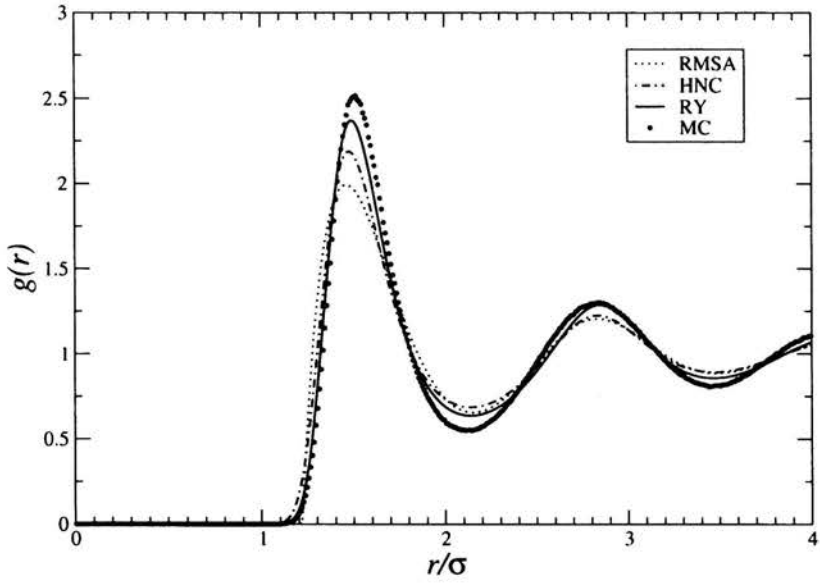

FIGURE 4.12. $g(r)$ of a concentrated suspension ($\Phi = 0.185$) of strongly coupled charge-stabilized colloidal spheres (salt-free: $\rho_s = 0$). System parameters: $\sigma = 125\,\text{nm}$, $Z = 155$, $L_B = 0.902\,\text{nm}$ (corresponding to $T = 294$ K and $\epsilon = 63$), monovalent counterions. Comparison of RY, HNC, and RMSA approximations with Monte-Carlo simulation results. After [20].

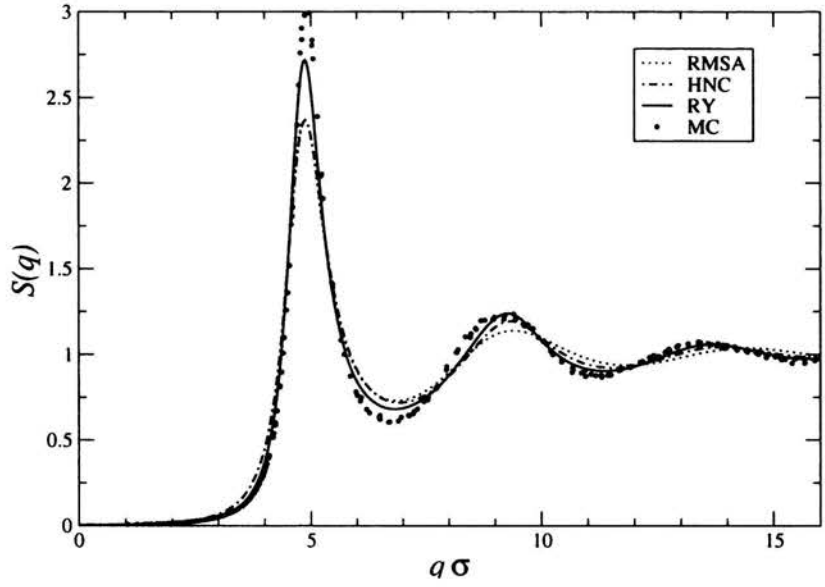

FIGURE 4.13. Static structure factor $S_c(q)$ corresponding to Fig. 4.12. After [20].

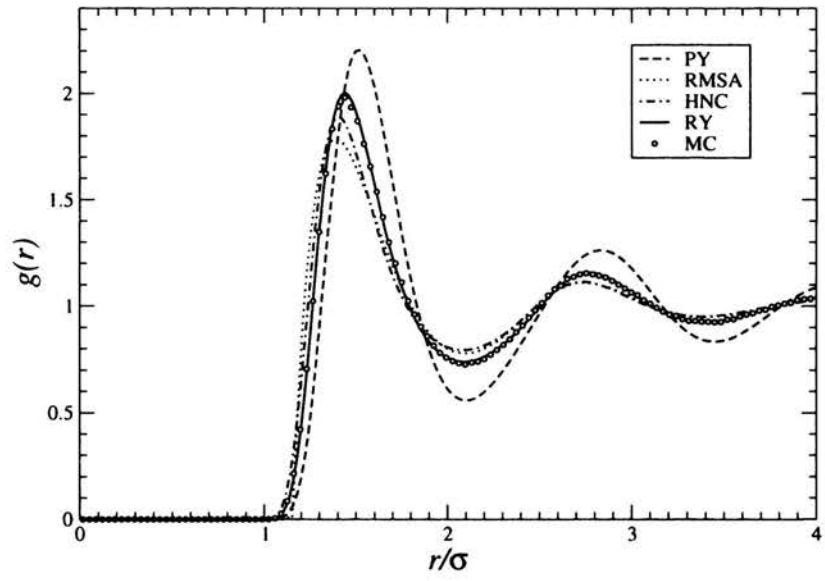

FIGURE 4.14. $g(r)$ for system parameters as in Fig. 4.13, but with 100 μM added 1-1 electrolyte. After [20].

amount of 100 μM 1-1 electrolyte to the salt-free system in Fig. 4.12 leads to a significant reduction in the microstructural ordering (cf. Fig. 4.14), and again to good agreement between the RY and MC-generated $g(r)$.

Chapter 5

Generalization to fluid mixtures

The concept of pair and direct correlations, and the Ornstein–Zernike integral equation schemes described in Secs. 4.3-4.5, can be generalized without difficulty to multi-component liquids and polydisperse (colloidal) systems. We will discuss these generalizations in the following section. As an interesting application of the many-component liquid state theory we will present a derivation of the effective pair potential in Eq. (2.3). This potential describes the screened electrostatic interaction of charged colloidal particles.

5.1. Partial correlation functions

Consider an atomic or colloidal liquid consisting of m components of spherical particles of diameters σ_α and partial number densities $\rho_\alpha = N_\alpha/V$. We employ Greek symbols, with $\alpha = 1, \ldots, m$, to label the m components which build up the liquid. The particles within each component are identical. We assume that the particle interactions can be described by pairwise additive forces. The following replacements

$$\begin{aligned} u(r) &\rightarrow u_{\alpha\beta}(r), \\ g(r) &\rightarrow g_{\alpha\beta}(r), \\ c(r) &\rightarrow c_{\alpha\beta}(r), \\ h(r) &\rightarrow h_{\alpha\beta}(r) = g_{\alpha\beta}(r) - 1, \end{aligned} \tag{5.1}$$

are needed for a generalization to a m-component mixture. There are $m(m+1)/2$ partial pair potentials $u_{\alpha\beta}(r)$, radial distribution functions $g_{\alpha\beta}(r)$, total correlation functions $h_{\alpha\beta}(r)$, and direct correlation functions $c_{\alpha\beta}(r)$ (with $\alpha, \beta \in \{1, \ldots, m\}$) necessary to characterize the fluid microstructure. Here, $u_{\alpha\beta}(r)$ is the pair potential of two particles belonging to component α and β, respectively. Furthermore, $g_{\alpha\beta}(r)$ gives the relative conditional probability of finding a β-type particle a distance r apart from a given α-type particle. The partial pair potentials are obviously symmetric in the two component indices, i.e. $u_{\alpha\beta}(r) = u_{\beta\alpha}(r)$. The remaining functions in Eq. (125) are also symmetric.

The one-component OZ equation is replaced in mixtures by a set of $m(m+1)/2$ coupled OZ equations, one for each $h_{\alpha\beta}(r)$. In case of a homogeneous and isotropic liquid mixture, these OZ equations are given by

$$h_{\alpha\beta}(r) = c_{\alpha\beta}(r) + \sum_{\gamma=1}^{m} \rho_\gamma \int d\mathbf{r}'\, c_{\alpha\gamma}(|\mathbf{r} - \mathbf{r}'|)\, h_{\gamma\beta}(r')\,. \tag{5.2}$$

Fourier-transformation gives the OZ equations in q-space:

$$h_{\alpha\beta}(q) = c_{\alpha\beta}(q) + \sum_{\gamma=1}^{m} \rho_\gamma\, c_{\alpha\gamma}(q)\, h_{\gamma\beta}(q)\,. \tag{5.3}$$

The total correlation function, $h_{\alpha\beta}$, between two particles of components α and β is thus written as the sum of a direct correlation part, $c_{\alpha\beta}$, and an indirect correlation part mediated through all other particles of components $\gamma = 1, \ldots, m$ with relative weight ρ_γ.

Since there are $m(m+1)/2$ unknown functions, $c_{\alpha\beta}(r)$, in the OZ equations one needs the same number of closure relations to obtain a complete set of integral equations determining the partial radial distribution functions. We quote here only the multi-component generalization of the MSA since it is used subsequently. All other integral equation schemes discussed previously can be generalized accordingly to mixtures. The multi-component MSA closure relations are

$$c_{\alpha\beta}(r) \approx -\beta u_{\alpha\beta}(r)\,, \quad r > \frac{\sigma_\alpha + \sigma_\beta}{2}\,. \tag{5.4}$$

Together with the exact non-overlap conditions

$$h_{\alpha\beta}(r) = -1\,, \quad r < \frac{\sigma_\alpha + \sigma_\beta}{2}\,, \tag{5.5}$$

and the OZ equations one obtains a closed set of integral equations for $h_{\alpha\beta}(r)$.

5.2. Effective interaction between charged colloidal particles

Our aim is to calculate the effective electrostatic interaction between two charge-stabilized colloidal particles of radius a and charge Ze immersed in a supporting electrolyte solution (cf. Fig. 5.1). For this purpose we model the colloidal particles, the counterions of charge $Z_c e$ dissociated from the colloidal particle surfaces, and the salt/electrolyte ions as uniformly charged hard spheres dispersed in a solvent which is described as a structure-less, uniform continuum of dielectric constant ϵ. This is the so-called Primitive Model which has been frequently used as a model for electrolytes and charge-stabilized colloidal dispersions. It is "primitive" in the sense that the structure of the solvent and particle surfaces, and polarization effects are completely disregarded.

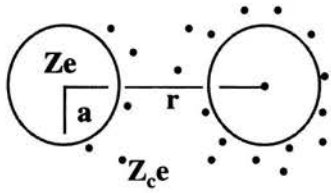

FIGURE 5.1. Primitive Model of charged colloidal hard spheres (macroions) of radius a and charge Ze plus point-like counterions of charge $Z_c e$.

The counterions and salt ions are much smaller than the colloidal particles (macroions). Therefore we assume these microions to be point-like, i.e. of zero diameter. For the sake of simplicity and to minimize the number of particle components to two, only the point-like counterions will be considered for the time being. Overall charge neutrality requires then that

$$\rho_1 Z + \rho_c Z_c = 0\,. \tag{5.6}$$

Typically, $|Z_c| = 1$ and $|Z| \gg |Z_c|$. According to Eq. (5.3), there are thus three coupled Ornstein–Zernike equations

$$h_{\alpha\beta}(q) = c_{\alpha\beta}(q) + \rho_1 c_{\alpha 1}(q)\, h_{1\beta}(q) + \rho_2 c_{\alpha 2}(q)\, h_{2\beta}(q) \tag{5.7}$$

for components 1 and 2, i.e. for the colloidal macroions of density ρ_1, and for the point-like counterions of density $\rho_2 = \rho_c$. The subscript c is used here to label the counterions, and not the colloidal particles. The three OZ equations

include information on macroion-macroion (11), macroion-counterion (12) and counterion-counterion (22) pair correlations. However, we are only interested here in the macroion-macroion correlations (11). To eliminate explicit reference to the counterions we define an effective one-component Ornstein–Zernike equation for the macroions alone as

$$h_{11}(q) = c_{eff}(q) + \rho_1 c_{eff}(q)\, h_{11}(q)\,. \tag{5.8}$$

By demanding h_{11} to be the same as in the original OZ equations, the effective direct correlation function, $c_{eff}(q)$, is determined by

$$c_{eff}(q) = c_{11}(q) + \frac{\rho_c c_{12}(q)^2}{1 - \rho_c c_{22}(q)}\,. \tag{5.9}$$

It is thus related to all three partial direct correlation functions. Eq. (5.8) is formally identical with the OZ equation of a genuinely one-component system. It describes the microstructure of particles 1 (macroions) immersed in a bath of particles of component 2 (counterions). The counterions do not appear explicitly in Eq. (5.8). Their effects are hidden in $c_{eff}(q)$.

Suppose $c_{eff}(q)$ and its Fourier-inverse, $c_{eff}(r)$, would be already known from Eq. (5.9). The effective pair potential, $u_{eff}(r)$, describing the interaction of two ("counterion-dressed") macroions follows then, at least asymptotically, from noting that

$$\lim_{\rho_1 \to 0} h_{11}(r) = \lim_{\rho_1 \to 0} c_{eff}(r) = -\beta u_{eff}(r) \quad \text{for} \quad r \to "\infty"\,, \tag{5.10}$$

where the second equality is valid in general only at large pair distances. The zero-macroion-density limit is performed at the end since we are interested only in the effective interaction of two isolated macroions (MacMillan-Mayer picture).

Our task is thus to calculate first the three partial direct correlation functions $c_{\alpha\beta}$ from solving the coupled Ornstein–Zernike equations with appropriate closure relations. Next, $c_{eff}(r)$ can be determined using Eq. (5.9). We will use here the linear MSA closure for analytical simplicity.

The direct correlation function of the point-like counterions is approximated in MSA by

$$c_{22}(r) = -\beta u_{22}(r)\,, \quad r > 0 \tag{5.11}$$

where

$$\beta u_{22}(r) = L_B \frac{Z_c^2}{r}\,, \quad r > 0\,. \tag{5.12}$$

Using Eqs. (3.34) and (3.35), Fourier inversion gives

$$c_{22}(q) = -4\pi L_B Z_c^2 \frac{1}{q^2} . \tag{5.13}$$

Notice in this context that in the limit of point-like ions, or for ionic systems at infinite dilution, the MSA reduces to what is known in electrolyte theory as the Debye–Hückel (DH) approximation. When dealing with direct correlation functions of charged particles, which have short-range (i.e. excluded volume) interaction contributions aside from the long-range Coulomb interactions, it is very helpful to split $c_{\alpha\beta}(r)$ into a short-range part, $c^s_{\alpha\beta}(r)$, and a long-range Coulomb part according to

$$c_{\alpha\beta}(r) = c^s_{\alpha\beta}(r) - L_B \frac{Z_\alpha Z_\beta}{r} , \tag{5.14}$$

since it holds quite generally that

$$c_{\alpha\beta}(r) \approx -\beta u_{\alpha\beta}(r) = -L_B \frac{Z_\alpha Z_\beta}{r} \quad r \to \infty . \tag{5.15}$$

In this way, the colloid-counterion direct correlations are expressed as

$$c_{12}(q) = c^s_{12}(q) - 4\pi L_B \frac{Z Z_c}{q^2} . \tag{5.16}$$

The colloid-colloid direct correlation function is written accordingly as

$$c_{11}(q) = c^s_{11}(q) - 4\pi L_B \frac{Z^2}{q^2} . \tag{5.17}$$

Substitution of Eqs. (5.13), (5.16) and (5.17) into Eq. (5.9) results in

$$c_{eff}(q) = c^s_{11}(q) + \rho_c [c^s_{12}(q)]^2 - 4\pi L_B \left[Z + \rho_c Z_c c^s_{12}(q)\right]^2 \frac{1}{\kappa^2 + q^2} \tag{5.18}$$

where we have introduced the Debye–Hückel screening length, κ^{-1}, with

$$\kappa^2 = 4\pi L_B \rho_c Z_c^2 . \tag{5.19}$$

Hence the screening parameter is determined by the concentration and charge ("ionic-strength") of dissociated counterions.

The large-r asymptotic behavior of $c_{eff}(r)$ is determined by the factor $\left[\kappa^2 + q^2\right]^{-1}$ in Eq. (5.18), since $c^s_{12}(q)$ and $c^s_{11}(q)$ are Fourier transforms of

short-range functions. Fourier inversion leads, with Eqs. (3.34) and (3.35), to the intermediate result

$$c_{eff}(r) = \frac{1}{(2\pi)^3} \int d\mathbf{r} e^{-i\mathbf{q}\cdot\mathbf{r}} c_{eff}(q) \sim -\beta g \frac{e^{-\kappa r}}{r} \quad r \to \infty \tag{5.20}$$

with a yet undetermined interaction strength g. The magnitude of g is determined by the pre-factor of $\left[\kappa^2 + q^2\right]^{-1}$ which includes $c_{12}^s(q)$. The effective macroion pair potential is asymptotically of the Yukawa-type, with a screening parameter determined by the Debye–Hückel relation Eq. (5.19). The counterions (and salt ions) distribute themselves around the macroions to screen the colloid-colloid Coulomb repulsion. The only approximation used to obtain the asymptotic result in Eq. (5.20) is the DH approximation for the counterion correlations $c_{22}(r)$.

To determine g analytically we further apply the MSA to the colloid-colloid and colloid-counterion direct correlation functions:

$$c_{11}(r) = -\beta u_{11}(r) = -L_B \frac{Z^2}{r}, \quad r > \sigma = 2a, \tag{5.21}$$

$$c_{12}(r) = -\beta u_{12}(r) = -L_B \frac{Z Z_c}{r}, \quad r > a. \tag{5.22}$$

In MSA the short-range direct correlation parts are thus zero outside the overlap region, i.e. $c_{11}^s(r) = 0$ for $r > \sigma = 2a$ and $c_{12}^s(r) = 0$, for $r > a$. As a consequence, the MSA predicts the counterion-colloid short-range direct correlation part to be a linear function of the colloid charge number. This linearity in Z is exactly valid for the true c_{12}^s only in the limit of weak particle charges. For larger macroion charges, the MSA underestimates the accumulation of counterions close to the surface of a colloidal macroion.

Using these properties of the MSA-$c_{\alpha\beta}^s(r)$, application of the convolution theorem to the second and third term on the right-hand-side of Eq. (5.18) shows that $g \propto Z^2$ and

$$-c_{eff}(r) = 4\pi L_B \mathcal{F}^{-1} \left\{ \frac{\left[Z + \rho_c Z_c c_{12}^s(q)\right]^2}{\kappa^2 + q^2} \right\} \propto Z^2 \frac{e^{-\kappa r}}{r} \quad r > \sigma. \tag{5.23}$$

That $c_{eff}(r) \propto \exp[-\kappa r]/r$ holds for all $r > \sigma$ and not only at asymptotically large distances is a consequence of the approximation $c_{12}^s(r > a) = 0$ used in MSA.

So far, we have accounted only for the counterions whose number density ρ_c, according to Eq. (5.6), and thus κ become zero when $\rho_1 \to 0$. One

can rather easily include the effects of point-like added salt ions of number density ρ_s and charge number Z_s (for each additional component s) by increasing accordingly the number of components in Eq. (5.7). For an overall neutral system

$$\sum_s \rho_s Z_s = 0\,, \tag{5.24}$$

where the sum runs over all components of salt ions. When the MSA closure is used again for the salt ion - salt ion direct correlation functions, Eq. (5.18) is easily generalized to

$$\begin{aligned} c_{eff}(q) = c_{11}^s(q) \;&+\; \sum_{\alpha=s,c} \rho_\alpha [c_{1\alpha}^s(q)]^2 \\ &-\; 4\pi L_B \left[Z + \sum_{\alpha=s,c} \rho_\alpha Z_\alpha c_{1\alpha}^s(q) \right]^2 \frac{1}{\kappa^2 + q^2}\,, \end{aligned} \tag{5.25}$$

where $c_{1\alpha}^s(q)$ is the short-range part of the colloid - microion direct correlations functions. The screening parameter is now determined by the ionic strengths of all microions, i.e. salt- and counterions:

$$\kappa^2 = 4\pi L_B \left[\rho_c Z_c^2 + \sum_s \rho_s Z_s^2 \right]. \tag{5.26}$$

In a final step, we employ the limit $\rho_1 \to 0$ of very small macroion concentrations, where the macroion-microion direct correlation functions, $c_{1\alpha}(r)$ and $h_{1\alpha}(r)$, can be calculated analytically in the MSA (= DH approximation). The details of these calculations are given in the following section, with final results results:

$$g_{1\alpha}(r) = \left[1 - L_B Z Z_\alpha \left(\frac{e^{\kappa a}}{1+\kappa a} \right) \frac{e^{-\kappa r}}{r} \right] \theta(r-a)\,, \tag{5.27}$$

$$c_{1\alpha}(r) = -\left[1 + \frac{L_B}{a} Z Z_\alpha \left(\frac{\kappa a}{1+\kappa a} \right) \right] \theta(a-r) - \left(L_B \frac{Z Z_\alpha}{r} \right) \theta(r-a)\,, \tag{5.28}$$

and

$$c_{1\alpha}^s(r) = -\left[1 + L_B Z Z_\alpha \left(\frac{\kappa}{1+\kappa a} - \frac{1}{r} \right) \right] \theta(a-r)\,. \tag{5.29}$$

The total correlation function, $h_{1\alpha}(r)$, describes the distribution of α-type microions around a colloidal sphere. It decays exponentially at large r

due to screening, whereas $c_{1\alpha}(r)$ still has the infinite range of the Coulomb potential. As noted already in Sec. 4.1, this feature distinguishes ionic from neutral liquids. An interesting observation for the DH-$g_{1\alpha}(r)$ in Eq. (137) is that

$$\sum_{\alpha=c,s} \rho_\alpha \int d\mathbf{r}\, g_{1\alpha}(r) Z_\alpha e = -Ze \tag{5.30}$$

which means that the total charge of the microionic cloud exactly cancels the charge of the colloidal particle in its centre. This is a special case of general local electroneutrality conditions for ionic systems [1]. One can show that the MSA and HNC closure relations are compatible with these exact conditions.

Using finally the DH expression for $c^s_{1\alpha}(r)$ in the Fourier-inverted form of Eq. (5.25), and noticing that in MSA

$$\left(c^s_{1\alpha} * c^s_{1\beta}\right)(r > 2a) = 0 \tag{5.31}$$

for the convolution of two colloid - microion short-range direct correlation function parts, we obtain our final result

$$\beta u_{eff}(r) = -\lim_{\rho_1 \to 0} c_{eff}(r) = -\lim_{\rho_1 \to 0} h_{11}(r) = L_B Z^2 \left(\frac{e^{\kappa a}}{1+\kappa a}\right)^2 \frac{e^{-\kappa r}}{r}, \qquad r > \sigma \tag{5.32}$$

for the effective macroion pair potential quoted already in Eq. (2.3). Within the linearization approximation of weak particle charges,

$$g_{11}(r) = e^{-\beta w_{11}(r)} \approx 1 - \beta w_{11}(r), \tag{5.33}$$

which is consistent with the DH-MSA approximation of direct correlations, $u_{eff}(r)$ can be identified, for a non-zero amount of excess electrolyte, with the macroion-macroion potential of mean force $w_{11}(r)$. One might expect from the mean-spherical-type approximations entering into its derivation that this form of the effective pair potential applies only at long distances r and for weakly charged particles. However, it has been shown that the range of applicability of Eq. (5.32) can be substantially extended when Z is treated not as the bare macroion charge, but as an effective or dressed colloid charge smaller than the bare one. In this way one accounts approximately for the stronger screening close to strongly charged macroion surfaces. For a determination of the effective macroion charge using a spherical Wigner–Seitz cell model calculation, consult [21, 22, 23].

5.3. MSA versus DH theory of electrolytes

The MSA reduces to the Debye-Hückel approximation for a special Primitive Model system of point-like microions and infinitely dilute macroionic species.

To see this explicitly consider an m-component Primitive Model system consisting of an infinitely dilute macroion species (tracer: $T = 1$, with $\rho_1 = 0$) with spheres of radius a and charge number Z_T, immersed in a $(m-1)$-component electrolyte solution of point-like ions ($\alpha \in \{2, \ldots, m\}$). Our aim is to calculate the tracer-microion two-body correlation functions using the MSA closure relations.

The $T - \alpha$ part of the Ornstein–Zernike equation follows here as

$$h_{T\alpha}(r) = c_{T\alpha}(r) + \sum_{\gamma=2}^{m} \rho_\gamma \int d\mathbf{r}'\, h_{T\gamma}(r')\, c_{\gamma\alpha}(|\mathbf{r} - \mathbf{r}'|)\,. \tag{5.34}$$

Application of the MSA closure for $r > a$ leads to

$$h_{T\alpha}(r) = -L_B \frac{Z_T Z_\alpha}{r} - L_B \sum_{\gamma=2}^{m} \rho_\gamma \int d\mathbf{r}'\, h_{T\gamma}(r')\, \frac{Z_T Z_\gamma}{|\mathbf{r} - \mathbf{r}'|}\,. \tag{5.35}$$

Since the MSA is linear in the pair potential, we may substitute

$$h_{T\alpha}(r) = Z_T Z_\alpha\, h(r)\,, \tag{5.36}$$

which gives a linear integral equation for h(r). Explicitly

$$h(r) = -\frac{L_B}{r} - \frac{\kappa^2}{4\pi} \int d\mathbf{r}'\, \frac{h(r')}{|\mathbf{r} - \mathbf{r}'|}\,, \qquad (r > a) \tag{5.37}$$

with

$$\kappa^2 = 4\pi L_B \sum_{\gamma=2}^{m} \rho_\gamma\, Z_\gamma^2\,. \tag{5.38}$$

Application of the Laplace operator on both sides of this equation results in the homogeneous Helmholtz equation,

$$(\Delta_r - \kappa^2)\, h(r) = 0 \qquad (r > a)\,, \tag{5.39}$$

with the isotropic general solution

$$h(r) = C_1 \frac{e^{-\kappa r}}{r} + C_2 \frac{e^{\kappa r}}{r}\,. \tag{5.40}$$

The outer boundary condition $h(r \to \infty) = 0$ implies that $C_2 = 0$. An inner boundary condition, and hence C_1, are obtained using the continuity $\gamma_{T\alpha}(a^+) = \gamma_{T\alpha}(a^-)$ of $\gamma_{T\alpha}(r) \equiv h_{T\alpha}(r) - c_{T\alpha}(r)$ at $r = a$:

$$C_1 Z_T Z_\alpha \frac{e^{-\kappa a}}{a} + L_B \frac{Z_T Z_\alpha}{a} = -\left[1 + c_{T\alpha}(a^-)\right] . \tag{5.41}$$

For $c_{T\alpha}(a^-)$, we invoke the OZ-MSA equation for $r < a$,

$$-\left[1 + c_{T\alpha}(r)\right] = -L_B Z_\alpha \sum_{\gamma=2}^{m} \rho_\gamma Z_\gamma \left\{ C_1 Z_T Z_\gamma \int_{r'>a} d\mathbf{r}' \frac{e^{-\kappa r'}}{r'|\mathbf{r} - \mathbf{r}'|} - \int_{r'<a} d\mathbf{r}' \frac{1}{|\mathbf{r} - \mathbf{r}'|} \right\} . \tag{5.42}$$

Next, we use electroneutrality and the integral over the unit sphere,

$$\int_{4\pi} d\Omega_r \frac{1}{r'|\mathbf{r} - \mathbf{r}'|} = \frac{4\pi}{(r')^2} , \qquad (r < a < r') \tag{5.43}$$

to show that

$$c_{T\alpha}(r < a) = -1 + C_1 Z_T Z_\alpha \kappa e^{-\kappa a} . \tag{5.44}$$

Thus, the direct correlation function is constant in the overlap region.

Finally, this determines the integration constant C_1 in Eq. (5.40) as

$$C_1 = -L_B \frac{e^{\kappa a}}{1 + \kappa a} , \tag{5.45}$$

with

$$c_{T\alpha}(r < a) = -\left[1 + \frac{L_B}{a} Z_T Z_\alpha \frac{\kappa a}{1 + \kappa a}\right] , \tag{5.46}$$

and (cf. Eq. (5.36))

$$g_{T\alpha}(r) = \theta(r - a)\left[1 - L_B Z_T Z_\alpha \left(\frac{e^{\kappa a}}{1 + \kappa a}\right) \frac{e^{-\kappa r}}{r}\right] . \tag{5.47}$$

We further quote the Fourier transforms of $c_{T\alpha}(r)$ and $h_{T\alpha}(r)$,

$$c_{T\alpha}(q) = -3V_T \left\{ \frac{j_1(qa)}{qa} + \frac{L_B}{a} Z_T Z_\alpha \left[\frac{\kappa a}{1 + \kappa a} \frac{j_1(qa)}{qa} + \frac{cos(qa)}{(qa)^2} \right] \right\} \tag{5.48}$$

and

$$h_{T\alpha}(q) = -3V_T \left\{ \frac{j_1(qa)}{qa} + \frac{L_B}{a} \frac{Z_T Z_\alpha}{(\kappa a)^2 + (qa)^2} \left[\cos(qa) + \frac{(\kappa a)(qa)}{1+\kappa a} j_1(qa) \right] \right\} \tag{5.49}$$

with $V_T = (4\pi/3)a^3$.

The matrix inverse of the microionic partial structure factors, $S_{\alpha\beta}(q) = \delta_{\alpha\beta} + (\rho_\alpha \rho_\beta)^{1/2} h_{\alpha\beta}(q)$, is given by

$$S^{-1}_{\alpha\beta}(q) = \delta_{\alpha\beta} + 4\pi L_B (\rho_\alpha \rho_\beta)^{1/2} \frac{Z_T Z_\alpha}{q^2} . \tag{5.50}$$

The DH-MSA tracer-microion direct and total correlation functions are related to each other by

$$\rho_\alpha{}^{1/2} c_{T\alpha}(q) = \sum_{\gamma=2}^{m} S^{-1}_{\alpha\gamma}(q) \rho_\gamma{}^{1/2} h_{T\gamma}(q) . \tag{5.51}$$

This is an exact relation valid for $n_T = 0$.

What is left to prove is that the MSA reduces to the linear DH approximation for the system under consideration. To this end, consider the total mean charge density, $n_T^{(el)}(\mathbf{r})$, with the tracer located at the centre of the co-ordinate system,

$$n_T^{(el)}(\mathbf{r}) = Z_T e\, \delta(\mathbf{r}) + \sum_{\gamma=2}^{m} \rho_\gamma Z_\gamma e\, g_{T\gamma}(r) . \tag{5.52}$$

Since we are interested only in the mean electric field outside of the core of the tracer sphere (i.e., r>a), we assume for simplicity that the charge Z_T is concentrated at the origin. Of course, any spherically symmetric volume or surface charge distribution localized to $r \leq a$ gives an identical field outside of the core. The mean charge density is related to the total mean electrostatic potential, $\phi_T(\mathbf{r})$, by the Poisson equation of electrostatics,

$$\Delta \phi_T(\mathbf{r}) = -\frac{4\pi}{\epsilon} n_T^{(el)}(\mathbf{r}) , \tag{5.53}$$

where we disregard any dielectric differences between solvent an tracer sphere (Primitive Model). The mean electric field follows from $\mathbf{E}_T = -\nabla \phi_T(\mathbf{r})$. In the Poisson-Boltzmann (PB) mean-field theory, $g_{T\alpha}(\mathbf{r})$ is approximated by

$$g_{T\alpha}(\mathbf{r}) = \exp\{-\frac{w_{T\alpha}(\mathbf{r})}{k_B T}\} \approx \exp\{-\frac{Z_\alpha e\, \phi_T(\mathbf{r})}{k_B T}\} . \tag{5.54}$$

Hence, the potential of mean force, $w_{T\alpha}(r)$, between the tracer and an α-type microion is approximated by the mean electrostatic energy of an α-type ion moving statistically independent from other ions in the presence of the mean electrostatic potential. The PB approximation amounts to disregarding local ion-correlation effects which can cause oscillations in $w_{T\alpha}(r)$ and $g_{T\alpha}(r)$. The non-linear PB equation for $\phi_T(\mathbf{r})$ reads explicitly

$$\Delta\phi_T(\mathbf{r}) = -\frac{4\pi e}{\epsilon}\left[Z_T\delta(\mathbf{r}) + \theta(r-a)\sum_{\gamma=2}^{m}\rho_\gamma Z_\gamma \exp\left\{-\frac{Z_\gamma e\,\phi_T(\mathbf{r})}{k_BT}\right\}\right]. \quad (5.55)$$

It must be supplemented by the outer boundary condition $\phi_T(r \to \infty) = 0$ in case of an infinite electrolyte solution. Integration over a sphere of radius a gives the inner boundary condition,

$$\frac{d}{dr}\phi_T(r = a^+) = -\frac{Z_T e}{\epsilon a^2}. \quad (5.56)$$

The electric field at the surface is of Coulombic form, since the tracer core is impenetrable to the microionic cloud.

For a dilute electrolyte solution and for sufficiently small ionic charges where it holds that $Z_T e\,\phi_T(r) \ll k_BT$, we can linearize with respect to $\phi_T(r)$,

$$g_{T\alpha}^{DH}(\mathbf{r}) \approx 1 - \frac{Z_\alpha e\,\phi_T(\mathbf{r})}{k_BT}, \qquad (r > a). \quad (5.57)$$

The potential is then more simply determined by the linear Debye–Hückel (DH) equation,

$$\Delta\phi_T(\mathbf{r}) = \theta(r-a)\kappa^2\phi_T(\mathbf{r}) - \frac{4\pi e}{\epsilon}Z_T\,\delta(\mathbf{r}), \quad (5.58)$$

where $\phi_T(\mathbf{r})$ is now linear in Z_T. The isotropic solution of Eq. (5.58) for $r > a$ is

$$\phi_T(r) = D_1\frac{e^{-\kappa r}}{r}, \quad (5.59)$$

conforming to the outer boundary condition $\phi_T(\infty) = 0$ (so that $g_{T\alpha}(r \to \infty) = 1$). The integration constant D_1 follows with Eq. (5.56) as

$$D_1 = \frac{Z_T e}{\epsilon}\frac{e^{\kappa a}}{1+\kappa a}. \quad (5.60)$$

According to Eq. (5.58), we have thus shown that $g_{T\alpha}^{DH}(r)$ is equal to the MSA result in Eq. (5.47). Finally, from Eqs. (5.59) and (5.60), we obtain the

following linear DH relation between the surface potential and the charge of the tracer sphere,

$$\beta e \phi_T(a) = \frac{L_B}{a} \frac{Z_T}{(1+\kappa a)} . \tag{5.61}$$

Chapter 6

Dynamic properties: introduction

In the second part of these lecture notes (Chapters 6-9), I discuss diffusional properties of suspensions consisting of spherically shaped colloidal particles, and of binary melts of homopolymers.

The most important experimental tool to study diffusion in these systems is dynamic light scattering (DLS). In Chapter 7, the principles of dynamic light scattering are discussed on a heuristic level, without involving Maxwell's equations. Various kinds of dynamic structure factors are introduced, which describe different types of diffusion processes like self-diffusion, collective diffusion, rotational diffusion, and interdiffusion.

These diffusion processes, and their relation to corresponding types of structure factors, are explored in Chapter 8, again on a heuristic and intuitive level. For pedagogical reasons, I will discuss first translational and rotational diffusion in very dilute systems (cf. Sec. 8.1). Diffusion processes of concentrated systems, where the particles interact both by direct forces and, in case of colloidal dispersions, by solvent-mediated hydrodynamic forces, are explored in Sec. 8.2. In my lectures, I am mostly concerned with diffusion mechanisms in one-component systems, except for interdiffusion which is particularly relevant to the dynamics in binary polymer melts.

In Chapter 9, various types of diffusion processes are quantified that were treated in Chapter 8 on a heuristic level. For this purpose, theoretical short- and long-time predictions and computer simulation results are explored and compared to experimental findings. In Sec. 9.1, I discuss various forms of

the generalized Smoluchowski equation (GSE) of colloidal systems. The GSE is a time evolution equation for the probability density function of particle positions and orientations. Most theoretical studies of diffusion in colloidal systems and polymer solutions are based on appropriately selected variants of the GSE. In fact, the GSE is nearly as important for the theory of colloid dynamics, as the Schödinger equation is for quantum mechanics.

In Sec. 9.2, theoretical tools and computer simulations based on the GSE are explained, and applied to calculate diffusional properties. Hereby, one neeeds to distinguish between short-time and long-time transport properties. Short-time properties are more easy to compute since only equilibrium distribution functions are involved in their calculation. A colloid scientist's life is more difficult in case of long-time transport properties, for one needs to account for so-called memory effects. The colloidal systems considered in Sec. 9.2 comprise one-component bulk dispersions of neutral and charged colloidal spheres, quasi-two-dimensional suspensions of charged particle monolayers between narrow plates, magnetically interacting particles confined to a liquid-gas interface, and mixtures of colloidal hard spheres.

Diffusion in binary polymer blends will be addressed in Sec. 9.3. Here, earlier discussed general relations for interdiffusion are explicitly quantified within the Flory–Huggins approach, using the dynamic random phase approximation (RPA). This Section shows that general concepts of many-component diffusion apply equally well to colloidal suspensions and polymer blends. In polymer blends, however, there is no solvent involved. Therefore, the dynamic RPA is used instead of the generalized Smoluchowski equation.

It should be realized from the many comparisons in this lecture notes between theoretical results and experimental findings, that there is an intense and very fruitful interplay between theory and experiment in the field of colloidal and polymeric soft matter.

Chapter 7

Principles of dynamic light scattering

Light scattering by colloidal suspensions and polymers is a major experimental tool to study the statistical properties of these systems. In this section, light scattering is introduced on a heuristic basis, without considering explicit solutions of the Maxwell equations. The content of this Section is much along the lines of [24]. Besides this reference, more about light scattering can be found in [25, 26, 27, 28].

7.1. The scattered electric field

Consider an assembly of points, fixed in space. These points will later be identified as infinitesimally small volume elements that constitute the colloidal particles or polymers. A plane wave of monochromatic light impinges onto this assembly of points. Each of the points is supposed to scatter the incident beam of light in such a way that neither the wave length nor its phase is changed. Such a scattering process is referred to *quasi-elastic*, since the only energy transfer between the photon and the scatterer is due to exchange of kinetic energy. Due to the extreme difference between the mass of an elementary scatterer and a photon, the change of the wave length after the collision of the photon with the scatterer is extremely small, and will be neglected. A scattering process of this sort can be thought of as follows. The incident electric field induces a dipole moment which oscillates with the same frequency as the incident field. This oscillating dipole then emits

electromagnetic radiation with the same frequency, and hence with the same wave length.

The scattered intensity is detected in a certain well-defined direction. The total electric field strength that is scattered in that direction is the sum of the scattered electric fields by the individual points. Clearly, the phase difference of the scattered light from two points depends on their relative positions, as well as on the direction in which the electric field strength is measured, as can be seen from the sketch in Fig. 7.1. Let us first calculate the phase difference of electric field strengths scattered by two point scatterers with position coordinates $\mathbf{r}$ and $\mathbf{r}'$ say, into a direction that is characterized by *the scattering angle* Θ_s, which is the angle between the propagation direction of the incident plane wave and the direction in which the scattered field is detected (see Fig. 7.1).

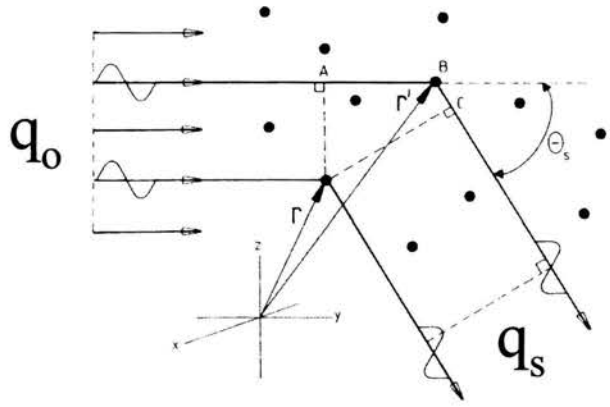

FIGURE 7.1. A schematic representation of the scattering of light by an assembly of point scatterers (•). Each macromolecule (a colloidal particle or a polymer molecule) comprises many of such point scatterers. After [24].

The *incident wavevector* $\mathbf{q}_0$ is the vector pointing in the propagation direction of the incident field, and its magnitude is $2\pi/\lambda$, where λ is the wave length of the light. Similarly, $\mathbf{q}_s$ is the *scattered wavevector*: its magnitude $q_s = |\mathbf{q}_s|$ is equal to that of the incident wavevector,

$$q_o = q_s = 2\pi/\lambda\,. \tag{7.1}$$

The phase difference $\Delta\Phi$ of the electric field strengths scattered by the two points located at $\mathbf{r}$ and $\mathbf{r}'$ under a scattering angle Θ_s is equal to $2\pi\Delta/\lambda$, where Δ is the difference in distance traversed by the two photons: $\Delta =$

$AB+BC$ (see Fig. 7.1). Now, $AB = (\mathbf{r}'-\mathbf{r})\cdot\mathbf{q}_o/q_o$, and $BC = (\mathbf{r}-\mathbf{r}')\cdot\mathbf{q}_s/q_s$. Hence, using this relation between phase difference and optical path length together with Eq. (7.1),

$$\Delta\Phi = (\mathbf{r}' - \mathbf{r})\cdot(\mathbf{q}_o - \mathbf{q}_s)\,. \tag{7.2}$$

One can thus associate to each point $\mathbf{r}$ a phase equal to $\mathbf{r}\cdot(\mathbf{q}_o-\mathbf{q}_s)$. The total scattered electric field strength $\mathbf{E}_s$ is then the sum of $\exp\{i\mathbf{r}\cdot(\mathbf{q}_o-\mathbf{q}_s)\}$ over all volume elements, weighted by the *scattering strength* of the point scatterers, which is defined as the fraction of the incident field strength that is actually scattered. Now, each point scatterer can be identified as an infinitesimally small volume element with volume $d\mathbf{r}$, from which the colloidal particle or polymer molecule is built. The scattering strength of a point scatterer is now written as $d\mathbf{r}\,F(\mathbf{r})$, where F is referred to here as *the scattering strength density*. Replacing the sum over point scatterers by integrals yields

$$\mathbf{E}_s = \int_{V_s} d\mathbf{r}\,F(\mathbf{r})\,\exp\{i(\mathbf{q}_o - \mathbf{q}_s)\cdot\mathbf{r}\}\,\mathbf{E}_0\,, \tag{7.3}$$

where $\mathbf{E}_0$ is the incident field strength, and V_s is *the scattering volume*, which is the volume from which scattered light is detected. The scattering strength density is proportional the polarizability $\alpha(\mathbf{r})$ of the volume element, relative to a constant background polarizability α_0 : the additional scattered field due to the macroscopically large, homogeneous background is zero for scattering angles unequal to 180^0. For a colloidal system, the background polarizability can be taken equal to that of the solvent, while for a binary polymer melt one can take the spatial average of the polarizability,

$$F(\mathbf{r}) \;\sim\; \alpha(\mathbf{r}) \;-\; \alpha_0\,. \tag{7.4}$$

We note that the polarizability is related to the refractive index for frequencies equal to that of light. The integral in Eq. (7.3) may be rewritten in order to make the distinction between interference of light scattered from volume elements within single particles and from distinct particles. Since the scattering strength is only non-zero within the colloidal particles or polymers, Eq. (7.3) can be written as a sum of integrals ranging over the volumes $V_j, j = 1, 2, \ldots, N$, occupied by the N particles in the scattering volume,

$$\mathbf{E}_s = \sum_{j=1}^{N} \int_{V_j} d\mathbf{r}\,F(\mathbf{r})\,\exp\{i(\mathbf{q}_o - \mathbf{q}_s)\cdot\mathbf{r}\}\,\mathbf{E}_0\,. \tag{7.5}$$

The integration range V_j is the volume that is occupied by the j^{th} particle. For non-spherical particles this volume depends on the orientation of the particle, and for any kind of particles, also for spherical particles, V_j depends on the location of the j^{th} particle. Let $\mathbf{r}_j$ denote a fixed point inside the j^{th} particle, which is referred to as its *position coordinate*. The position coordinate dependence of V_j can easily be accounted for explicitly, by changing for each j the integration variable to $\mathbf{r}' = \mathbf{r} - \mathbf{r}_j$. The new integration range V_j^0 is the volume occupied by the particle with its position coordinate at the origin. For spherical particles, with their positions chosen at the center of the spheres, V_j^0 is the volume of a sphere with its center at the origin. For non-spherical, possibly flexible particles, V_j^0 depends on the orientation and the internal configuration of particle j. In terms of these new integration variables Eq. (7.5) reads

$$\mathbf{E}_s = \sum_{j=1}^{N} B_j(\mathbf{q}) \exp\{i\,\mathbf{q}\cdot\mathbf{r}_j\}\,\mathbf{E}_0\,, \tag{7.6}$$

where we abbreviated

$$B_j(\mathbf{q}) = \int_{V_j^0} d\mathbf{r}'\,F(\mathbf{r}')\exp\{i\mathbf{q}\cdot\mathbf{r}'\}\,. \tag{7.7}$$

Here, B_j is referred to as *the scattering amplitude of particle* j, and

$$\mathbf{q} = \mathbf{q}_o - \mathbf{q}_s\,, \tag{7.8}$$

which is referred to as *the scattering wavevector*. From Eq. (7.1) it is easily verified that the magnitude of this scattering wavevector is equal to

$$q = \frac{4\pi}{\lambda}\sin\{\Theta_s/2\}\,, \tag{7.9}$$

where Θ_s is the scattering angle that was introduced before as the angle between $\mathbf{q}_o$ and $\mathbf{q}_s$, and λ is the wave length of the light in the scattering volume. The exponential functions in Eq. (7.6) containing the position coordinates $\mathbf{r}_j$ describe the interference of light scattered from different colloidal particles, while the scattering amplitudes B_j describe interference of light scattered from different volume elements within single particles.

In the above analysis we did not consider polarization effects. Consider the oscillating dipole $\mathbf{P}$ that is induced by the incident electric field, from

which emitted radiation is detected in the direction $\mathbf{q}_s$. The component of the dipole parallel to $\mathbf{q}_s$ does not contribute to the electric field emitted in that direction : looking "onto the head" of a dipole, one can not tell whether the dipole oscillates or not, and therefore it can not radiate in that direction. The part of the dipole that gives rise to emitted radiation in the direction $\mathbf{q}_s$ is the part that is perpendicular to $\mathbf{q}_s$ (see Fig. 7.2). This "effective dipole" is equal to

$$\mathbf{P}^{eff} = \left[\hat{\mathbf{I}} - \hat{\mathbf{q}}_s\hat{\mathbf{q}}_s\right] \cdot \mathbf{P}\,, \tag{7.10}$$

where $\hat{\mathbf{q}}_s = \mathbf{q}_s/q_s$ is the unit vector in the direction of $\mathbf{q}_s$.

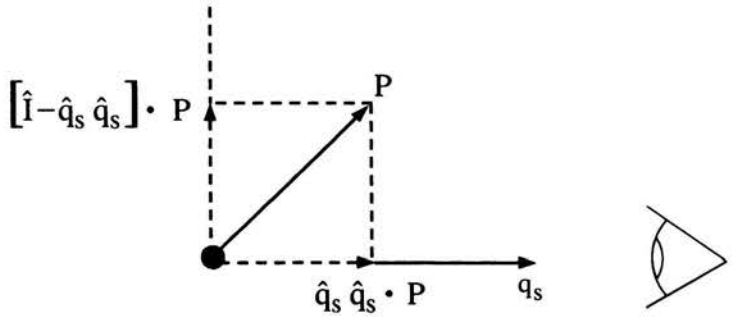

FIGURE 7.2. An observer only probes that part of an oscillating dipole $\mathbf{P}$ that is perpendicular to the observation direction $\sim \mathbf{q}_s$.

Secondly, the polarizability may be anisotropic, that is, the polarizability may depend on the polarization direction of the incident field. For example, for long and thin rods, the polarizability for light with a polarization direction parallel to the rods long axis may be different from the polarizability of light that is polarized in a direction perpendicular to the long axis. Such an anisotropic polarizability is the result of the anisotropic microstructure of the rods material. For such anisotropic polarizabilities, the induced dipole generally has a different orientation than the incident electric field. In such a case, the scattering strength F in Eq. (7.4) is a tensor, denoted as $\mathbf{F}$, rather than a scalar. Thirdly, in an experiment one usually measures, by means of a polarization filter, the scattered intensity with a prescribed polarization direction, which is characterized by the unit vector $\hat{\mathbf{n}}_s$. The detected electric field strength is simply $\hat{\mathbf{n}}_s \cdot \mathbf{E}_s$. Taking these polarization effects into account,

generalizes Eq. (7.6) to

$$E_s \equiv \hat{\mathbf{n}}_s \cdot \mathbf{E}_s = \hat{\mathbf{n}}_s \cdot \left[\hat{\mathbf{I}} - \hat{\mathbf{q}}_s \hat{\mathbf{q}}_s\right] \cdot \sum_{j=1}^{N} \mathbf{B}_j(\mathbf{q}) \exp\{i\,\mathbf{q} \cdot \mathbf{r}_j\} \cdot \mathbf{E}_0\,, \qquad (7.11)$$

where $\mathbf{B}_j$ is now defined by Eq. (7.7), with the scalar F replaced by the tensor $\mathbf{F}$. Note that the polarization direction is always perpendicular to the propagation direction, so that, $\hat{\mathbf{n}}_s \cdot \hat{\mathbf{q}}_s = 0$. Introducing the polarization direction $\hat{\mathbf{n}}_o$ of the incident field, where $\mathbf{E}_0 = \hat{\mathbf{n}}_o E_0$, with E_0 the magnitude of the incident electric field strength, Eq. (7.11) simplifies to

$$E_s = \sum_{j=1}^{N} [\hat{\mathbf{n}}_s \cdot \mathbf{B}_j(\mathbf{q}) \cdot \hat{\mathbf{n}}_o] \exp\{i\,\mathbf{q} \cdot \mathbf{r}_j\}\, E_0\,. \qquad (7.12)$$

This equation is at the basis of the analysis of quasi-elastic light scattering experiments.

Two assumptions, which are implicit in the above analysis, should be mentioned. First of all it is assumed here that the incident field strength is the same at every point in the scattering volume. This is only true if the various scattering elements scatter only a very small fraction of the light. This amounts to what is commonly referred to as "the first Born approximation". Secondly, multiple scattering is neglected. That is, scattered light is assumed not to be scattered by a second and further volume elements. Both these assumptions are satisfied when, according to Eq. (7.4), differences in polarizability of the material within the scattering volume are small.

The value of the scattering wavevector q is of special importance. Since the exponential function in Eq. (7.12) hardly changes when the position coordinates $\mathbf{r}_j$ are changed by an amount less than about $2\pi/q$, the scattered electric field strength changes when particles move over distances of at least $\sim 2\pi/q$. Equivalently, from Eq. (7.7) it follows that particle orientations and internal modes can only be probed when the scattering angle is chosen such that the linear dimensions of the scattering particles is at most $\sim 2\pi/q$. We can therefore introduce an effective wave length

$$\Lambda = 2\pi/q\,, \qquad (7.13)$$

which sets the structural length scale on which dynamics is probed. For example, if the length of a colloidal rod is smaller than Λ, rotation of the rod leaves the scattering amplitude (7.7) virtually unchanged, and does therefore

not affect the scattered electric field strength. For such a wavevector, nothing can be learned from a light scattering experiment about the rotational dynamics of these rods. Similarly, if one is interested in the dynamics of internal degrees of freedom of a polymer molecule, the scattering angle should be so large, that Λ is smaller than the linear dimension of the polymers. For larger Λ, only translational motion of the polymers is probed. For the same reason, displacements of particles that are smaller than Λ are not seen in a light scattering experiment. According to Eq. (7.9), the scattering angle thus sets the length scale on which the dynamics is probed by light scattering.

7.2. Dynamic light scattering

Due the Brownian motion of the center of mass $\mathbf{r}_j$, and of the orientation of particles and their internal fluctuations (which renders the scattering amplitude $\mathbf{B}_j$ time dependent), the scattered intensity fluctuates with time. Clearly, these fluctuations contain information about the dynamics of these degrees of freedom, which are generally affected by interactions between the colloidal particles or polymers. In a dynamic light scattering experiment one measures the so-called *intensity auto-correlation function* $g_I(\mathbf{q},t)$, hereafter abbreviated as IACF, which is defined as

$$g_I(\mathbf{q},t) \equiv < i(\mathbf{q},t_0)\, i(\mathbf{q},t+t_0) > , \tag{7.14}$$

where the brackets $< \cdots >$ denote ensemble averaging. For an equilibrium system, the IACF is independent of the reference time t_0, which we shall therefore set equal to 0 from now on. The IACF contains information about the dynamics of the above mentioned degrees of freedom. The instantaneous intensity is related to the scattered electric field strength as

$$i(\mathbf{q},t) \sim E_s(\mathbf{q},t)\, E_s^\star(\mathbf{q},t) , \tag{7.15}$$

where the wavevector and time dependence of the scattered electric field strength is denoted explicitly. The asterisk denotes the operation of complex conjugation. The IACF is thus an ensemble average of a product of four electric field strengths,

$$g_I(\mathbf{q},t) \sim < E_s(\mathbf{q},t)\, E_s^\star(\mathbf{q},t)\, E_s(\mathbf{q},t=0)\, E_s^\star(\mathbf{q},t=0) > . \tag{7.16}$$

The scattered field strength in Eq. (7.12) can be written as a sum over many statistically independent terms, where each term itself is a sum over "clusters"

of interacting particles. The linear dimension of a cluster is the distance over which interactions between particles extends. These clusters of particles are statistically independent. The central limit theorem implies that the scattered electric field strength is a Gaussian variable (with zero average), provided that the scattering volume contains a large number of such independent clusters of particles. According to Wick's theorem for Gaussian-distributed random variables [24], the four-point ensemble average in Eq. (7.16) can thus be written as a sum of products of two-point averages (henceforth we simply write $E_s(0)$ instead of $E_s(t=0)$),

$$\begin{aligned} g_I(\mathbf{q},t) \;\sim\; & < E_s(0)E_s^*(0) >< E_s(t)E_s^*(t) > \\ & + < E_s(0)E_s(t) >< E_s^*(0)E_s^*(t) > \\ & + < E_s(0)E_s^*(t) >< E_s^*(0)E_s(t) > \; . \end{aligned} \tag{7.17}$$

For systems in equilibrium, the first of these terms is nothing but I^2, where I is the mean scattered intensity. Defining the *electric field auto-correlation function* (EACF) g_E as

$$g_E(\mathbf{q},t) \;\equiv < E_s(0)\, E_s^*(t) > , \tag{7.18}$$

the third term in Eq. (7.17) is equal to $\mid g_E \mid^2$. This will turn out to be the interesting quantity in DLS. The second term in Eq. (7.17) is equal to zero for non-zero wavevectors. This can be seen as follows. The second term consists of ensemble averages of the following form

$$< \exp\{i\mathbf{q}\cdot(\mathbf{r}_i(0)+\mathbf{r}_j(t))\} > ,$$

where i and j are either different or equal. Let $P(\mathbf{r}_j,t \mid \mathbf{r}_i,0)$ be the conditional probability density function (pdf) for the position $\mathbf{r}_j$ of particle j at time t, given that the position of particle i at time $t=0$ is $\mathbf{r}_i$. This probability density function is only a function of the difference coordinate $\mathbf{r}_i - \mathbf{r}_j$ for homogeneous systems : $P(\mathbf{r}_j,t \mid \mathbf{r}_i,t=0) \equiv P(\mathbf{r}_i-\mathbf{r}_j,t)$. The ensemble average is then equal to (with $\mathbf{r}' = \mathbf{r}_i(t=0)$ and $\mathbf{r} = \mathbf{r}_j(t)$)

$$\begin{aligned} & < \exp\{i\mathbf{q}\cdot(\mathbf{r}_i(t=0)+\mathbf{r}_j(t))\} > \\ & \quad = \int_{V_s} d\mathbf{r}' \int_{Vs} d\mathbf{r}\, P(\mathbf{r}'-\mathbf{r},t)\, P(\mathbf{r}')\, \exp\{i\mathbf{q}\cdot(\mathbf{r}'+\mathbf{r})\} , \end{aligned}$$

where $P(\mathbf{r}')$ is the equilibrium probability density function for the position coordinate. Since $P(\mathbf{r}') \equiv 1/V_s$ for the homogeneous equilibrium system considered here, this can be written, in the thermodynamic limit (where $V_s \to \infty$

and $\bar{\rho}$ constant) as

$$\frac{1}{8}\left[\lim_{V_s\to\infty}\frac{1}{V_s}\int_{V_s} d(\mathbf{r}'+\mathbf{r})\,\exp\{i\mathbf{q}\cdot(\mathbf{r}'+\mathbf{r})\}\right]\times\int d(\mathbf{r}'-\mathbf{r})\,P(\mathbf{r}'-\mathbf{r},t)\,,$$

where the factor $1/8$ is the Jacobian determinant of the variable transformation

$$(\mathbf{r}',\mathbf{r})\to(\mathbf{r}'+\mathbf{r},\mathbf{r}'-\mathbf{r})\,.$$

The integral with respect to $(\mathbf{r}'-\mathbf{r})$ is well behaved, since the probability density function is a normalized function. The integral between the square brackets is equal to unity for $\mathbf{q}=\mathbf{0}$, and is zero for $\mathbf{q}\neq\mathbf{0}$, since that integral is proportional to the delta distribution of $\mathbf{q}$ (for sufficiently large scattering volumes). Hence, the ensemble average is zero for non-zero wavevectors, so that the second term in Eq. (7.17) does not contribute. The IACF can thus be written in terms of the mean scattered intensity and the EACF (7.18),

$$g_I(\mathbf{q},t)=I^2+\mid g_E(\mathbf{q},t)\mid^2\,. \tag{7.19}$$

This equation is usually referred to as the *Siegert relation*. The IACF is measured, and interpreted through the more simple EACF via the Siegert relation.

7.3. Dynamic structure factors

Several types of dynamic structure factors can be defined, each of which describes a different type of diffusion process. The experimental relevance of these structure factors relates to the Siegert relation (7.19). Substitution of Eq. (7.12) into the definition (7.18) of the EACF leads to

$$g_E(q,t)\;\sim\;\sum_{l,j=1}^{N}<B_l^p(\mathbf{q},t)\,B_j^{p\,\star}(\mathbf{q},0)\exp\{i\,\mathbf{q}\cdot(\mathbf{r}_i(l)-\mathbf{r}_j(0))\}>\,, \tag{7.20}$$

where $\mathbf{r}_j(0)$ is the position coordinate at $t=0$. For brevity, we have introduced,

$$B_j^p(\mathbf{q},t)=\hat{\mathbf{n}}_s\cdot\mathbf{B}_j(\mathbf{q},t)\cdot\hat{\mathbf{n}}_o\,, \tag{7.21}$$

where a superscript "p" is used to indicate that polarization effects are taken into account. Time dependencies are denoted explicitly here. The *collective dynamic structure factor* is now defined as

$$S_c(q,t) = \langle \sum_{l,j=1}^{N} \frac{1}{N} \exp\{i\,\mathbf{q}\cdot(\mathbf{r}_l(t) - \mathbf{r}_j(0))\}\rangle\,. \tag{7.22}$$

This structure factor is proportional to the experimentally obtained EACF, when the scattering amplitudes B_j^p can be omitted in Eq. (7.20). These scattering amplitudes contributes to the EACF due to rotation and possibly fluctuations of internal degrees of freedom of a particle. Rotation and internal degrees of freedom are not probed when either the wave length Λ in Eq. (7.13) is larger than the linear dimensions of the scattering particles, or when the particles are rigid and spherically symmetric. In the latter case, rotation does not change the scattered intensity and internal degrees of freedom that could contribute to scattering are absent. For such cases, the scattering amplitudes can be omitted in Eq. (7.20). It should always be kept in mind, that DLS-data on non-spherical particles at relatively large wavevectors can not be interpreted directly in terms of the collective dynamic structure factor; the time dependence of the latter is solely determined by the translational dynamics of the center-of-mass positions.

The collective dynamic structure factor can be related to density fluctuations as follows. The microscopic density is defined as

$$\rho(\mathbf{r},t) = \sum_{j=1}^{N} \delta(\mathbf{r} - \mathbf{r}_j(t))\,, \tag{7.23}$$

where δ is the Dirac delta distribution. On ensemble averaging the right-hand side, it is easily shown that the macroscopic density is obtained. The Fourier transform of the microscopic density with respect to $\mathbf{r}$ yields

$$\rho(\mathbf{q},t) = \sum_{j=1}^{N} \exp\{i\mathbf{q}\cdot\mathbf{r}_j(t)\}\,, \tag{7.24}$$

where $\mathbf{q}$ is the Fourier variable conjugate to $\mathbf{r}$. The collective dynamic structure factor (7.22) can thus be written as

$$S_c(\mathbf{q},t) = \langle \frac{1}{N}\,\rho(\mathbf{q},t)\,\rho^{\star}(\mathbf{q},0)\rangle\,. \tag{7.25}$$

The collective dynamic structure factor is thus related to collective motion of many particles. In the next Section it will be shown how this structure factor is related to the so-called collective diffusion coefficient, which under certain conditions reduces to the Fickian or gradient diffusion coefficient.

Consider now an experiment on a binary mixture of particles, where one sort of particles is very dilute and one sort possibly concentrated. Suppose that the possibly concentrated species does not scatter any light, that is, their scattering amplitudes B_j^p in Eq. (7.20) are 0. These particles are referred to as *the host particles.* All the scattered intensity originates from the dilute species, the so-called *tracer particles.* The concentration of tracer particles is chosen so small, that they do not mutually interact. The summations in Eq. (7.20) range only over the tracer particles, since the scattering amplitudes are 0 for the host particles. Let us furthermore assume once more, that the wavevector is small enough in order to neglect the contribution of the scattering amplitudes B_j^p. Since the tracer particles do not interact, we then have, for $i \neq j$,

$$< \exp\{i\mathbf{q} \cdot (\mathbf{r}_i - \mathbf{r}_j)\} > = < \exp\{i\mathbf{q} \cdot \mathbf{r}_i\} > < \exp\{-i\mathbf{q} \cdot \mathbf{r}_j\} > . \quad (7.26)$$

Since the exponential functions are equally often positive and negative (for $\mathbf{q} \neq \mathbf{0}$), this ensemble average is 0. For monodisperse tracer particles the EACF is now proportional to the so-called *self-dynamic structure factor,*

$$S_s(q,t) = < \exp\{i\,\mathbf{q} \cdot (\mathbf{r}(t) - \mathbf{r}(0))\} > , \quad (7.27)$$

where $\mathbf{r}(t)$ is the position coordinate of a tracer particle. This structure factor contains information about the dynamics of a single particle, possibly interacting with other particles. Its relation to the mean-square displacement and the so-called self-diffusion coefficient is discussed in the next section.

A third kind of dynamic structure factor, which is of importance, is the *distinct dynamic structure factor* S_d, defined as

$$S_d(q,t) = \langle \frac{1}{N} \sum_{l \neq j=1}^{N} \exp\{i\,\mathbf{q} \cdot (\mathbf{r}_l(t) - \mathbf{r}_j(0))\} \rangle . \quad (7.28)$$

The distinct dynamic structure factor is that part of the collective dynamic structure factor which describes time-correlations between distinct pairs of particles only.

Chapter 8

Heuristic considerations on diffusion processes

For dispersions of rigid colloidal particles in a solvent and for polymer melts, there are three fundamental types of diffusion processes to be distinguished, which are related to translational particle motion: *self-diffusion*, *collective diffusion*, and *exchange* or *interdiffusion* between different particle species. In addition to translational diffusion, the particles or polymers undergo further rotational diffusion which is coupled in general to the translational motion. In this section, we shall discuss each of these diffusion processes on an intuitive level, for a colloidal system of the most simple particle shape: a suspension (i.e. an assembly) of rigid colloidal spheres embedded in a low-molecular-weight fluid (i.e. the solvent) of small molecules as compared to the size of the spheres. The various translational diffusion mechanisms will be further exemplified for binary blends of polymer chains, within time- and length scales accessible to dynamic light scattering.

The basic understanding of diffusion of rigid colloidal spheres is very helpful in improving the understanding of diffusion mechanisms of more complicated non-rigid macromolecules in solution, like polymers and polyelectrolytes, where the fluctuating internal degrees of freedom related to the motion of monomers affect the diffusion properties of the macromolecules. We consider first very dilute colloidal dispersions where the interactions between the colloidal spheres can be disregarded. For this most simple case, only a single diffusion mechanism is present, namely self-diffusion. We then focus on the general case of diffusion in systems of interacting particles.

8.1. Diffusion in very dilute colloidal systems

Translational self-diffusion refers to the random walk of the center of mass of a tagged colloidal sphere (the "tracer particle") in a quiescent and homogeneous suspension caused by thermal collisions with surrounding solvent molecules and other colloidal particles (the so-called "host particles"). For very small sphere concentrations, the dynamics of the colloidal tracer is governed only by the thermal bombardment of the solvent molecules.

The most important quantity that characterizes the translational self-diffusion of the center of mass of a particle is the so-called mean-square displacement $W(t)$ (hereafter abbreviated as MSD), which is defined as

$$W(t) \equiv \frac{1}{2d} <|\mathbf{r}(t) - \mathbf{r}(t=0)|^2> \ . \tag{8.1}$$

Here, $\mathbf{r}(t)$ is the position vector of the center of mass of the tracer sphere at time t, and hence, $\Delta\mathbf{r}(t) \equiv \mathbf{r}(t) - \mathbf{r}(t=0)$ is the sphere displacement during a time interval t. A factor $1/2d$ has been included into the definition of the MSD for later convenience, where d denotes the system dimension. For a homogeneous suspension in thermal equilibrium, the reference time "$t = 0$" is of no significance (stationarity property). The brackets $< \cdots >$ denote, in general, an ensemble averaging.

Suppose that at time $t = 0$ a colloidal tracer sphere in an unbound solvent has a translational velocity $\mathbf{v}_0$. For very short times, say $t \ll \tau_B$, when the sphere velocity has hardly changed under the impact of solvent molecules, $\mathbf{r}(t) - \mathbf{r}(0) \approx \mathbf{v}_0\, t$, and hence,

$$W(t) \sim t^2 , \qquad t \ll \tau_B . \tag{8.2}$$

For times large as compared to the momentum relaxation time τ_B, when the sphere has experienced many collisions with solvent molecules, the MSD has changed into a linear function of time, i.e.,

$$W(t) = D_0\, t , \qquad t \gg \tau_B , \tag{8.3}$$

where D_0 is referred to as the single particle or *Stokes–Einstein* diffusion coefficient.

The time scale τ_B can be inferred from the following reasoning originally due to Langevin. A sphere with velocity $\mathbf{v}$ experiences through the solvent impacts an average friction force that is equal to $-\gamma\,\mathbf{v}$, where γ is referred to

as the friction coefficient, and a fluctuating force $\mathbf{f}(t)$. For a sphere, the friction coefficient γ is given by the Stokes law $\gamma = 6\pi\eta_0 R$, where η_0 is the shear viscosity of the solvent and R is the radius of the sphere. For times large as compared with the mean collision time, τ_s, of solvent molecules (typically, $\tau_s \approx 10^{-13}$ s), the colloidal sphere has experienced many collisions by the solvent molecules. Then the force $\mathbf{f}(t)$ can be described as a Gaussian distributed fluctuating quantity completely characterized by its first and second moments

$$< \mathbf{f}(t) > = 0\,, \qquad < \mathbf{f}(t) \cdot \mathbf{f}(t') > = 2dB\,\delta(t - t')\,. \tag{8.4}$$

Here, $< \cdots >$ is an average over the fast solvent collisions, and B is a measure of the strength of the fluctuating force. In thermal equilibrium, $B = k_B T\gamma$, i.e. the strength is proportional to the temperature and friction coefficient. The delta function in time indicates that, as seen from a coarse-grained time level $t \gg \tau_s$, there is no correlation between solvent impacts at different times.

The Newtonian equation of motion for a Brownian sphere of mass M is thus given, for times $t \gg \tau_s$, by

$$M\,\frac{d\mathbf{v}}{dt} = -\gamma\,\mathbf{v}(t) + \mathbf{f}(t). \tag{8.5}$$

with the solution

$$< \mathbf{v}(t) > = \mathbf{v}_0\,\exp\left\{-\frac{\gamma}{M}\,t\right\} \tag{8.6}$$

for the solvent-collision-averaged velocity. As seen, the velocity remains on average almost equal to the initial velocity $\mathbf{v}_0$ for times $t \ll M/\gamma$, which sets the time scale

$$\tau_B \equiv \frac{M}{\gamma} = \frac{M}{6\pi\eta_0 R} \tag{8.7}$$

for the average velocity relaxation of a colloidal sphere. For times $t \gg \tau_B$, the average velocity of a tagged particle decays towards zero. Using typical values for aqueous colloidal dispersions, one finds that $\tau_B \approx 10^{-8} \div 10^{-9}$ s, so that $\tau_B \gg \tau_s$.

So far we have considered the Brownian motion of a sphere with given *fixed* initial velocity $\mathbf{v}_0$. In dynamic light scattering experiments, an additional average is performed with respect to a Maxwellian distribution of initial particle velocities since light is scattered from many spheres in thermal

equilibrium. Multiplication of Eq. (8.5) by $\mathbf{v}_0$ and subsequent averaging over solvent collisions *and* initial velocities gives

$$\phi_v(t) \equiv \frac{1}{d} < \mathbf{v}(t) \cdot \mathbf{v}(0) > = \frac{k_B T}{M} \exp\left\{-\frac{t}{\tau_B}\right\} \tag{8.8}$$

for the velocity auto-correlation function (VAF), $\phi_v(t)$, of an isolated Brownian sphere. Here and in the following, $< \cdots >$ means a full equilibrium ensemble average. Due to equipartition of energy at equilibrium, $< \mathbf{v}^2(t) > = dk_B T/M$. Using that $\mathbf{r}(t) - \mathbf{r}_0 = \int_0^t dt' \mathbf{v}(t')$ one can easily show for stationary systems that $\phi_v(t)$ is related to the MSD by

$$W(t) = \int_0^t du\,(t-u)\,\phi_v(u)\,. \tag{8.9}$$

This relation is valid also for non-dilute system of interacting particles. The MSD of an isolated sphere follows from the substitution of Eq. (8.8) into Eq. (8.9) as

$$W(t) = D_0 t \left[1 - \frac{\tau_B}{t}\left(1 - e^{-t/\tau_B}\right)\right] \rightarrow \begin{cases} \frac{k_B T}{2M}\, t^2\,, & \tau_c \ll t \ll \tau_B\,, \\ D_0\, t\,, & t \gg \tau_B\,, \end{cases} \tag{8.10}$$

where D_0 is related to the friction coefficient by the Stokes–Einstein relation

$$D_0 = \frac{k_B T}{\gamma}\,. \tag{8.11}$$

Equation (8.10) interpolates between random ballistic flight for $t \ll \tau_B$ and linear diffusive behavior for $t \gg \tau_B$.

The sphere displacement $\Delta\mathbf{r}(t)$ during time t is a Gaussian random variable, since it is linearly related to $\mathbf{v}(t)$ and to $\mathbf{f}(t)$. The probability density function, $P(\Delta\mathbf{r}, t)$, for such a displacement is thus

$$P(\Delta\mathbf{r}, t) = \{4\pi\, W(t)\}^{-d/2} \exp\{-\frac{(\Delta\mathbf{r})^2}{4W(t)}\} \tag{8.12}$$

with

$$W(t) = \frac{1}{2d} \int d\mathbf{r}^d\, P(\Delta\mathbf{r}, t)\, (\Delta\mathbf{r})^2\,. \tag{8.13}$$

The probability density function is the solution of the diffusion-like equation

$$\frac{\partial}{\partial t} P(\Delta \mathbf{r}, t) = \mathcal{D}(t) \nabla^2 P(\Delta \mathbf{r}, t) , \tag{8.14}$$

where

$$\mathcal{D}(t) \equiv \frac{d}{dt} W(t) = D_0 \left[1 - e^{-t/\tau_B} \right] , \tag{8.15}$$

subject to the initial condition $P(\Delta \mathbf{r}, t = 0) = \delta(\Delta \mathbf{r})$. The latter follows from Eq. (8.12) specialized to $t = 0$. Here, ∇ is the d-dimensional gradient operator. Knowing the probability density function we can calculate from Eq. (8.12) the self-dynamic structure factor

$$S_s(q, t) = \int d(\Delta \mathbf{r})\, e^{i\mathbf{q}\cdot\Delta\mathbf{r}}\, P(\Delta \mathbf{r}, t) = \exp\{-q^2\, W(t)\} , \tag{8.16}$$

which, for uncorrelated spheres, depends on time only through $W(t)$. Note that for the dilute dispersions of uncorrelated particles considered here the collective dynamic structure factor $S_c(q, t)$ reduces to the self-dynamic one.

In typical dynamic light scattering experiments on colloidal suspensions, times $t > 10^{-6}\,\mathrm{s} \gg \tau_B$ and hence distances large compared to $(D_0 \tau_B)^{1/2}$ are resolved. In this so-called diffusive regime, Eq. (8.14) reduces to the one-particle diffusion equation

$$\frac{\partial}{\partial t} P(\Delta \mathbf{r}, t) = D_0 \nabla^2 P(\Delta \mathbf{r}, t) , \tag{8.17}$$

which has Eq. (8.12) specialized to $W(t) = D_0\, t$ as its fundamental solution. The diffusion Eq. (8.17) is statistically equivalent to the overdamped Langevin equation

$$\mathbf{v}(t) = \frac{1}{\gamma}\, \mathbf{f}(t) , \tag{8.18}$$

and $\mathbf{f}$ according to Eq. (8.4), which expresses a force balance, i.e an inertia-free sphere motion for times $t \gg \tau_B$.

In fact, Brownian motion of a colloidal particle is adequately described by the Langevin Eq. (8.5) with δ-correlated random force only when solvent inertia is negligible, i.e. for times $t \gg \tau_B$ only, where it reduces to Eq. (8.18). The Langevin equation disregards, for shorter times $t \approx \tau_B$, the feedback on the particle velocity from the surrounding solvent. The solvent can not

instantaneously follow the changes in the particle velocity. Through the retarded response of the solvent, the sphere velocity is influenced by its values at earlier times. This leads to an enlarged persistence in the velocity autocorrelations. These solvent memory effects on the sphere velocity can be adequately described, for $d = 3$, by the retarded (one-particle) Langevin equation

$$M \frac{d\mathbf{v}}{dt} = - \int_{-\infty}^{t} du\, \gamma(t-u)\, \mathbf{v}(u) + \mathbf{f}(t)\,, \tag{8.19}$$

which includes a time-dependent friction function $\gamma(t)$ obeying a generalized fluctuation-dissipation relation

$$< \mathbf{f}(t) \cdot \mathbf{f}(t') > = 3k_B T\, \gamma(t-t')\,. \tag{8.20}$$

The random force in the retarded Langevin equation is still Gaussian, however it is now correlated for different times, due to cooperative effects of the fluid motion. The friction function can be calculated, for times $t \gg \tau_s$, using macroscopic equations of motion for the solvent flow. Substitution of the hydrodynamically determined $\gamma(t)$ into the retarded Langevin equation results in closed expressions for the MSD and $\phi_V(t)$. We only quote the asymptotic forms valid for $t \gg \tau_\eta$, viz. [29, 31, 30]

$$W(t) \approx D_0 t \left[1 - \frac{2}{\sqrt{\pi}} \left(\frac{\tau_\eta}{t}\right)^{1/2}\right] \tag{8.21}$$

and

$$\phi_v(t) = \frac{d^2}{dt^2} W(t) \approx \frac{1}{9\sqrt{\pi}} \frac{k_B T}{m} \left(\frac{t}{\tau_\eta}\right)^{-3/2}, \tag{8.22}$$

where $\tau_\eta = a^2 \rho_s / \eta_0 = (9/2)(\rho_s/\rho_M)\tau_B$ is the time needed for a viscous shear wave in the solvent of mass density ρ_s to diffuse across a particle radius. The mass density, ρ_M, of colloidal particles is close to ρ_s, and τ_η and τ_B are thus of the same order of magnitude.

The positive feedback of the solvent flow on the sphere velocity implies an algebraic rather than exponential decay of the VAF. Moreover, the algebraic approach of the single-particle MSD to its long-time-limiting form $W(t) = D_0 t$ is much slower than prediced by Eq. (8.10). The occurrence of an algebraic decay in an auto-correlation function is generally referred to as a

long-time tail. An algebraic tail proportional to $t^{-1/2}$ in $W(t)$ was indeed observed in dynamic light scattering experiments on very large colloidal spheres (since $\tau_B \propto a^2$) through the measurement of $S_s(q,t)$ and using Eq. (8.16) to infer $W(t)$ [32]. While the non-retarded Langevin equation does not describe dilute colloidal dispersions for times $t \approx \tau_B$, it can be applied instead for $t \approx \tau_B$ to aerosols like dust or smoke particles in air, since for these systems one has $\rho_s \ll \rho_M$ and hence $\tau_\eta \ll \tau_B$.

The surrounding solvent molecules exert in addition to a random force a random torque, $\mathbf{f}_r(t)$, on the colloidal sphere, which causes a rotational Brownian motion of its angular velocity $\boldsymbol{\omega}(t)$. Neglecting solvent inertia, the erratic sphere rotation can be described in analogy to translational motion by a rotational Langevin equation, given for $d = 3$ and $t \gg \tau_s$ by

$$M_r \frac{d\boldsymbol{\omega}}{dt} = -\gamma_r \boldsymbol{\omega}(t) + \mathbf{f}_r(t)\,, \tag{8.23}$$

with a stochastic torque of zero mean and δ-correlated covariance

$$< \mathbf{f}_r(t) \cdot \mathbf{f}_r(t') > = 6k_BT\gamma_r\,\delta(t-t')\,. \tag{8.24}$$

According to this Langevin equation, the solvent-collisions-averaged angular velocity and the equilibrium angular VAF are, respectively,

$$< \boldsymbol{\omega}(t) > = \boldsymbol{\omega}_0 \exp\left\{-\frac{t}{\tau_B^r}\right\} \tag{8.25}$$

and

$$\phi_\omega(t) \equiv \frac{1}{3} < \boldsymbol{\omega}(t) \cdot \boldsymbol{\omega}(0) > = \frac{k_BT}{M_r} \exp\left\{-\frac{t}{\tau_B^r}\right\} \tag{8.26}$$

with the damping time

$$\tau_B^r = \frac{M_r}{\gamma_r}\,. \tag{8.27}$$

Here, $\gamma_r = 8\pi\eta_0 a^3$ is the so-called Stokes-Debye friction coefficient of a freely rotating sphere, and $M_r = (2/5)Ma^2$ is the moment of inertia of a homogeneous sphere. The damping times for the translational and rotational velocity are of the same order of magnitude, since $\tau_B^r = (3/10)\tau_B$.

When the hydrodynamic solvent-sphere coupling is accounted for through a time-dependent rotational friction function similar to the translational case,

the exponential decay of the rotational VAF is changed for times $t \gg \tau_\eta$ into the power-law decay [33, 34]

$$\phi_\omega(t) \approx \frac{1}{60\sqrt{\pi}} \frac{k_B T}{M_r} \left(\frac{t}{\tau_\eta}\right)^{-5/2}, \tag{8.28}$$

which is one power in t faster than the asymptotic decay of the translational VAF. Depolarized dynamic light scattering is a convenient experimental tool to measure rotational Brownian motion of optically anisotropic spheres in the diffusive regime $t \gg \tau_B$. As mentioned in Sec. 7.1, the polarizability, $\boldsymbol{\alpha}$, of an optically anisotropic uniaxial sphere is a tensor

$$\boldsymbol{\alpha}(\hat{\mathbf{u}}) = \alpha_\parallel \, \hat{\mathbf{u}}\hat{\mathbf{u}} + \alpha_\perp \, (\mathbf{1} - \hat{\mathbf{u}}\hat{\mathbf{u}}) = \alpha \, \mathbf{1} + \beta \left(\hat{\mathbf{u}}\hat{\mathbf{u}} - \frac{1}{3}\mathbf{1}\right), \tag{8.29}$$

where $\alpha_\parallel$ and $\alpha_\perp$ are the incremental (relative to the solvent) polarizabilities parallel and perpendicular to the optical axis of the sphere, with $\alpha = (\alpha_\parallel + 2\alpha_\perp)/3$ and $\beta = \alpha_\parallel - \alpha_\perp$, and $\hat{\mathbf{u}}(t)$ is the unit orientation vector pointing along the optical axis. The orientation vector is related to the angular velocity of the sphere by $\boldsymbol{\omega}(t) = \hat{\mathbf{u}}(t) \times (d/dt)\hat{\mathbf{u}}(t)$.

In depolarized dynamic light scattering, the polarization of the incident electric light field is chosen perpendicular to the scattering plane spanned by the incident and detected light beam (i.e. $\hat{\mathbf{n}}_0 = \hat{\mathbf{n}}_V$), and one detects the in-plane component (i.e. $\hat{\mathbf{n}}_s = \hat{\mathbf{n}}_H$) of the scattered electric field. In this VH-geometry

$$\hat{\mathbf{n}}_s \cdot \boldsymbol{\alpha}(\hat{\mathbf{u}}) \cdot \hat{\mathbf{n}}_0 = \beta \left(\frac{2\pi}{15}\right)^{1/2} [Y_{2,1}(\hat{\mathbf{u}}) + Y_{2,-1}(\hat{\mathbf{u}})], \tag{8.30}$$

where $Y_{2,m}$ is a second order spherical harmonic function. Together with Eq. (7.15), this results in the EACF [26]

$$g_E^{VH}(q,t) \propto \beta^2 \, S_s(q,t) \, S_r(t), \tag{8.31}$$

where we have introduced the rotational self-dynamic correlation function

$$S_r(r) = 4\pi < Y_{2,-1}(\hat{\mathbf{u}}(0)) \, Y_{2,1}(\hat{\mathbf{u}}(t)) > = < P_2(\hat{\mathbf{u}}(t) \cdot \hat{\mathbf{u}}(0)) >, \tag{8.32}$$

which includes information on the rotational diffusion. The second equality follows from spatial isotropy, i.e. from the m-independence of $S_r(t)$, with P_2 denoting here the second-order Legendre polynomial (no to be confused

with a two-particle probability density function). In deriving Eq. (8.32), it has been assumed that the rotational motion of a sphere is decoupled from the translational motion for all $t \gg \tau_B$. While this decoupling is strictly valid for dilute dispersions of non-interacting spheres, it is an approximation for non-spherical particles and for concentrated sphere dispersions. Note that $\beta = 0$ for optically isotropic spheres. Then there is no depolarized scattered light as long as multiple light scattering is negligibly small.

The function $S_s(q,t)$ of non-interacting spheres can be calculated for $t \gg \tau_B$ from the rotational diffusion equation (Debye equation)

$$\frac{\partial}{\partial t} P_1(\hat{\mathbf{u}},t) = D_0^r \, \hat{\mathbf{L}}^2 \, P_1(\hat{\mathbf{u}},t) \,, \tag{8.33}$$

which determines the single-sphere probability density function $P_1(\hat{\mathbf{u}},t)$ of finding the sphere with orientation $\hat{\mathbf{u}}$ at time t. We have introduced here the diffusion coefficient of a single and freely rotating sphere, related to the rotational friction coefficient by the Einstein-Debye relation

$$D_0^r = \frac{k_B T}{\gamma_r} \,. \tag{8.34}$$

The Debye equation is the analogue of the translational diffusion Eq. (8.17), with $\hat{\mathbf{L}} = \hat{\mathbf{u}} \times \partial/(\partial \hat{\mathbf{u}})$ denoting the gradient operator in orientation space. It describes the random walk of the tip of $\hat{\mathbf{u}}(t)$ on the unit sphere. Eq. (8.33) has the fundamental solution [26]

$$P_1(\hat{\mathbf{u}},t|\hat{\mathbf{u}}_0) = \sum_{l=1}^{\infty} \sum_{m=-l}^{l} Y_{lm}(\hat{\mathbf{u}}) \, Y_{l,-m}(\hat{\mathbf{u}}_0) \, \exp\{-l(l+1) D_0^r \, t\} \,, \tag{8.35}$$

which is the probability density for a sphere to have orientation $\hat{\mathbf{u}}$ at time t given that it had orientation $\hat{\mathbf{u}}_0$ at initial time $t = 0$. The rotational function $S_r(t)$ is then calculated as

$$S_r(t) = \int d\hat{\mathbf{u}} \int d\hat{\mathbf{u}}_0 \, Y_{2,1}(\hat{\mathbf{u}}) \, Y_{2,-1}(\hat{\mathbf{u}}_0) P_1(\hat{\mathbf{u}},t|\hat{\mathbf{u}}_0) = \exp\{-6 D_0^r t\} \tag{8.36}$$

where we have employed the orthogonality relations of the spherical harmonics. As a consequence, the depolarized EACF of non-interacting sphere dispersions is

$$g_E^{VH}(q,t) \propto \beta^2 \, \exp\left\{-\left(q^2 D_0 + 6 D_0^r\right) t\right\} \,. \tag{8.37}$$

One can determine D_0 and D_0^r simultaneously from the EACF by plotting the time derivative of $-\ln g_E^{VH}(q,t)$ versus q^2, yielding a straight line of slope D_0 and intercept D_0^r. Plots of this kind are shown in Fig. 8.1 for depolarized DLS experiments on a dilute dispersion of anisotropic teflon spheres [35]. The particle diameters determined from D_0 and D_0^r, respectively, are indeed nearly identical.

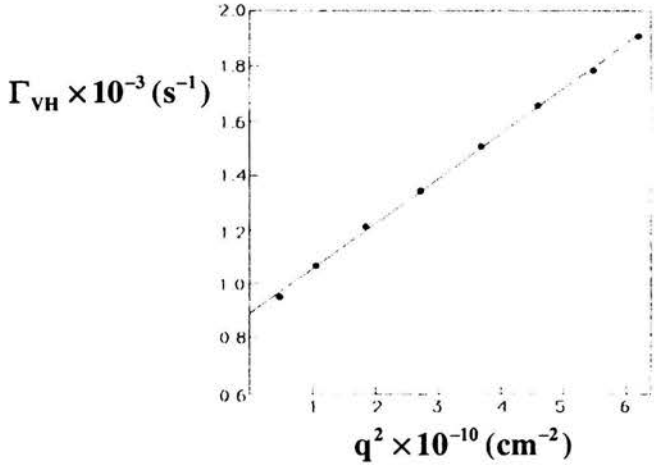

FIGURE 8.1. Initial decay rate $\Gamma_{VH} = -\lim_{t\to 0}(d/dt)\ln g_E^{VH}(q,t)$ of depolarized EACF versus q^2, for a dilute dispersion of anisotropic teflon spheres ($\Phi = 0.02$). After [35].

From employing the fundamental solution, one can further calculate the orientation auto-correlation function

$$< \hat{\mathbf{u}}(t) \cdot \hat{\mathbf{u}}(0) > = \exp\{-t/\tau_r\} \tag{8.38}$$

and the orientation MSD [36]

$$< [\hat{\mathbf{u}}(t) - \hat{\mathbf{u}}(0)]^2 > = 2\left[1 - e^{-t/\tau_r}\right] \rightarrow \begin{cases} 4D_0^r\, t\,, & \tau_B^r \ll t \ll \tau_r\,, \\ 2\,, & t \gg \tau_r\,, \end{cases} \tag{8.39}$$

where $\tau_r = 1/(2D_0^r)$ is the orientation relaxation time. The tip of $\hat{\mathbf{u}}(t)$ performs, for $t \ll \tau_r$, a two-dimensional random walk on the tangential surface touching the unit sphere at $\hat{\mathbf{u}}_0$. The MSD saturates to 2 for times $t \gg \tau_r$, since $|\hat{\mathbf{u}}(t) - \hat{\mathbf{u}}(0)| \leq 2$ for all t. Typical values of τ_r are $10^{-4} \div 10^{-3}$ s which implies the following sequence of time scale separations

$$\tau_s \ll \tau_\eta \approx \tau_B \approx \tau_B^r \ll \tau_r \tag{8.40}$$

valid for the translational/orientational self-diffusion of non-interacting globular particles

8.2. Diffusion in concentrated colloidal systems

While the diffusion of a non-interacting sphere is completely described by its MSD, which is linear in time in the diffusive time regime $t \gg \tau_B$, various diffusion processes have to be distinguished in non-dilute dispersions of interacting colloidal spheres. These diffusion processes are controlled by different diffusion coefficients, which become equal to each other only in the dilute limit when the sphere interactions can be ignored. The spheres influence each other indirectly through the solvent flow field in which they move. These so-called hydrodynamic interactions (HI) propagate on a time scale $\tau_\eta \approx \tau_B$, so that they act quasi-instantaneously on the diffusive time scale where the fast momentum relaxations of the spheres are not resolved any more. HI affects the sphere dynamics but not the equilibrium microstructure, since as dissipative forces they are not describable in terms of an interaction potential. In addition to the HI, the spheres can have potential interactions with each other through excluded volume, van der Waals and screened electrostatic forces. These direct forces become operative on the interaction time scale τ_I, which is the time after which a particle experiences a substantial change of the potential interactions through a perceptible change in its next neighbor sphere configuration. Very roughly, τ_I can be estimated for a fluid-like suspension as the time needed for a sphere to diffuse across its own radius, viz.

$$\tau_I \approx \frac{a^2}{D_0}, \tag{8.41}$$

with typical values of $10^{-4} \div 10^{-3}$ s. The short-time regime $\tau_B \ll t \ll \tau_I$, for DLS is thus well separated from the long-time regime $t \gg \tau_I$.

Self-diffusion

For short times $\tau_B \ll t \ll \tau_I$, a sphere diffuses only over a distance small as compared to its own size, and the dynamic "cage" of neighboring spheres has thus hardly changed (as sketched in the left part of Fig. 8.2). The sphere diffuses then, on the average, in a potential minimum of the neighboring particles and is thus influenced only by the instantaneously acting HI. A linear

increase

$$W(t) = D_s^s\, t \qquad \tau_B \ll t \ll \tau_I \tag{8.42}$$

of the MSD is thus observed at short times, with a *short-time* self-diffusion coefficient, D_s^s, smaller than the Stokesian diffusion coefficient, D_0, at infinite dilution, owing to the slowing influence of HI. Note that the subscript s in D_s^s stands for "self" and the superscript for "short". At intermediate times $t \approx \tau_I$, the cage becomes distorted from its equilibrium spherical symmetry and the sphere experiences an additional hindrance by potential forces. The cage distortion implies a sub-linear time dependence of $W(t)$. For long times $t \gg \tau_I$, a sphere has experienced many independent collisions with neighboring spheres, as sketched in the right part of Fig. 8.2.

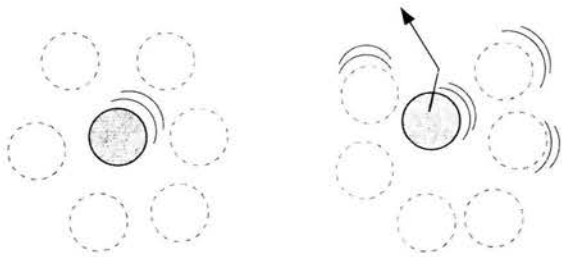

FIGURE 8.2. Schematic view of a particle cage around a colloidal sphere for short times $\tau_B \ll t \ll \tau_I$ (left), and long times $t \gg \tau_B$ (right).

This leads again to a linear time dependence of $W(t)$

$$W(t) = D_s^l\, t\,, \qquad t \gg \tau_I\,, \tag{8.43}$$

but with a *long-time* self-diffusion coefficient, D_s^l, smaller than the short-time one. Summarizing,

$$0 \le D_s^l \le D_s^s \le D_0\,, \tag{8.44}$$

and one can show that this ordering is valid independent of the type of potential interactions. All three diffusion coefficients are equal to D_0 in the absence of interactions only, whereas D_s^l is substantially smaller than D_0 for strongly interacting particles. On approach of a glass-transition point, a particle gets eventually trapped in its next-neighbor cage, with a complete blocking of its long-range motion characterized by $D_s^l \approx 0$ (idealized glass

transition scenario). In contrast, $D_s^s > 0$ since a sphere in a glass can still perform short-time Brownian motion within its cage.

Using Eq. (8.9), D_s^l can be expressed as a Green–Kubo relation

$$D_s^l = \int_0^\infty dt\, \phi_v(t)\,, \tag{8.45}$$

i.e. in form of a time integral over the VAF. On the coarse-grained level $t \gg \tau_B$, the VAF

$$\phi_v(t) = 2D_s^s\delta(t) - \Delta\phi_v(t) \tag{8.46}$$

of interacting spheres consists of a singular part proportional to D_s^s, such that Eq. (8.42) is retained from Eq. (8.9), and a long-lived negative part, $-\Delta\phi_v(t)$, originating from particle interactions (caging). One can show that $\Delta\phi_v(t) > 0$ and $(d/dt)\Delta\phi_v(t) < 0$, consistent with $D_s^l < D_s^s$. The regular part of the VAF is thus negative and increases strictly monotonically towards its final value zero. As one expects intuitively, the collective retarding effect of neighboring spheres leads to anti-correlations in the particle velocity. The positive-valued singular part in the VAF is the residual of the fast initial decay of velocity correlations mediated through the intervening solvent. The initial decay of the VAF manifests itself as a δ-function for times $t \gg \tau_B$ (see Fig. 8.3).

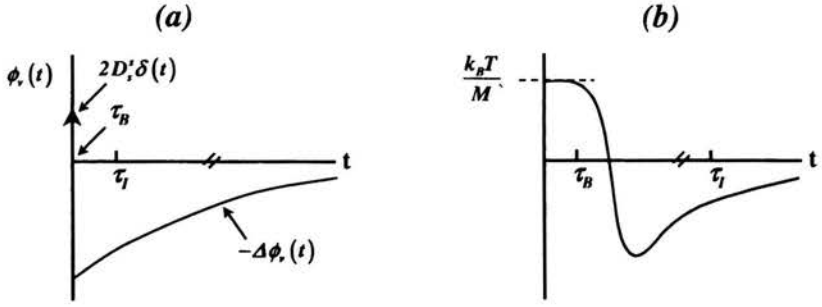

FIGURE 8.3. Schematic VAF in: (a) the diffusive regime $t \gg \tau_B$, and (b) at very short times so that the initial δ-peak is resolved.

Substitution of Eq. (8.46) into Eq. (8.9) gives

$$W(t) = D_s^l t + \tau_m\left(D_s^s - D_s^l\right) - \int_t^\infty du(u-t)\Delta\phi_v(u)\,, \tag{8.47}$$

where

$$\tau_m \equiv \frac{\int_0^\infty dt\; t\; \Delta\phi_v(t)}{\int_0^\infty dt\; \Delta\phi_v(t)} \tag{8.48}$$

is the mean relaxation time of $\Delta\phi_v(t)$. It is roughly comparable to τ_I. The last term on the right-hand-side of Eq. (8.47) is the difference between $W(t)$ and its long-time asymptote. The asymptote crosses the vertical axis at the point $\tau_m \left(D_s^s - D_s^l\right)$. A remarkable feature of $W(t)$ is that the approach towards its long-time form in Eq. (8.43) is very slow. In three dimensions, the VAF of a suspension of hard colloidal spheres has a negative long-time tail [37]

$$\phi_v(t) = -\Delta\phi_v(t) \approx -A\left(\frac{t}{\tau_m}\right)^{-5/2}, \quad t \gg \tau_m\,, \tag{8.49}$$

with an amplitude $A > 0$ that depends on the sphere concentration. The MSD for large t is consequently

$$W(t) \approx D_s^l t + \tau_m \left(D_s^s - D_s^l\right)\left[1 - \left(\frac{t}{\tau_l}\right)^{-1/2}\right] + \mathcal{O}(t^{-1})\,, \tag{8.50}$$

where τ_l is a typical time scale related to τ_m. Fig. 8.4 displays a sketch of a three-dimensional MSD.

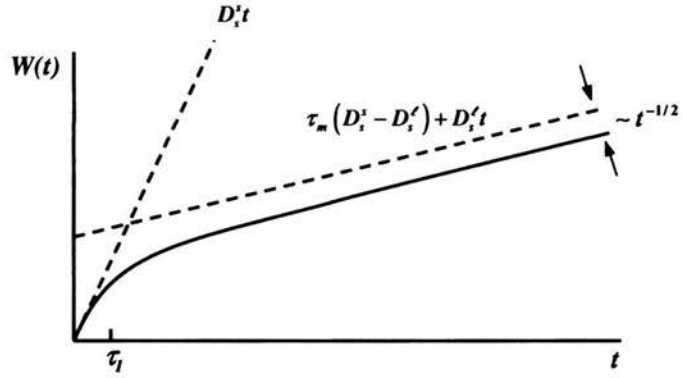

FIGURE 8.4. Mean-square displacement in three dimensions (for $t \gg \tau_B$).

The relaxation of the VAF becomes extremely slow in two dimensions where $\phi_v(t)$ decays asymptotically as t^{-2} for all concentrations, independent of the nature of the interactions. Therefore, the two-dimensional MSD

includes a logarithmic long-time correction [38]

$$W(t) \approx D_s^l t + \tau_m \left(D_s^s - D_s^l\right) \ln\left(\frac{t}{\tau_l}\right) + \mathcal{O}(1) \tag{8.51}$$

with diffusion coefficients and decay times different from the three-dimensional case. We emphasize that the negative VAF long-time tails discussed above are due to configurational rearrangements of interacting spheres, and they should not be confused with the positive long-time tail in Eq. (8.22). The latter is due to unsteady solvent flow around a sphere in isolation, and appears on a much shorter time scale $t \approx \tau_\eta$.

The long-time decay of the VAF in one dimension is proportional to $-t^{-(d+2)/2}$, with d specialized to one. For particles diffusing along an infinite line which are not allowed to pass each other (single-filing condition) there is, however, a subtle difference to diffusion in higher dimensions. Due to the strong mutual hindrance of particles moving along a line the MSD at long times grows only proportional to $t^{1/2}$. Without HI, the MSD reads thus explicitly [39]

$$W(t) \to \begin{cases} 2D_0 t\,, & \tau_B \ll t \ll \tau_I\,, \\ \dfrac{1}{n}\left(\dfrac{4D_0 t}{\pi}\right)^{1/2}, & t \gg \tau_I, \end{cases} \tag{8.52}$$

with n denoting the line density of particles and interaction time $\tau_I = 1/(D_0 n^2)$. It is most likely that only the pre-factor of $t^{1/2}$ will be affected when HI is included. The long-time limiting form of the probability density function, $P(x,t)$, for a particle displacement x during time t is given by the Gaussian form in Eq. (8.12) for $d = 1$, with $W(t)$ according to Eq. (8.52) for $t \gg \tau_I$. The absence of a linear long-time term in $W(t)$ implies a vanishing long-time self-diffusion coefficient for an infinite line. Single-file diffusion can be observed, e.g., in superionic conduction, in diffusion of bio-molecules through narrow-sized channels in membranes, and in the channel arrays of crystalline nanoporous materials (zeolites).

Self-diffusion coefficients can be measured by a variety of techniques including NMR, isotope labelling, light scattering experiments with partial refractive index matching, and by means of specialized techniques that use fluorescently labelled spheres. In the following, we restrict ourselves to dynamic light scattering. To measure self-diffusion over an extended time range the system now consists of a possibly concentrated suspension of host spheres,

with a few tracer spheres, such that the tracer spheres do not mutually interact with each other. The system must be prepared such, that the scattered intensity from the host particles and the solvent molecules can be neglected against that of the tracer particles. As explained in Sec. 7.2, the measured EACF is proportional to the self-dynamic structure factor $S_s(q,t)$ defined in Eq. (7.27), provided tracer and host spheres are different from each other only in terms of their scattering properties. The self-dynamic structure factor may be expanded in a Taylor series for small wavevectors,

$$S_s(q,t) = 1 - \frac{1}{6}q^2 <|\mathbf{r}(t=0) - \mathbf{r}(t)|^2> + \mathcal{O}(q^4)\,, \tag{8.53}$$

meaning that

$$S_s(q,t) = \exp\{-q^2 W(t)\}\left[1 + \mathcal{O}(q^2)\right]\,. \tag{8.54}$$

There is a time-dependent non-Gaussian correction of $\mathcal{O}(q^2)$ to $S_s(q,t)$ originating from particle interactions. This correction is rather small for a fluid-like suspension and becomes zero when the small-q limit is considered. Equation (8.54) allows for measuring the full time dependence of the MSD. To this end, $-\ln\{S_s(q,t)\}/q^2$ is plotted for a given time t against q^2, and linearly extrapolated to $q = 0$. The intercept is equal to $W(t)$. Such data

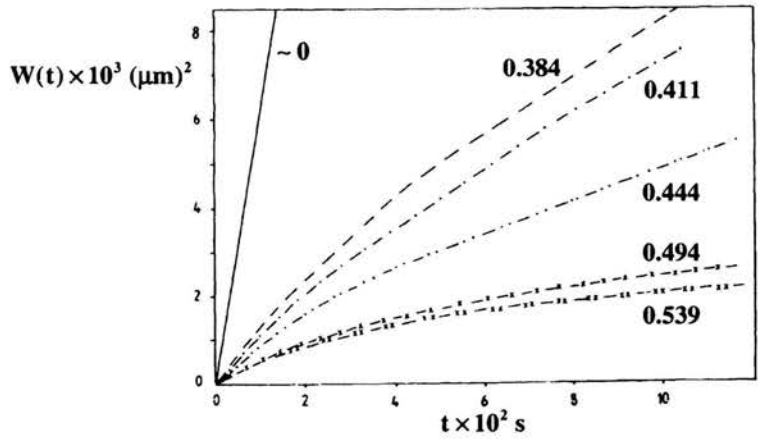

FIGURE 8.5. Mean-square displacement $W(t)$ of silica tracer spheres in an index-matched host suspension of PMMA spheres (of same size as the silica particles). The curves are labelled by volume fraction Φ. The last two volume fractions represent the co-existing fluid ($\Phi_{freez} \approx 0.494$) and crystalline ($\Phi_{melt} \approx 0.539$) phases. After [40].

obtained from dynamic light scattering experiments on hard-sphere suspensions are given in Fig. 8.5, for various volume fractions [40]. The cross-over from short- to long-time behavior is clearly seen. Further note the diminishing difference between the short- and long-time self-diffusion coefficients when the concentration is decreased.

At infinite dilution, $D_s^s = D_0$, $W(t) = D_0 t$ and, hence

$$S_s(q,t) = \exp\{-q^2 D_0 t\}\,, \tag{8.55}$$

i.e. $S_s(q,t)$ reduces to the single-sphere dynamic structure factor of independent particles.

Collective diffusion

In contrast to self-diffusion, which is the Brownian motion of a tagged particle in a sea of others, collective diffusion refers to the isothermal relaxation of density gradients by the coordinated motion of many colloidal particles. Imagine a colloidal system where the density of colloidal particles, at some instant in time, varies sinusoidally (such a sinusoidal density profile is referred to as a *density wave* or *density mode*). That is, at time $t = 0$ say, the number density $\overline{\rho}(\mathbf{r}, t = 0)$ at position $\mathbf{r}$ is equal to

$$\overline{\rho}_q(\mathbf{r}, t = 0) = \rho_0 + \overline{\rho}(\mathbf{q}, t = 0)\, \sin\{\mathbf{q} \cdot \mathbf{r}\}\,, \tag{8.56}$$

with $\rho_0 = N/V$ the average number density, and $\overline{\rho}(\mathbf{q}, t = 0)$ the amplitude of the density wave. The bar indicates an ensemble average over a non-equilibrium initial particle distribution. The wavevector $\mathbf{q}$ determines both the direction and wave length of the sinusoidal density variation. For changes of the position $\mathbf{r}$ in the suspension perpendicular to $\mathbf{q}$, the phase of the sine function does not change, so that the direction of $\mathbf{q}$ is in the "propagation direction" of the sinusoidal variation. A change $\Delta\mathbf{r}$ of the position $\mathbf{r}$ parallel to $\mathbf{q}$ leaves the sine function unchanged when $|\Delta\mathbf{r}| = m \times 2\pi/q$, with m an arbitrary integer. Hence, the wave length of the density variation is

$$\Lambda = 2\pi/q\,. \tag{8.57}$$

The density wave will relax away to the homogeneous state due to the collective motion of particles. In the initial stage of relaxation (i.e. for $\tau_B \ll t \ll \tau_I$), the decay of the density wave is single exponential in time. At

a later stage ($t \approx \tau_I$), the decay becomes non-exponential and slower than initially as a result of interactions between the colloidal particles. In the final long-time regime ($t \gg \tau_I$), the density variation may decay once again exponentially in time for selected values of q, however with a decay rate that is usually smaller than the initial one. For a density wave of large amplitude, different wave lengths come into play at a later stage and its shape is then no longer sinusoidal. Long-time collective diffusion describes the final stage of relaxation of a density wave, where the density profile generally strongly deviates from a sinusoidal profile.

A phenomenological description of the relaxation of density waves can be accomplished by using what is known as generalized hydrodynamics. The starting point in a generalized hydrodynamic description is the continuity equation

$$\frac{\partial}{\partial t}\,\overline{\rho}(\mathbf{r},t) = -\nabla\cdot\overline{\mathbf{j}}(\mathbf{r},t)\,, \tag{8.58}$$

which relates the particle density to the particle flux density, $\overline{\mathbf{j}}(\mathbf{r},t)$, and it expresses the conservation of the number of particles. The overbar indicates an average over a non-equilibrium ensemble. The flux density $\overline{\mathbf{j}}(\mathbf{r},t)$ denotes the number of colloidal particles that cross the point $\mathbf{r}$ in the direction in which $\overline{\mathbf{j}}$ points, per unit area and unit time.

For small amplitudes in the density variation, and close to thermal equilibrium, the flux is linearly related to gradients in the density, that is (note that at time $t = 0$ relaxation begins)

$$\overline{\mathbf{j}}(\mathbf{r},t) = -\int d\mathbf{r}' \int_0^t dt'\, \boldsymbol{D}_c(\mathbf{r}-\mathbf{r}', t-t')\cdot\nabla'\overline{\rho}(\mathbf{r}',t')\,, \tag{8.59}$$

where the integral kernel tensor $\mathbf{D}_c(\mathbf{r},t)$ is referred to as the real-space *collective diffusion kernel*. This phenomenological expression can be interpreted as the leading term in an expansion of the flux $\overline{\mathbf{j}}$ with respect to the amplitude of density gradients. The "Taylor coefficient" $\mathbf{D}_c$ is independent of the magnitude of gradients whenever these are sufficiently small. Density modes of different wave numbers decay then independently from each other due to linearity in $\overline{\rho}(\mathbf{r},t)$. The non-local space- and time dependence of $\overline{\mathbf{j}}$ on $\nabla\overline{\rho}$ can be understood as follows. The flux at a point $\mathbf{r}$ can depend on density gradients at another point $\mathbf{r}'$, through interactions between the spheres. Hence, $\boldsymbol{D}_c(\mathbf{r}-\mathbf{r}', t-t') = 0$ when $|\mathbf{r}-\mathbf{r}'| \gg R_I$, where R_I is a measure for the distance

over which colloidal particles are correlated. Moreover, the flux at time t can depend on $\nabla\overline{\rho}$ at earlier times, due to the finite time it takes interactions to propagate. Such time-delayed effects are commonly referred to as *memory effects*. As a consequence, $\mathbf{D}_c(\mathbf{r}-\mathbf{r}', t-t') = 0$ when $t - t' \gg \tau_I$. Note that causality requires that $\mathbf{D}_c(\mathbf{r}, t) = 0$ whenever $t < 0$. The diffusion kernel is a tensor since flux and density gradient may not be collinear. Spatial isotropy requires further that $\mathbf{D}_c(\mathbf{r}, t) = \mathbf{D}_c(|\mathbf{r}|, t)$. The so-called *non-local Fickian law* in Eq. (8.59) is valid on a mesoscopically coarse-grained level of spatial resolution $\sim (D_0\tau_I)^{1/2}$ and time resolution $\sim \tau_I$.

Spatial Fourier transformation of Eq. (8.58) with the use of Eq. (8.59) leads to

$$\frac{\partial}{\partial t}\,\overline{\rho}(\mathbf{q}, t) = -q^2 \int_0^t dt'\, D_c(q, t-t')\,\overline{\rho}(\mathbf{q}, t')\,. \tag{8.60}$$

where $D_c(q,t) = \hat{\mathbf{q}} \cdot \mathbf{D}_c(q,t) \cdot \hat{\mathbf{q}}$ is the longitudinal part (parallel to $\mathbf{q}$) of the Fourier transform of the diffusion kernel, and $\hat{\mathbf{q}} = \mathbf{q}/q$. For notational brevity we use the same symbols for the original and Fourier transformed functions, where their argument (either $\mathbf{r}$ or $\mathbf{q}$) indicates which function is meant. Spatial isotropy requires the Fourier transform of $\mathbf{D}_c(\mathbf{r}, t)$ to depend only on the magnitude q of the wavevector $\mathbf{q}$. We learn from Eq. (8.60) that the time rate of change of a density mode becomes increasingly slow with decreasing wavenumber, since particles need to diffuse over an increasingly large distance $\Lambda = 2\pi/q$ to smooth out density variations.

According to the definition of the collective dynamic structure factor, we find from Eq. (8.60) (using that the non-equilibrium average density $\overline{\rho}$ satisfies near equilibrium the same linear equation of motion as the equilibrium density auto-correlation function, which is known as an application of Onsager's hypothesis) that

$$\frac{\partial}{\partial t} S_c(q,t) = -\,q^2 \int_0^t dt'\, D_c(q, t-t') S_c(q, t')\,. \tag{8.61}$$

The solution of this equation for S_c can be formulated in terms of time-Laplace transforms. The Laplace transform of a function f is defined as

$$f(z) \equiv \int_0^\infty dt\, f(t)\, \exp\{-zt\}\,. \tag{8.62}$$

In terms of such Laplace transforms, the solution of Eq. (8.61) reads

$$S_c(q,z) = \frac{S_c(q)}{z + q^2\, D_c(q,z)}\,, \tag{8.63}$$

with a wavenumber- and frequency- (i.e. z) dependent collective diffusion kernel $D_c(q,z)$. As explained above, the q-dependence of $D_c(q,z)$ describes the coupling between the colloidal particle flux at a certain point with density gradients at other points. The z-dependence of D_c describes memory effects, that is, the coupling between the flux at a certain time with density gradients that existed at earlier times. For strongly interacting particles memory effects give rise to a complicated time dependence of $S_c(q,t)$, characterized by a whole spectrum of relaxation times. The collective dynamic structure factor (as well as $S_s(q,t)$) is a strictly monotonically decaying function in time, for fixed q, with negative slope $(d/dt)S_c(q,t) < 0$. This exemplifies an important rule stating that any auto-correlation function is strictly monotonically decaying in time when described within the overdamped colloid dynamics, i.e., for $t \gg \tau_B$ [3]. It follows readily that $S_c(q,z) > 0$ and $zS_c(q,z) < S(q)$.

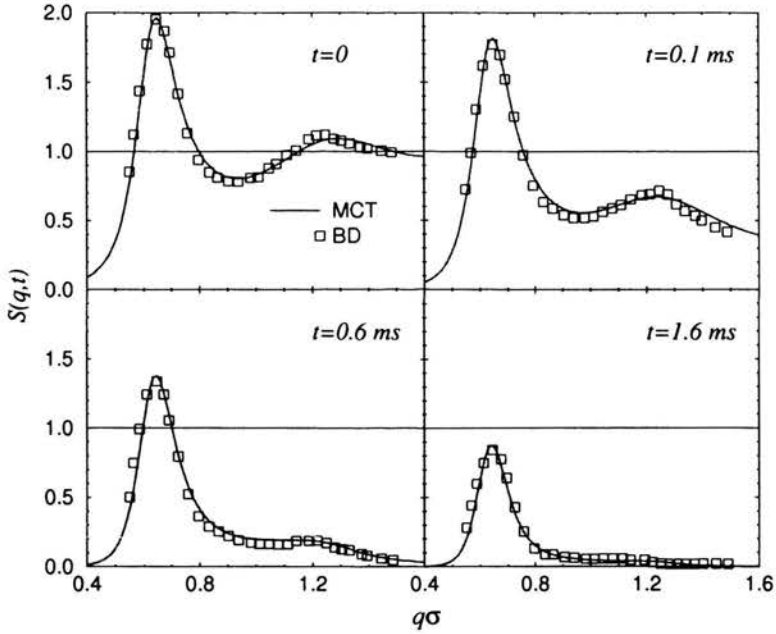

FIGURE 8.6. Collective dynamic structure factor of a charge-stabilized colloidal dispersion. Open squares: Brownian dynamics (BD) computer simulations (after [41]); solid line: Mode coupling theory (MCT) result.

These inequalities in turn imply with Eq. (8.63) that $D_c(q,z)$ and its associated collective diffusion coefficients are all non-negative, as one expects on physical grounds. For fixed t, $S_c(q,t)$ shows damped oscillations in q. A typical q-dependence of $S_c(q,t)$ at various t is illustrated in Fig. 8.6, which shows theoretical and computer simulation results of $S_c(q,t)$ for a suspension of charge-stabilized colloidal spheres.

There exists a special regime where Eq. (8.63) predicts an exponential decay of $S_c(q,t)$. In this so-called hydrodynamic regime, only density wave relaxations are resolved with a wave length much larger than R_I (typically $\sim 1\,\mathrm{mm}$), and with a time resolution that is much larger than τ_I (typically $\sim 1\,\mathrm{s}$). On this strongly coarse-grained level, one can neglect non-local spatial dependencies and memory effects. The collective diffusion kernel is then equal to

$$\mathbf{D}_c(\mathbf{r}-\mathbf{r}',t-t') = D_c^l\ \mathbf{1}\ \delta(\mathbf{r}-\mathbf{r}')\ \delta(t-t')\,. \tag{8.64}$$

The coefficient D_c^l is independent of position and time when the amplitude of the density profile is sufficiently small. Hence, from Eq. (8.59),

$$\bar{\mathbf{j}}(\mathbf{r},t) = -D_c^l\ \nabla\ \bar{\rho}(\mathbf{r},t)\,, \tag{8.65}$$

which is *Fick's local law* of macroscopic gradient diffusion. $S_c(q,t)$ and the associated density wave $\bar{\rho}_q(\mathbf{r},t)$ in Eq. (8.56) decay thus exponentially, for $q \ll {R_I}^{-1}$ and $t \gg \tau_I$, according to

$$S_c(q,t) = S_c(q)\ \exp\{-q^2 D_c^l t\} \tag{8.66}$$

and

$$\bar{\rho}_q(\mathbf{r},t) = \rho_0 + \exp\{-q^2 D_c^l t\}\ \bar{\rho}(\mathbf{q},t=0)\sin\{\mathbf{q}\cdot\mathbf{r}\}\ , \tag{8.67}$$

respectively, where $S_c(q) = S_c(q,t=0)$ is the static structure factor. The correlation length R_I can be roughly estimated by $1/q_m$, where q_m is the wave number where the static structure factor attains its principal maximum. The average extension of the next-neighbor cage around a sphere is roughly equal to $2\pi/q_m$. The local microstructure around a sphere is not resolved in the hydrodynamic limit. This means that $S_c(q \ll q_m)$ in Eq. (8.66) is practically equal to the long wave length limit

$$S_c(0) \equiv \lim_{q\to 0} S_c(q) = \rho_0 k_B T \chi_T \quad \text{with} \quad \chi_T = \frac{1}{\rho_0}\left(\frac{\partial \rho_0}{\partial p}\right)_T\,, \tag{8.68}$$

where, for a one-component suspensions, χ_T is the isothermal *osmotic* compressibility of colloidal spheres.

The transport coefficient D_c^l is referred to as the *long-time collective* or *gradient* diffusion coefficient, since it can be determined, e.g., from macroscopic gradient diffusion experiments near equilibrium. Note here that Eq. (8.66) is equivalent to

$$S_c(q,z) = \frac{S_c(0)}{z + q^2 D_c^l}\,, \tag{8.69}$$

which shows with Eq. (8.63) that D_c^l is equal to the small-wavenumber and small-frequency (i.e. long-time) limit of the collective diffusion kernel. Explicitly

$$D_c^l = \lim_{z\to 0} \lim_{q\to 0} D_c(q,z)\,, \tag{8.70}$$

where q^2/z (i.e. $q^2 t$) is kept fixed to a value of order one. The long-time (i.e. zero-frequency) limit $t \to \infty$ (i.e. $z \to 0$) means in physical terms that $t \gg \tau_I$ (i.e. $z \ll \tau_I^{-1}$). Likewise, the short-time (infinite-frequency) limit $t \to 0$ ($z \to \infty$) should be interpreted as $\tau_B \ll t \ll \tau_I$ (${\tau_I}^{-1} \ll z \ll \tau_B^{-1}$).

As a phenomenological approach, generalized hydrodynamics provides no methods to predict the collective diffusion kernel $D_c(q,z)$ and its associated long-time diffusion coefficient D_c^l. An actual calculation of $D_c(q,z)$ can be accomplished only on the basis of a microscopic theory that relies on a many-sphere extension of the single-particle diffusion Eq. (8.17) as the appropriate time evolution equation. A microscopic theory of diffusion will be discussed in Chapter 9. We will address here only general features of collective diffusion.

At short times, $\tau_B \ll t \ll \tau_I$, memory effects are not felt yet and

$$S_c(q,t) = S_c(q) \exp\{-q^2 D_c^s(q) t\}\,, \tag{8.71}$$

i.e there is an exponential short-time decay of $S_c(q,t)$ for all q. We recall that short-time collective diffusion relates to the initial stage of relaxation of a density wave, where it still retains its original form, but just has decreased its amplitude. This process is described by a wavenumber-dependent (i.e. apparent) diffusion coefficient $D_c^s(q) = D_c(q, z \to \infty)$, which quantifies the initial de-correlation of density modes of wavenumber q. Equation (8.71) and the monotonicity of $S_c(q,t)$ imply that the longitudinal collective diffusion kernel in Eq. (8.61) is decomposable as [42, 3]

$$D_c(q,t) = 2D_c^s(q)\delta(t) - \Delta D_c(q,t)\,, \tag{8.72}$$

corresponding to

$$\frac{\partial}{\partial t} S_c(q,t) = -q^2 \, D_c^s(q) \, S_c(q,t) + q^2 \int_0^t dt' \, \Delta D_c(q, t-t') S_c(q,t') \quad (8.73)$$

with a memory function contribution $\Delta D_c(q,t) \geq 0$. The non-local memory effect on density relaxations inherent in $\Delta D_c(q,t)$ is operative only for times exceeding the short-time regime, and it causes a slower and, in general, non-exponential decay of $S_c(q,t)$.

The short-time collective diffusion coefficient is defined as the zero-q limit of the apparent diffusion coefficient

$$D_c^s = \lim_{q \to 0} D_c^s(q) \,, \quad (8.74)$$

and relates to the long-time collective diffusion coefficient through

$$D_c^l = D_c^s - \lim_{q \to 0} \int_0^\infty dt \, \Delta D_c(q,t) \,. \quad (8.75)$$

The collective diffusion coefficients obey thus the same ordering

$$D_c^l \leq D_c^s \quad (8.76)$$

as the short-time and long-time self-diffusion coefficients. The coefficient D_c^l quantifies the relaxation of constant density gradients over times $t \gg \tau_I$, through cooperative diffusion of spheres opposite to the gradient direction $\hat{\mathbf{q}}$. Therefore D_c^l is intimately related to the average sedimentation velocity, U^l, as measured relative to the laboratory frame of reference, of a homogeneous suspension of slowly sedimenting colloidal spheres. To understand this explicitly, consider a homogeneous suspension of equal spheres in a closed macroscopic vessel at constant temperature, which sediment slowly (so that $Pe \equiv U^l a / D_0 \ll 0$) under the influence of a constant force of buoyancy $\mathbf{F} = F\hat{\mathbf{q}}$. This force acting on each sphere drives a sedimentation flux

$$\mathbf{j}_s = \rho_o \, U^l \, \hat{\mathbf{q}} \,. \quad (8.77)$$

At equilibrium, the small concentration gradient, $\nabla \overline{\rho}$, thereby generated will produce an equal, but opposite diffusive flux, $\mathbf{j}_d$, so that

$$\mathbf{0} = \mathbf{j}_s + \mathbf{j}_d = \rho_o \, U^l \, \hat{\mathbf{q}} - D_c^l \, \nabla \overline{\rho} \,. \quad (8.78)$$

The force on the solvent exerted by the sedimenting particles is balanced through a pressure gradient, $\nabla p = \rho_0 \mathbf{F}$, generated by the base of the vessel (which is perpendicular to $\hat{\mathbf{q}}$). The pressure gradient drives a back-flow of solvent such that the zero-volume-flux condition is fulfilled: due to incompressibility, the net volume flux of solvent and spheres through any plane perpendicular to $\hat{\mathbf{q}}$ is zero. The concentration gradient follows next from

$$\nabla \overline{\rho} = \left(\frac{\partial \rho_0}{\partial p} \right)_{T,\mu_s} \nabla p = \beta S_c(0) \rho_0 F \, \hat{\mathbf{q}} \,, \tag{8.79}$$

where μ_s is the chemical potential of the solvent (osmotic equilibrium). Finally, substitution into Eq. (8.78) leads to the general relation [43, 44]

$$D_c^l = \frac{D_0}{S_c(0)} \frac{U^l}{U_0} \tag{8.80}$$

between D_c^l and U^l, where $U_0 = \beta D_0 F$ is the sedimentation velocity at infinite dilution. Equation (8.80) can be derived more rigorously from linear response theory, which provides us further with a microscopic expression for D_c^l.

Very interestingly, the configurational probability density function of identical colloidal spheres is not distorted from the equilibrium distribution during sedimentation, as long as HI between spheres can be considered as pairwise additive. This holds true for dilute monodisperse suspensions. The long-time sedimentation velocity U^l, which is measured in standard sedimentation experiments, becomes then equal to the short-time sedimentation velocity U^s. The latter is related to the short-time collective diffusion coefficient once again by Eq. (8.80), with l replaced by s. Consequently, we have

$$D_c^l = D_c^s \tag{8.81}$$

for pairwise-additive HI. There is thus no distinction between short-time and long-time collective diffusion, which corresponds to a vanishing memory contribution to D_c^l in Eq. (8.75). A density wave retains its sinusoidal shape during the entire process of relaxation whenever the wave length is much larger than the correlation length R_I. This result is in marked contrast to self-diffusion where the long-time self-diffusion coefficient of interacting particles is substantially smaller than the short-time one even when HI is totally disregarded.

Three-body or more-body HI become highly relevant for concentrated dispersions. In these systems, their effect is to distort the suspension microstructure from the initial equilibrium distribution for times $t \sim \tau_I$, which causes additional hindrance of particle motion. For $t \gg \tau_I$, a new steady-state distribution has been reached, accompanied by a small decrease in the sedimentation velocity such that $U^l < U^s$ and $D_c^l < D_c^s$. Recent calculations for dense hard-sphere suspensions have revealed, however, that the differences between D_c^l and D_c^s are quite small (less than 6%), which makes them difficult to detect using DLS [45].

DLS and small-angle quasi-elastic neutron scattering experiments on colloidal particles which scatter equally strongly, are convenient and widely used tools to determine $S_c(q,t)$ over an extended range of times and wave numbers. These methods allow to study in detail relaxation of density waves for a wave length set by the experimental scattering angle. The short-time and long-time collective diffusion coefficients can be extracted from linearly extrapolating $-\ln\{S_c(q,t)\}/q^2$, measured for fixed $t \ll \tau_I$ and $t \gg \tau_I$, respectively, to $q = 0$. The sedimentation velocity derives then from Eq. (8.80) when in addition $S_c(q \ll q_m)$ is determined by static light scattering.

In dispersions of strongly repelling particles, D_c^s and D_c^l can be substantially larger than the Stokesian diffusion coefficient D_0. This feature is mainly due to the low osmotic compressibility (i.e. $S_c(0) \ll 0$), which acts as a thermodynamic force driving the relaxation of local density gradients (cf. Fig. 8.7).

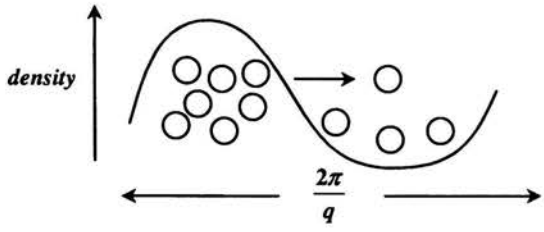

FIGURE 8.7. Enhanced relaxation of density fluctuations through low osmotic compressibility.

A typical concentration dependence of D_c^s for a suspension of moderately charged colloidal spheres is shown in Fig. 8.8 for low and moderately large amounts of excess electrolyte. Note that both $S_c(0)$ and U^s decrease with increasing volume fraction Φ of spheres (cf. Eq. (8.80)). At small vol-

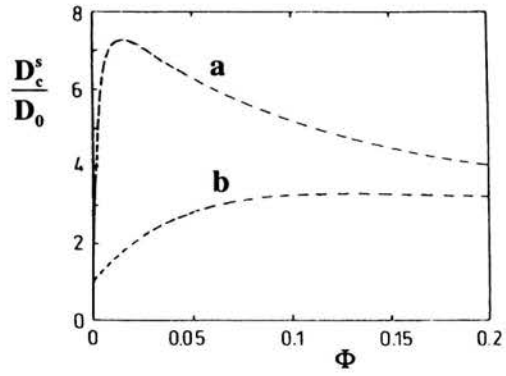

FIGURE 8.8. Theoretical prediction for the (reduced) collective diffusion coefficient D_c^s/D_0 versus volume fraction, for typical aqueous solutions of weakly charged spherical micelles. Shown are two curves with (a) low amount and (b) moderately large amount of added electrolyte. After [3].

ume fraction Φ, U^s decreases less strongly than $S_c(0)$ leading to an initial increase in D_c^s. With Φ further increasing, hydrodynamic hindrance starts to overcompensate the electrostatic particle repulsion so that D_c^s goes through a maximum. The maximum in $D_c^s(\Phi)$ becomes smaller with increasing amount of added electrolyte, i.e. with enlarged screening of the electrostatic repulsion. While $D_s^s/D_0 \leq 1$ independent of the type of interactions, D_c^s/D_0 is found to be larger than one for repulsive pair interactions. For dispersions with attractive interaction contributions close to a critical point, however, $D_c^s/D_0 \approx 0$ due to the large osmotic compressibility of near-critical systems. The dynamics of such systems is thus very slow (critical slowing down).

On various places we have noted that, aside from small wavenumbers $q \ll q_m$, $S_c(q,t)$ decays in general non-exponentially in time. However, recent calculations of $S_c(q,t)$ for concentrated suspensions with pronounced particle caging have revealed that the dynamic structure factor of these systems does decay exponentially for *long* times, for wavenumbers centered around q_m. The existence of such a collective long-time mode

$$S_c(q_m,t) \propto \exp\{-q^2 D_c^l(q_m)t\}\,, \quad t \gg \tau_I \tag{8.82}$$

characterized by a collective long-time diffusion coefficient, $D_c^l(q_m)$, at the finite wave number q_m has been observed indeed in DLS experiments on concentrated suspensions of hard spheres. This peculiar mode describes the decay of concentration fluctuations linked to the average extension of a nearest-

neighbor cage. According to theory, the long-time mode ceases to exist when the volume fraction of hard spheres is reduced below 0.2. The caging effect is then too small and $S_c(q_m, t)$ decays non-exponentially at long times.

The long-time coefficient $D_c^l(q_m)$ should be distinguished from the q-dependent *mean* collective diffusion coefficient, $\overline{D}_c(q)$. The latter is defined by

$$\overline{D}_c(q) \equiv D_c(q, z=0) = D_c^s(q) - \int_0^\infty dt \Delta D_c(q,t)\,, \tag{8.83}$$

and is related to the mean relaxation time, $\overline{\tau}(q)$, of $S_c(q,t)$ through

$$\overline{\tau}(q) \equiv \int_0^\infty dt\, \frac{S_c(q,t)}{S_c(q)} = \frac{1}{q^2 \overline{D}_c(q)}\,. \tag{8.84}$$

Contrary to $D_c^l(q)$, the coefficient $\overline{D}_c(q)$ is not a true long-time diffusion coefficient although this has been erroneously claimed. If $D_c(q,t)$ would decay sufficiently faster than $S_c(q,t)$, the memory integral in Eq. (8.61) could then

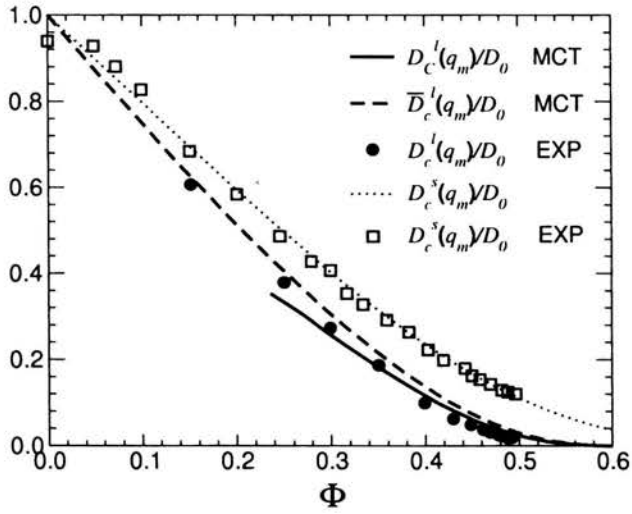

FIGURE 8.9. Mode coupling theory (MCT) prediction (from [46]) for the concentration dependence of the collective long-time coefficient $D_c^l(q_m)$, and for the mean collective coefficient $\overline{D}_c(q_m)$ of hard-sphere suspensions. The experimental data for $D_c^l(q_m)$ are from [47]. For comparison, we include experimental data (from [48]) for the short-time $D_c^s(q_m)/D_0$ with corresponding theoretical predictions from Eqs. (9.74), (9.75).

be de-convoluted for $t \gg \tau_I$ as

$$\int_0^t dt' D_c(q, t-t')\, S_c(q, t') \approx D_c(q, z=0)\, S_c(q, t)\,. \tag{8.85}$$

If this holds true then $\overline{D}_c(q)$ would be a genuine long-time diffusion coefficient with $S_c(q, t \gg \tau_I) \propto \exp\{-q^2 \overline{D}_c(q) t\}$. However, $D_c(q,t)$ decays so slowly for finite q that the de-convolution is strictly valid only in the hydrodynamic limit, where $\overline{D}_c(q)$ reduces to D_c^l. Contrary to $D_c^l(q)$ the mean collective diffusion coefficient is defined for any concentration and all values of q, even those where $S_c(q,t)$ is non-exponential at long times. Note that the ordering relations

$$D_c^s(q) > \overline{D}_c(q) > D_c^l(q) \tag{8.86}$$

are valid for the range of q and Φ where $D_c^l(q)$ exists. A comparison between the coefficients $D_c^l(q_m)$ and $\overline{D}_c(q_m)$ of hard spheres, as predicted by theory, is made in Fig. 8.9. This figure includes also DLS data for $D_c^l(q_m)$ which agree well with theory. The difference between both coefficients is rather small over the complete range of volume fractions where $D_c^l(q_m)$ exists.

Interdiffusion in mixtures

So far we have explored diffusion processes in one-component systems of identical particles, as far as the sizes and interaction properties are concerned. In colloidal mixtures, and of course also in atomic and polymer mixtures, an additional interdiffusion mechanism comes into play related to the relaxation of thermal fluctuations in the relative concentration of two components. For simplicity, we will discuss only the most simple case of interdiffusion in binary colloidal dispersions of spherical particles, and in a ternary incompressible melt of two homopolymer species mingled in a matrix of a third homopolymer species. We will address in particular the question whether the interdiffusion coefficient can be expressed alone in terms of the self-diffusion coefficients of both components.

The interdiffusion process mediates the relaxation of thermal fluctuations (under isothermal and isobaric conditions) in the relative particle (monomer) concentration of two components, say component 1 and 2, towards their equilibrium values. There might be additional components present but we focus here on the concentration exchange between components 1 and 2. The

Fourier transform of the *incremental* microscopic number density of component $\alpha = 1, 2$, relative to its mean density $\rho_{\alpha 0} = N_\alpha / V_s$, reads

$$\rho_\alpha(q,t) = \sum_{j=1}^{N_\alpha} \exp\{i\mathbf{q} \cdot \mathbf{r}_j^\alpha\} - N_\alpha \delta_{\mathbf{q},\mathbf{0}} \,, \tag{8.87}$$

with $\langle \rho_\alpha(q,t) \rangle = 0$. Here, $\mathbf{r}_j^\alpha$ is the center-of-mass position vector of the j-th sphere (monomer) of component α, and N_α is the number of particles of species α in the scattering volume. Small fluctuations in the relative local concentrations of 1-particles with respect to component 2 are quantified by the microscopic concentration variable

$$\rho_{in}(\mathbf{q},t) \equiv \frac{1}{\sqrt{N}} \left[x_2 \rho_1(\mathbf{q},t) - x_1 \rho_2(\mathbf{q},t) \right] \,, \tag{8.88}$$

with $N = N_1 + N_2$ and partial molar fraction $x_\alpha = N_\alpha / N$. The interdiffusion process is thus related to the relaxation of $\rho_{in}(\mathbf{q},t)$, whose de-correlation in time is described by the interdiffusion auto-correlation function

$$\begin{aligned} S_{in}(q,t) &= < \rho_{in}(\mathbf{q},t)\, \rho_{in}(-\mathbf{q},0) > \\ &= x_1 x_2 \left[x_2 S_{11}(q,t) + x_1 S_{22}(q,t) - 2\,(x_1 x_2)^{1/2}\, S_{12}(q,t) \right] \,. \end{aligned} \tag{8.89}$$

The interdiffusion function $S_{in}(q,t)$ has been further denoted in the literature on X-ray and neutron scattering as the Bhatia–Thornton dynamic concentration-concentration structure factor. It is a special linear combination of three partial collective dynamic structure factors [3]

$$S_{\alpha\beta}(q,t) = \frac{1}{(N_\alpha N_\beta)^{1/2}} < \rho_\alpha(\mathbf{q},t) \rho_\beta(-\mathbf{q},0 > \,, \tag{8.90}$$

with $\alpha, \beta \in \{1,2\}$ and $S_{12} = S_{21}$. The partial structure factors, $S_{\alpha\beta}(q,t)$, describe time-correlations in the density fluctuations of components α and β, and they form the elements of a symmetric and positive definite 2×2 matrix $\mathbf{S}(q,t)$. This matrix is the extension of the collective dynamic structure factor $S_c(q,t)$ of a monodisperse system to binary mixtures. Note that the factors $N^{-1/2}$ and $(N_\alpha N_\beta)^{-1/2}$ in Eq. (8.88) and Eq. (8.90), respectively, have been introduced to make $S_{in}(q,t)$ and $\mathbf{S}(q,t)$ intensive. The EACF for polarized single scattering from a binary mixture can be expressed in terms of the dynamic structure factor matrix as

$$\begin{aligned} g_E(q,t) &\propto f_1^2 S_{11}(q,t) + f_2^2 S_{22}(q,t) + 2 f_1 f_2 S_{12}(q,t) \\ &= \mathbf{f}(q)^T \cdot \mathbf{S}(q,t) \cdot \mathbf{f}(q) \,, \end{aligned} \tag{8.91}$$

where we have introduced the column vector $\mathbf{f} = [f_1, f_2]^T$ of partial scattering strengths $f_\alpha = x_\alpha^{1/2} b_\alpha$. For a binary colloidal suspension, b_α is the *excess* scattering amplitude of a sphere of component $\alpha = 1, 2$ relative to the solvent. For a ternary homopolymer blend, b_α is the scattering amplitude of an α-type monomer relative to the scattering strength of a matrix monomer. In principle, the three partial dynamic structure factors could be measured individually by index matching each of the two interdiffusing components separately to the solvent (matrix). Unfortunately, such an index matching is quite difficult to do from an experimental point of view and has been achieved to date only for a few selected systems. The index matching method is to some extent analogous to the isotope substitution technique used in neutron scattering.

We are interested here in the hydrodynamic regime (i.e. $q \to 0$ and $t \to \infty$ with $q^2 t$ fixed) where the internal structure of the colloidal spheres and homopolymers, and the internal dynamics of the individual homopolymers are not resolved. In this regime, the scattering amplitudes become independent of q. The time evolution of the matrix $\mathbf{S}(q,t)$ is shown in the hydrodynamic limit to be governed by

$$\mathbf{S}(q,t) = \exp\{-q^2 \mathbf{D}_c^l t\}\, \mathbf{S}(0)\,, \tag{8.92}$$

where $\mathbf{D}_c^l$ is the 2×2 long-time collective diffusion matrix, and $\mathbf{S}(0) = \mathbf{S}(q \to 0, t = 0)$ is the matrix of partial static structure factors in the small-q limit. Equation (8.92) extends Eq. (8.66) to (binary) mixtures. It is found that $\mathbf{D}_c^l$ is in general not symmetric. However, it can be diagonalized and it possesses real and positive eigenvalues d_+ and d_-, as one expects for an overdamped system. To see this, we introduce the symmetric and positive definite matrix, $\boldsymbol{\mu}^l$, of long-time partial mobilities $\mu_{\alpha\beta}$ through [50, 49]

$$\mathbf{D}_c^l = k_B T\, \boldsymbol{\mu}^l \cdot \mathbf{S}(0)^{-1}\,. \tag{8.93}$$

A trivial example is provided for a system of non-interacting particles, where $\mu_{\alpha\beta}^l = \delta_{\alpha\beta} D_{0\alpha}/(k_B T)$. The symmetry and positive definiteness of $\boldsymbol{\mu}^l$ is a consequence of the symmetry of $\mathbf{S}(q,t)$, and its monotonic decay in the hydrodynamic limit. That $\mathbf{D}_c^l$ is diagonalizable with positive eigenvalues arises then from the possibility to express it as the product of a symmetric and positive definite matrix $\boldsymbol{\mu}^l$ and a symmetric matrix $\mathbf{S}^{-1}$. Explicit diagonalization of $\mathbf{D}$ leads to the normal-mode expansion [50]

$$\mathbf{S}(q,t) = \mathbf{A}_+ \exp\{-q^2 d_+ t\} + \mathbf{A}_- \exp\{-q^2 d_- t\} \tag{8.94}$$

of $\mathbf{S}(q,t)$ as a sum of two exponentially decaying diffusive modes. The amplitudes $\mathbf{A}_+$ and $\mathbf{A}_-$ can be expressed in terms of the elements of $\mathbf{S}(0)$ and $\boldsymbol{\mu}^l$. The eigenvalues of $\mathbf{D}$ are given by

$$d_\pm = D_{av} \pm \sqrt{D_{av}^2 - |\mathbf{D}|} \tag{8.95}$$

with $D_{av} = [D_{11} + D_{22}]/2$ and $|\mathbf{D}| = D_{11}D_{22} - D_{12}D_{21}$. In case of a binary colloidal dispersion, the bimodal relaxation described by Eq. (8.94) arises from the large differences in the relaxation times of colloidal particles and solvent molecules. In contrast, the relaxation time of the polymer matrix, which plays the role of the "solvent" in the ternary homopolymer mixture, is comparable to those of the other two components. The bimodal relaxation is here a consequence of the incompressibility constraint

$$\rho_1(\mathbf{q}) + \rho_2(\mathbf{q}) + \rho_3(\mathbf{q}) = 0\,, \tag{8.96}$$

valid in the diffusive limit, which enables one to express the dynamics of one component, identified as the "matrix", in terms of the other ones. For simplicity, we have assumed here that the segmental volumes of all three homopolymer species are equal to each other. It is clear that $\mathbf{S}(q,t)$ in the general case will contain as many exponentially decaying modes as the number of independent components.

It follows from Eqs. (8.89) and (8.94) that

$$S_{in}(q,t) = x_1 x_2\, \mathbf{e}^T \cdot \mathbf{S}(q,t) \cdot \mathbf{e}\,, \tag{8.97}$$

with $\mathbf{e} = \left[\sqrt{x_2}, -\sqrt{x_1}\right]^T$, is a superposition of two decaying modes. Nevertheless, the initial decay of $S_{in}(q,t)$ in the hydrodynamic limit can be described for $t \ll 1/d_+$ by the single exponential form

$$S_{in}(q,t) \;\propto\; \exp\{-q^2 D_{in}^l t\}\,, \tag{8.98}$$

which defines the long-time interdiffusion coefficient, D_{in}^l, as

$$D_{in}^l = \lim_{t\to\infty} \lim_{q\to 0} \left[-\frac{1}{q^2}\frac{\partial}{\partial t} \ln S_{in}(q,t)\right]\,. \tag{8.99}$$

By matching the initial relaxation rates in Eqs. (8.97) and (8.98), we find, using Eq. (8.93), that

$$D_{in}^l = \frac{\Lambda_{in}^l}{S_{in}(0)}\,, \tag{8.100}$$

with

$$\begin{aligned}\Lambda_{in}^{l} &= k_B T x_1 x_2 \, \mathbf{e}^T \cdot \boldsymbol{\mu}^l \cdot \mathbf{e} \\ &= k_B T x_1 x_2 \left[x_2 \mu_{11}^l + x_1 \mu_{22}^l - 2 \, (x_1 x_2)^{1/2} \, \mu_{12}^l \right] . \end{aligned} \tag{8.101}$$

We note that D_{in}^{l} is expressed here as a product of a *kinetic factor*, $\Lambda_{in}^{l} > 0$, and a *thermodynamic factor* equal to $1/S_{in}(q=0)$. For a binary mixture of particles nearly identical in their interactions, $S_{in}(0) \approx x_1 x_2$. For systems with $S_{in}(0) < x_1 x_2$ ($S_{in} > x_1 x_2$) the particles of components 1 and 2 have the tendency to mix (de-mix).

The kinetic factor can be expressed by the Green–Kubo formula

$$\Lambda_{in}^{l} = \lim_{q \to 0} \int_0^\infty dt \; < j_{in}(\mathbf{q}, t) \; j_{in}(-\mathbf{q}, 0) > , \tag{8.102}$$

where

$$j_{in}(\mathbf{q}, t) = \sqrt{N} x_1 x_2 \left[\frac{1}{N_1} \sum_{j=1}^{N_1} v_j^{(1)} \exp\{ i\mathbf{q} \cdot \mathbf{r}_j^{(1)} \} - \frac{1}{N_2} \sum_{j=1}^{N_2} v_j^{(2)} \exp\{ i\mathbf{q} \cdot \mathbf{r}_j^{(2)} \} \right] \tag{8.103}$$

is the interdiffusion flux related to $\rho_{in}(\mathbf{q}, t)$. Here, $v_j^{(1)}$ and $v_j^{(2)}$ denote the longitudinal (i.e. parallel to $\mathbf{q}$) velocities of component 1 and 2 particles. The interdiffusion flux is seen to be closely related to the *relative velocity of the center-of-masses* of the two components in the mixture. The derivation of Eq. (8.102) can be represented quite generally [50, 51] for any density function $\rho(\mathbf{q}, t)$ in Fourier space satisfying the continuity equation

$$\dot{\rho}(\mathbf{q}, t) = iq \, j(\mathbf{q}, t) . \tag{8.104}$$

Here $j(\mathbf{q}, t)$ is the longitudinal component of the flux vector $\mathbf{j}(\mathbf{q}, t)$ associated with $\rho(\mathbf{q}, t)$, and the dot denotes differentiation with respect to time. The long wave length limit of the current auto-correlation function follows then as

$$\begin{aligned}\lim_{q \to 0} \langle j(\mathbf{q}, t) \; j(-\mathbf{q}, 0) \rangle &= \lim_{q \to 0} \frac{1}{q^2} < \dot{\rho}(\mathbf{q}, t) \; \dot{\rho}(-\mathbf{q}, 0) > \\ &= - \lim_{q \to 0} \frac{1}{q^2} \frac{\partial^2 S(q, t)}{\partial t^2} \end{aligned} \tag{8.105}$$

where $S(q,t) = < \rho(\mathbf{q},t)\rho(-\mathbf{q},0) >$. For the most right equality we have used the stationarity property, which states that equilibrium time-correlation functions are invariant to a shift in the time origin. Next we integrate Eq. (8.105) with respect to time to obtain

$$\lim_{q\to 0}\int_0^t dt' \, \langle j(\mathbf{q},t') \, j(-\mathbf{q},0)\rangle = -\lim_{q\to 0}\frac{1}{q^2}\frac{\partial}{\partial t} S(q,t)\,, \tag{8.106}$$

where the initial condition

$$\frac{\partial}{\partial t} S(q,t)|_{t=0} = 0 \tag{8.107}$$

has been used. This initial condition is a consequence of time reversibility, i.e. $< A(t)A(0) > = < A(-t)A(0) >$ for any dynamic variable A obeying the deterministic Liouville equation. The initial slope of any auto-correlation function is thus zero in Liouville dynamics. Of course, this does not hold for the irreversible dynamical regime described by diffusion equations (e.g., Eq. (8.17)), wherein the microscopic short-time regime $t \ll \tau_B$ remains unresolved. The transition to the hydrodynamic regime follows from taking the long-time limit of Eq. (8.107). This gives the exact relation

$$\lim_{q\to 0}\int_0^\infty dt \, \langle j(\mathbf{q},t) \, j(-\mathbf{q},0)\rangle = -\lim_{t\to\infty}\lim_{q\to 0}\frac{1}{q^2}\frac{\partial}{\partial t} S(q,t)\,, \tag{8.108}$$

where the order of the limits is not interchangeable. In specializing this equation to interdiffusion, the Green–Kubo formula for Λ_{in}^l is readily obtained from substituting the hydrodynamic limit form of $S_{in}(q,t)$ as given in Eq. (8.94). When Eq. (8.108) is specialized to self-diffusion by choosing $\rho(\mathbf{q},t) = \exp\{i\mathbf{q}\cdot\mathbf{r}_1(t)\}$ and using that $S_s(q,t) = \exp\{-q^2 D_s^l t\}$ in the hydrodynamic limit, one is led to the Green–Kubo formula for the VAF given in Eq. (8.45). For self-diffusion, $\Lambda_s^l = D_s^l$, since the thermodynamic factor $1/S_s(q,t=0)$ is equal to one even for finite q.

For colloidal mixtures, one needs to distinguish between the short-time and long-time interdiffusion coefficient. The definition of $D_{in}^s = \Lambda_{in}^s/S_{in}(0)$ and of its associated short-time kinetic factor Λ_{in}^s follows from considering the time evolution equation

$$\frac{\partial}{\partial t}\mathbf{S}(q,t) = -q^2\,\mathbf{D}_c^s(q)\cdot\mathbf{S}(q,t) + q^2\int_0^t dt' \, \Delta\mathbf{D}_c(q,t-t')\cdot\mathbf{S}(q,t') \tag{8.109}$$

for $\mathbf{S}(q,t)$, which constitutes the generalization of Eq. (8.73) to colloidal mixtures. Here $\Delta\mathbf{D}_c(q,t)$ is a 2×2-matrix of collective memory functions, related to the long-time collective diffusion matrix in Eq. (8.93) by (cf. Eq. (8.75))

$$\mathbf{D}_c^l = \mathbf{D}_c^s - \lim_{q\to 0}\int_0^\infty dt\,\Delta\mathbf{D}_c(q,t)\,, \tag{8.110}$$

with the short-time collective diffusion matrix $\mathbf{D}_c^s = \lim_{q\to 0}\mathbf{D}_c^s(q)$. Introducing the short-time mobility matrix through $\mathbf{D}_c^s = k_BT\boldsymbol{\mu}^s\cdot\mathbf{S}(\mathbf{0})^{-1}$, Λ_{in}^s can be defined in analogy to the long-time kinetic coefficient as

$$\Lambda_{in}^s = k_BT\,x_1x_2\mathbf{e}^T\cdot\boldsymbol{\mu}^s\cdot\mathbf{e}\,. \tag{8.111}$$

Contrary to the one-component case, where $D_c^s = D_c^l$ for systems with pairwise additive HI, one finds for mixtures that $\mathbf{D}_c^s \neq \mathbf{D}_c^l$, and hence $\Lambda_{in}^l < \Lambda_{in}^s$ and $D_{in}^l < D_{in}^s$, even so when HI is neglected. The reason for the different physical behavior of mixtures is that particles of different components diffuse differently fast under a constant density gradient. Hence, the equilibrium microstructure becomes distorted at longer times. For the memory matrix this implies that $\lim_{q\to 0}\Delta\mathbf{D}(q,t) \neq 0$.

The interdiffusion coefficient describes the relaxation of thermally excited fluctuations in the relative composition through the collective motion of particles. Therefore, there is no reason to expect that, except for a few limiting cases, D_{in}^l can be expressed solely in terms of the self-diffusion coefficients

$$D_{s\alpha}^l = \int_0^\infty dt < v_i^\alpha(t)\,v_i^\alpha(0) > \tag{8.112}$$

of both components, with v_i^α denoting the longitudinal velocity of a component α particle. That there are collective contributions to D_{in}^s which are not contained in the self-diffusion coefficients was explicitly shown for fluid atomic mixtures in [52]. The importance of collective contributions to D_{in} will be exemplified in Sec. 9.2 for mixtures of colloidal hard spheres.

An ideal binary mixture is characterized by

$$\Lambda_{in}^l \;\propto x_2\,D_{s1}^l + x_1\,D_{s2}^l\,, \tag{8.113}$$

i.e. the kinetic factor can be expressed solely in terms of a weighted sum of the self-diffusion coefficients. Such an ideal situation is implied, in particular,

according to Eq. (8.102), when velocity cross-correlations $< v_i(t)v_j(0) >$ between different particles $i \neq j$ vanish or mutually cancel each other for all t. A trivial example of an ideal system is a binary suspension of non-interacting particles, where

$$D_{in}^{l} = D_{in}^{s} = x_2 D_{01} + x_1 D_{02} . \tag{8.114}$$

Here, $D_{0\alpha}$ is the free diffusion coefficient of an α-type particle. Eq. (8.113) is the *fast-mode* expression for interdiffusion since for $D_{s1} \gg D_{s2}$, D_{in} is dominated by the self-diffusion coefficient of the fast component 1. The fast-mode form of D_{in} is approximately valid for mixtures of Lennard–Jones-type fluids like argon-krypton. However, there are severe deviations from the fast-mode form for mixtures of strongly dissymmetric particles. Perfect situation is reached only for symmetric bimodal systems, where the particles of both components differ only in their labelling (e.g. in their optical properties). In this limiting case, $S_{in}(0) = x_1 x_2$, and

$$D_{in} = D_s \tag{8.115}$$

for arbitrary concentration and particle interactions. Not unexpectedly, this means that the concentration exchange between the two components is only driven by self-diffusion. The interdiffusion coefficient in a symmetric mixture is thus identical with the self-diffusion coefficient. Since all particles are identical regarding their sizes and interactions, there is no gradient in the local chemical potential difference of both species. Each particle experiences a uniform environment as in the case of self-diffusion. An ideal bimodal system in the hydrodynamic limit is further characterized by

$$d_- = D_{in} , \quad d_+ = D_c \tag{8.116}$$

with $d_- < d_+$. The eigenmode with decay constant d_- (d_+) is thus identified with the interdiffusion (collective diffusion) process, and D_{in} and D_c can be extracted, using index matching, from a single measurement of the EACF of the unmatched (labelled) component α, since then $g_E(q,t) \propto S_{\alpha\alpha}(q,t)$. The two normal modes cannot be identified, in general, as interdiffusion and collective diffusion processes. Moreover, D_{in} cannot be extracted, in general, from the measurement of a single dynamic structure factor, say $S_{11}(t)$, of one component. One needs a second experiment, in which the first component is matched away and $S_{22}(q,t)$ is determined.

Exact microscopic expressions have been derived for the interdiffusion coefficient of colloidal mixtures. These expressions form the basis of its actual calculation (cf. Chapter 9). In the case of incompressible polymer melts, an analogous microscopic description is of little use from a computational point of view. Therefore one resorts to approximate schemes like the (dynamic) random phase approximation (RPA), which relates the dynamics of polymer mixtures to the dynamics of a single polymer chain in the mixture. In Sec. 9.3, we will discuss the application of the RPA to ternary blends of homopolymers. We only mention here that for a incompressible binary blend, the RPA predicts the *slow-mode* expression

$$\frac{1}{\Lambda_{in}} \propto \frac{x_2}{D_{s1}} + \frac{x_1}{D_{s2}} \tag{8.117}$$

for the kinetic factor, with $D_{s\alpha}$ the self-diffusion coefficient of an α-type monomer in the melt, and x_α the molar fraction of α-type monomers. The kinetic factor is dominated here by the slow component, as the name "slow mode" implies. The RPA states thus that, due to incompressibility, the dynamics of the fast component is slaved by the slow one. The binary blend is thus an opposite limiting case to ideal solutions of weakly interacting particles and to mixtures of nearly identical components where the fast-mode expression applies.

Rotational diffusion

We proceed to discuss salient features of rotational diffusion in suspensions of colloidal spheres with spherically symmetric potential interactions, within the time regime accessible by depolarized DLS. As discussed already in Sec. 8.1, the decoupling approximation of the depolarized EACF holds then exactly to linear order in t. Consider first the (hypothetical) case of particles, which interact by direct potential forces only, and not by HI. Then the rotational self-dynamic correlation function reduces, for all times $t \gg \tau_B \approx \tau_B^r$, to an exponentially decaying function

$$S_r(t) = \exp\{-6D_0^r t\}\,. \tag{8.118}$$

This result follows from realizing that the orientational Brownian motion of a sphere with radially symmetric pair interactions is independent of the orientational and translational motion of other spheres, as long as HI is not considered. Recall that, contrary to $S_r(t)$, the translational self-dynamic structure

factor $S_s(q,t)$ is single exponential without HI only at short times. Consequently,

$$g_E^{VH}(q,t) \propto \beta^2 \exp\{-(q^2 W(t) + 6D_0^r t)\} \tag{8.119}$$

is valid for all $t \gg \tau_B$, provided small non-Gaussian corrections to $S_s(q,t)$ can be discarded. In reality, however, Eq. (8.119) is of little use since the HI are very long-ranged. HI decay for long interparticle distances r as r^{-1} regarding collective diffusion, and as r^{-4} and r^{-6}, respectively, in case of translational and rotational self-diffusion. Therefore, HI cannot be neglected in comparison to direct interactions. With HI, $S_r(t)$ decays exponentially only at short times. The initial decay of $S_r(t)$ can be quantified by the short-time rotational self-diffusion coefficient D_r^s, defined as

$$D_s^r = -\lim_{t\to 0} \frac{\partial \ln S_r(t)}{\partial t}, \tag{8.120}$$

where $t \to 0$ should be interpreted as $\tau_B \ll t \ll \tau_I \approx \tau_r$. The HI between the spheres cause a hindrance of short-time rotational motion so that $D_s^r < D_0^r$. At infinite dilution, $D_s^r \to D_0^r$. As will be exemplified in Sec. 9.2, D_s^r depends crucially on system parameters like the volume fraction, and the particle charge in case of charge-stabilized dispersions.

Memory effects come into play at longer times and lead to deviations of $S_r(t)$ from the single exponential decay. For the rotational Brownian motion of the tip of the orientation vector $\hat{\mathbf{u}}$ on the compact unit sphere, there is no analogue of the hydrodynamic $q \to 0$ limit known from translational self- and collective motion. At long times, $S_r(t)$ decays in principle non-exponentially, with an average decay rate somewhat smaller than the initial one. Such a non-Debye-like relaxation of $S_r(t)$ at long times has been observed experimentally and theoretically for various systems. For dilute suspensions of colloidal hard spheres, e.g., it has been shown theoretically that $S_r(t)$ is non-exponential at intermediate and long times, according to [53]

$$\frac{S_r(t)}{S_r^0(t)} = 1 + \gamma_2(t)\Phi + \mathcal{O}(\Phi^2) \tag{8.121}$$

with a positive-valued function $\gamma_2(t)$. Here, $S_r^0(t)$ is the rotational self-function at infinite dilution, given by Eq. (8.118). While a genuine long-time rotational self-diffusion coefficient does not exist, one can always define instead a *mean* orientational self-diffusion coefficient, $\overline{D}_r$, which depends on

the overall time dependence of $S_r(t)$ through [53]

$$\frac{1}{6\overline{D}_r} \equiv \int_0^\infty dt\, S_r(t) = \frac{1}{6D_0^r}\left[1 + C_r\Phi + \mathcal{O}(\Phi^2)\right] \tag{8.122}$$

with $C_r = 0.67$ for hard spheres, resulting in $\overline{D}_r/D_0^r = 1 - 0.67\Phi + \mathcal{O}(\Phi^2)$. This should be compared with the first-order virial result for the short-time rotational self-diffusion coefficient of hard spheres, given by $D_s^r/D_0^r = 1 - 0.63\Phi + \mathcal{O}(\Phi^2)$. Thus, memory effects in $S_r(t)$ lead to a mean diffusion coefficient only slightly smaller than the short-time one, to first order in Φ.

Whereas a true long-time rotational self-diffusion coefficient, D_l^r, does not exist in monodisperse suspensions, we expect D_l^r to be a well-defined long-time property when interpreted as the long-time coefficient describing the rotation of a large tracer sphere immersed in a dispersion of small host spheres. Depolarized DLS measurements indicate that a tracer/host size ratio larger than 10 is large enough for D_l^r to be well-defined. Due to the separation of time scales between the slow motion of the tracer and the fast motion of the host spheres, the tracer experiences the host dispersion as an unstructured effective fluid, characterized by the effective viscosity η_H of the host dispersion. Thus, one expects that D_l^r obeys the generalized Stokes–Einstein relation for a perfectly sticking effective fluid, i.e.,

$$D_l^r = \frac{k_B T}{6\pi\eta_H a_T}, \tag{8.123}$$

where a_T denotes the radius of the tracer. This expectation is supported experimentally, and by calculating the short-time rotational self-diffusion coefficient of the tracer in a dilute host dispersion of hard spheres [54]. For the latter case, D_s^r is described to good accuracy by [54]

$$D_s^r = D_0^r\left[1 - \frac{2.5}{1 + 3\lambda^{-1}}\,\Phi + \mathcal{O}(\Phi^2)\right], \tag{8.124}$$

with $\lambda = a_T/a_H$, and Φ the volume fraction of host spheres. This equation describes a monotonic decline of the tracer coefficient from $D_s^r = D_0^r$ at $\lambda = 0$ towards $D_s^r = D_0^r(1 - 2.5\Phi) = k_B T/[6\pi\eta_0(1 + 2.5\Phi)] + \mathcal{O}(\Phi^2)$ for $\lambda \to \infty$ (see Fig. 8.10). For very large λ, the tracer sphere experiences thus the host solution as an effective one-component fluid, with an effective shear viscosity given to first order in Φ by the Einstein relation $\eta_H = \eta_0(1 + 2.5\Phi)$. In the opposite limit $\lambda \ll 1$, the point-like (relative to the host) tracer rotates for

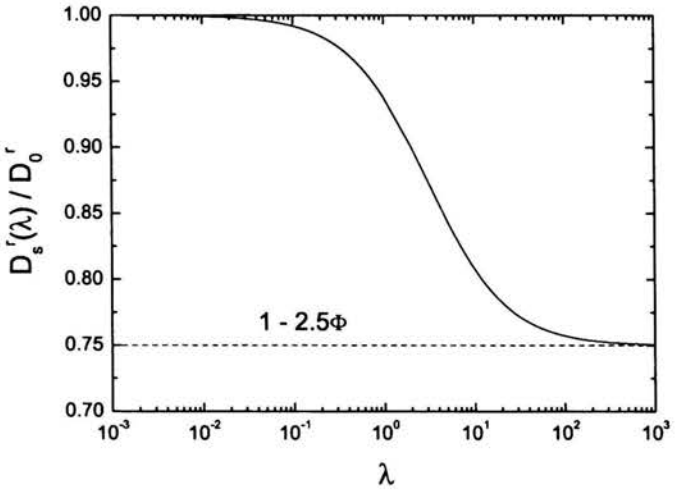

FIGURE 8.10. Reduced short-time self-diffusion coefficient, D_s^r/D_0^r versus size ratio $\lambda = a_T/a_H$ of a colloidal tracer sphere immersed in a dilute host dispersion of colloidal hard spheres. The volume fraction of host spheres is $\Phi = 0.1$. After [54, 55].

short times in an essentially stationary environment of host spheres so that its dynamic cage is affected only by the viscosity η_0 of the pure solvent.

Chapter 9

Theory of diffusion

9.1. Many-particle Smoluchowski equation

For $t \gg \tau_B$, which is the time regime of most DLS experiments, the velocities of the colloidal spheres have relaxed to Maxwellian equilibrium, so that only the slow relaxation of the particle positions and orientations is probed. Therefore, the dynamics of interacting spheres is entirely described on this coarse-grained level in terms of a many-particle probability density function, $P(\mathbf{r}^N, \hat{\mathbf{u}}, t)$, in the configuration space of positional and orientational degrees of freedom. The probability density function depends thus, in principle, on the position vectors $\mathbf{r}^N = (\mathbf{r}_1, \ldots, \mathbf{r}_N)$ and orientation vectors $\hat{\mathbf{u}}^N = (\hat{\mathbf{u}}_1, \ldots, \hat{\mathbf{u}}_N)$ of all N spheres in the suspension (scattering volume V_s). In compact notation, $X = (\hat{\mathbf{u}}^N, \mathbf{r}^N)$ denotes a $6N$-dimensional vector specifying the momentary positions and orientations of all N spheres. The equation of motion for $P(\mathbf{r}^N, \hat{\mathbf{u}}^N, t)$ is a generalization of the one-particle diffusion Eq. (8.17) to interacting particle systems. This many-particle diffusion equation is known among colloid scientists as the generalized Smoluchowski equation (GSE). In the polymer science community, a particular version of the GSE is known as the Kirkwood–Riseman–Zimm equation [36, 56].

The description of the configurational evolution by means of the GSE is founded on the separation of time scales between the strongly fluctuating particle velocities, and the slow configurational changes. Such a description cannot be applied to polymer blends since the relaxation of the matrix, which

plays the role of the solvent, is comparable to those of the other components. To explore the polymer dynamics in the diffusion limit (or Markovian limit) of small wavenumbers and long times, we resort therefore to the semi-phenomenological dynamic RPA. Using the RPA, we will study the interdiffusion process in a ternary homopolymer mixture.

In the following, we give a heuristic derivation of the generalized Smoluchowski equation, on assuming quasi-inertia-free motion of solvent and spheres. Consider N identical colloidal spheres immersed in an unbounded Newtonian solvent. The interpretation of $P(X,t)$ as an N-particle probability density function normalized to

$$\int dX\, P(X,t) = 1\,, \tag{9.1}$$

requires that $P(X,t)$ obeys a generalized continuity equation of the form [3, 24]

$$\frac{\partial}{\partial t} P(X,t) + \left(\nabla^N \cdot \mathbf{v}^N + \hat{\mathbf{L}}^N \cdot \boldsymbol{\omega}^N\right) P(X,t) = 0\,. \tag{9.2}$$

Here, $\mathbf{v}^N = (\mathbf{v}_1, \ldots, \mathbf{v}_N)$ and $\boldsymbol{\omega}^N = (\boldsymbol{\omega}_1, \ldots, \boldsymbol{\omega}_N)$ are coarse-grained translational and rotational velocities of the spheres. Moreover, $\nabla^N = (\nabla_1, \ldots, \nabla_N)$ and $\hat{\mathbf{L}}^N = (\hat{\mathbf{L}}_1, \ldots, \hat{\mathbf{L}}_N)$, with $\hat{\mathbf{L}}_i = \hat{\mathbf{u}}_i \times \partial/(\partial \hat{\mathbf{u}}_i)$ denoting the orientational 'gradient' operator applied to sphere i. The continuity equation can be formulated in a more compact form by introducing the $6N$-dimensional gradient operator $\nabla_X = (\nabla^N, \hat{\mathbf{L}}^N)$. For pedagogical reasons, however, we prefer to distinguish explicitly the translational variables from the rotational ones.

For $t \gg \tau_B \approx \tau_\eta$, we assume that inertial effects in the particle velocities and the fluid velocity field have relaxed away. It follows that the hydrodynamic forces, $\mathbf{F}^H = (\mathbf{F}_1, \ldots, \mathbf{F}_N)$, and torques $\mathbf{T}^H = (\mathbf{T}_1, \ldots, \mathbf{T}_N)$, which are exerted *on* the surfaces of the spheres by the surrounding fluid are balanced by the sum over all non-hydrodynamic forces, i.e. [3, 24, 42]

$$\begin{aligned} -\mathbf{F}^H &= \mathbf{F}^p + \mathbf{F}^{ex} + \mathbf{F}^B = -\nabla^N U - \nabla^N U^{ex} - k_B T\, \nabla^N \ln P\,, \\ -\mathbf{T}^H &= \mathbf{T}^p + \mathbf{T}^{ex} + \mathbf{T}^B = -\hat{\mathbf{L}}^N U - \hat{\mathbf{L}}^N U^{ex} - k_B T\, \hat{\mathbf{L}}^N \ln P\,. \end{aligned} \tag{9.3}$$

Here, $\mathbf{F}_i^p = -\nabla_i U(X)$ and $\mathbf{T}_i^p = -\hat{\mathbf{L}}_i U(X)$ are the force and torque, respectively, exerted on sphere i through inter-particle interactions described by the potential energy function $U(X)$ (cf. Eq. (2.6)). The latter can also depend

on particle orientations (through, e.g., dipole-dipole interactions). Likewise, $\mathbf{F}^{ex}$ and $\mathbf{T}^{ex}$ are the forces and torques exerted on the spheres by an external force field (e.g., gravitational, electric or magnetic forces) with potential $U^{ex}(X)$.

The Brownian forces and torques,

$$\begin{aligned} \mathbf{F}_i^B &= -k_B T \nabla_i \ln P, \\ \mathbf{T}_i^B &= -k_B T \hat{\mathbf{L}}_i \ln P, \end{aligned} \tag{9.4}$$

are due to the integrated effect (on the slow colloidal time scale) of the thermal motion of the fluid molecules in presence of the spheres of fixed configuration X. These 'thermodynamic' forces drive the colloidal system, for zero external forces and zero incident flow, to thermal equilibrium,

$$P(X, t \to \infty) \to P_{eq}(X) \propto \exp\{-\beta U(X)\}, \tag{9.5}$$

when the system has been prepared initially in a non-equilibrium state.

On the time- and length scales relevant to colloidal motion ($t \gg \tau_B$ and $\Delta r \gg (D_0 \tau_B)^{1/2}$), the fluid can be described by the creeping flow equation, i.e. by the stationary and linearized Navier-Stokes equation for (quasi-) incompressible flow and small Reynolds number. This equation is also frequently referred to as the Stokes' equation. For creeping flow, the hydrodynamic forces and torques are linearly related to the (angular) particle velocities in form of a generalized Stokes' law [24, 57, 58, 59],

$$\begin{pmatrix} \mathbf{v}^N - \mathbf{v}_c^N \\ \boldsymbol{\omega}^N - \boldsymbol{\omega}_c^N \end{pmatrix} = -\frac{1}{k_B T} \begin{pmatrix} \mathbf{D}^{tt}(X) & \mathbf{D}^{tr}(X) \\ \mathbf{D}^{rt}(X) & \mathbf{D}^{rr}(X) \end{pmatrix} \cdot \begin{pmatrix} \mathbf{F}^H \\ \mathbf{T}^H \end{pmatrix}. \tag{9.6}$$

The advective velocities $\mathbf{v}_c^N(X;[\mathbf{u}_0]) = (\mathbf{v}_{c1}, \ldots, \mathbf{v}_{cN})$ and $\boldsymbol{\omega}_c^N(X;[\mathbf{u}_0]) = (\boldsymbol{\omega}_{c1}, \ldots, \boldsymbol{\omega}_{cN})$ are acquired by the spheres when they are force- and torque-free. These velocities are linear functionals of $\mathbf{u}_0$, and they vanish for zero incident flow, i.e. for a quiescent suspension. To be compatible with creeping suspension flow, the incident flow must be a solution of the homogeneous Stokes' equation [59],

$$\begin{aligned} -\nabla p(\mathbf{r}) + \eta_0 \Delta \mathbf{u}(\mathbf{r}) &= 0, \\ \nabla \cdot \mathbf{u}(\mathbf{r}) &= 0, \end{aligned} \tag{9.7}$$

where $\mathbf{u}(\mathbf{r})$ and $p(\mathbf{r})$ are the fluid flow and pressure fields, respectively.

The incident flow can be considered as arising from forces acting at the infinitely distant boundaries of the fluid. An important example for $\mathbf{u}_0$ is simple linear shear flow. Here,

$$\mathbf{u}_0(\mathbf{r}) = \dot{\gamma}\,\mathbf{\Gamma}\cdot\mathbf{r} = \boldsymbol{\omega}_0 \times \mathbf{r} + \mathbf{e}_0\cdot\mathbf{r} \tag{9.8}$$

with shear rate, $\dot{\gamma}$, and velocity gradient tensor

$$\mathbf{\Gamma} = \begin{pmatrix} 0 & 1 & 0 \\ 0 & 0 & 0 \\ 0 & 0 & 0 \end{pmatrix}. \tag{9.9}$$

The tensor $\mathbf{\Gamma}$ is traceless, since $\nabla\cdot\mathbf{u}_0(\mathbf{r}) = 0$. For convenience, we have split the flow field into a rotational part, characterized by the local angular velocity $\boldsymbol{\omega}_0(\mathbf{r})$ with

$$\boldsymbol{\omega}_0(\mathbf{r}) = \frac{1}{2}\left(\nabla\times\mathbf{u}_0\right)(\mathbf{r}) = \frac{1}{2}\dot{\gamma}\,\epsilon : \mathbf{\Gamma}\,, \tag{9.10}$$

and a purely extensional flow part, characterized by the symmetric and traceless rate-of-strain tensor,

$$\mathbf{e}_0(\mathbf{r}) = \frac{1}{2}\left[(\nabla\mathbf{u}_0)(\mathbf{r}) + (\nabla\mathbf{u}_0)^T(\mathbf{r})\right] - \frac{1}{3}\,\mathbf{1}\,Tr(\nabla\mathbf{u}_0(\mathbf{r})) = \frac{1}{2}\dot{\gamma}\,\left[\mathbf{\Gamma} + \mathbf{\Gamma}^T\right]. \tag{9.11}$$

In addition, we have introduced the totally anti-symmetric and third-rank tensor ϵ. For simple linear shear flow, $\boldsymbol{\omega}_0$ and $\mathbf{e}_0$ are constants.

Replacing the translational-rotational velocities in the continuity Eq. (9.2) by Eq. (9.6), and using further the force balance equations, leads to the generalized Smoluchowski equation for $P(X,t)$:

$$\begin{aligned}\frac{\partial}{\partial t}P(X,t) = & \sum_{i,j=1}^{N}\Big\{\left(\nabla_i\cdot\mathbf{D}_{ij}^{tt} + \hat{\mathbf{L}}_i\cdot\mathbf{D}_{ij}^{rt}\right)\cdot\left(\nabla_j + \beta\left[\nabla_j U + \nabla_j U^{ex}\right]\right) \\ & + \left(\nabla_i\cdot\mathbf{D}_{ij}^{tr} + \hat{\mathbf{L}}_i\cdot\mathbf{D}_{ij}^{rr}\right)\cdot\left(\hat{\mathbf{L}}_j + \beta\left[\hat{\mathbf{L}}_j U + \hat{\mathbf{L}}_j U^{ex}\right]\right)\Big\}\,P(X,t) \\ & - \sum_{i=1}^{N}\left\{\nabla_i\cdot\mathbf{v}_{ci} + \hat{\mathbf{L}}_i\cdot\boldsymbol{\omega}_{ci}\right\}P(X,t)\,. \end{aligned} \tag{9.12}$$

Here, $\nabla_i U$, $\hat{\mathbf{L}}_i U$, $\nabla_i U^{ex}$ and $\hat{\mathbf{L}}_i U^{ex}$ are vector functions and not differential operators. The generalized Smoluchowski equation in this very general form applies both to suspensions of spheres, and to suspensions of thin uniaxial rods. In the latter case, $\hat{\mathbf{u}}_i$ points into the long-axis direction of rod i.

In Eq. (9.12), the solvent enters only through the time-independent translational-translational (tt), translational-rotational (tr), rotational-translational (rt) and rotational-rotational (rr) hydrodynamic diffusivity tensors. These tensors describe the solvent-mediated many-body hydrodynamic interactions (HI) between the particles.

The propagation of hydrodynamic disturbances (via sound and diffusion of shear waves) appears to be infinitely fast for times $t \gg \tau_\eta$. Therefore, HI between colloidal spheres act quasi-instantaneously, and the $\mathbf{D}_{ij}^{pq}(X)$, with $p, q \in \{t, r\}$, can be determined by solving the Stokes' equation, augmented by stick boundary conditions on the sphere surfaces, and by outer boundary conditions related to $\mathbf{u}_0$. Yet, actual analytical calculations of the $\mathbf{D}_{ij}^{pq}(X)$ are very difficult even in the case of spheres, and have been fully achieved only on the pairwise-additive level, mainly in form of inverse distance expansions [57, 58, 59]. Hereby one disregards the influence of other spheres on the HI between a given pair of spheres, an approximation which is valid only for large interparticle distances. Note for spheres that $\mathbf{D}_{ij}^{p,q}(\mathbf{r}^N)$ depends only on the position variables. The leading-order long-distance forms of $\mathbf{D}^{tt}$ and $\mathbf{D}^{rr}$ are discussed following Eqs. (9.67) and (9.83), respectively. For non-spherical particles like thin rods, position and orientation variables are coupled by HI. The diffusivity tensors of uniaxial rods depend both on the position and orientation vectors of the rods. Contrary to spheres, little is known about these many-rod tensors even for very thin (needle-like) rods. Note that for non-spherical particles, even the single-particle friction and diffusivity coefficients are of tensorial nature.

We consider in the following only suspensions of spheres. If we ignore HI, then $\mathbf{D}^{tt} = D_0\mathbf{1}, \mathbf{D}^{tr} = \mathbf{0} = \mathbf{D}^{rt}$, and $\mathbf{D}^{rr} = D_0^r\,\mathbf{1}$, with D_0 and D_0^r the single-sphere translational and rotational diffusion coefficients, and $\mathbf{1}$ the $3N \times 3N$-dimensional unit matrix. The advective sphere velocities without HI follow directly from the first and second Faxén theorem for stick boundary conditions (cf., e.g., [24]), namely from

$$\begin{aligned} \mathbf{v}_{ci}(\mathbf{r}) &= -\frac{1}{6\pi\eta_0 a}\left(\mathbf{F}_i^H = 0\right) + \mathbf{u}_0(\mathbf{r}_i) + \frac{a^2}{6}\nabla^2\,\mathbf{u}_0(\mathbf{r}_i)\,, \\ \boldsymbol{\omega}_{ci}(\mathbf{r}) &= -\frac{1}{8\pi\eta_0 a^3}\left(\mathbf{T}_i^H = 0\right) + \frac{1}{2}\left(\nabla \times \mathbf{u}_0\right)(\mathbf{r}_i)\,. \end{aligned} \tag{9.13}$$

These theorems are generalizations, for arbitrary incident flow, of the standard single-sphere translational-rotational Stokes' laws. They express mean

value properties since the solutions of the homogeneous Stokes' equations are bi-harmonic functions, i.e. $\nabla^4 \mathbf{u}_0 = 0$.

With Eq. (9.13) for the convective velocities, one arrives at the Smoluchowski equation for $P(X,t)$ without HI in simple incident shear flow. Explicitly

$$\begin{aligned}\frac{\partial}{\partial t} P(X,t) = \sum_{i=1}^{N} \Big\{ & D_0 \nabla_i \cdot [\nabla_i + \beta (\nabla_i [U + U^{ex}])] \\ & + D_0^r \hat{\mathbf{L}}_i \cdot \left[\hat{\mathbf{L}}_i + \beta \left(\hat{\mathbf{L}}_i [U + U^{ex}]\right)\right] \\ & - \dot{\gamma} \left(\nabla_i \cdot (\mathbf{\Gamma} \cdot \mathbf{r}_i) + \frac{1}{2} \hat{\mathbf{L}}_i \cdot (\epsilon : \mathbf{\Gamma})\right) \Big\} P(X,t) . \end{aligned} \tag{9.14}$$

Restricting ourselves to orientation-independent potential functions $U(\mathbf{r}^N)$ and $U^{ex}(\mathbf{r}^N)$, we can integrate Eq. (9.14) with respect to the positional degrees of freedom, using that

$$\int d\mathbf{r}_i \, \nabla_i \cdot [\ldots] = 0 , \tag{9.15}$$

for P vanishing in the system boundary (e.g., by assuming an infinite wall potential). This gives rise to the orientational Smoluchowski equation without HI,

$$\frac{\partial}{\partial t} P(\hat{\mathbf{u}}^N, t) = \sum_{i=1}^{N} \left\{ D_0^r \hat{\mathbf{L}}_i^{\,2} - \frac{1}{2} \dot{\gamma} \hat{\mathbf{L}}_i \cdot (\epsilon : \mathbf{\Gamma}) \right\} P(\hat{\mathbf{u}}^N, t) , \tag{9.16}$$

with the orientational probability density function, $P(\hat{\mathbf{u}}^N, t)$, defined as

$$P(\hat{\mathbf{u}}^N, t) = \int d\mathbf{r}^N \, P(X,t) . \tag{9.17}$$

For orientation-independent potentials and vanishing HI, each sphere rotates thus independently from all the others. For zero incident flow, Eq. (9.16) reduces to the single-sphere Debye Eq. (8.3) discussed already in Sec. 8.1.

We can alternatively integrate Eq. (9.14) with respect to the orientational variables, introducing hereby the positional probability density function

$$P(\mathbf{r}^N, t) = \int d\hat{\mathbf{u}}^N \, P(X,t) . \tag{9.18}$$

Application of Stokes' integral theorem to a *closed* unit sphere, where

$$\int_{4\pi} d\hat{\mathbf{u}} \, \hat{\mathbf{L}} (\ldots) = 0 , \tag{9.19}$$

leads then to the translational Smoluchowski equation without HI [24]

$$\frac{\partial}{\partial t} P(\mathbf{r}^N, t) = \sum_{i=1}^{N} \Big\{ D_0 \nabla_i \cdot \left[\nabla_i + \beta \left(\nabla_i \left[U(\mathbf{r}^N) + U^{ex}(\mathbf{r}^N) \right] \right) \right] - \dot{\gamma} \, \nabla_i \cdot (\mathbf{\Gamma} \cdot \mathbf{r}_i) \Big\} P(\mathbf{r}^N, t) \,. \quad (9.20)$$

So far we have formulated the translational and rotational variants of the generalized Smoluchowski equation without HI only. We proceed to describe the forms of the convective velocities in presence of HI. For linear incident flow, only the first order derivatives in $\mathbf{u}(\mathbf{r}) - \mathbf{u}_0(\mathbf{r})$, evaluated at the sphere centers, need to be considered. In the so-called friction problem, one prescribes the translational and rotational velocities $\mathbf{v}^N$ and $\boldsymbol{\omega}^N$, and the incident flow $\mathbf{u}_0(\mathbf{r})$. The resulting hydrodynamic forces and torques, and the force stresslets [4, 59],

$$\mathbf{S}_i^H = \int d\mathbf{r} \left\{ \left[(\mathbf{r} - \mathbf{r}_i) \, \mathbf{f}_i(\mathbf{r}) \right]_S - \frac{1}{3} \mathbf{1} \, Tr \left[(\mathbf{r} - \mathbf{r}_i) \mathbf{f}_i(\mathbf{r}) \right] \right\} , \quad (9.21)$$

acting *on* spheres $i = 1, \ldots, N$, are then obtained by the linear relations [57]

$$\begin{pmatrix} \mathbf{F}^H \\ \mathbf{T}^H \\ \mathbf{S}^H \end{pmatrix} = - \begin{pmatrix} \zeta^{tt}(\mathbf{r}) & \zeta^{tr}(\mathbf{r}) & \zeta^{ts}(\mathbf{r}) \\ \zeta^{rt}(\mathbf{r}) & \zeta^{rr}(\mathbf{r}) & \zeta^{rs}(\mathbf{r}) \\ \zeta^{st}(\mathbf{r}) & \zeta^{sr}(\mathbf{r}) & \zeta^{ss}(\mathbf{r}) \end{pmatrix} \cdot \begin{pmatrix} \mathbf{v}^N - \mathbf{u}_0^N \\ \boldsymbol{\omega}^N - \boldsymbol{\omega}^N{}_0^N \\ -\mathbf{e}_0^N \end{pmatrix} . \quad (9.22)$$

Here, $\mathbf{S}^H = (\mathbf{S}_1^H, \ldots, \mathbf{S}_N^H)$, $\mathbf{e}_0^N = (\mathbf{e}_0(\mathbf{r}_i), \ldots, \mathbf{e}_0(\mathbf{r}_i))$, as well as $\mathbf{u}_0^N$ and $\boldsymbol{\omega}_0^N$ are evaluated at the sphere centers. The translational-rotational submatrix of the grand friction matrix in Eq. (9.22) is linearly related to the mobility matrix in Eq. (9.6) through [57]

$$\begin{pmatrix} \zeta^{tt}(\mathbf{r}) & \zeta^{tr}(\mathbf{r}) \\ \zeta^{rt}(\mathbf{r}) & \zeta^{rr}(\mathbf{r}) \end{pmatrix} = k_B T \begin{pmatrix} \mathbf{D}^{tt}(\mathbf{r}) & \mathbf{D}^{tr}(\mathbf{r}) \\ \mathbf{D}^{rt}(\mathbf{r}) & \mathbf{D}^{rr}(\mathbf{r}) \end{pmatrix}^{-1} . \quad (9.23)$$

In the definition for the symmetric and traceless force dipole moment tensor, $\mathbf{S}_i^H$, given in Eq. (9.21),

$$\mathbf{f}_i(\mathbf{r}) = \delta(|\mathbf{r} - \mathbf{r}_i| - a^+) \, \sigma(\mathbf{r}) \cdot \hat{\mathbf{n}}_i(\mathbf{r}) \quad (9.24)$$

is the force density exerted on the surface of sphere i by the surrounding fluid. The surface normal vector $\hat{\mathbf{n}}(\mathbf{r})$ points hereby into the fluid. Moreover,

$$\sigma(\mathbf{r}) = -p(\mathbf{r}) \, \mathbf{1} + \eta_0 \left[\nabla \mathbf{u}(\mathbf{r}) + (\nabla \mathbf{u}(\mathbf{r}))^T \right] = -p(\mathbf{r}) \, \mathbf{1} + 2\eta_0 \, \mathbf{e}(\mathbf{r}) \quad (9.25)$$

is the Newtonian fluid stress tensor. The single-sphere stresslet is related to the incident flow field by [4]

$$\mathbf{S}_i^H = \frac{20}{3}\pi\eta_0 a^3 \left(1 + \frac{a^2}{10}\nabla^2\right) \mathbf{e}_0(\mathbf{r}_i)\,. \tag{9.26}$$

This equation is referred to as the third Faxén theorem. According to the first and second Faxén theorems, $\mathbf{F}^H = 0 = \mathbf{T}^H$ is possible even when $\mathbf{u}_0 \neq 0$. In contrast, the third Faxén theorem demands $\mathbf{S}^H \neq 0$ when the incident flow differs from a constant rotation. The reason for this behavior of the stresslet is that rigid spheres can not deform under shear. The (high-frequency-limiting) average suspension viscosity is therefore larger than the solvent viscosity.

The advective velocities entering into the generalized Smoluchowski equation with incident flow, follow from Eq. (9.22) by setting $\mathbf{F}^H = 0 = \mathbf{T}^H$, solving then successively for $\mathbf{v}_c^N - \mathbf{u}_0^N$ and $\boldsymbol{\omega}_c^N - \boldsymbol{\omega}_0^N$. This gives

$$\begin{aligned} \mathbf{v}_c^N &= \mathbf{u}_0^N + \beta\left(\mathbf{D}^{tt}\cdot\boldsymbol{\zeta}^s\right)\cdot\mathbf{e}_0^N, \\ \boldsymbol{\omega}_c^N &= \boldsymbol{\omega}_c^N - (\boldsymbol{\zeta}^{rr})^{-1}\left[\boldsymbol{\zeta}^{rs} - \beta\,\boldsymbol{\zeta}^{rt}\cdot\mathbf{D}^{tt}\cdot\boldsymbol{\zeta}^s\right]\cdot\mathbf{e}_0^N\,, \end{aligned} \tag{9.27}$$

with

$$\mathbf{D}^{tt} = k_B T\left[\boldsymbol{\zeta}^{tt} - \boldsymbol{\zeta}^{tr}\cdot(\boldsymbol{\zeta}^{rr})^{-1}\cdot\boldsymbol{\zeta}^{rt}\right]^{-1} \tag{9.28}$$

and

$$\boldsymbol{\zeta}^s = \boldsymbol{\zeta}^{ts} - \boldsymbol{\zeta}^{tr}\cdot(\boldsymbol{\zeta}^{rr})^{-1}\cdot\boldsymbol{\zeta}^{rs}\,. \tag{9.29}$$

For simple incident shear flow, the translational advective velocity of sphere i is given by

$$\mathbf{v}_{ci}(\mathbf{r}) = \boldsymbol{\Gamma}\cdot\mathbf{r}_i + \mathbf{C}_i(\mathbf{r}^N) : \boldsymbol{\Gamma}_S\,, \tag{9.30}$$

with $\boldsymbol{\Gamma}_S = \left[\boldsymbol{\Gamma} + \boldsymbol{\Gamma}^T\right]/2$. We have introduced here the third-rank shear mobility tensor, $\mathbf{C}_i(\mathbf{r}^N)$, by

$$\mathbf{C}_i(\mathbf{r}^N) = \beta\sum_{l=1}^{N}\left[\mathbf{D}^{tt}(\mathbf{r}^N)\cdot\boldsymbol{\zeta}^s(\mathbf{r}^N)\right]_{il}\,. \tag{9.31}$$

The long-distance asymptotic form of the shear mobility tensor is of order r^{-2}. Its divergence, however, decays like r^{-6} for large sphere separations [24].

Substitution of the advective velocities for simple incident shear flow into Eq. (9.12), followed by an integration over the orientational degrees of freedom, leads to the translational generalized Smoluchowski equation [24],

$$\frac{\partial}{\partial t} P(\mathbf{r}^N, t) = \sum_{i,j=1}^{N} \nabla_i \cdot \mathbf{D}_{ij}^{tt} \cdot \left[\nabla_j + \beta \left(\nabla_i \left[U(\mathbf{r}^N) + U^{ex}(\mathbf{r}^N)\right]\right)\right] P(\mathbf{r}^N, t) - \sum_{i=1}^{N} \nabla_i \cdot \left[\boldsymbol{\Gamma} \cdot \mathbf{r}_i + \mathbf{C}_i(\mathbf{r}^N) : \boldsymbol{\Gamma}_S\right] P(\mathbf{r}^N, t) . \quad (9.32)$$

This equation describes hydrodynamically interacting spheres under simple shear.

Although these lecture notes are focused on the statics and dynamics of spherical colloidal particles, it is of interest to discuss briefly the form of the GSE for a suspension of N identical long and thin rods. For these suspensions, the volume fractions corresponding to the isotropic phase are very small. Therefore hydrodynamic interactions are probably far less important than for suspensions of spheres [60]. However, this assertion should be checked carefully in future studies.

Without HI between the rods, $\mathbf{D}^{rt} = \mathbf{0} = \mathbf{D}^{tr}$. Moreover, all cross terms, $i \neq j$, of $\mathbf{D}_{ij}^{tt}$ and $\mathbf{D}_{ij}^{rr}$ do vanish. The only non-vanishing diffusivity components (tensors) in Eq. (9.12) are the self-terms

$$\begin{aligned} \mathbf{D}_{ii}^{tt} &= D_0^{\parallel} \hat{\mathbf{u}}_i \hat{\mathbf{u}}_i + D_0^{\perp} (\mathbf{1} - \hat{\mathbf{u}}_i \hat{\mathbf{u}}_i) , \\ \mathbf{D}_{ii}^{rr} &= D_0^r \mathbf{1} . \end{aligned} \quad (9.33)$$

In Eq. (9.33), the single-rod translational diffusion coefficients for motion of the rod center parallel and perpendicular to the long axis, respectively, are given by [60]

$$\begin{aligned} D_0^{\parallel} &= \frac{k_B T \ln\{L/D\}}{2\pi\eta_0 L} , \\ D_0^{\perp} &= \frac{1}{2} D_0^{\parallel} , \end{aligned} \quad (9.34)$$

where L and D, with $L \gg D$, are the rod length and thickness. End effects are disregarded here. The single-rod rotational diffusion coefficient, D_0^r,

quantifies the rotation of a rod with angular velocity perpendicular to the long axis. It reads

$$D_0^r = \frac{3k_BT\ln\{L/D\}}{\pi\eta_0 L^3}\,. \tag{9.35}$$

For very large and thin rods, one can disregard rotation along the long axis. After inserting Eq. (9.33) into Eq. (9.12), we are led to the intermediate result

$$\frac{\partial}{\partial t}P(X,t) = \sum_{i=1}^{N}\Big\{\nabla_i\cdot\Big(D_0^{\parallel}\,\hat{\mathbf{u}}_i\hat{\mathbf{u}}_i + D_0^{\perp}\,(\mathbf{1}-\hat{\mathbf{u}}_i\hat{\mathbf{u}}_i)\Big)\,[\nabla_i + \beta\,(\nabla_i\,[U+U^{ex}])]$$
$$+ D_0^r\,\hat{\mathbf{L}}_i\cdot\Big[\hat{\mathbf{L}}_i + \beta\Big(\hat{\mathbf{L}}_i\,[U+U^{ex}]\Big)\Big] - \Big(\nabla_i\cdot\mathbf{v}_{ci} + \hat{\mathbf{L}}_i\cdot\boldsymbol{\omega}_{ic}\Big)\Big\}\,P(X,t)\,. \tag{9.36}$$

The center of a hydrodynamically non-interacting rod i, located at $\mathbf{r}_i$ is advected, in presence of simple incident shear flow, with the velocity

$$\mathbf{v}_{ci} = \dot{\gamma}\,\boldsymbol{\Gamma}\cdot\mathbf{r}_i\,. \tag{9.37}$$

To obtain the advective angular velocity $\boldsymbol{\omega}_{ci}$ of a rod we select a co-moving co-ordinate system centered at $\mathbf{r}_i$. The tip of $\hat{\mathbf{u}}_i$ would be dragged along by the flow with velocity $\dot{\gamma}\,\boldsymbol{\Gamma}\cdot\hat{\mathbf{u}}_i$, if there would not be the length constraint ${\hat{\mathbf{u}}_i}^2 = 1$ which demands that $\dot{\hat{\mathbf{u}}}_i \perp \hat{\mathbf{u}}_i$. Hence, $\dot{\hat{\mathbf{u}}}_i$ must be equal to the projection of the vector $\dot{\gamma}\,\boldsymbol{\Gamma}\cdot\hat{\mathbf{u}}_i$ onto a direction perpendicular to $\hat{\mathbf{u}}_i$, viz.

$$\dot{\hat{\mathbf{u}}}_i = \dot{\gamma}\,(\mathbf{1}-\hat{\mathbf{u}}_i\hat{\mathbf{u}}_i)\cdot\boldsymbol{\Gamma}\cdot\hat{\mathbf{u}}_i = \dot{\gamma}\,\boldsymbol{\Gamma}\cdot\hat{\mathbf{u}}_i + \dot{\gamma}\,(\hat{\mathbf{u}}_i\cdot\boldsymbol{\Gamma}\cdot\hat{\mathbf{u}}_i)\,\hat{\mathbf{u}}_i\,. \tag{9.38}$$

We only need to consider that part of the flow-induced angular velocity which changes the orientation of the rod. This part must be perpendicular to $\hat{\mathbf{u}}_i$. Therefore, we have [36, 60]

$$\boldsymbol{\omega}_{ci} = \hat{\mathbf{u}}_i\times\dot{\hat{\mathbf{u}}}_i = \dot{\gamma}\,\hat{\mathbf{u}}_i\times(\boldsymbol{\Gamma}\cdot\hat{\mathbf{u}}_i) \tag{9.39}$$

for the advective angular velocity of a single rod.

In Eq. (9.36), we rewrite

$$D_0^{\parallel}\,\hat{\mathbf{u}}_i\hat{\mathbf{u}}_i + D_0^{\perp}\,(\mathbf{1}-\hat{\mathbf{u}}_i\hat{\mathbf{u}}_i) = \frac{3}{4}\,\overline{D}\,(\mathbf{1}-\hat{\mathbf{u}}_i\hat{\mathbf{u}}_i) \tag{9.40}$$

introducing hereby the single-rod mean translational diffusion coefficient

$$\overline{D} = \frac{1}{3}\left[D_0^{\parallel} + 2\,D_0^{\perp}\right] = \frac{4}{3}\,D_0^{\perp}\,. \tag{9.41}$$

Insertion of Eqs. (9.37) and (9.39) into Eq. (9.36) gives the final result,

$$\frac{\partial}{\partial t} P(X,t) = \sum_{i=1}^{N} \Big\{ \frac{3}{4} \overline{D} \nabla_i \cdot (\mathbf{1} - \hat{\mathbf{u}}_i \hat{\mathbf{u}}_i) \cdot [\nabla_i + \beta (\nabla_i [U + U^{ex}])] + D_0^r \hat{\mathbf{L}}_i \cdot \Big[\hat{\mathbf{L}}_i + \beta \Big(\hat{\mathbf{L}}_i [U + U^{ex}] \Big) \Big] - \dot{\gamma} \nabla_i \cdot (\boldsymbol{\Gamma} \cdot \mathbf{r}_i) - \dot{\gamma} \hat{\mathbf{L}}_i (\cdot \hat{\mathbf{u}}_i \times (\boldsymbol{\Gamma} \cdot \hat{\mathbf{u}}_i)) \Big\} P(X,t), \quad (9.42)$$

for the Smoluchowski equation (without HI) of long and thin rods in simple shear flow. This equation is the starting point for investigations on various interesting dynamic aspects of colloidal rod dispersions, like translational-rotational diffusion, sedimentation, shear-induced paranematic-to-nematic transitions, viscoelasticity, and shear banding in inhomogeneous rod suspensions (cf., e.g., [24, 60, 61, 62]).

9.2. Dynamics of colloidal spheres

In this section, we concentrate on quiescent suspensions of colloidal spheres without external fields, and with orientation-independent pair forces. Equation (9.32) reduces then further to the translational GSE,

$$\frac{\partial}{\partial t} P(\mathbf{r}^N, t) = \widehat{O}(\mathbf{r}^N) P(\mathbf{r}^N, t), \quad (9.43)$$

where

$$\widehat{O}(\mathbf{r}^N) = \sum_{i,j=1}^{N} \nabla_i \cdot \mathbf{D}_{ij}(\mathbf{r}^N) \cdot [\nabla_j - \beta \mathbf{F}_j] \quad (9.44)$$

is the Smoluchowski differential operator, and $\mathbf{F}_j = -\nabla_j U(\mathbf{r}^N)$. Here and subsequently, the abbreviation $\mathbf{D}_{ij}(\mathbf{r}^N) = \mathbf{D}_{ij}^{tt}(\mathbf{r}^N)$ is used for the translational diffusivity tensors.

In equilibrium, $(\partial/\partial t)P = 0$, and the GSE is satisfied by the equilibrium probability density function $P_{eq}(\mathbf{r}^N) \propto \exp\{-\beta U(\mathbf{r}^N)\}$. The latter is independent of the $\mathbf{D}_{ij}(\mathbf{r}^N)$, which shows that the HI are dynamic forces with no effect on static equilibrium properties.

Using the GSE (9.43), one can express equilibrium time-correlation functions like $S_c(q,t)$ and $S_s(q,t)$ as

$$S_A(q,t) = \langle \rho_A(-\mathbf{q}) \Big(\exp\{\widehat{O}_B t\} \rho_A(\mathbf{q}) \Big) \rangle, \quad (9.45)$$

with $A = a, c$ and microscopic densities $\rho_c(\mathbf{q}) = \rho(\mathbf{q})$ (see Eq. (7.24)) and $\rho_s(\mathbf{q}) = \exp\{i\mathbf{q} \cdot \mathbf{r}_1\}$. Here

$$\widehat{O}_B(\mathbf{r}^N) = \sum_{i,j=1}^{N} \left[\nabla_i + \frac{1}{k_B T} \mathbf{F}_i \right] \cdot \mathbf{D}_{ij}(\mathbf{r}^N) \cdot \nabla_j \tag{9.46}$$

is the adjoint (or backward) Smoluchowski operator, and

$$\langle \cdots \rangle = \int d\mathbf{r}^N P_{eq}(\mathbf{r}^N) \, (\cdots) \tag{9.47}$$

is the equilibrium ensemble average. Note that the time evolution operator $\exp\{\widehat{O}_B t\}$ in Eq. (9.45) operates only on ρ_A, and not on P_{eq}.

In the following two subsections, we describe theoretical methods based on the GSE. From a theoretical point of view, it is appropriate to treat short-time diffusion and long-time diffusion separately, since the former is needed as an input to the latter one.

Short-time diffusion

In general, $S_A(q,t)$ can not be calculated exactly from Eq. (9.45), owing to the complicated form of the operator $\widehat{O}_B$ for interacting particles. However, for short times $t \ll \tau_I$, $S_A(q,t)$ can be expressed in a series of cumulants, that is

$$\begin{aligned} S_A(q,t) &= S_A(q) \, \exp\{ \sum_{l=1}^{\infty} (-t)^l \, \frac{\Gamma_A^{(l)}(q)}{l!} \} \\ &= S_A(q) \, \exp\{ -\Gamma_A^{(1)}(q) t + \frac{1}{2} \Gamma_A^{(2)}(q) t^2 + \cdots \} \end{aligned} \tag{9.48}$$

with $S_A(q) = S_A(q,t)$. The higher-order cumulants, $\Gamma_A^{(l)}$, with $l = 2, 3, \ldots$, measure the deviation of $S_A(q,t)$ from a single exponential decay. Cumulant analysis is a customary tool to analyze DLS data at short times, whereby mainly the first and second cumulants have been determined. One can alternatively expand $S_A(q,t)$ in a time Taylor series, resulting in the so-called moment expansion

$$S_A(q,t) = \sum_{n=0}^{\infty} \frac{t^n}{n!} \, S_A^{(n)}(q) = S_A(q) + t S_a^{(1)}(q) + \frac{1}{2} t^2 \, S_A^{(2)}(q) \,, \tag{9.49}$$

with moments

$$S_A^{(n)}(q) = \frac{1}{N}\langle \rho_A(-\mathbf{q})(\widehat{O}_B)^n \rho_A(\mathbf{q})\rangle \,. \tag{9.50}$$

In deriving Eq. (9.50), we have expanded the time evolution operator $\exp\{\widehat{O}_B\}$ in Eq. (9.45) in powers of t. From a small-t expansion of Eq. (9.48), it follows for the two leading cumulants that

$$\begin{aligned} \Gamma_A^{(1)}(q) &= -\frac{S_A^{(2)}(q)}{S_A(q)} \,, \\ \Gamma_A^{(2)}(q) &= \frac{S_A^{(2)}(q)}{S_A(q)} - \left[\frac{S_A^{(1)}(q)}{S_A(q)}\right]^2 \,. \end{aligned} \tag{9.51}$$

In specializing to $A = c$, the first cumulant of the collective dynamic structure factor follows as

$$\Gamma_c^{(1)}(q) = q^2 D_c^s(q) = q^2 D_0 \frac{H(q)}{S_c(q)} \,. \tag{9.52}$$

Here, $D_c^s(q)$ is the apparent short-time collective diffusion coefficient already defined in Eq. (8.70), and $H(q)$ is given by

$$H(q) = \frac{1}{ND_0} \sum_{l,j=1}^{N} \langle \hat{\mathbf{q}} \cdot \mathbf{D}_{lj}(\mathbf{r}^N) \cdot \hat{\mathbf{q}} \exp\{i\mathbf{q} \cdot [\mathbf{r}_l - \mathbf{r}_j]\}\rangle \,. \tag{9.53}$$

The function $H(q) \geq 0$ contains, through the diffusion tensors $\mathbf{D}_{lj}$, the influence of HI on the short-time collective diffusion. For this reason, $H(q)$ is known as the *hydrodynamic function*. Without HI, $H(q) \equiv 1$, so that $D_c^s(q) = D_0/S_c(q)$ in this case. Any q-dependence of $H(q)$ is thus an indicator for the non-negligible influence of HI. Comparison with the phenomenological Eq. (8.80) shows that

$$\lim_{q\to 0} H(q) = \frac{U^s}{U_0} \,. \tag{9.54}$$

Hence, the long wave length limit of the hydrodynamic function is equal to the relative (short-time) sedimentation velocity in a homogeneous suspension. According to Eq. (9.53), $H(q)$ is indeed a short-time equilibrium average. For $q > 0$, $H(q)$ can be interpreted as a generalized (short-time) sedimentation coefficient: assume a spatially periodic and weak external force of amplitude $F(q)$ to act on each colloidal sphere according to

$$\mathbf{F}_j = \hat{\mathbf{q}} F(q) \exp\{-i\mathbf{q} \cdot \mathbf{r}_j\} \,, \tag{9.55}$$

with $j = 1, \ldots, N$, and all forces collinear with the unit vector $\hat{\mathbf{q}}$. Then, a simple linear response analysis shows for $\tau_B \ll t \ll \tau_I$ that,

$$\frac{U_s(q)}{U_0(q)} = H(q) \,, \tag{9.56}$$

where

$$U_s(q) = < \frac{1}{N} \sum_{l=1}^{N} V_l \exp\{i\mathbf{q} \cdot \mathbf{r}_l\} >_{st} \tag{9.57}$$

is the wave-number dependent generalized velocity response to the applied forces, and $\langle \cdots \rangle_{st}$ is a stationary short-time average. Here, $U_0(q) = \beta D_0 F(q)$. For non-macroscopically large q^{-1}, there is no macroscopic solvent backflow, since the applied force-field changes sign each half wave length, π/q, along the direction of $\hat{\mathbf{q}}$. Therefore no renormalization method is needed for calculating $H(q > 0)$. Obviously, $\lim_{q \to 0} U_s(q) = U_s$.

Next, the first cumulant for the self-dynamic structure factor is determined as (see Eq. (9.50))

$$\Gamma_s^{(1)}(q) = q^2 D_s^s \,, \tag{9.58}$$

with the microscopic expression

$$D_s^s = \langle \hat{\mathbf{q}} \cdot \mathbf{D}_{11}(\mathbf{r}^N) \cdot \hat{\mathbf{q}} \rangle \tag{9.59}$$

for the translational short-time self-diffusion coefficient. Without HI, $D_s^s = D_0$ since at short times, the Brownian motion of a sphere is not influenced by direct forces.

For large $q \gg q_m$, strong oscillations in the exponential factors in Eq. (9.53) cancel each other for $l \neq j$, and $H(q)$ becomes therefore equal to the reduced short-time self-diffusion coefficient, i.e.

$$H(q \gg q_m) \approx \frac{D_s^s}{D_0} \,. \tag{9.60}$$

Likewise, $D_c^s(q \gg q_m) \approx D_s^s$ since $S_c(q \gg q_m) = 1$. Thus, it is in principle possible to determine short-time self-diffusion properties from DLS experiments performed at long wavenumbers without a need for contrast variation. Index matching is needed, however, to determine the MSD at longer times.

Moments up to the third order have been calculated for $S_A(q,t)$. The expression for the second moment of $S_c(q,t)$ reads without HI

$$S_c^{(2)}(q) = (q^2 D_0)^2 \left\{ 1 + \frac{\beta\rho_0}{q^2} \int d\mathbf{r}\, g(r)\,(1 - \cos(\mathbf{q}\cdot\mathbf{r}))\,(\hat{\mathbf{q}}\cdot\nabla)^2 u(r) \right\}. \quad (9.61)$$

It is given in terms of the pair distribution function $g(r)$, and derivatives of the pair potential, $u(r)$, between two spheres. Hereby it is assumed that the total potential energy is pairwise additive, that is $U(\mathbf{r}^N) = \sum_{i<j} u(|\mathbf{r}_i - \mathbf{r}_j|)$. The second cumulant, $S_s^{(2)}(q)$, of $S_s(q,t)$ is given by Eq. (9.61) with the $\cos(\mathbf{q}\cdot\mathbf{r})$ term omitted, since

$$S_c(q \gg q_m, t) = S_s(q,t) \quad (9.62)$$

due to smallness of the distinct part, $S_d(q,t)$, of $S_c(q,t)$ for $q \gg q_m$ (cf. Eq. (7.28)).

Little is known about the higher-order moments. With HI, even the second moment becomes quite complicated, invoking now up to four-particle static distribution functions. Thus moment expansions are not very helpful in gaining information on $S_A(q,t)$ for intermediate and long times. In the following section, we will describe a projection operator method, which is far better suited for analyzing the dynamics at long times.

Incidentally, the second moment of $S_A(q,t)$ does not exist for systems with singular pair potentials like suspensions of colloidal hard spheres. For the latter case, the non-analytical short-time expansion of $S_A(q,t)$ is given by

$$S_A(q,\tau) = S_A(q) - \tau + \frac{4\sqrt{\pi}}{3} C_A(q;\Phi)\tau^{3/2} + \cdots \quad (9.63)$$

with $\tau = q^2 D_0 t$. Explicit expressions for the expansion coefficients $C_s(q;\Phi)$ and $C_c(q;\Phi)$ can be found in [63, 46].

In order to obtain explicit results for the short-time translational property $H(q)$ and its limiting values U^s and D_s^s, it is necessary to specify the translational diffusivity tensors $\mathbf{D}_{ij}(\mathbf{r}^N)$. For this purpose, it is useful to expand $\mathbf{D}_{ij}(\mathbf{r}^N)$, according to

$$\mathbf{D}_{ij}(\mathbf{r}^N) = D_0 \mathbf{1}\delta_{ij} + \mathbf{D}_{ij}^{(2)}(\mathbf{r}^N) + \mathbf{D}_{ij}^{(3)}(\mathbf{r}^N) + \cdots, \quad (9.64)$$

into contributions, $\mathbf{D}_{ij}^{(n)}(\mathbf{r}^N)$, originating from increasingly large clusters of n hydrodynamically interacting spheres.

For (very) small volume fractions, it is justified to assume pairwise additivity of the HI. In this case

$$\mathbf{D}_{ij}(\mathbf{r}^N) \approx D_0 \mathbf{1}\delta_{ij} + \mathbf{D}_{ij}^{(2)}(\mathbf{r}^N), \tag{9.65}$$

with

$$\mathbf{D}_{ij}^{(2)}(\mathbf{r}^N) = D_0\left[\delta_{ij}\sum_{l\neq i}^{N}\boldsymbol{\omega}_{11}(\mathbf{r}_i - \mathbf{r}_l) + (1-\delta_{ij})\,\boldsymbol{\omega}_{12}(\mathbf{r}_i - \mathbf{r}_j)\right]. \tag{9.66}$$

The first term of Eq. (9.66) determines $\mathbf{D}_{11}$ in Eq. (9.59) so that the tensor $\boldsymbol{\omega}_{11}$ modifies the short-time self-diffusion coefficient as compared to its value, D_0, at infinite dilution. The tensor $\boldsymbol{\omega}_{12}$ determines the distinct part, $i \neq j$, of $H(q)$. For one-component suspensions of spheres, series expansions of $\boldsymbol{\omega}_{11}(\mathbf{r})$ and $\boldsymbol{\omega}_{12}(\mathbf{r})$ are known, in principle, to arbitrary order. The leading terms in these long-distance expansions are

$$\begin{aligned}
\boldsymbol{\omega}_{11}(\mathbf{r}) &= -\frac{15}{4}\left(\frac{a}{r}\right)^4 \hat{\mathbf{r}}\hat{\mathbf{r}} + \mathcal{O}\left[\left(\frac{a}{r}\right)^6\right], \\
\boldsymbol{\omega}_{12}(\mathbf{r}) &= \frac{3}{4}\left(\frac{a}{r}\right)[\mathbf{1} + \hat{\mathbf{r}}\hat{\mathbf{r}}] + \frac{1}{2}\left(\frac{a}{r}\right)^3[\mathbf{1} - 3\hat{\mathbf{r}}\hat{\mathbf{r}}] + \mathcal{O}\left[\left(\frac{a}{r}\right)^7\right]
\end{aligned} \tag{9.67}$$

where $\hat{\mathbf{r}} = \mathbf{r}/r$. The long-distance (i.e. far-field) expression for $\boldsymbol{\omega}_{12}(\mathbf{r})$ up to $\mathcal{O}(r^{-3})$ is the well-known Rotne–Prager (RP) tensor [64]. In general, $\mathbf{D}_{ij}^{(s)} \sim \mathcal{O}(r^{-(3s-5)})$ at large r.

Substitution of Eq. (9.66) into Eqs. (9.53) and (9.59) leads to the expressions

$$D_s^s = D_0\left[1 + \rho_0 \int d\mathbf{r}\, g(r)\,\hat{\mathbf{q}}\cdot\boldsymbol{\omega}_{11}(\mathbf{r})\cdot\hat{\mathbf{q}}\right], \tag{9.68}$$

$$H(q) = \frac{D_s^s}{D_0} + \rho_0 \int d\mathbf{r}\, g(r)\,\hat{\mathbf{q}}\cdot\boldsymbol{\omega}_{12}(\mathbf{r})\cdot\hat{\mathbf{q}}\cos(\mathbf{q}\cdot\mathbf{r}), \tag{9.69}$$

valid for pairwise additive HI. The only input needed to calculate D_s^s and $H(q)$ from these expressions is the pair distribution function $g(r)$. The latter gives the conditional probability of finding a second sphere a distance r apart from a given one. For given pair potential $u(r)$, $g(r)$ can be determined using standard integral equation methods or computer simulations [1, 3]. For neutral hard spheres, $g(r)$ has its maximum at contact distance, $r = 2a$, whereas it is practically equal to zero for charged spheres up to the nearest-neighbor distance, where it attains a rather pronounced peak. This implies

that, contrary to dilute suspensions of charge-stabilized spheres, where only the leading far-field terms in ω_{ij} are of importance, many more terms need to be summed up for neutral hard spheres.

The most accurate virial expansion result for the D_s^s of monodisperse hard spheres valid to second order in Φ reads [65]

$$\frac{D_s^s}{D_0} = 1 - 1.832\Phi - 0.219\Phi^2 + \mathcal{O}(\Phi^3)\,. \tag{9.70}$$

This result has been obtained from summing up a large number of terms in the inverse distance expansions of $\mathbf{D}_{11}^{(2)}$ and $\mathbf{D}_{11}^{(3)}$, and by further accounting for short-range lubrication interactions between nearly touching pairs or triplets of spheres. Three-body terms in $\mathbf{D}_{11}$, which contribute to D_s^s to order Φ^2, first appear in order r^{-7}. For comparison, the leading-order three-body contribution to $\mathbf{D}_{12}$ is of order r^{-4}.

Figure 9.1 depicts D_s^s, determined according to Eq. (9.70), in comparison with DLS and depolarized DLS data on hard spheres, and with the semi-empirical formula,

$$\frac{D_s^s}{D_0} = (1 - 1.56\Phi)\,(1 - 0.27\Phi)\;, \tag{9.71}$$

proposed by Lionberger and Russel [66]. The latter formula conforms to the (numerically) exact $\mathcal{O}(\Phi)$ limit in Eq. (9.70), and it predicts D_s^s to vanish

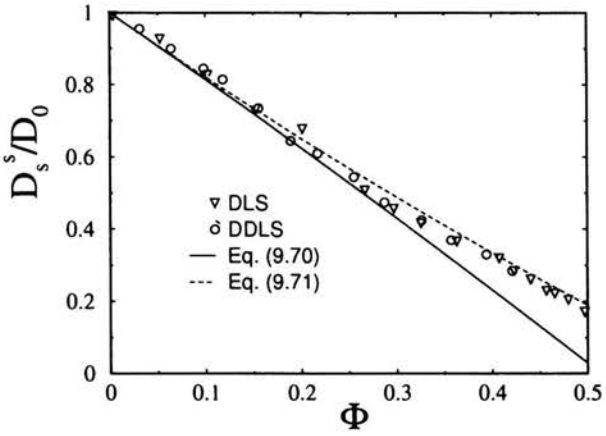

FIGURE 9.1. Reduced short-time translational self-diffusion coefficient, D_s^s/D_0, of monodisperse hard-sphere suspensions. We compare experimental DLS [48] and depolarized DLS [53] data with the $\mathcal{O}(\Phi^2)$ expression in Eq. (9.70), and the semi-empirical expression in Eq. (9.71). After [54, 69].

at the volume fraction $\Phi_{rcp} \approx 0.64$ where random close packing occurs. As seen in Fig. 9.1, the second-order virial form is applicable for $\Phi < 0.3$. The experimental data are overall well described by Eq. (9.71) up to $\Phi \approx 0.5$, where the systems begins to freeze into an ordered solid state.

To first order in Φ, the sedimentation velocity of hard spheres has been determined by Batchelor [67]. Very recently, the second virial coefficient of U_s was derived by Cichocki and co-workers [68]. The second-order virial expansion reads explicitly [68]

$$\frac{U^s}{U_0} = 1 - 6.546\Phi + 21.918\Phi^2 + \mathcal{O}(\Phi^3)\,. \tag{9.72}$$

Using that $S_c(q = 0) = 1 - 8\Phi + 34\Phi^2 + \mathcal{O}(\Phi^3)$, the short-time collective diffusion coefficient of hard spheres at low concentrations is determined as

$$\frac{D_c^s}{D_0} = 1 + 1.454\Phi - 0.45\Phi^2 + \mathcal{O}(\Phi^3)\,, \tag{9.73}$$

indicating that $D_c^s > D_0$. The modest initial increase in D_c^s with Φ described by Eq. (9.73) is counter-operated by HI through the factor $H(0)$, which causes D_c^s to decay towards zero for larger Φ.

For hard spheres up to $\Phi = 0.5$, it has been shown in comparison to exact low-density calculations [70], experimental data [48] and so-called Lattice-Boltzmann computer simulation results for $H(q)$ [48], that [46, 70]

$$H(q_m) = 1 - 1.35\Phi\,. \tag{9.74}$$

The Lattice-Boltzmann simulation method combines Newtonian dynamics of the solid colloidal particles with a discretized Boltzmann-type equation for the fluid phase (see, e.g., [71]). It is particularly suited to analyze the effect of many-body HI on the colloidal short-time dynamics.

The principal peak height, $S_c(q_m)$, of the hard-sphere static structure factor is well described, within $0 < \Phi < 0.5$, by [46, 72]

$$S_c(q_m) = 1 + 0.644\Phi\, g(r = 2a^+)\,, \tag{9.75}$$

where $g(r = 2a^+) = (1 - 0.5\Phi)/(1 - \Phi)^3$ is the Carnahan–Starling contact value of $g(r)$. Note that $S_c(q_m) \approx 2.85$ at $\Phi = 0.494$, in accord with the empirical Hansen–Verlet freezing criterion [17]. This criterion states for one-component atomic and colloidal liquids that freezing into an ordered state sets in when $S_c(q_m)$ exceeds $2.8 \div 3.0$. Substitution of Eqs. (9.74) and (9.75)

into $D_c^s(q_m) = D_0 H(q_m)/S_c(q_m)$ gives an analytic expression for the short-time apparent collective diffusion coefficient, $D_c^s(q_m)$, which, according to Fig. 8.9, is in perfect agreement with experimental data.

Calculations of the hard-sphere H(q) in dependence on q have been performed by Beenakker and Mazur [73]. These involved calculations account in an approximate way for many-body HI contributions (through so-called ring diagrams), with results for $H(q)$ which agree, up to $\Phi \approx 0.3$, quite well with experimental data and Lattice-Boltzmann computer simulations [48].

The shape of $H(q)$ is rather similar to that of $S_c(q)$ for the same Φ. The maximum of $H(q)$ is located close to q_m. However, according to Eq. (9.74), $H(q_m)$ decreases linearly in Φ, while $S_c(q_m)$ is instead a monotonically increasing function in Φ (see Eq. (9.75)).

Having discussed the short-time properties of colloidal suspensions with short-range, i.e. hard-sphere-like, pair interactions, we proceed to discuss the opposite case of charge-stabilized suspensions with long-range electrostatic repulsions among the particles. We examine in particular systems with small amounts of excess electrolyte (in addition to the neutralizing counterions). The highly charged colloidal particles in these systems are already strongly correlated at volume fractions as low as $\Phi \approx 10^{-4}$. The strong electrostatic repulsion keeps the particles apart from each other such that contact configurations are extremely unlikely. Contrary to hard-sphere dispersions in which near-field hydrodynamic lubrication forces are important, the diffusion of charged colloidal spheres is thus influenced only by the far-field part of the HI. This salient difference in the effect of the HI leads to remarkable qualitative differences in the dynamic behavior of charge-stabilized dispersions and suspensions of hard spheres.

The usual virial expansion in Φ, which is so successful for semi-dilute hard-sphere suspensions, does not apply to charge-stabilized suspensions. Non-linear volume fraction dependencies have been predicted instead by Nägele and co-workers for the short-time transport properties of monodisperse charge-stabilized dispersions [75, 79, 3, 77, 78, 74, 76]. In particular, D_s^s obeys a fractional Φ-dependence of the form [3]

$$\frac{D_s^s}{D_0} = 1 - a_t \Phi^{4/3}, \tag{9.76}$$

with a parameter $a_t \approx 2.5$, which depends only weakly on the charge of the colloidal particle, provided that the charge remains large enough to mask the physical hard core of the particle. Eq. (9.76) is valid typically for $\Phi \leq 0.05$.

At larger volume fractions, three- and more-body HI come into play, and Eq. (9.76) becomes invalid. The $\Phi^{3/4}$-dependence of D_s^s has been verified in recent DLS measurements on charge-stabilized suspensions with the excess electrolyte (i.e. excess salt ions) removed form the suspension using an ion exchange resin [80]. According to Eq. (9.76), the D_s^s of charged spheres is less strongly reduced by HI than for hard spheres at the same volume fraction. In case of hard spheres, lubrication forces between nearby spheres are operating whereas the dynamics of charged spheres is dominated by far-field HI.

HI have a stronger effect on charged spheres than on neutral ones, when instead of D_s^s, the sedimentation velocity in a homogeneous system is considered. In this case, theory predicts for charge-stabilized suspensions with $\Phi < 0.1$ that

$$\frac{U^s}{U_0} = 1 - a_s \Phi^{1/3}, \tag{9.77}$$

with a nearly charge- and particle size-independent coefficient $a_s \approx 1.8$ [75, 3, 76]. The fractional exponent 1/3 has been subsequently confirmed by measurements of the sedimentation velocity in deionized charge-stabilized suspensions [79]. Equation (9.77) predicts, for $\Phi = 10^{-3}$, a reduction in U^s from the zero-density limit U_0 by as much as 15%, whereas the reduction for hard spheres at the same Φ is as small as 0.4% (cf. Eq. (9.72)). This is quite remarkable, for in the past the influence of HI on dilute charge-stabilized dispersions had been frequently considered to be negligibly small. The origin for the smaller sedimentation velocity of charged spheres as compared to uncharged ones at the same Φ is that charged particles are more strongly exposed to laminar solvent friction arising from the cumulative backflow of displaced fluid. This backflow friction is more effective for charged particles since, contrary to neutral spheres, nearby particle pairs are very unlikely.

The strong influence of (far-field) HI on charged particles can be observed further in the significant wavenumber dependence of $H(q)$. For charged spheres at $\Phi \leq 10^{-2}$, it is sufficient to substitute in Eq. (9.53) the Rotne–Prager limiting form of $\mathbf{D}_{ij}$ given in Eq. (9.67). This leads to [81]

$$H(y) = 1 - 15\Phi \frac{j_1(y)}{y} + 18\Phi \int_1^\infty dx\, x\, [g(x) - 1] \left\{ j_0(xy) - \frac{j_1(xy)}{xy} + \frac{j_2(xy)}{6x^2} \right\} \tag{9.78}$$

with $y = 2qa$, $x = r/(2a)$, and j_n the spherical Bessel function of order n. DLS data of Härtl and co-workers [82] for the hydrodynamic function of dilute charge-stabilized suspensions are displayed in Fig. 9.2 for three different concentrations. Notify the pronounced oscillations of $H(q)$ even for the smallest $\Phi \approx 10^{-4}$ considered. The experimental $H(q)$ are overall in very good agreement with the theoretical result in Eq. (9.78). The differences at small q can be attributed to the scattering contribution of residual particle

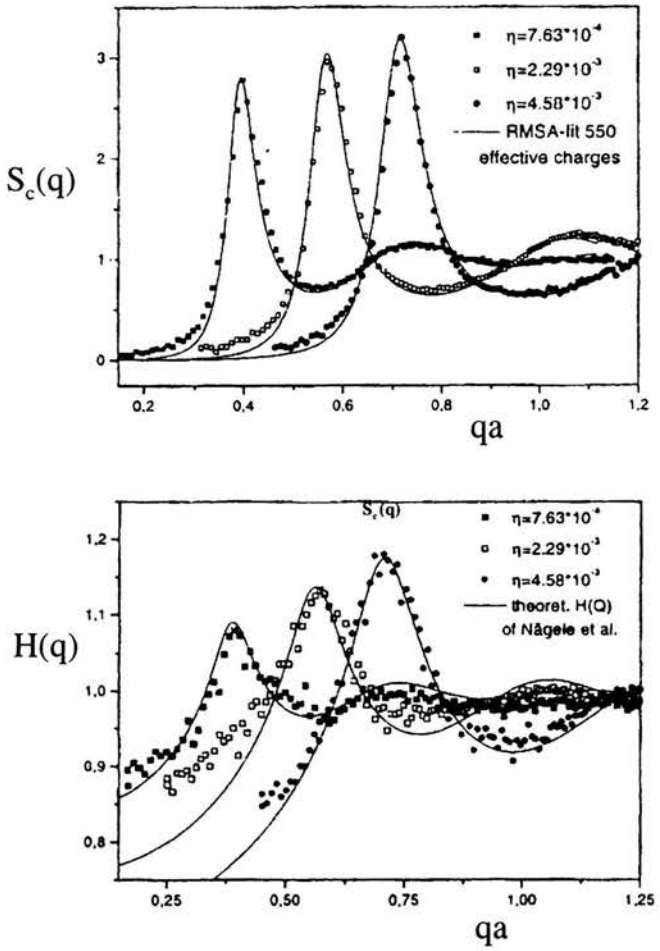

FIGURE 9.2. Static structure factor $S_c(q)$(top) and hydrodynamic function $H(q)$ (bottom) versus qa for aqueous dispersions of strongly charged spheres at $\Phi = 7.63 \cdot 10^{-4}$, $2.29 \cdot 10^{-3}$, and $4.58 \cdot 10^{-3}$ (curves from left to right). Note that without HI, $H(q) \equiv 1$. After [82].

aggregates in the experimental probes and to polydispersity effects, which are most influential at small q. The radial distribution function in Eq. (9.78) was determined from fitting the peak heights, $S_c(q_m)$, of the experimental $S(q)$ in Fig. 9.2 by static structure factors calculated by means of the rescaled mean spherical integral equation scheme (RMSA).

Contrary to hard spheres, the peak height, $H(q_m)$, of dilute and deionized charged sphere suspensions is larger than one, and it grows with increasing Φ. For $\Phi \leq 10^{-2}$, this peak height is well described by [70, 46]

$$H(q_m) = 1 + p\,\Phi^{0.4}\,, \tag{9.79}$$

with a coefficient $p = 1 - 1.5$ moderately dependent on particle size and charge.

So far we have dealt with *translational* short-time properties. The *rotational* short-time self-diffusion coefficient, D_s^r, of interacting colloidal spheres defined in Eq. (8.120) can be calculated in analogy with the translational case by accounting also for the orientational degrees of freedom [42, 53, 24, 77, 54]. In this way, one obtains the microscopic expression

$$D_s^r = \langle \hat{\mathbf{q}} \cdot \mathbf{D}_{11}^{rr}(\mathbf{r}^N) \cdot \hat{\mathbf{q}} \rangle \tag{9.80}$$

for D_s^r. The rotational diffusivity tensor, $\mathbf{D}_{11}^{rr}$, relates the hydrodynamic torque, $\mathbf{T}_1^H$, acting on a representative sphere 1 to its angular velocity, $\boldsymbol{\omega}_1$, by

$$\boldsymbol{\omega}_1 = -\frac{1}{k_B T}\,\mathbf{D}_{11}^{rr}(\mathbf{r}^N) \cdot \mathbf{T}_1^H\,, \tag{9.81}$$

on assuming that no hydrodynamic torques and forces are exerted on the remaining $(N-1)$ spheres. To leading order in the a/r expansion, $\mathbf{D}_{11}^{rr}(\mathbf{r}^N)$ is given by [58]

$$\mathbf{D}_{11}^{rr}(\mathbf{r}^N) = D_0^r \Big[\mathbf{1} + \sum_{l \neq i}^{N} \boldsymbol{\omega}_{11}^{rr}(\mathbf{r}_i - \mathbf{r}_l)\Big]\,, \tag{9.82}$$

with

$$\boldsymbol{\omega}_{11}^{rr}(\mathbf{r}) = -\frac{15}{4}\left(\frac{a}{r}\right)^6 [\mathbf{1} - \hat{\mathbf{r}}\hat{\mathbf{r}}] + \mathcal{O}\left[\left(\frac{a}{r}\right)^8\right]\,. \tag{9.83}$$

The leading-order three-body contribution to $\mathbf{D}_{11}^{rr}(\mathbf{r}^N)$ is of order r^{-9} [65, 54].

On the basis of Eq. (9.80), Cichocki et al. [65] have derived for hard spheres the second-order virial expansion result

$$\frac{D_s^r}{D_0^r} = 1 - 0.631\Phi - 0.726\Phi^2 . \tag{9.84}$$

This expression describes experimental data and Lattice-Boltzmann computer simulation results for D_s^r quite well up to surprisingly large volume fractions $\Phi = 0.4$ [53, 69, 83].

Calculations of D_s^r for charge-stabilized suspensions with leading-order three-body HI included, reveal for small excess electrolyte concentration a purely quadratic Φ-dependence, viz.,

$$\frac{D_s^r}{D_0^r} = 1 - a_r \Phi^2 , \tag{9.85}$$

with the parameter $a_r \approx 1.3$ rather insensitive to particle size and charge. Eq. (9.85) has been confirmed by Lattice-Boltzmann computer simulations, which show that it applies quite accurately even up to $\Phi \approx 0.3$ [83].

Figure 9.3 includes the comparison between the theoretical prediction for D_s^r in Eq. (9.85), and depolarized DLS measurements of Bitzer et al. [84] on deionized suspensions of highly charged and optically anisotropic fluorinated

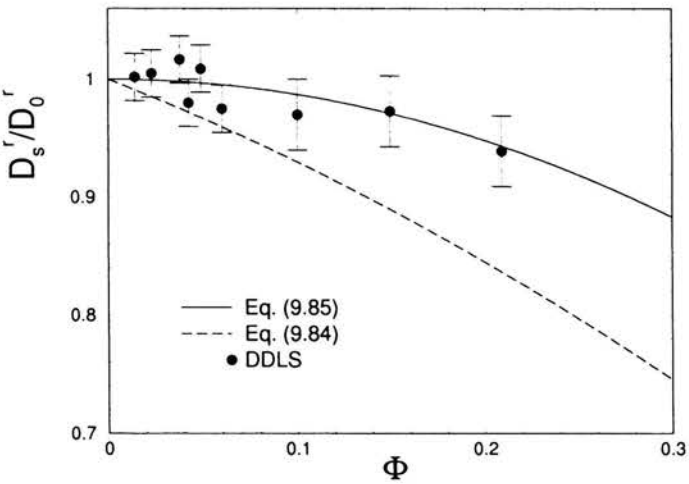

FIGURE 9.3. Depolarized DLS data (from [84]) and Eq. (9.85) for the reduced short-time rotational self-diffusion coefficient, D_s^r/D_0^r, versus Φ of charge-stabilized colloidal spheres. The second-order virial expansion result in Eq. (9.84) for monodisperse hard spheres is included for comparison.

teflon spheres. For comparison, Fig. 9.3 contains further the hard-sphere D_s^r according to Eq. (9.84). The experimental data for D_s^r are seen to be in qualitative agreement with the predicted Φ^2-dependence.

The non-linear volume fraction dependence of the short-time properties of charged spheres arises from the peculiar concentration dependence of the mean diameter, r_m, of the average next-neighbor cage around a charged sphere. The length r_m coincides with the location of the first maximum, $g(r_m)$, of the radial distribution function and is very nearly equal to the mean interparticle distance, $\rho_0^{-1/3}$, which scales in Φ as $\Phi^{-1/3}$. Using this characteristic property of deionized charge-stabilized suspensions, the exponents in Eqs. (9.76), (9.77), (9.79), (9.85) can be derived quite easily on the basis of a simplified model of effective hard spheres of diameter $2r_m$. We refer to [3, 78, 76] for more details on the effective hard-sphere model.

Long-time diffusion

Theoretical calculations of the intermediate time and long-time behavior of $S_c(q,t)$ and $S_s(q,t)$, the MSD and the associated translational long-time self-diffusion coefficient are very demanding, since these quantities are affected simultaneously by direct and hydrodynamic interactions. These interactions give rise to time-retarded caging effects. At long times $t \gg \tau_I$, the dynamic cage around a sphere is distorted away from its, on the average, spherical symmetry. This implies that, contrary to D_s^s, D_s^l can not be expressed in terms of a genuine equilibrium average as the one in Eq. (9.59).

A frequently used route to a direct calculation of time dynamic properties at intermediate to long times invokes Brownian Dynamics (BD) computer simulations without and, to a certain degree of approximation, with HI included. The BD method allows to generate numerically the trajectories $\{\mathbf{r}_i(t)\}$ of colloidal spheres, and it is *statistically* equivalent to solving the GSE (9.43) for the many-sphere probability density function. The (translational) displacements of N identical colloidal spheres during a time step Δt, with $\tau_B \ll t \ll \tau_I$, are generated in this scheme through solving the coupled stochastic finite difference equations [85]

$$\mathbf{r}_i(t+\Delta t) - \mathbf{r}_i(t) = \sum_{j=1}^{N} [-\beta \mathbf{D}_{ij}(\mathbf{r}^N) \cdot \nabla_j U(\mathbf{r}^N) + \nabla_j \cdot \mathbf{D}_{ij}(\mathbf{r}^N)]\Delta t + \Delta \mathbf{x}_i + \mathcal{O}(\Delta t^2). \quad (9.86)$$

Here, $\Delta\mathbf{x}_i$ is a Gaussian-distributed random displacement vector of zero mean $\langle\Delta\mathbf{x}_i\rangle = 0$ due to isotropy, and the covariance matrix

$$\langle\Delta\mathbf{x}_i\,\Delta\mathbf{x}_j\rangle = 2\,\mathbf{D}_{ij}(\mathbf{r}^N)\Delta t\,. \tag{9.87}$$

For dilute suspensions with long-range repulsive interactions, we have argued before that it is sufficient to account only for the leading asymptotic form of $\mathbf{D}_{ij}$, given for an unbound three-dimensional suspension by the Rotne–Prager form in Eq. (9.66). Eq. (9.86) reduces then to a more simple form, since $\nabla_j \cdot \mathbf{D}_{ij} = 0$ within RP approximation. The RP approximation for $\mathbf{D}_{ij}$ amounts to neglecting reflections, through other (caging) spheres, of the hydrodynamic flow field created by a moving sphere onto itself. Therefore, $D_s^s = D_0$ within RP approximation. For dilute charge-stabilized suspensions, DLS experiments show indeed that $D_s^s \approx D_0$.

In a typical BD simulation, several hundred to several thousand particles confined in a periodically repeated simulation box are equilibrated using, e.g., a canonical ensemble Monte-Carlo method. After equilibration has been reached, several ten thousand production time steps are generated by the algorithm in Eq. (9.86) to obtain diffusional (and structural) properties like the particle MSD through

$$W(t) = \frac{1}{2d}\left\langle \frac{1}{N}\sum_{i=1}^{N}[\mathbf{r}_i(t) - \mathbf{r}_i(0)]^2 \right\rangle , \tag{9.88}$$

with t some multiple of Δt. The long-range nature of the HI requires to include an Ewald-type summation technique on the RP level into the BD algorithm, as developed by Beenakker [86]. The influence of HI on dynamic properties can be analyzed through comparison with BD calculations where HI are disregarded, by setting $\mathbf{D}_{ij} = D_0\delta_{ij}\mathbf{1}$. An example for a BD calculation of $S_c(q,t)$ without HI has been discussed already in Fig. 8.6, in comparison with a mode coupling theory scheme which will be explained further down. BD simulations with far-field HI included have been performed, e.g., for the in-plane diffusion of planar monolayers of charge-stabilized colloidal spheres [87] and for one-component [88, 89, 90, 72] and bidisperse [91] systems of super-paramagnetic colloidal spheres confined to a liquid-gas interface, and exposed to an external magnetic field perpendicular to the interface. The induced magnetic moments in the particles lead to long-range dipolar repulsions. A BD study of three-dimensional charge-stabilized suspensions with far-field HI has been discussed in [92].

For an interesting example of a quasi-two-dimensional colloidal suspension, consider a monolayer of electrostatically repelling colloidal spheres diffusing in the midplane between two narrow parallel (charged) walls of separation $h = 2\sigma$, with $\sigma = 2a$ (see Fig. 9.4).

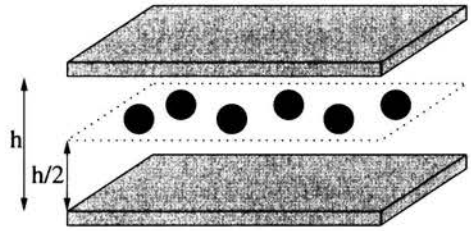

FIGURE 9.4. Charged colloidal spheres diffusing in the midplane between two charged plates. The spheres interact by the screened Coulomb potential $u(r) = Q^2 \exp\{-\kappa r\}/r$ for $r > 2a$, with particle charge Q and screening parameter $\kappa = \pi/(h\sqrt{2})$ (see [87] for details).

Due to the stronger influence of HI in such confined systems, it is necessary to account for many-body near-field HI (where $\nabla_j \cdot \mathbf{D}_{ij} \neq 0$) between particles and walls (p-w HI), and among the particles themselves (p-p HI), including also lubrication corrections. Lubrication effects arise when two or more spheres or a sphere and a wall are close to contact: for stick boundary conditions, which we assume here to apply, the mobility for relative motion goes to zero at contact, due to strong lubrication stresses required to expel the solvent from the thin gap between the surface points of closest approach. Moreover, in the present system there is a non-negligible hydrodynamic coupling between the translational and rotational motion of the spheres. To include all these hydrodynamic features of the system one can use the so-called Stokesian Dynamics (SD) simulation method. This method is a more sophisticated extension of the BD scheme, pioneered and advanced by Brady and Bossis [93], which accounts to a good approximation for many-body HI contributions and lubrication effects.

Figure 9.5 includes SD simulation results [87] for the self-dynamic and distinct space-time van Hove functions $G_s(r,t)$ and $G_d(r,t)$, respectively, defined as [3] (see, also, Sec. 7.3)

$$G_s(r,t) = \left\langle \frac{1}{N} \sum_{i=1}^{N} \delta(\mathbf{r} - \mathbf{r}_i(t) + \mathbf{r}_i(0)) \right\rangle \approx [4\pi W(t)]^{-d/2} \exp\left\{ - \frac{r^2}{4W(t)} \right\} \tag{9.89}$$

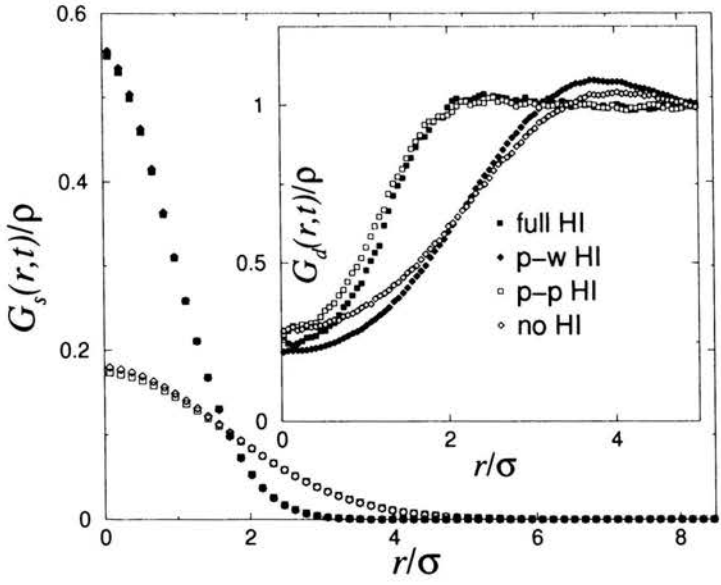

FIGURE 9.5. Reduced self-dynamic and distinct van Hove functions, $G_s(r,t)/\rho_0$ and $G_d(r,t)\rho_0$ versus $r/(2a)$, for time $t = 3.5\tau_I$, particle surface fraction $\Phi = 0.062$, and an effective particle charge Q of 10^3 elementary charges. Figure reproduced from [87].

and

$$G_d(r,t) = \left\langle \frac{1}{N} \sum_{i \neq j}^{N} \delta(\mathbf{r} - \mathbf{r}_i(t) + \mathbf{r}_j(0)) \right\rangle . \tag{9.90}$$

The second approximate equality in Eq. (9.89) applies only when non-Gaussian contributions to $G_s(r,t)$ are very small. The function $G_s(r,t)$ gives the conditional probability density that a particle undergoes a displacement r during the time interval t. The distinct van Hove function, with $G_d(r,0) = \rho_0 g(r)$, gives the conditional probability density of finding, at time t, a particle a distance r apart from another one at earlier time $t = 0$. Up to the density factor ρ_0, $G_d(r,t)$ is thus the time-dependent generalization of the radial distribution function. Real-space quantities like $G_s(r,t)$, $G_d(r,t)$ and $W(t)$ can be *directly* measured in quasi-two-dimensional systems of micron-sized colloidal particles using video microscopy imaging [94, 95]. The functions $G_s(r,t)$ and $G_d(r,t)$ are the Fourier transform pairs, respectively,

of $S_s(q,t)$ and of the distinct part, $S_d(q,t) = S_c(q,t) - S_s(q,t)$, of $S_c(q,t)$, viz.

$$\begin{aligned} S_s(q,t) &= \int d\mathbf{r}\, \exp\{i\mathbf{q}\cdot\mathbf{r}\}\, G_s(r,t)\,, \\ S_d(q,t) &= \int d\mathbf{r}\, \exp\{i\mathbf{q}\cdot\mathbf{r}\}\, G_d(r,t)\,. \end{aligned} \tag{9.91}$$

The time $t = 3.5\tau_I$, at which the reduced van Hove functions $G_s(r,t)/\rho_0$ and $G_d(r,t)/\rho_0$ are depicted in Fig. 9.5 versus the radial distance r, corresponds to the intermediate time regime characterized by a sub-linear increase in $W(t)$. Interestingly enough, the shape of $G_d(r,t)$ with full HI (i.e p-p *and* p-w HI) is seen from the figure to be mainly determined by p-p HI. In comparison, the p-w HI has only a minor effect on $G_d(r,t)$, giving rise to a somewhat slower decay of interparticle correlations. In sharp contrast to $G_d(r,t)$, $G_s(r,t)$ is mainly influenced hydrodynamically by the walls (i.e. by p-w HI), which act to slow down the self-diffusion. This is the reason why the $G_s(r,t)$ with full HI and with p-w HI alone, which are nearly equal to each other, are much larger for smaller r than the $G_s(r,t)$ for the non-confined cases of of p-p HI only and with no HI at all.

Beside from BD and SD computer simulations, various approximate theoretical methods have been developed [97, 103, 101, 96, 63, 99, 98, 49, 102, 100] for calculating long-time diffusional and rheological properties from the knowledge of $S_c(q)$ or, likewise, $g(r)$. These methods are all based, regarding $S_c(q,t)$, on the microscopic equivalent of the phenomenological memory Eq. (8.73), with different approximations involved in each of these methods for the memory function $\Delta D_c(q,t)$. Out of these methods, we discuss here only the mode coupling theory (MCT) for the overdamped dynamics of dense colloidal suspensions [103, 101, 81, 98, 49]. The MCT for Brownian systems has been established, through comparison with experiment and computer simulations, as a versatile tool for calculating dynamic transport coefficients and density correlation functions [104, 70, 46].

In order to derive a microscopic evolution equation for $S_c(q,t)$ it should be realized that the microscopic densities $\rho_A(\mathbf{q},t)$, with $A \in \{s,c\}$, are the only slowly relaxing dynamic variables, at least for small q (cf. Eq. (8.104)), since momentum and energy of the colloidal spheres are very quickly exchanged with the surrounding fluid. From introducing the projection operator into the subspace of configurational dynamic variables:

$$\hat{P}_c(\cdots) = \frac{\langle(\cdots)\rho_c(-\mathbf{q})\rangle}{NS_c(q)}\,\rho_c(\mathbf{q})\,, \tag{9.92}$$

Nägele and Baur [81] have derived the following exact evolution equation for $S_c(q,t)$:

$$\frac{\partial}{\partial t} S_c(q,t) = -q^2 D_c^s(q) S_c(q,t) - \int_0^t du\, M_c^{irr}(q,t-u) \frac{\partial}{\partial u} S_c(q,u)\,. \quad (9.93)$$

This equation relates $S_c(q,t)$ to the so-called irreducible collective memory function $M_c^{irr}(q,t)$. The function $M_c^{irr}(q,t)$ is given by an exact but formal equilibrium average invoking $\hat{P}_c$ and the adjoint Smoluchowski operator $\hat{O}_B(\mathbf{r}^N)$ (see [81, 49] for details).

Time-Laplace transformation of Eq. (9.93) leads to

$$S_c(q,z) = \frac{S_c(q)}{z + \dfrac{q^2 D_c^s(q)}{1 + M_c^{irr}(q,z)}}\,, \quad (9.94)$$

with $M_c^{irr}(q,z)$ the Laplace transform of $M_c^{irr}(q,t)$. It follows from this equation that the collective diffusion kernel, $D_c(q,z)$, in Eq. (8.63) can be expressed in terms of $M_c^{irr}(q,t)$ via

$$D_c(q,z) = \frac{D_c^s(q)}{1 + M_c^{irr}(q,z)}\,. \quad (9.95)$$

At this point, it becomes obvious that $M_c^{irr}(q,z)$ renormalizes the short-time decay rate, $q^2 D_c^s(q)$, of $S_c(q,t)$ due to the presence of memory effects. As a generalization of the single-particle Stokes–Einstein relation $D_0 = k_B T/\gamma$ to interacting particle systems, a wavenumber and frequency-dependent friction function, $\gamma_c(q,z)$, can be introduced through $D_c(q,z) = k_B T/\gamma_c(q,z)$. Hence, with Eq. (9.95), $M_c^{irr}(q,z)$ is identified as being proportional to the frequency-dependent part of the generalized friction function. For given $M_c^{irr}(q,z)$, the long-time collective diffusion coefficient can be calculated from

$$D_c^l = \frac{D_c^s}{1 + M_c^{irr}(q \to 0, z \to 0)}\,. \quad (9.96)$$

On the basis of the microscopic expression for $M_c^{irr}(q,t)$, it can be shown for vanishing or pairwise additive HI that $M_c^{irr}(q,t)/q^2 \to 0$ for $q \to 0$, which implies that $D_c^l = D_c^s$.

The MCT privides a self-consistent approximation for $M_c^{irr}(q,t)$, which preserves the positive definiteness of the exact $D_c(q,z)$. It is particularly

suitable for fluid suspensions of strongly correlated particles. Moreover, as shown in the salient work of Götze and co-workers (see [105, 106, 107, 108]), it predicts a consistent dynamic glass transition scenario in good accord with experiment and computer simulation. This scenario is characterized by the appearance of non-ergodicity above a certain concentration threshold, where $S_c(q,t)$ and $S_s(q,t)$ do not relax any more to zero, and where the suspension viscosity diverges.

In the most commonly used version of the MCT, $M_c^{irr}(q,t)$ is approximated without HI by

$$M_c^{irr}(q,t) = \frac{D_0}{2\rho_0(2\pi)^3} \int d\mathbf{k}\, [V_c(\mathbf{q},\mathbf{k})]^2\, S_c(k,t)\, S_c(|\mathbf{q}-\mathbf{k}|,t) \qquad (9.97)$$

with the vertex amplitude [105, 106, 103, 99],

$$V_c(\mathbf{q},\mathbf{k}) = \hat{\mathbf{q}}\cdot\mathbf{k}\,\rho_0 c(k) + \hat{\mathbf{q}}\cdot(\mathbf{q}-\mathbf{k})\,\rho_0 c(|\mathbf{q}-\mathbf{k}|)\,, \qquad (9.98)$$

related to collective diffusion. Here, $c(q) = [1 - 1/S_c(q)]/\rho_0$ is the Fourier-transform of the two-body direct correlation function $c(r)$ [1]. The vertex amplitude $V_c(\mathbf{q},\mathbf{k})$ in Eq. (9.97) has been derived in the so-called convolution approximation, where the contribution of static three-point direct correlations is neglected. The convolution approximation for the collective vertex amplitude is used in most of the recent applications of the MCT to atomic [107, 108, 109] and colloidal dynamics [103, 49, 46, 102, 100].

The MCT has been formulated further for self-diffusional properties related to self-dynamic structure factor $S_s(q,t)$. The time evolution of $S_s(q,t)$ is described by the exact memory equation [81],

$$\frac{\partial}{\partial t} S_s(q,t) = -q^2 D_s^s\, S_s(q,t) - \int_0^t du\, M_s^{irr}(q,t-u) \frac{\partial}{\partial u} S_s(q,u)\,, \qquad (9.99)$$

which includes the irreducible memory function, $M_s^{irr}(q,t)$, related to self-diffusion. Without HI, $D_s^s = D_0$, and $M_s^{irr}(q,t)$ is then approximated in MCT by

$$M_s^{irr}(q,t) = \frac{D_0}{(2\pi)^3\rho_0} \int d\mathbf{k}\, [V_s(\mathbf{q},\mathbf{k})]^2 S_c(k,t)\, S_s(|\mathbf{q}-\mathbf{k}|,t)\,, \qquad (9.100)$$

with the vertex function [99]

$$V_s(\mathbf{q},\mathbf{k}) = \hat{\mathbf{q}}\cdot\mathbf{k}\left(1 - \frac{1}{S_c(k)}\right). \qquad (9.101)$$

Equations (9.93), (9.97) and (9.98) constitute a self-consistent set of nonlinear equations determining $S_c(q,t)$ for a given static structure factor $S_c(q)$. The latter can be calculated independently for given pair potential using well-established integral equation schemes [1, 3].

Once $S(q,t)$ has been determined, $S_s(q,t)$ is obtained from solving Eqs. (9.99)-(9.101). Knowing $S_s(q,t)$, the MSD can be determined from

$$W(t) = -\lim_{q\to 0} \frac{\log S_s(q,t)}{q^2} . \tag{9.102}$$

The long-time self-diffusion coefficient, D_s^l, follows then from

$$D_s^l = \lim_{t\to\infty} \frac{W(t)}{t} = \frac{D_s^s}{1 + M_s^{irr}(q \to 0, z \to 0)} , \tag{9.103}$$

where $M_s^{irr}(q,z)$ is the Laplace transform of $M_s^{irr}(q,t)$.

An approximate incorporation of far-field HI into the MCT equations of monodisperse systems and colloidal mixtures was provided by Nägele and co-workers [110, 98, 49]. This leads to modifications in the wavenumber dependence of $V_c(\mathbf{q},\mathbf{k})$ and $V_s(\mathbf{q},\mathbf{k})$, and hydrodynamic functions like $H(q)$ are needed as additional external inputs. The MCT with far-field HI aims at describing the dynamics of charge-stabilized suspensions in the fluid regime. So far it has been applied with good success to the self-diffusion of moderately correlated charged particles (see below), and to the electrolyte friction effect experienced by a charged colloidal sphere immersed in an electrolyte solution [111].

Figure 8.6 shows BD results without HI for the $S_c(q,t)$ of a charge-stabilized dispersion, in comparison with corresponding MCT prediction without HI. There is no adjustable parameter involved in this comparison. The good agreement between MCT and BD for all times and wavenumbers considered confirms our earlier statement that the MCT is well suited for dense (in the sense of strongly correlated) particle systems. The effect of far-field HI, which is predominant in charge-stabilized suspensions, is to enlarge D_s^l moderately, and to enhance the decay of $S_c(q,t)$. The enhancement of D_s^l had been originally predicted in [81] from partially self-consistent simplified MCT calculations of D_s^l with far-field HI included (see Fig. 9.6), and from exact low-density calculations. Meanwhile, hydrodynamic enhancement of long-time self-diffusion has been observed in various colloidal systems characterized by strong and long-range particle repulsions [88, 89, 92, 87, 90]. The

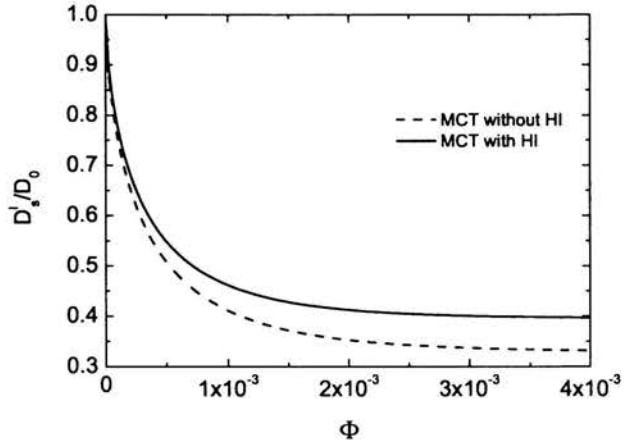

FIGURE 9.6. MCT long-time self-diffusion coefficient of a typical deionized charge-stabilized suspension. HI leads here to an enhancement of long-time diffusion (see [81, 99]).

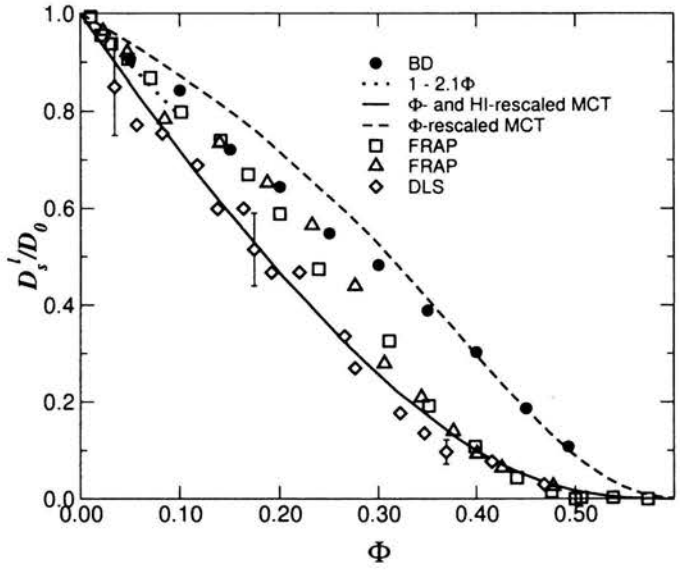

FIGURE 9.7. Reduced long-time self-diffusion coefficient for hard spheres as function of volume fraction. Comparison between MCT and experimental data. Filled circles: BD data of Moriguchi et al. [112]. Open diamonds: DLS data of van Megen and Underwood [113]. Open squares and triangles: two sets of FRAP data by Imhof and Dhont [114]. Figure partially reproduced from [46].

far-field HI prevailing in these systems promotes the diffusion of a sphere out of its momentary cage.

A neutral sphere diffusing out of its cage of neighboring hard spheres will, contrary to charges spheres, most probably pass by very closely to one of the caging particles, since the $g(r)$ of hard spheres is maximal at contact. Due to the strongly reduced relative mobility of two spheres near contact, the long-time self-diffusion of a hard sphere is hydrodynamically reduced accordingly. Consider here Fig. 9.7, which shows BD results for the D_s^l of hard spheres without HI included, versus experimental data obtained from fluorescence recovery after photobleaching (FRAP) and DLS measurements. For hard spheres, $D_s^l/D_0 = 1 - 2.1\Phi$ to leading order in the density. While there are significant differences in D_s^l for the various sets of experimental data, the hydrodynamically induced de-enhancement of D_s^l for hard spheres is clearly observable. The diverging experimental results for D_s^l arise from difficulties in determining the volume fraction unambiguously. Figure 9.7 includes further the MCT predictions for D_s^l without and with HI. The MCT locates the glass transition of hard-sphere suspensions at $\Phi = 0.525$, which is lower than the experimental value of approximately 0.58. To correct for this, Φ is rescaled in the MCT results according to $\Phi \to \Phi \times \Phi_g/0.525$, with a value $\Phi_g = 0.62$ selected somewhat larger than the experimental one, so that the MCT-D_s^l without HI conforms well with the BD data at large concentrations. The influence of many-body HI is accounted for in a semi-heuristic fashion by multiplying (i.e. rescaling) D_s^l without HI, calculated using the MCT, by the factor D_s^s/D_0 where D_s^s is determined from Eq. (9.71). A rationale for this hydrodynamic rescaling is provided from noting for hard spheres that a particle diffusing out of its cage will move very slowly for a considerable amount of time in the immediate neighborhood of a caging sphere, as adequately described by the short-time self-diffusion coefficient, before it leaves the cage. According to Fig. 9.7, the D_s^l from the HI-rescaled MCT is overall in good accord with experimental data, in particular for larger concentrations.

An empirical dynamic freezing rule, due to Löwen et al. [115], states that freezing sets in in a three-dimensional monodisperse suspension when the threshold value $D_s^l/D_s^s \approx 0.1$ has been reached. A value of 0.1 for D_s^l/D_0 corresponds to $\Phi = 0.949$ within the HI-rescaled MCT. Since $S_c(q_m; \Phi = 0.494) = 2.85$, this is also the freezing volume fraction predicted by the static Hansen–Verlet freezing criterion [17]. This observation suggests that

both freezing criteria are in fact equivalent, since dynamic properties are derived in MCT from knowledge of the static property $S_c(q)$. The equivalence of both freezing criteria, and of their two-dimensional analogues, has been further established for systems with long-range repulsive interactions [46, 90]. The equivalence of static and dynamic criteria derives from a general dynamic scaling behavior (cf. [90, 72] for details on this dynamic scaling), which has led to the formulation of additional dynamic freezing criteria in terms of long-time collective diffusion coefficients [72].

As an example of dynamic scaling, consider Fig. 9.8(a). This figure includes the master curve for D_s^l versus $S(q_m)$, calculated using the MCT without HI for a three-dimenisional suspension of highly charged spheres. Note here that a height of 2.85 in the static structure factor peak corresponds to $D_s^l/D_0 = 0.1$. Recall further that $D_s^s \approx D_0$ for charge-stabilized systems with prevailing far-field HI. BD simulation results of D_s^l/D_0 versus $S_c(q_m)$ with and without far-field HI included are shown in Fig. 9.8b for magnetically and electrostatically repelling particles. We observe here that $D_s^l/D_0 \approx 0.085$ for $S_c(q_m) \approx 5.5$, in excellent agreement with an empirical dynamic criterion for two-dimensional freezing proposed by Löwen [116], which states that $D_s^l/D_0 \approx 0.085$ at the freezing line, independent of the pair potential and the nature of the freezing process. Moreover, a value of $S_c(q_m) = 5.5$ at freezing is indeed found in computer simulations of two-dimensional systems [117]. As seen from Fig. 9.8(b), values of D_s^l close to freezing are only slightly enhanced by HI. This indicates that the dynamic freezing rules remain essentially untouched when far-field HI is included.

As an application of the MCT to colloidal mixtures, we consider long-time interdiffusion in a dilute binary mixture of colloidal hard spheres. To this end, one needs to employ the generalizations of the one-component MCT equations to colloidal mixtures, as provided, e.g., in [49]. The long-time mobility matrix $\boldsymbol{\mu}^l$, defined in Eq. (8.93), can be calculated analytically without HI to yield [49]

$$k_B T\, \mu_{\alpha\beta}^l = \delta_{\alpha\beta}\, D_{s\alpha}^l + \frac{1}{3}\, D_\alpha^0\, (\Phi_\alpha\, \Phi_\beta)^{1/2}\, \frac{(1+\lambda_{\alpha\beta})^2}{(\lambda_{\alpha\beta})^{3/2}} + \mathcal{O}(\Phi^2) \qquad (9.104)$$

where

$$D_{s\alpha}^l = D_{0\alpha}\left[1 - \frac{1}{3}\sum_{\gamma=1}^{2} \Phi_\gamma\, (1+\lambda_{\gamma\alpha})^2\right] + \mathcal{O}(\Phi^2) \qquad (9.105)$$

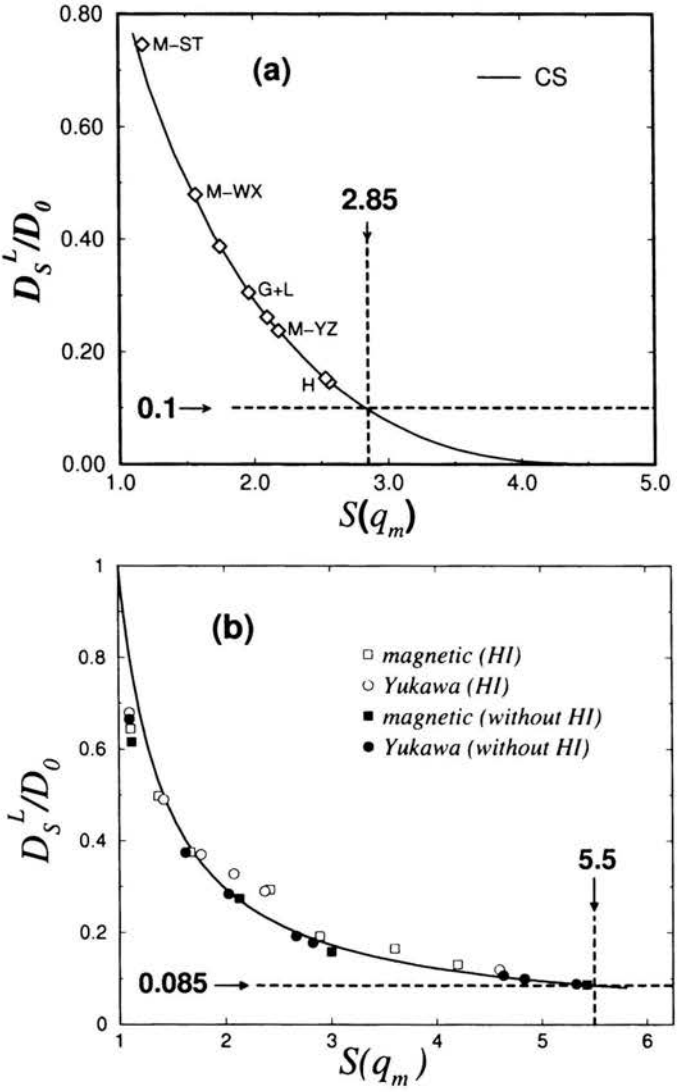

FIGURE 9.8. Reduced long-time self-diffusion coefficient, D_s^l/D_0, versus liquid static structure factor peak height $S_c(q_m)$. MCT results without HI are (from [46]) for deionized three-dimensional suspensions of charge-stabilized spheres are shown in (a). The particle interactions in (a) are described by a Yukawa-like screened Coulomb potential. BD simulation results with and without HI for magnetic and charge-stabilized (Yukawa-like) quasi-two-dimensional systems are depicted in (b) (after [72]).

is the long-time self-diffusion coefficient, without HI, of an α-type hard sphere in the mixture. Here, Φ is the total volume fraction of both components, and $\lambda_{\alpha\beta} = a_\beta/a_\alpha$ is the size ratio of β to α spheres. The MCT result in Eqs. (9.104) and (9.105) is not an exact one: the exact expression for $D^l_{s\alpha}$ is given by Eq. (9.105) with the factor 1/3 replaced by 1/2 [3], so that $D^l_s/D_0 = 1 - 2\Phi + \mathcal{O}(\Phi^2)$ in the mondisperse case. The MCT does not describe the dynamics at low densities exactly, since the low-density binary collision part is treated in an approximative way.

Substitution of Eq. (9.104) for $\boldsymbol{\mu}^l$ in Eq. (8.101) yields the following MCT result for the kinetic factor of a dilute binary hard sphere suspension [49]:

$$\begin{aligned} \frac{\Lambda^l_{in}}{x_1\, x_2} &= \left(x_2\, D^l_{s1} + x_1\, D^l_{s2}\right) + \frac{4}{3}\left(x_1\, \Phi_2\, D_{02} + x_2\, \Phi_1 D_{01}\right) \\ &- \frac{2}{3}\left(x_1 x_2 \Phi_1 \Phi_2\right)^{1/2} D_{01}\, \frac{(1+\lambda_{12})^2}{(\lambda_{12})^{3/2}}\,. \end{aligned} \tag{9.106}$$

As has been discussed already in the part of Sec. 8.2 on interdiffusion, an ideal binary mixture is characterized by $\Lambda^l_{in} \propto \left(x_2\, D^l_{s1} + x_1\, D^l_{s2}\right)$; i.e., Λ^l_{in} can then be expressed completely in terms of the self-diffusion coefficients. Equation (9.106) implies that a binary mixture of hard spheres is non-ideal already at small concentrations. Ideality is reached only when $a_1 = a_2$, i.e. for labelled but otherwise identical particles. It has been shown very recently that HI have a strong influence on the interdiffusion process in semi-dilute hard-sphere mixtures (cf. the second citation in [49]).

9.3. Interdiffusion in polymer blends

In this section, we analyze the interdiffusion process in binary polymer blends of homopolymers, labelled as A and B. We further consider the interdiffusion of A and B polymers in a matrix of C polymers. Our analysis is restricted to length scales accessible to dynamic light scattering. The lengths $2\pi/q$ resolved in typical DLS experiments on polymer blends are much larger than the average extent of a polymer coil. The average coil size is quantified by the radius of gyration, R_G, with $R_G = pa^2/6$ for a Gaussian chain. Here, p is the degree of polymerization, i.e. the number of statistical segments or monomers [36, 56, 14], of a homopolymer chain, and a is the length of a statistical segment. DLS experiments performed in the macroscopic regime, i.e. in the diffusive limit where $qR_G \ll 1$ holds, resolve times which are large

as compared to the internal modes of a chain in the melt. Hence, only the center-of-mass diffusion of a chain is resolved.

As discussed earlier in Sec. 8.2, the partial static structure factors in a mixture are expressible, in the hydrodynamic limit, as a linear superposition of exponentially decaying hydrodynamic modes (cf. Eq. (8.94)). To make contact with the notation commonly used in the polymer field with regard to interdiffusion [50, 51], we slightly redefine the partial collective dynamic structure factor, $S_{\alpha\beta}(q,t)$, for the density correlations of α and β-type monomers as $S_{\alpha\beta}(q,t) = \langle \rho_\alpha(\mathbf{q},t)\rho_\beta(-\mathbf{q},0)\rangle$, which differs from the definition given in Eq. (8.90) by a factor of $(N_\alpha N_\beta)^{1/2}$. In the context of polymer blends, N_α denotes the total number of α-type monomers in the melt, with $\alpha \in \{A,B,C\}$, and $\rho_\alpha(\mathbf{q},t)$ is the incremental number density given in Eq (8.87), with $\mathbf{r}_j^\alpha$ pointing to the location of the j-th monomer of type α.

Using this redefinition of the $S_{\alpha\beta}(q,t)$, the EACF for a binary blend is (cf. Eq. (8.91))

$$g_E(q,t) \propto b_A^2\, S_{AA}(q,t) + b_B^2\, S_{BB}(q,t) + 2\, b_A\, b_B\, S_{AB}(q,t)\,, \qquad (9.107)$$

where b_α is the scattering amplitude of an α-type monomer (q-independent in the diffusive limit), related to its dielectric polarizability. Eq. (9.107) applies also to an *incompressible* ternary blend, with b_A and b_B interpreted now as the excess scattering amplitudes relative to the amplitude, b_C, of matrix monomers. The incremental number density, ρ_C, of matrix molecules is hereby contracted out of the description, by using the local incompressibility constraint (cf. Eq. (8.96)),

$$\overline{\rho}_A(\mathbf{q},t) + \overline{\rho}_B(\mathbf{q},t) + \overline{\rho}_C(\mathbf{q},t) = 0\,, \qquad (9.108)$$

for the coarse-grained incremental number densities, $\overline{\rho}_\alpha(\mathbf{q},t)$. In Eq. (9.108), it is assumed that the thermodynamic segmental volumes of the three polymer species are equal.

The interdiffusion of A chains into B chains in the ternary mixture is described by the interdiffusion auto-correlation function,

$$S_{in}(q,t) = \frac{1}{N_A^2}\, S_{AA}(q,t) + \frac{1}{N_B^2}\, S_{BB}(q,t) - \frac{2}{N_A N_B}\, S_{AB}(q,t)\,, \qquad (9.109)$$

which differs from the definition of $S_{in}(q,t)$ in Eq. (8.89) by a factor $(N x_A x_B)^{-1}$, with $N = N_A + N_B$. Here, $x_A = N_A/N$ is the molar fraction, i.e. the volume fraction for equal molar volumes, of A monomers relative to

A and B, with $x_B = 1 - x_A$. The long-time interdiffusion coefficient has been defined in Eq. (8.98) in terms of the initial decay rate of $S_{in}(q,t)$ as

$$D_{in}^{l} = -\frac{1}{q^2}\frac{\partial}{\partial t} \ln S_{in}(q,t)|_{t=0} \,, \tag{9.110}$$

where it is understood that the diffusive limit of $S_{in}(q,t)$ is taken before its evaluation at $t = 0$. The 2×2-matrix, $\boldsymbol{\mu}^l$, of long-time partial mobilities $\mu_{\alpha\beta}$ for the components A and B is introduced, in accordance with Eq. (8.93), by

$$k_B T \mu_{\alpha\beta}^{l} = -\frac{1}{q^2}\frac{\partial}{\partial t} S_{\alpha\beta}(q,t)|_{t=0} \,. \tag{9.111}$$

Then, D_{in}^{l} in Eq. (9.110) can be re-expressed as [50]

$$D_{in}^{l} = \frac{\Lambda_{in}^{l}}{S_{in}} = k_B T \, \frac{\frac{\mu_{AA}^{l}}{N_A^2} + \frac{\mu_{BB}^{l}}{N_B^2} - \frac{2\mu_{AB}^{l}}{N_A N_B}}{\frac{S_{AA}}{N_A^2} + \frac{S_{BB}}{N_B^2} - \frac{2S_{AB}}{N_A N_B}} \,. \tag{9.112}$$

This equation relates D_{in}^{l} to the long-time and long wave length limiting partial mobilities and partial static structure factors of A and B monomers. The definition of the $\mu_{\alpha\beta}$ in Eq. (9.111) differs from the one in Eq. (8.93) by the same factor $(N_A N_B)^{1/2}$ as for the partial static structure factors, so that D_{in}^{l} in Eq. (9.112) is not affected by these redefinitions.

In the interdiffusion part of Sec. 8.2, we have pointed out that, in general, D_{in}^{l} can not be determined by a single scattering experiment. An important exemption from this rule is a *incompressible* binary blend of A and B polymer chains, void of any vacancies or C polymers. In this case, local incompressibility, $\overline{\rho}_A + \overline{\rho}_B = 1$, implies that

$$S_{AA}(q,t) = S_{BB}(q,t) = -S_{AB}(q,t) \,, \tag{9.113}$$

from which follows with Eqs. (9.107) and (9.109) that

$$g_E(q,t) \propto S_{in}(q,t) = \left(\frac{1}{N_A} + \frac{1}{N_B}\right)^2 S_{\alpha\alpha}(q) \exp\{-q^2 D_{in}^{l} t\} \,, \tag{9.114}$$

with $\alpha = A$ or B. It can be shown that the amplitude $\mathbf{A}_+$ in the normal-mode expansion of Eq. (8.94) vanishes in case of an incompressible binary blend, so that the (+)-mode with eigenvalue d_+ is not observable. The relaxation coefficient d_+ is identified here with the so-called cooperative diffusion coefficient, which quantifies the long-time relaxation of fluctuations in the

total number density $\rho_A + \rho_B$ [50]. In identifying the normal mode d_- with D_{in}^l, we can state that in an incompressible binary blend, a measurement of $g_E(q,t)$ yields the interdiffusion coefficient, given here as

$$D_{in}^l = k_B T \frac{\mu_{\alpha\alpha}^l}{S_{\alpha\alpha}}, \tag{9.115}$$

since $\mu_{\alpha\alpha}^l = \mu_{\beta\beta}^l = -\mu_{\alpha\beta}^l$ according to Eqs. (9.111) and (9.113).

To make further progress in determining the interdiffusion coefficient of binary and ternary melts, a method is needed for calculating the $\mu_{\alpha\beta}^l$ and $S_{\alpha\beta}$ in Eq. (9.112). For an approximate calculation of the $\mu_{\alpha\beta}^l$, we employ a dynamic extension of the random phase approximation (RPA) of polymer blends. The dynamic RPA is a self-consistent mean-field-type approach based on linear response theory, which relates the (Laplace-transformed) linear response function , $-\beta(d/dt)S_{\alpha\beta}(q,t)$, of the actual system of interacting chains, to the response function, $-\beta(d/dt)S_{\alpha\beta}^o(q,t)$, of a bare reference system of non-interacting chains. For a derivation of the dynamic RPA, we refer to the work of de Gennes [118], Brochard and de Gennes [119], and for the extension of the RPA to incompressible polymer mixtures with an arbitrary number of components to Akcasu and Tombakoglu [120].

In the dynamic RPA, the static and dynamic properties of the bare system are assumed to be known. The bare system is commonly chosen as one which is identical to the original mixture in all respects except for the absence of interactions between the monomers and the incompressibility constraint, but with the chain connectivity maintained. As a mean-field-type theory, the (dynamic) RPA should apply only to dense systems (i.e. melts) of sufficiently long polymer chains where density fluctuations are small. Furthermore, its predictions are most reliable for small values of q (as the ones probed in the diffusive limit) since, as the name RPA implies, it involves an averaging over the directions (phase) of $\mathbf{q}$.

The mobilities $\{\mu_{\alpha\beta}^l\}$, with $\alpha, \beta \in \{A, B\}$, of an incompressible ternary mixture are expressed in the dynamic RPA in terms of the mobilities, $\mu_{\alpha\beta}^o$, of the bare system as [120]

$$\begin{aligned} \frac{1}{\mu_{\alpha\alpha}^l} &= \frac{1}{\mu_{\alpha\alpha}^o} + \frac{1}{\mu_{\beta\beta}^o} + \frac{1}{\mu_{\beta\beta}^o + \mu_{CC}^o}, \\ \frac{1}{\mu_{\alpha\beta}^l} &= -\left[\frac{1}{\mu_{\alpha\alpha}^o} + \frac{1}{\mu_{\beta\beta}^o} + \frac{\mu_{CC}^o}{\mu_{\alpha\alpha}^o \mu_{\beta\beta}^o}\right], \quad \alpha \neq \beta, \end{aligned} \tag{9.116}$$

where μ^o_{CC} is the mobility of a C-matrix monomer in the bare system. The mobilities $\mu^o_{\alpha\beta}$ are related to the self-diffusion coefficients in the bare system by

$$\mu^o_{\alpha\beta} = \delta_{\alpha\beta} \frac{N_\alpha D_{0\alpha}}{k_B T}, \tag{9.117}$$

with $D_{0\alpha} = k_B T/\gamma_\alpha$ the self-diffusion coefficient of an α-type monomer related to the monomer friction coefficient γ_α. This result for $\mu^o_{\alpha\beta}$ is obtained from adopting for the bare system the Rouse model for the dynamics of non-interacting and non-self-avoiding Gaussian chains [14, 36]. Here, we use the fact that in a dense system of chains like in a melt, each chain is to a good approximation Gaussian and ideal, with $R_G \propto N^{1/2}$. Within the Rouse model of non-interacting chains,

$$S^o_{\alpha\beta}(q,t) = \delta_{\alpha\beta} N_\alpha p_\alpha \exp\{-q^2 D^p_{0\alpha} t\} \tag{9.118}$$

for $qR_G \ll 1$ and for times t large compared to the relaxation times of the internal modes of a Rouse chain. Here, $D^p_{0\alpha}$ is the center-of-mass self-diffusion coefficient of a polymer chain, related to the monomer diffusion coefficient by $D^p_{0\alpha} = D_{0\alpha}/p_\alpha$, and p_α is the degree of polymerization of an α-chain. Note that $S^o_{\alpha\alpha}(q,t)/N_\alpha$ is the dynamic structure factor of a single Rouse chain. The monomer friction coefficient, γ_α, enters the Rouse dynamics as a parameter that must be specified as an input from elsewhere. Hence, γ_α and $D_{0\alpha}$ are usually interpreted as the friction coefficient and self-diffusion coefficient of an α-monomer in the actual mixture of interacting chains. As such they depend implicitly on the composition and temperature of the mixture. Moreover, it is then necessary to distinguish between systems of unentangled chains, where $D^p_\alpha = D_\alpha/p_\alpha$, and systems of very long chains governed by the reptation process, where $D^p_\alpha = D_\alpha/p^2_\alpha$ [14, 51].

For an application of the RPA, consider first an incompressible binary blend, without any additional matrix molecules or vacancies. Substitution of Eqs. (9.116) and (9.117), with μ^o_{CC} set equal to zero, into Eq. (9.115) leads for unentangled chains to

$$(N x_A x_B)\Lambda^l_{in} = \left[\frac{x_B}{p_A D^p_{0A}} + \frac{x_A}{p_B D^p_{0B}}\right]^{-1}, \tag{9.119}$$

which is the *slow-mode* form for the long-time kinetic coefficient (cf. Eq. (8.117)). Recall here that the definitions of Λ^l_{in} and S_{in} in Eqs. (129)

and (8.89), respectively, differ from the ones used in the present section by a factor of $N(x_A x_B)^2$. This factor renders them into *intensive*, i.e. N-independent, quantities. According to Eq. (9.119), the RPA predicts thus that the interdiffusion process in a binary incompressible blend is dominated, for $D_{0A}^p \ll D_{0B}^p$, by the slow component A, which enslaves the dynamics of the fast component B in the absence of voids.

To obtain D_{in}^l, we need to divide Λ_{in}^l by $S_{in}(q=0)$. The latter is obtained, for consistency, from the static limit of the RPA. For an incompressible ternary blend of A and B chains in a matrix of C chains, the static RPA relates the 2×2 static structure factor matrix, $\mathbf{S}(q,t)$, of A and B monomers in the interacting system to the static structure factor matrix, $\mathbf{S}^o(q,t)$, of the bare system via (for details see [14, 120, 50])

$$\mathbf{S}(q)^{-1} = (\mathbf{S}^o(q))^{-1} + \mathbf{v}(q)\,. \tag{9.120}$$

Here, $\mathbf{v}(q)$ is a 2×2 excluded volume matrix of elements $v_{\alpha\beta}(q)$, with $\alpha,\beta \in \{A,B\}$, which accounts for the interactions between monomers of type α and β, and for the incompressibility constraint.

The partial static structure factors of the bare system of non-interacting Gaussian chains are explicitly

$$S^o_{\alpha\beta}(q) = \delta_{\alpha\beta} p_\alpha f_D([qR_{G\alpha}]^2)\,, \tag{9.121}$$

where $f_D(x)$ is the Debye function [14], with $f_D(x) \approx 1 - x/3$ for $x \ll 1$, and $R_{G\alpha}$ is the radius of gyration of an α-type chain. Using Eq. (9.121) specialized to $qR_{G\alpha} \ll 1$, the RPA result in Eq. (9.120) simplifies for a binary incompressible melt to

$$\frac{1}{S_{\alpha\alpha}} = \left(\frac{1}{N_a} + \frac{1}{N_B}\right)^2 \frac{1}{S_{in}} = \frac{1}{N}\left(\frac{1}{x_A p_A} + \frac{1}{x_B p_B} - 2N\chi_{AB}\right)\,. \tag{9.122}$$

The Flory–Huggins interaction parameter, χ_{AB}, is related to the spatial Fourier transforms, $w_{\alpha\beta}(q)$, of the local interaction potentials, $w_{\alpha\beta}(r)$, of α and β monomers by [14, 50]

$$\chi_{AB} = \lim_{q\to 0} \frac{1}{k_B T V}\left[w_{AB}(q) - \frac{1}{2}\left(w_{AA}(q) + w_{BB}(q)\right)\right]\,, \tag{9.123}$$

so that $\chi \equiv N\chi_{AB}$ can be interpreted as the Flory–Huggins interaction parameter per segmental volume $v_s = V/N$, for equal segmental volumes

of both polymer components. Typically, χ exhibits an inverse temperature dependence. Finally, Eqs. (9.119) and (9.122) yield

$$D_{in}^{l} = \left(\frac{1}{x_A p_A} + \frac{1}{x_B p_B} - 2\chi\right)\left[\frac{1}{x_A p_A D_{0A}^{p}} + \frac{1}{x_B p_B D_{0B}^{p}}\right]^{-1}. \quad (9.124)$$

Experiments on binary blends (see the discussion given below) have revealed that the slow-mode result does not satisfactorily describe, in general, the dependence of Λ_{in}^{l} on the molecular weight (say p_A) of its constituents. The observed discrepancy between the slow-mode result for binary incompressible melts and experiment may be due to the presence of vacancies, which add some amount of compressibility to the mixture. When instead of a binary melt, a ternary incompressible blend of A and B chains in a matrix of C-chains is considered, Λ_{in}^{l} can be derived within the dynamic RPA from substituting Eqs. (9.116) and (9.117) into Eq. (9.112). This leads to the so-called ANK expression,

$$(N x_A x_B)\Lambda_{in}^{l} = \Big[x_B p_A D_{0A}^{p} + x_A p_B D_{0B}^{p} - \frac{x_A x_B \left(p_A D_{0A}^{p} - p_B D_{0B}^{p}\right)^2}{x_A p_A D_{0A}^{p} + x_B p_B D_{0B}^{p} + x_C p_C D_{0C}^{p}}\Big] \quad (9.125)$$

for the kinetic coefficient of unentangled chains, originally derived by Akcasu et al. [50]. Quite remarkably, this expression reduces to the *fast-mode* form (cf. Eq. (8.113)),

$$(N x_A x_B)\Lambda_{in}^{l} = \left[x_B p_A D_{0A}^{p} + x_A p_B D_{0B}^{p}\right], \quad (9.126)$$

in the limit of a large self-diffusivity and/or large concentration of matrix molecules, that is for $x_C p_C D_{0C}^{p} \gg x_\alpha p_\alpha D_{0\alpha}^{p}$. In this 'solution-like' limit, $g_E(q,t)$ decays in a superposition of two normal modes where, contrary to the incompressible case, d_- and, likewise, d_+ can not be identified with the interdiffusion process [50]. The slow-mode result is recaptured from the ANK formula when the matrix is removed, i.e. for $x_C p_C D_{0C}^{p} \to 0$, resulting again in an incompressible mixture of A and B chains. If one is allowed to stretch the validity of the RPA result in Eq. (9.125) by allowing the matrix to consist of vacancies instead of homopolymers, the ANK formula predicts a gradual transition from the fast-mode form to the slow-mode form of Λ_{in}^{l}, when the vacancy concentration, or compressibility, of the mixture is reduced.

The approximate fast-mode and slow-mode expressions for Λ_{in}^{l} do apply only to selected polymer mixtures, with varying degree of accuracy in each case. The fast-mode or vacancy model appears to be more consistent with lower molecular weight blends, whereas the slow-mode or incompressible model is more consistent in the high molecular weight regime. For an example of this trend, consider Figs. 9.9 and 9.10, which display time-resolved static light scattering data of Feng et al. [121] for the kinetic interdiffusion factor (called mobility M in the notation of [121]) of a poly(styrene)/poly(vinylmethylether) blend (PS/PVME) for varying molecular weight N_{PS} of PS. In the experiments by Feng et al., the interdiffusion coefficient has been determined from temperature quench experiments within the miscible one-phase region. The measured decay of density (composition) fluctuations right after the quench has been interpreted in these experiments in terms of the celebrated Cahn-Hilliard-Cook (CHC) expression for the time-resolved average scattered intensity of binary blends (cf. [121, 51]). We remark that the CHC expression is commonly used also to interpret the early

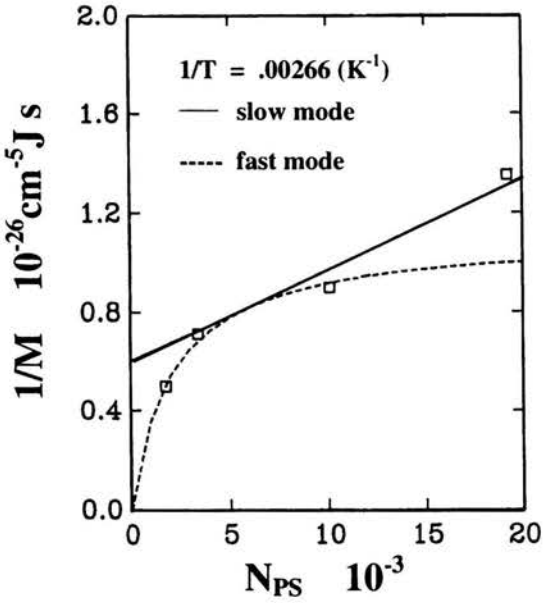

FIGURE 9.9. Inverse mobility data, $M^{-1} \propto 1/\Lambda_{in}^{l}$, versus molecular weight, N_{PS}, of PS in PS/PVME blends. The dashed line (solid line) is a fit of the fast-mode (slow-mode) model to the experimental data. Both models show systematic deviations from the data. After [121].

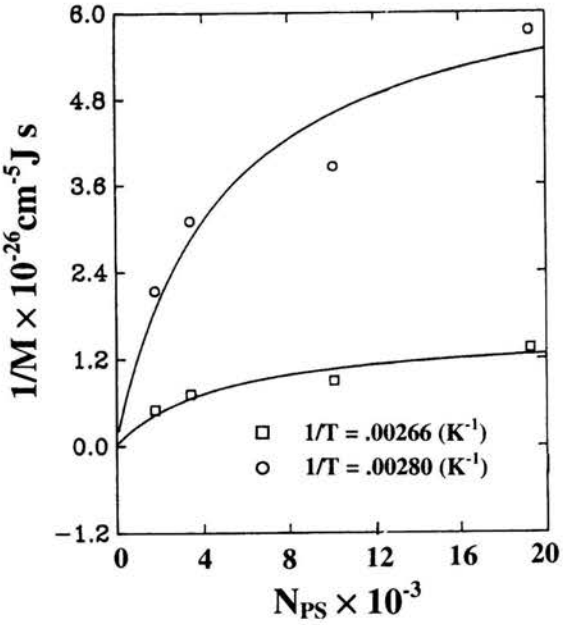

FIGURE 9.10. Inverse mobility data, M^{-1}, versus N_{PS}, in PS/PVME blends at two different temperatures as indicated. The solid lines are fits of the ANK formula (9.125) to the data, demonstrating the applicability of the ANK-theory over the whole range of PS molecular weights. After [121].

stages of spinodal composition of binary mixtures right after a sudden quench into the mechanically unstable two-phase region.

The chains in the PS/PVME blend are in a bulk-entangled state, so that the self-diffusion coefficient of a chain scales, different from Rouse chains, with the inverse *square* of the molecular weight. In the entanglement case, W^o is not any more a local property independent of molecular weights. Substitution of $D^p_{0\alpha} = D_{0\alpha}/p^2_\alpha$ into Eqs. (9.119), (9.126) and (9.125) leads for the inverse mobility $1/M \propto 1/(x_A x_B \Lambda^l_{in})$, according to the slow-mode expression, to linear dependence on the degree of polymerization p_α. On the other hand, the fast-mode model predicts a concave curve for $1/M$ plotted versus p_α, with an infinite slope at $p_\alpha = 0$ and a horizontal asymptote for large p_α [51]. Figure 9.9 includes experimental data of $1/M$ for four different molecular weights, N_{PS}, of PS. Neither the fast-mode nor the slow-mode expression can adequately fit the data. The fast-mode model applies only to the low-molecular-weight side, and the slow-mode model only for large values of N_{PS} (cf. Fig. 9.9).

Inverse mobility data of PS/PVME versus N_{PS} for two different temperatures are depicted in Fig. 9.10, in comparison with the predictions of the ANK formula. As one can see, the molecular-weight-dependence of the kinetic factor in PS/PVME is well described by the ANK model, with the (third) matrix component interpreted as 'vacancies'. The solid curves in Fig. 9.10 were plotted using the matrix parameter $x_C D_{C0}/p_C$ occurring in the entanglement version of the ANK formula as a fitting parameter. However, this matrix parameter can be related to the cooperative diffusion coefficient in a binary mixture, which is a measurable quantity [51]. This deliberates us from needing to assign a meaning to the diffusion coefficient of a vacancy.

Chapter 10

Summary and outlook

The aim of my lecture notes was to provide an introductory overview over salient theoretical methods and concepts used in colloidal physics. Let me note here that part of the material in Chapters 1-5 is published in [122]. Part of the material in Chapters 6-9 will be published in [123]. However, a substantial amount of material in my AMAS lecture notes is not covered by these two references

In my notes, I have followed the traditional approach by considering first the static properties of colloidal (and atomic) systems of spherically shaped particles, followed by a discussion of their dynamic properties. The second part on colloid dynamics was focused on diffusion mechanisms only, and on the theoretical methods used for calculating diffusion coefficients, and density correlation functions associated with dynamic light scattering techniques.

Transport mechanisms different from diffusion like viscoelasticity, for example, have not been treated in the notes. I should mention in this context that possible theoretical links between diffusional and viscoelastic transport properties are currently of large interest, since certain generalized Stokes–Einstein relations (cf. [55]) are basic to so-called micro-rheological measurements on biological systems like actin networks, protein solutions and cells.

In the first part of my notes, I have discussed integral equation schemes for static properties of liquids. These schemes are based on the Ornstein–Zernike equation and the concept of direct correlations. The OZ-based integral equa-

tion schemes provide an extremely versatile framework for predicting microstructural and thermodynamic properties of simple and colloidal liquids, from the knowledge of the pair potential. In addition, these schemes can be used to obtain effective pair potentials in colloidal systems of various particle species, by contracting the unwanted species out of the description.

Due to the approximate nature and, usually, non-perturbative character of an integral equation scheme, one can not make decisive a priori statements on its accuracy. The accuracy of a scheme depends in general on the range and attractive or repulsive nature of $u(r)$, the system dimensionality, and on the degree of thermodynamic consistency. So-called (partially) self-consistent integral equation theories like the RY approximation, in which different routes to the same thermodynamic properties are enforced, are therefore superior to standard integral equation schemes, for the price of a larger numerical effort.

The importance of OZ integral equation schemes goes well beyond the calculation of $g(r)$ and $S(q)$ from a given pair potential. In combination with powerful density functional theory methods, one can study first-order liquid-solid phase transitions, and calculate structural properties of inhomogeneous fluids near a boundary or at a liquid-gas interface (e.g., layering and wetting phenomena). Integral equation approaches form also the basis of inversion schemes to deduce information on the pair potential from an experimentally determined $g(r)$ or $S_c(q)$. From the knowledge of $g(r)$, $c(r)$ can be determined using the OZ equation. The pair potential follows then directly (and approximatively) from a closure relation like the HNC closure. HNC based inversion scheme calculations of $u(r)$ for a monolayer of charged colloidal spheres between to closely spaced glass plates suggest, for instance, the possibility of longer-ranged effective attractions between like-charged particles (cf. [124] for such a determination of $u(r)$, and [87] for a consistency check based on computer simulations). Whether such an attraction really occurs and whether existing physical explanations for its existence do really apply is still very controversially debated.

My lecture notes on static properties have been restricted to fluids of spherical particles with spherically symmetric pair interactions. The integral equation schemes and their closure relations have been broadened in the past to deal also with fluids of non-spherical particles, like molecules, rod-like viruses and polymers. The so-called reference interaction-site model (RISM) method has been used to calculate the site-site distribution function of rigid molecules whose interactions are modelled by an interaction-site po-

tential. The molecule is hereby represented by a discrete set of interaction sites located at the places of the atomic nuclei [1]. The site-site distribution of non-rigid molecules like polymer chains and polyelectrolytes has been successfully determined on the basis of polymer reference interaction-site model (PRISM) calculations [125]. The structure of liquids adsorbed in a porous medium, like in a gel or in an arrested particle matrix, can be approximately predicted using the method of Replica Ornstein–Zernike (ROZ) equations [126].

The second part of my lecture notes has been devoted to the physics of various diffusion processes observed in colloidal fluids of spherical particles, and in binary polymer melts. I have explained theoretical methods and computer simulation techniques, which allow to calculate diffusional transport properties and scattering functions probed in dynamic light scattering.

While DLS is nowadays a standard technique, it is certainly not the only experimental method to measure diffusion properties of colloids and polymers. The new developments in this area are in the direction of scattering geometries, where the dynamics under the influence of external fields (shear flow, pressure, electric field and temperature gradients), near walls and within interfaces can be probed. In addition, somewhat slower dynamical processes are studied nowadays by means of optical microscopy, such as Confocal Laser Scanning Microscopy. Time-resolved phosphorescence anisotropy has recently been used to measure rotational diffusion of colloids [127, 128]. Fluorescence recovery after photobleaching (FRAP) has been applied to probe long-time diffusion under oscillatory shear flow. A similar method is Forced Rayleigh Scattering (FRS), where a refractive index grating is created by means of an interference pattern, from which grating scattered intensities are measured. FRAP and FRS are specialized to measure long-time translational (and rotational) self-diffusion coefficients of various kinds of macromolecules (also non-spherical molecules).

The concentration dependence of translational and rotational diffusion coefficients, and of sedimentation coefficients, and the time dependence of mean-square displacements, van Hove functions and dynamic structure factors have been analyzed in these lecture notes by means of several theoretical methods. The performances of these methods (short-time cluster expansion, MCT, BD and SD simulations) have been scrutinized through a comparison with experimental results obtained from various experimental techniques.

I have pointed to qualitative differences in the dynamics of colloidal particles with short-range interactions (i.e., hard spheres), and systems with long-range repulsive interactions like charge-stabilized dispersions and magnetic systems. In particular, charge-stabilized suspensions at low salinity are characterized by peculiar non-linear density dependencies of their short-time transport properties. For long times, dynamic scaling is observed, which has interesting implications on the equivalence of certain static and dynamic freezing criteria.

For systems of monodisperse colloidal spheres in the fluid phase, meanwhile a quantitative level of understanding has been reached, at least with regard to translational diffusion. As yet, a first-principle inclusion of many-body HI into the theoretical description of concentrated suspensions remains as a major theoretical challenge. For mixtures of colloidal spheres, a semi-quantitative level of accuracy has been reached by existing theoretical methods. Far less is known, however, about diffusion in systems of non-spherical particles like, to mention the most simple case, colloidal hard rods. In these systems, translational particle motion is coupled to the rotational one even at short times.

Recent theoretical efforts are devoted to understand diffusion in confined geometries like in colloidal matrices and gels, to electrokinetic effects on charged colloidal macroions arising from the dynamics of the neutralizing microion clouds, and to anisotropic diffusion and shear banding in suspensions under shear.

Bibliography

1. J.-P. HANSEN AND I.R. MCDONALD, *Theory of Simple Liquids* (2nd Edition, Academic Press, London, 1986)
2. P.A. EGELSTAFF, *An Introduction to the Liquid State* (2nd Edition, Clarendon Press, Oxford, 1992)
3. G. NÄGELE, *Phys. Rep.* **272**, 215-372 (1996)
4. W.B. RUSSEL, D.A. SAVILLE, and W.R. SCHOWALTER, *Colloidal Dispersions* (Cambridge University Press, Cambridge, 1989)
5. J. MAHANTY and B.W. NINHAM, *Dispersion Forces* (Academic Press, New York, 1976)
6. V.I. KALIKMANOV, *Statistical Theory of Fluids* (Springer, Berlin, 2001)
7. M.J. GRIMSON and M. SILBERT, *Mol. Phys.* **74**, 397 (1991)
8. A.R. DENTON, *Phys. Rev. E* **62**, 3855 (2000)
9. P.M. CHAIKIN and T.C. LUBENSKY, *Principles of Condensed Matter Physics* (Cambrigde University Press, Cambrigde, 1995)
10. J.J. BINNEY, N.J. DOWRICK, A.J. FISHER, and M.E.J. NEWMAN, *The Theory of Critical Phenomena* (Oxford University Press, New York, 1993)
11. H.E. STANLEY, *Introduction to Phase Transitions and Critical Phenomena* (Oxford University Press, New York, 1971)
12. I.K. SNOOK and J.B. HAYTER, *Langmuir* **8**, 2280 (1992)
13. G. NÄGELE, O. KELLERBAUER, R. KRAUSE, and R. KLEIN, *Phys. Rev. E* **47**, 2562 (1993)
14. P.-G. DE GENNES, *Scaling Concepts in Polymer Physics* (Cornell University Press, Ithaca, 1979)
15. M.S. WERTHEIM, *J. Math. Phys.* **5**, 643 (1964)
16. L. VERLET and J.J. WEIS, *Phys. Rev. A* **5**, 939 (1972)

17. J.P. HANSEN and L. VERLET, *Phys. Rev.* **184**, 151 (1969)

18. F.J. ROGERS and D.A. YOUNG, *Phys. Rev. A* **30**, 999 (1984)

19. J.M. MENDÉZ-ALCARAZ, Ph.D. thesis, University of Konstanz (1993)

20. A.J. BANCHIO and G. NÄGELE, unpublished results

21. S. ALEXANDER, P.M. CHAIKIN, P. GRANT, G.J. MORALES, and P. PINCUS, *J. Chem. Phys.* **80**, 5776 (1984)

22. L. BELLONI, *Colloids and Surfaces A* **140**, 227 (1998)

23. E. TRIZAC, L. BOCQUET, M. AUBOUY, and H.H. VON GRÜNBERG, *Langmuir* **19**, 4027 (2003)

24. J.K.G. DHONT, *An Introduction to Dynamics of Colloids* (Elsevier, Amsterdam, 1996)

25. B. CHU, *Laser Light Scattering: Basic Principles and Practice* (Academic Press, London, 1991)

26. R. PECORA, *Dynamic Light Scattering: Applications of Photon Correlation Spectroscopy* (Plenum Press, New York, 1985)

27. W. BROWN, *Dynamic Light Scattering: The Method and some Applications* (Clarendon Press, Oxford, 1993)

28. D. MACINTYRE and F. GORNICK (Eds.), *Light Scattering from Dilute Polymer Solutions* (Gordon and Breach Science Publishers, New York, 1964)

29. R. ZWANZIG and M. BIXON, *J. Fluid Mech.* **69**, 21 (1975)

30. H.J.H. CLERCX, *Phys. Rev. E* **56**, 2950 (1997)

31. E.J. HINCH, *J. Fluid Mech.* **72**, 499 (1975)

32. G.N. PAUL and P.N. PUSEY, *J. Phys. A* **14**, 3301 (1981)

33. N.K. AILAWADI and B.J. BERNE, *J. Chem. Phys.* **54**, 3569 (1971)

34. B. CICHOCKI and B.U. FELDERHOF, *Physica A* **289**, 409 (2001)

35. R. PIAZZA and V. DEGIORGIO, *Physica A* **182**, 576 (1992)

36. M. DOI and S.F. EDWARDS, *The Theory of Polymer Dynamics* (Clarendon Press, Oxford, 1986)

37. B. CICHOCKI and K. HINSEN, *Physica A* **166**, 473 (1990)

38. B. CICHOCKI and B.U. FELDERHOF, *J. Phys. Condens. Matter* **6**, 7287 (1994)

39. H. VAN BEIJEREN, K.W. KEHR, and R. KUTNER, *Phys. Rev. E* **28**, 5711 (1983)

40. W. VAN MEGEN, S.M. UNDERWOOD, and I. SNOOK, *J. Chem. Phys.* **85**, 4065 (1986)

41. K.J. GAYLOR, I.K. SNOOK, W. VAN MEGEN, and R.O. WATTS, *J. Phys. A* **13**, 2513 (1980)

42. R.B. JONES and P.N. PUSEY, *Annu. Rev. Phys. Chem.* **42**, 137 (1991)

43. A.B. GLENDINNING and W.B. RUSSEL, *J. Colloid Interface Sci.* **89**, 124 (1982)

44. W.B. RUSSEL and A.B. GLENDINNING, *J. Chem. Phys.* **74**, 948 (1981)

45. P. SZYMCZAK and B. CICHOCKI, *Europhys. Lett.* **59**, 465 (2002)

46. A.J. BANCHIO, G. NÄGELE, and J. BERGENHOLTZ, *J. Chem. Phys.* **113**, 3381 (2000)

47. P.N. SEGRÈ, S.P. MEEKER, P.N. PUSEY, and W.C.K. POON, *Phys. Rev. Lett.* **75**, 958 (1995)

48. P.N. SEGRÈ, O.P. BEHREND, and P.N. PUSEY, *Phys. Rev. E* **52**, 5070 (1995)

49. G. NÄGELE, J. BERGENHOLTZ, and J.K.G. DHONT, *J. Chem. Phys.* **110**, 7037 (1999); G. NÄGELE AND H. ZHANG, submitted (2004)

50. A.Z. AKCASU, G. NÄGELE, and R. KLEIN, *Macromolecules* **24**, 4408 (1991)

51. A.Z. AKCASU, *Macromol. Theory Simul.* **6**, 679 (1997)

52. W. HESS, G. NÄGELE, and A.Z. AKCASU, *J. Polym. Sci. B* **28**, 2233 (1990)

53. V. DEGIORGIO, R. PIAZZA, and R.B. JONES, *Phys. Rev. E* **52**, 2707 (1995)

54. H. ZHANG and G. NÄGELE, *J. Chem. Phys.* **117**, 5908 (2002)

55. G. NÄGELE, *J. Phys.: Condens. Matter* **15**, S407 (2003)

56. H. YAMAKAWA, *Modern Theory of Polymer Solutions* (Harper & Row, New York, 1971)

57. R. SCHMITZ and B.U. FELDERHOF, *Physica A* **116**, 163 (1982)

58. D.J. JEFFREY and Y. ONISHI, *J. Fluid. Mech.* **139**, 261 (1984)

59. S. KIM and S.J. KARRILA, *Microhydrodynamics: Principles and Selected Applications* (Butterworth-Heinemann, Boston, 1991)

60. J.K.G. DHONT, in: J.K.G. Dhont, G. Gompper and D. Richter (Eds.), *Lecture Manuscripts of the 33rd IFF Winter School* (Schriften des Forschungszentrums Jülich, Series: Materials and Matter, Vol. 10, 2002)

61. J.K.G. DHONT and W.J. BRIELS, *Colloids & Surfaces A: Physicochem. Eng. Aspects* **213**, 131 (2003)

62. J.K.G. DHONT and W.J. BRIELS, *J. Chem. Phys.* **118**, 1466 (2002)

63. B. CICHOCKI AND B.U. FELDERHOF, *Physica A* **204**, 152 (1994)

64. J. ROTNE and S. PRAGER, *J. Chem. Phys.* **50**, 4831 (1969)

65. B. CICHOCKI, M.L. EKIEL-JEZEWSKA, and E. WAJNRYB, *J. Chem. Phys.* **111**, 3265 (1999)

66. R.A. LIONBERGER and W.B. RUSSEL, *J. Rheology* **38**, 1885 (1994)

67. G.K. BATCHELOR, *J. Fluid Mech.* **52**, 245 (1972)

68. B. CICHOCKI, M.L. EKIEL-JEZEWSKA, P. SZYMCZAK, and E. WAJNRYB, *J. Chem. Phys.* **117**, 1231 (2002)

69. G.H. KOENDERINK, H. ZHANG, D.G.A.L. AARTS, M.P. LETTINGA, A.P. PHILIPSE, and G. NÄGELE, *Faraday Discuss.* **123**, 335 (2003)

70. A.J. BANCHIO, G. NÄGELE, and J. BERGENHOLTZ, *J. Chem. Phys.* **111**, 8721 (1999)

71. A.J.C. LADD, *J. Fluid Mech.* **271**, 285 (1994); *J. Fluid Mech.* **271**, 311 (1994)

72. G. NÄGELE, M. KOLLMANN, R. PESCHÉ, and A.J. BANCHIO, *Mol. Phys.* **100**, 2921 (2002)

73. C.W.J. BEENAKKER and P. MAZUR, *Physica A* **126**, 349 (1984); *Physica A* **120**, 388 (1983)

74. G. NÄGELE, M. WATZLAWEK, and R. KLEIN, *Progr. Colloid Polym. Sci.* **104**, 31 (1997)

75. G. NÄGELE, B. STEININGER, U. GENZ, and R. KLEIN, *Physica Scripta* **T55**, 119 (1994)

76. M. WATZLAWEK and G. NÄGELE, *J. Colloid Interface Sci.* **214**, 170 (1999)

77. M. WATZLAWEK and G. NÄGELE, *Physica A* **235**, 56 (1997)

78. M. WATZLAWEK and G. NÄGELE, *Phys. Rev. E* **56**, 1258 (1997)

79. D.M.E. THIES-WEESIE, A.P. PHILIPSE, G. NÄGELE, B. MANDL, and R. KLEIN, *J. Colloid Interface Sci.* **176**, 43 (1995)

80. E. OVERBECK, CH. SINN, and M. WATZLAWEK, *Phys. Rev. E* **60**, 1936 (1999)

81. G. NÄGELE and P. BAUR, *Physica A* **245**, 297 (1997)

82. W. HÄRTL, CH. BECK, and R. HEMPELMANN, *J. Chem. Phys.* **110**, 7070 (1999)

83. M.H.J. HAGEN, D. FRENKEL, and C.P. LOWE, *Physica A* **272**, 376 (1999)

84. F. BITZER, T. PALBERG, and P. LEIDERER, University of Konstanz, unpublished results

85. D.L. ERMAK and J.A. MCCAMMON, *J. Chem. Phys.* **69**, 1352 (1978)

86. C.W.J. BEENAKKER, *J. Chem. Phys.* **85**, 1581 (1983)

87. R. PESCHÉ and G. NÄGELE, *Phys. Rev. E* **62**, 5432 (2000)

88. K. ZAHN, J.M. MENDEZ-ALCARAZ, and G. MARET, *Phys. Rev. Lett.* **79**, 175 (1997)

89. B. RINN, K. ZAHN, P. MAASS, and G. MARET, *Europhys. Lett.* **46**, 537 (1999)

90. R. PESCHÉ, M. KOLLMANN, and G. NÄGELE, *J. Chem. Phys.* **114**, 8701 (2001)

91. M. KOLLMANN, R. HUND, B. RINN, G. NÄGELE, K. ZAHN, H. KÖNIG, G. MARET, R. KLEIN, and J.K.G. DHONT, *Europhys. Lett.* **58**, 919 (2002)

92. W. HÄRTL, J. WAGNER, CH. BECK, F. GRIERSCHNER, and R. HEMPELMANN, J. Phys. Condens. Matter **12**, A287 (2000)

93. J.F. BRADY and G. BOSSIS, *Annu. Rev. Fluid Mech.* **20**, 111 (1988)

94. A.E. LARSEN and D.G. GRIER, *Nature* **385**, 230 (1997)

95. H. ACUÑA-CAMPA, M.D. CARBAJAL-TINOCO, J.L. ARAUZ-LARA, and M. MEDINA-NOYOLA, *Phys. Rev. Lett.* **80**, 5802 (1998)

96. B. CICHOCKI and B.U. FELDERHOF, *J. Chem. Phys.* **98**, 8186 (1993)

97. M. MEDINA-NOYOLA, *Faraday Discuss. Chem. Soc.* **83**, 21 (1987)

98. G. NÄGELE and J.K.G. DHONT, *J. Chem. Phys.* **108**, 9566 (1998)

99. G. NÄGELE AND P. BAUR, *Europhys. Lett.* **38**, 557 (1997)

100. R. VERBERG, I.M. DE SCHEPPER, and E.G.D. COHEN, *Europhys. Lett.* **48**, 397 (1999)

101. M. FUCHS, W. GÖTZE, I. HOFACKER, and A. LATZ, *J. Phys. (France)* **3**, 5047 (1991)

102. M. FUCHS and M.R. MAYR, *Phys. Rev. E* **60**, 5742 (1999)

103. G. SZAMEL and H. LÖWEN, *Phys. Rev. A* **44**, 8215 (1991)

104. A.J. BANCHIO, J. BERGENHOLTZ, and G. NÄGELE, *Phys. Rev. Lett.* **82**, 1792 (1999)

105. L. SJÖGREN, *Phys. Rev. A* **22**, 2883 (1980)

106. U. BENGTZELIUS, W. GÖTZE, and A. SJÖLANDER, *J. Phys. C* **17**, 5915 (1984)

107. W. GÖTZE, in: *Liquids, Freezing and Glass Transition*, edited by: J.-P. Hansen, D. Levesque, and J. Zinn-Justin (North-Holland, Amsterdam, 1991)

108. W. GÖTZE and L. SJÖGREN, *Rep. Prog. Phys.* **55**, 241 (1992)

109. M. FUCHS, *Transp. Theory Stat. Phys.* **24**, 855 (1995)

110. G. NÄGELE and J. BERGENHOLZ, *J. Chem. Phys.* **108**, 9893 (1998)

111. M. KOLLMANN and G. NÄGELE, *J. Chem. Phys.* **113**, 7672 (2000)

112. I. MORIGUCHI, *J. Chem. Phys.* **106**, 8624 (1997)

113. W. VAN MEGEN and S.M. UNDERWOOD, J. Chem. Phys. **91**, 552 (1989)

114. A. IMHOF and J.K.G. DHONT, *Phys. Rev. E* **52**, 6344 (1995)

115. H. LÖWEN, T. PALBERG, and R.G. SIMON, *Phys. Rev. Lett.* **70**, 1557 (1993)

116. H. LÖWEN, *Phys. Rev. E* **53**, R29 (1996)

117. J.Q. BROUGHTON, G.H. GILMER, and Y.D. WEEKS, *Phys. Rev. B* **25**, 4651 (1982)

118. P.G. DE GENNES, *J. Chem. Phys.* **72**, 4756 (1980) 679 (1997)

119. F. BROCHARD and P.G. DE GENNES, *Physica A* **118**, 289 (1983)

120. A.Z. AKCASU and M. TOMBAKOGLU, *Macromolecules* **23**, 1511 (1990)

121. Y. FENG, C.C. HAN, M. TAKENAKA, and T. HASHIMOTO, *Polymer* **33**, 2729 (1992)

122. G. NÄGELE, in: J.K.G. Dhont, G. Gompper, and D. Richter (Eds.), *Lecture Manuscripts of the 33rd IFF Winter School* (Schriften des Forschungszentrums Jülich, Series: Materials and Matter, Vol. 10, 2002)

123. G. NÄGELE, J.K.G. DHONT, and G. MEIER, in: P. Heitjans and J. Kärger (Eds.), *Diffusion in Condensed Matter* (to appear in Springer-Verlag, Berlin, 2004)

124. H. ACUNA-CAMPA, M.D. CARBAJAL-TINOCO, J.L. ARAUZ-LARA, and M. MEDINA-NOYOLA, *Phys. Rev. Lett.* **80**, 5802 (1998)

125. T. HOFMANN, R.G. WINKLER, and P. REINEKER, *J. Chem. Phys.* **114**, 10181 (2001)

126. J.A. GIVEN and G. STELL, *J. Chem. Phys.* **97**, 4573 (1992)

127. M.P. LETTINGA, M.A.M.J. VAN ZANDVOORT, C.M. VAN KATS, and A.P. PHILIPSE, *Langmuir* **16**, 6156 (2000)

128. G.H. KOENDERINK, H. ZHANG, M.P. LETTINGA, G. NÄGELE, and A.P. PHILIPSE, *Phys. Rev. E* **64**, 022401 (2001).

Institute of Fundamental Technological Research
publishes the following periodicals:

Archives of Mechanics — bimonthly (in English)
Archives of Acoustics — quarterly (in English)
Archives of Civil Engineering — quarterly (in English)
Engineering Transactions — quarterly (in English)
Computer Assisted Mechanics and Engineering Sciences
— quarterly (in English)
Journal of Technical Physics — quarterly (in English)

Subscription orders for all journals edited by IFTR may be sent directly to:
Editorial Office
Institute of Fundamental Technological Research
Świętokrzyska 21, p. 508
00-049 Warszawa, POLAND